NUMERICAL ANALYSIS OF ISOTHERMAL VARIATION OF CONCENTRATION-DEPENDENT INTERDIFFUSION COEFFICIENT

BY

OSAMUDIAMEN OLAYE

A Thesis Submitted to the Faculty of Graduate Studies of the University of Manitoba

in Partial Fulfillment of the Requirements for the Degree of

DOCTOR OF PHILOSOPHY

Department of Mechanical Engineering,

University of Manitoba

Winnipeg

Copyright © 2022 by Osamudiamen Olaye

ABSTRACT

The accuracy of theoretical predictions and analyses of diffusion-controlled phase transformations in materials is significantly influenced by the concentration-dependent interdiffusion coefficient (**D(C)**). It is generally assumed in the literature that the dependence of the interdiffusion coefficient on concentration is isothermally constant. However, this may not be the case because of the evolution of diffusion stresses and strains, which result from factors that can change the concentration gradients at the same solute concentration. This work aims to theoretically and experimentally study how factors that change concentration gradient and, by implication, the diffusion-induced stress/strain (**DIS**) influence the solute concentration dependence of the interdiffusion coefficient.

In this research work, six factors that are postulated to influence the D(C) have been theoretically studied, and the results are experimentally validated using diffusion couples. The six factors studied are time, temperature, non-uniform initial solute distribution, time-varying surface concentration (SC), solute source concentrations, and diffusion geometry. A theoretical model based on DIS and its relaxation is used to simulate concentration profiles and calculate the D(C). Key theoretical predictions are experimentally verified using a newly developed and validated numerical model to reliably extract the D(C) from experimental data. The theoretical and experimental data analyses show that the concentration dependence of interdiffusion coefficient can significantly change when any of the six factors changes. This study shows that the common practice of using a single interdiffusion coefficient to predict isothermal diffusion effects can become significantly unreliable when the dependence of diffusivity on concentration changes. Neglecting the fundamental concept elucidated in this study can lead to the consequential misidentification of the mechanism of microstructural changes through phase transformation reactions.

DEDICATION

This thesis is dedicated to my mom and in honour of my late father.

ACKNOWLEDGEMENTS

I would like to thank my advisor, Dr. Olarenwaju Akanbi Ojo, for his guidance and help throughout my entire Ph.D. research study. This study could not have been accomplished without Professor Ojo's support and academic advice. I also appreciate his timely advice, financial support, and the provision of all the materials and equipment required to complete my doctoral program. I also want to express my gratitude to the other committee members, Dr. Guozhen Zhu and Dr. Masoud Asadzadeh, for their valuable advice and contribution to the success of this research work. Their invaluable contributions have greatly improved the work. I appreciate Dr. Lina Zhang and Mike Boskwick for their technical assistance.

I wish to express my gratitude for the financial assistance from the University of Manitoba through the University of Manitoba Graduate Fellowship, scholarships, and bursary. The financial support from NSERC towards the research work in this study is also acknowledged.

I want to thank my mom, Mary O. Olaye, for her strong support throughout my life. I appreciate my fiancée, Chidinma Emmanuella Monyei, my siblings, and my friends, including Oguntuase Oluwasanmi, Emmanuel Adejumo, Yemi Aina, Dr. Gbenga Asala, Nnaemeka Ugodilinwa, Akinshilo Akinbowale, James Adu, Chidinma Anyanwu, Taiwo Dada, Deborah Michael, Mallikarjuna Thammaiah, Hassan Oyeleja, Hamid Reza Abed, Olusola Bamidele, Oluwadara Afolabi, Paul Fase, and Hassan Sada for always being there for me.

Finally, my most revered appreciation goes to God Almighty for bringing me thus far in life.

LIST OF ABBREVIATIONS AND SYMBOLS

J: Flux

C: Composition or mole fraction

C*: Specific composition

r: Distance

D: Diffusion coefficient

D(C): Concentration-dependent interdiffusion coefficient

DIS: Diffusion-induced stress

SC: Surface concentration

Cs: Solute source

λ: Boltzmann parameter

t: Time

1D: One dimensional

2D: Two dimensional

3D: Three dimensional

D^*: Tracer diffusion coefficient

M: Mobility

K: Boltzmann constant

T: Temperature

Tm: Melting temperature

a: Activity

μ: Chemical potential

F: Force

Φ: Component potential

L_{11} and L_{1Q}: Onsager coupling coefficients

$Q_{1:}$ Associated charge

ϕ: Electrostatic potential

$\vec{E}_1$: Electric field

β: Constant in electropotential

$\bar{s}_1$: Partial atomic entropy

Q_1^{Trans}: Heat of transport

D_T: Thermal diffusion coefficient

D_{eff}: Effective diffusivity

V: Molar volume

P: Hydrostatic pressure

C_0: Constant in tracer experiment

γ^*: Activity coefficient

θ: Thermodynamic factor

y: Concentration ratio

$\tilde{D}$: Interdiffusion coefficient

D_i: Intrinsic diffusivity

c: Concentration

D_{ave}: Average interdiffusion coefficient or Average diffusivity

r_m: Matano Interface position

BM: Boltzmann-Matano

SF: Sauer-Freise

ρ : Molar density

α : Constant in the equation of thermodynamic factor

E: Young's modulus

υ : Poisson ratio

ε : Strain

σ : Stress

η : Viscosity

x: horizontal distance

n: Geometry factor

s: Interface position

L : Diffusion length

$\lambda\lambda$: Geometrical condition

p: Concentration in first phase

q: Concentration in last phase

z: Concentration in intermediate phase

v: Normalized distance in the last phase

u: Normalized distance in the first phase

w: Normalized distance in the inner phases

k: Time step

m: Space step

nn: intermediate phase

nf: Number of phases

N_A: Avogadro's number

Q(C): Concentration-dependent activation energy

D_0(C): Concentration-dependent pre-exponential factor

Ms: Mass of solute

Vo: Volume

A: Area

A_c: Area under curve

I(x): Initial conditions

Common subscripts:

1,2: The component of diffusion

i: Initial

f: Final

L: Left

R: Right

Superscript:

': Dimensionless values of a symbol

TABLE OF CONTENTS

LIST OF TABLES

LIST OF FIGURES

CHAPTER ONE

1 INTRODUCTION

Mass transport by atomic motion, known as atomic diffusion, is vital for studying phase changes in metals and semiconductors. The properties of engineering materials can be changed by altering their microstructures through processes that produce phase transformations in materials. Researchers have studied this phenomenon for over a century and a half due to its indispensable applications in several industrial sectors, including the energy, aerospace, biomedical, and automobile industries. These sectors use the principle of mass transport in solids to control and predict the properties of engineering materials. Mass transport in metals results in phase change or microstructural transformation. Physical metallurgists are primarily interested in the relationship between phase change and variation in the properties of metals. Materials processing industries commonly use phase transformation processes such as coating, diffusion bonding, sintering, and heat treatments to enhance the properties of engineering materials for improving material performance.

Presently, diffusion is found in most metallurgical processes such as carburizing, where atomic carbon is diffused into the surface of an iron element or steel alloys; nitriding where atomic nitrogen is diffused into the surface of an iron element or steel alloys; the production of bimetallic strips, which requires diffusion to join different alloys and metals; the production of heat and corrosion-resistant surfaces through a diffusion coating process which coats them with metallic elements (chromizing, siliconizing); age-hardening; homogenization of casting; manufacture of penny coins by the diffusion of zinc into copper; metal joining processes such as solid-solid diffusion bonding, transient liquid phase (TLP) bonding, etc. Adolf Fick, a German physician and

physiologist, first used the laws of diffusion in 1855 to describe the diffusion of gas through another substance [1]. The first successful use of Fick's laws in solid-state diffusion was done by William Chandler Roberts-Austen, a physicist, in 1896. He extended a study of the diffusion of gold in lead by the renowned chemist Thomas Graham. Fick's laws are now the prominent equations used to analyze diffusion-controlled processes in gases, liquids, and solids [2]. Even though Fick's laws were originally developed for diffusion in fluids, the laws presently form the core understanding of diffusion in solids.

Fick's first law of diffusion is:

$$J = -D\frac{\partial C}{\partial r} \tag{1.1}$$

Fick's second law of diffusion is:

$$\frac{\partial C}{\partial t} = \frac{\partial}{\partial r}\left(D\frac{\partial C}{\partial r}\right) \tag{1.2}$$

The Fick's equations (Equations 1.1 and 1.2) require a crucial parameter called the diffusion coefficient, which is a vital component of the diffusion equations and for diffusion analyses and predictions (Figure 1.1). Therefore, the accuracy of analyses of diffusion-controlled processes, which affects the predicted performance of materials, depends on a reliable diffusion coefficient for each composition [3]. It is well established in the literature that diffusion coefficient is concentration-dependent, which is referred to as concentration-dependent interdiffusion or chemical diffusion coefficient [4], [5]. Also, there is a common implied assumption that D(C) is a material constant and should not isothermally change. However, this assumption may not always

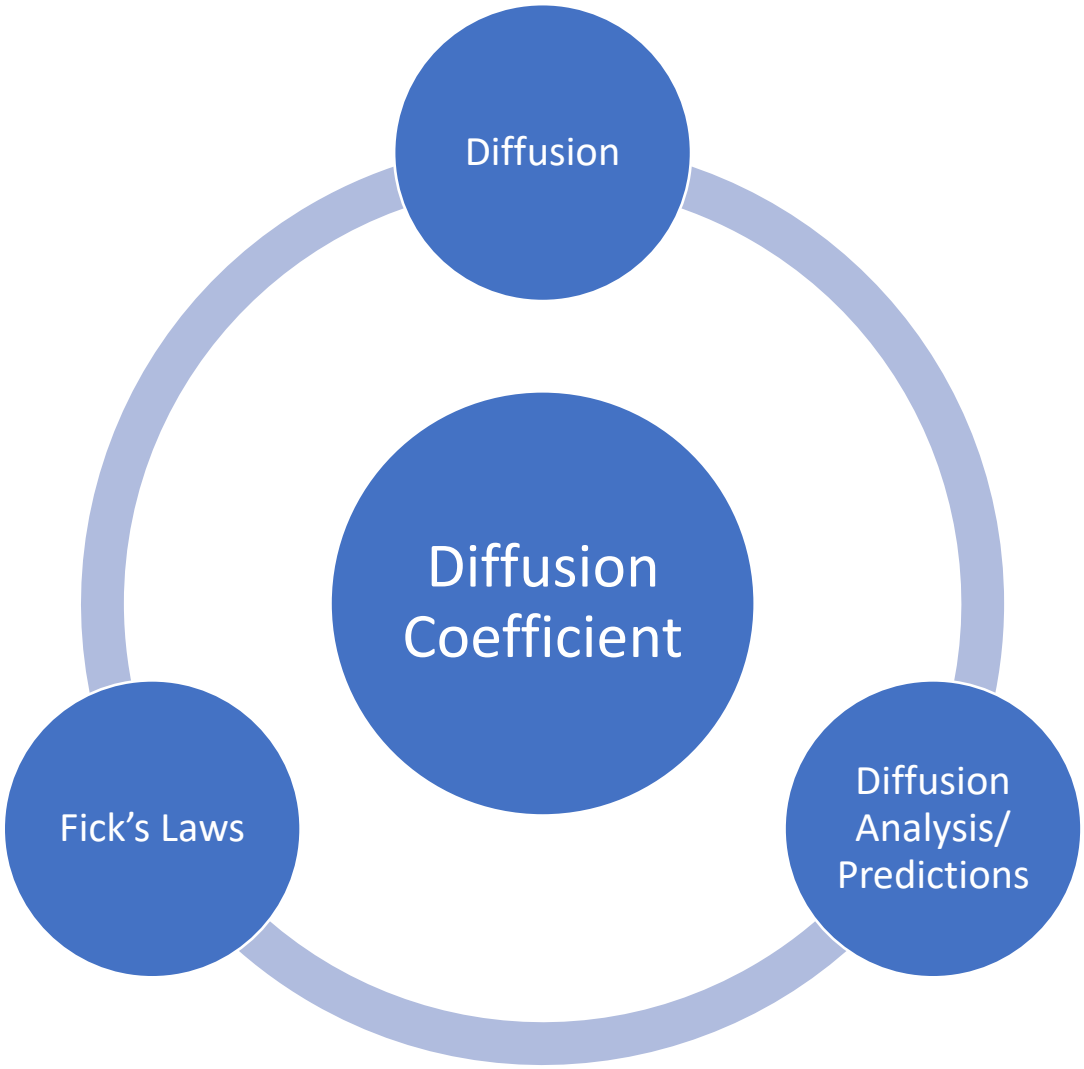

Figure 1.1 Significance of diffusion coefficient in equations of diffusion, diffusion analysis, and predictions

hold. Fundamentally, due to the atomic mismatch caused by the difference between the solute and solvent atomic sizes, the lattice parameter of the host material changes during diffusion. As can be observed in Figure 1.2, the variation of the lattice parameter within a crystal, caused by solute concentration gradients induced by diffusion, results in the generation of strains within the crystal lattice of the host material [6]–[9]. The strain-induced during diffusion is called diffusion-induced strain, and the resulting atomic stress due to this strain is called diffusion-induced stress (**DIS**). Interestingly, strains in crystals influence atomic diffusion coefficients [10]–[15]. Hence, the solute concentration gradient in a crystal is a factor that affects diffusion-induced strain, and by implication, the diffusion coefficient [8]. The existence of DIS has been proven both theoretically [6], [14], [16] and experimentally [9], [12], [14], [17]. Studies have shown that the DIS influences the diffusion coefficient [6], [9], [11], [14], [15], [18]. During diffusion, the concentration gradient changes with solute concentration (Figure 1.3), and since the solute concentration influences the concentration gradient, and the concentration gradient affects the DIS, which controls the diffusion coefficient, therefore, theoretically, diffusion coefficients can vary with solute concentration. Several studies in the literature have confirmed that diffusion coefficient changes with solute concentration [4], [19].

1.1 Research Hypothesis

Generally, the concentration dependence of interdiffusion coefficient (**D(C)**) is assumed to be isothermally constant in the literature. However, at any given concentration, several other factors can change the concentration gradient during diffusion and, by implication, the stress/strain in the

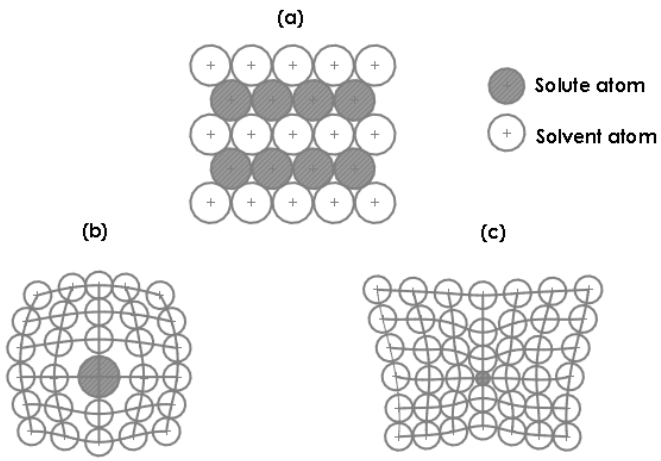

Figure 1.2 Effect of solute atom gradient in a crystal lattice (a) unstrained crystal lattice with no concentration gradient (b) strained crystal lattice with a substitutional solute concentration gradient, and (c) strained crystal lattice with an interstitial solute concentration gradient [20]

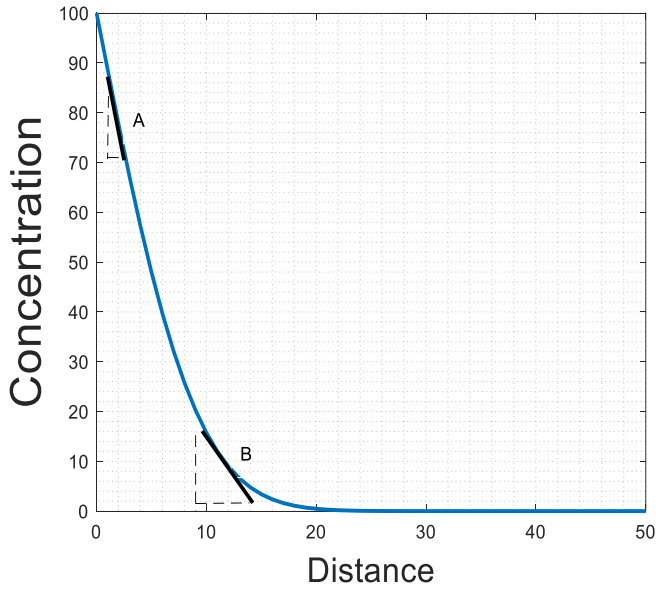

Figure 1.3 Typical concentration profile with the concentration-dependent gradient shown by different gradients at concentrations A and B

diffusion system (Figure 1.4). Changes in stress/strain influence diffusion coefficients. Therefore, it may be possible that the solute concentration dependence of the interdiffusion coefficient is not isothermally constant but changes with other factors that can alter the concentration gradient at any given solute concentration. Some of these factors are (1) time, (2) temperature, (3) non-uniform initial solute distribution, (4) time-varying surface concentration, (e) concentration of solute source, and (f) diffusion interface geometry. These factors affect the magnitude of a solute concentration gradient and how the gradients change with each concentration (Figure 1.5). Therefore, it is postulated that the D(C) may not be isothermally constant, as generally assumed in the literature, but can isothermally change by other factors that can alter the solute concentration gradient, due to DIS.

1.2 Problem Statement

There are two major challenges to verifying the hypothesis of this study. To determine if **D(C)** is affected by any of the six factors listed in the hypothesis, there should be a reliable way to determine DIS influenced **D(C) theoretically and experimentally**. The challenges therefore are:

First Major Challenge: To theoretically use the concept of DIS to study the isothermal variation D(C), DIS model equations that incorporate stress generation and stress relaxation need to be derived and solved simultaneously and reliably for the cases where the diffusion interface migrates in 1D, 2D and 3D.

Second Major Challenge: Analytical methods used to extract D(C) from experiment data, such as the Boltzmann- Matano, Sauer-Freise, Halls and Wagner methods, cannot be used because they

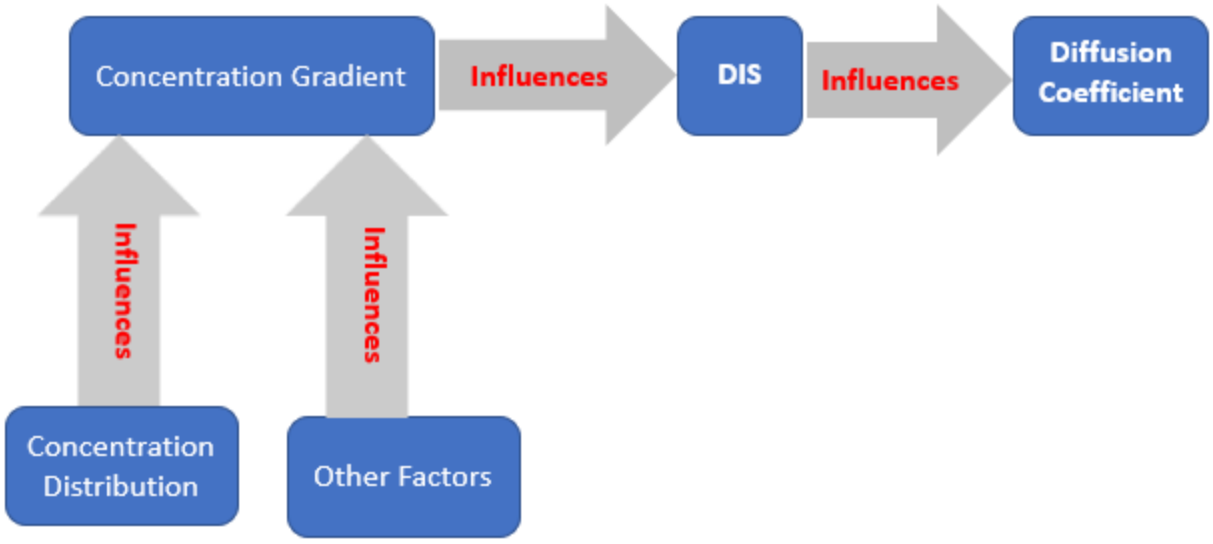

Figure 1.4 Chart of hypothesis

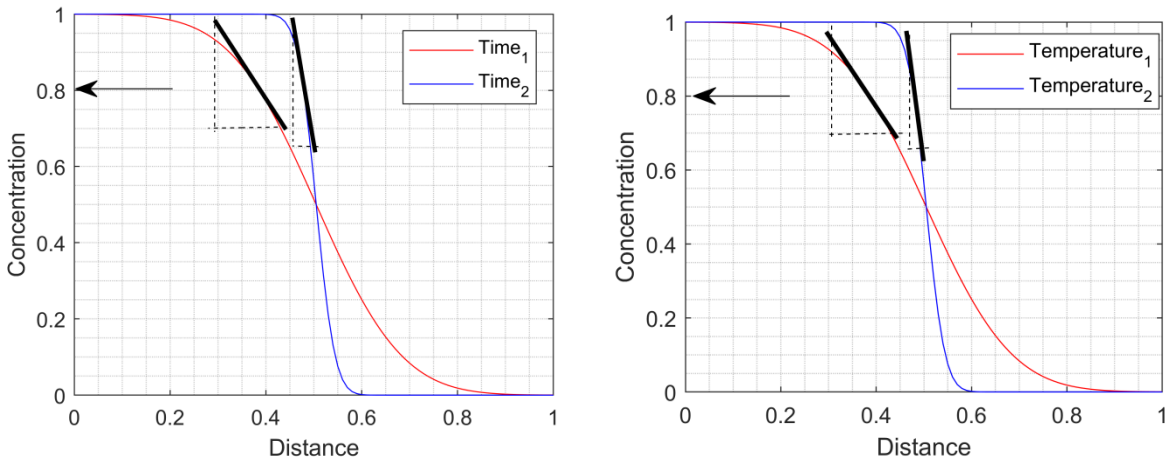

(a) (b)

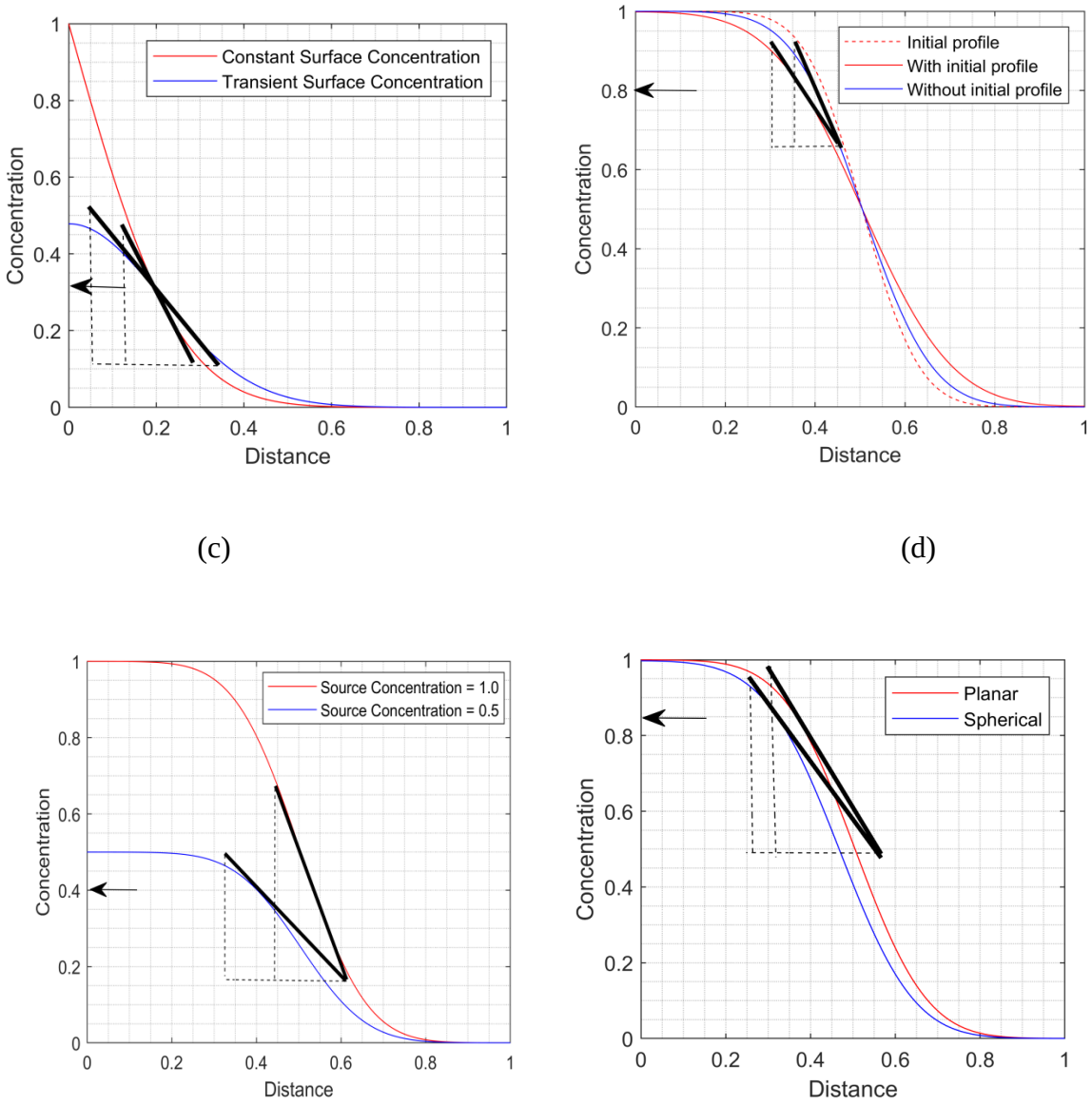

Figure 1.5 Review of factors which alter the concentration gradient at the same concentration (arrow) for (a) Time, (b) Temperature, (c) Transient surface concentration, (d) Initial concentration gradient (e) Source concentration, and (f) Sample geometry

have some common limitations: (1) the initial condition of the concentration distribution must be a step-function in space, which prevents in-between time analyses and multistage analyses, (2) the Boltzmann parameter $\left(\lambda = r/\sqrt{t}\right)$, which is the ratio of diffusion penetration $\left(r\right)$ to the square root of time $\left(\sqrt{t}\right)$, is assumed to be constant in analytical methods, and this is not the case for (i) changing surface concentration cases and (ii) non-planar diffusion interface geometry. Recent work [21]–[30] have shown that the forward simulation method (FSM) is a reliable way of overcoming all the above limitations of analytical methods. The FSM, however, requires a robust numerical simulation model that is stable, reliable, and efficient. This type of model needs to be developed in a way that solute is conserved.

1.3 Thesis Objectives

A. The first major objective of this Ph.D. study is to develop and use a DIS model that incorporates the principles of diffusion-induced stress generation and relaxation to theoretically calculate and study the isothermal variation of D(C).
B. The second major objective of this study is to develop a new numerical model and couple it with the FSM to extract D(C) from experimental data to verify key findings from the theoretical analysis.

1.4 Scope

Six factors that influence the concentration gradient at a given solute concentration during diffusion, which could isothermally alter the interdiffusion coefficient, will be studied in this work. The factors to be studied are (1) time, (2) temperature, (3) non-uniform initial solute distribution,

(4) time-varying surface concentration, (e) concentration of solute source, and (f) diffusion interface geometry.

1.5 Major Work Performed and Key Finding

The first phase of this work involves developing sets of equations to model interdiffusion under DIS. The three key equations that are developed are: (i) pressure equation under DIS, (ii) solute distribution equation under DIS, and (iii) D(C) equation under DIS. The pressure equation is developed using the concept of pressure generation and relaxation during diffusion. The solute distribution equation is developed from the first principles of deriving a solute distribution equation. The innovative approach used in this work involves using the intrinsic diffusivity that combines the chemical potential and pressure/stress potential for diffusion. The D(C) equation is derived by comparing the solute distribution equation under DIS and Fick's laws of diffusion. This is an ingenious approach to calculate the D(C) equation under DIS, which is operative when applying Fick's law to diffusion data. The D(C) equation was theoretically verified as it reproduced the Darken and Nernst-Planck diffusion limits of interdiffusion coefficients. Subsequently, the three equations are discretized and solved simultaneously. The new theoretical model equations developed from the first principles are used to theoretically study the effects of 6 different factors that alter concentration gradient on D(C). The factors studied are (1) time, (2) temperature, (3) non-uniform initial solute distribution, (4) time-varying surface concentration, (e) concentration of solute source, and (f) diffusion interface geometry.

The second phase of this research involves verifying the key theoretical predictions on the effect of the six factors on D(C). This phase is achieved by using a new approach that uses a robust numerical model solution to Fick's laws of diffusion in single-phase, multi-phase, planar, and non-

planar systems with varying D(C). The required numerical model is developed by applying the Landau transformation to the Fick's laws of diffusion. The transformed equations are stabilized using the leapfrog and Duforth-Frankel schemes. Solute balance is made certain by calculating the future interface position, which ensures the total solute in the system remains the same at all diffusion times. This research finds a correlation between the effects predicted by the theoretical model and experimental observations. In contrast to what is commonly assumed, D(C) is not an isothermally constant parameter but can change isothermally by the six factors that alter concentration gradient. The results are published or accepted in seven journals, one paper with minor correction, and two conference presentations.

1.6 Thesis Structure

This thesis consists of the twelve following chapters.

Chapter 1: This is the introduction, and the chapter provides the background information on this research work, the research hypothesis, problem statement, objectives, scope, major work performed, key findings, and thesis structure.

Chapter 2: This chapter is the literature review and consists of three sections. The first section briefly reviews the phenomenon of diffusion and its application in Materials Science. The second section reviews the different methods used to calculate the D(C). Finally, the third section discusses the numerical methods that can be coupled with the FSM.

Chapter 3: In this chapter, the theoretical and experimental research methodologies used in this study are presented. This chapter is divided into three sections. The first section briefly introduces

the chapter, while the second section derives from the first principles, the theoretical equations used to study diffusion under DIS conditions. Subsequently, the third section derives the new numerical model for extracting the experimental data for verification purposes.

Chapter 4: The effect of the diffusion time on the D(C) is investigated in this chapter. This chapter is presented in four parts. The first part introduces the concept. In the second part, the effect of time is theoretically studied, while the third part experimentally verifies the theoretical findings. Finally, the last part investigates the implications of the results.

Chapter 5: The effect of temperature on the D(C) is studied in this chapter. This chapter is presented in four sections. The first section introduces the concept investigated. In the second section, the effect of the diffusion temperature is theoretically studied. The third section experimentally verifies the theoretical findings. The fourth section examines the implications of the time variation of the concentration-dependent activation energy and pre-exponential factor.

Chapter 6: The effect of the initial solute distribution on D(C) is examined in this chapter. This chapter is presented in four parts. The first part introduces the concept, and the second part is a theoretical study on the effect of initial solute distribution. The third section experimentally verifies the theoretical findings, and the fourth section investigates the implications of the investigation.

Chapter 7: The effect of time-varying surface concentration on the D(C) is studied in this chapter. The four sections of this chapter are as follows: introduction of the concept, theoretical study, experimental verification, and implications of the investigation.

Chapter 8: The effect of surface concentration on the D(C) is investigated in this chapter. The four sections of this chapter are as follows: introduction of the concept, theoretical study, experimental verification, and implications of the investigation.

Chapter 9: In this chapter, the effect of one-dimensional (1D) and two-dimensional (2D) migration of the interface on D(C) is studied. The four sections of this chapter are as follows: an introduction, a section on the reliability of using 1D models for migrating interfaces to extract the D(C) from diffusion systems with 2D and 3D migration of the interface, the new method for calculating the initial position of the interface, and the effect of the diffusion geometry on the D(C).

Chapter 10: The development of an analytical equation to calculate the D(C) in a binary diffusion system with a non-uniform initial solute profile is presented in this chapter. This chapter is in six parts. The first section is the introduction, while the second section elaborates on developing the new analytical equation. In the third section, the numerical experimental procedure for validation is presented. The fourth section validates the new method. Subsequently, the fifth section presents an error analysis of the new method by comparing the error from the new method to that from the Sauer-Freise (SF) method. The last section of this chapter verifies the new method with experimental data obtained from the literature.

Chapter 11: This chapter is a detailed summary and conclusions from the major findings of this research work.

Chapter 12: This chapter comprises the limitations of the present work and recommendations for future work.

Chapter 13: In this chapter, the research contributions from this work are presented.

CHAPTER TWO

2 LITERATURE REVIEW

2.1 Introduction

This chapter consists of three (3) sections. The first part, which is a review of the phenomenon of diffusion and its application in Materials Science, will provide a better understanding of diffusion to the reader. This section discusses the different types of diffusion and some of the previous works on diffusion related to material processes. This section will also discuss the mechanisms and the driving force of diffusion. The second section reviews the different methods used to calculate the D(C), with emphasis on the FSM. The third section will discuss the numerical methods that can be coupled with the FSM. This section will also review some published literature on numerical methods used to simulate Fick's second law in several phases.

2.2 The Diffusion Phenomenon

Diffusion plays an important role in microstructural transformations and material processing because the phenomenon is a mass flow process with atomic migration. Diffusion results in microstructural changes, which causes a corresponding change in the properties and performance of the engineering materials (Figure 2.1) [31]. The rate of diffusion, which is the number of atoms that diffuse across a unit area (flux) with time [32]–[35], is directly proportional to the diffusion potential [36]. When the diffusion potential is a concentration gradient, the relationship follows

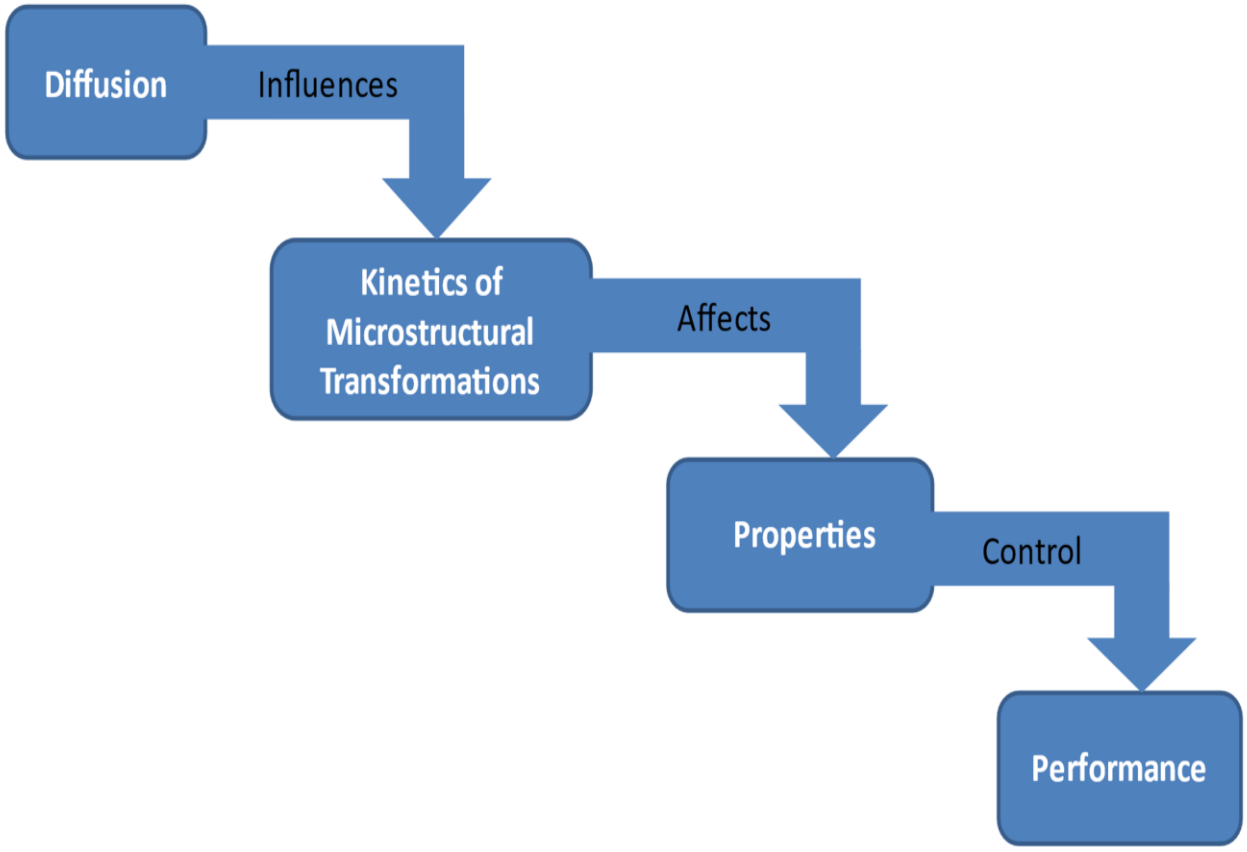

Figure 2.1 Influence of diffusion on the performance of engineering materials

Fick's first law of diffusion, and the constant of the proportionality is a diffusion coefficient. The next section will discuss the diffusion mechanisms, followed by the driving force of diffusion and the types of diffusion coefficients.

2.3 Mechanisms of Diffusion

As defined earlier, diffusion involves the movement of atoms, and there are several mechanisms for such movement. In this subsection, four predominantly relevant mechanisms of diffusion will be discussed: the vacancy, interstitial, interstitialcy mechanisms, and diffusion involving extended defects.

2.3.1 Vacancy diffusion mechanism

Vacancy migration is a common mechanism of diffusion. At thermal equilibrium, vacancies can be found in crystalline materials [37]; see Figure 2.2 for an example. The neighbouring atoms surrounding the vacancy in Figure 2.2 are the hatched atoms. When an atom on an adjacent site jumps into the vacancy to exchange places, the atom is said to have diffused by a vacancy mechanism [38], [39]. The vacancy mechanism can be found in the self-diffusion of pure metals and substitutional solutes in alloys. In pure metals, the atoms are essentially the same. However, atoms that share the same chemical properties can be tagged. A tagged atom is called a tracer atom. The movement of these tracer atoms can track their diffusion. When a tracer atom jumps into a vacancy, the previous site of the tracer atom becomes a new vacancy site (Figure 2.3). The migrated tracer atom is also one of the nearest neighbours to the new vacancy site because the tracer atom can move back to its former site. Therefore, the migration of vacancies can be a completely random event, except when there is a force field [40].

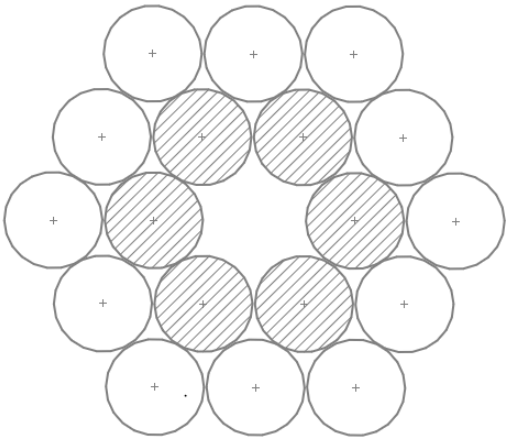

Figure 2.2 A plane of close-packed crystal with a vacancy [40]

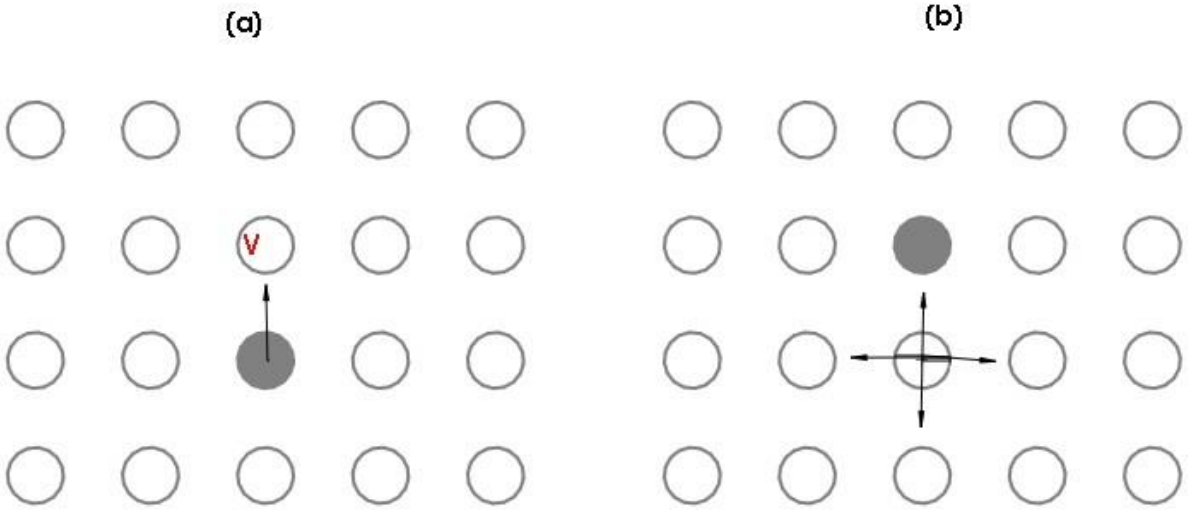

Figure 2.3 Vacancy migration (a) Initial positions (b) After the first jump, the vacancy can move in any of the four directions [40]

2.3.2 Interstitial diffusion mechanism

In the interstitial mechanism of diffusion, atoms diffuse through the interstitial spaces between other atoms in their normal lattice sites without permanently displacing any of the matrix atoms (Figure 2.4). This diffusion type occurs without substantial distortions and occurs more rapidly than vacancy diffusion [40]. In this case, the interstitial defects must be continuous over several interatomic distances [38], [39]. In general, small interstitial atoms diffuse through lattices using this mechanism. Examples of interstitial atoms are hydrogen (H), boron (B), carbon (C), nitrogen (N), oxygen (O), etc. [37].

2.3.3 Interstitialcy diffusion mechanism

The interstitialcy mechanism of diffusion is one in which the solute atoms are large and equal to or greater than the host matrix atoms. This diffusion mechanism differs from interstitial diffusion, where the solutes are smaller than the host matrix atoms. In interstitialcy diffusion, a solute atom jumps from an interstitial site to occupy a lattice site [38], [39]. The migration of the solute atoms displaces the host atoms that previously occupied the lattice site, and the host atom moves to an interstitial site. This mechanism is also referred to as “the indirect interstitial mechanism” [40], and it is illustrated in Figure 2.5.

2.3.4 Mechanisms of diffusion involving extended defects

The three previously explained mechanisms of diffusion in crystalline materials occur in the presence of point defects which results in volume/bulk/lattice diffusion. Nevertheless, some crystalline materials might have one-dimensional defects, such as dislocations and planar defects,

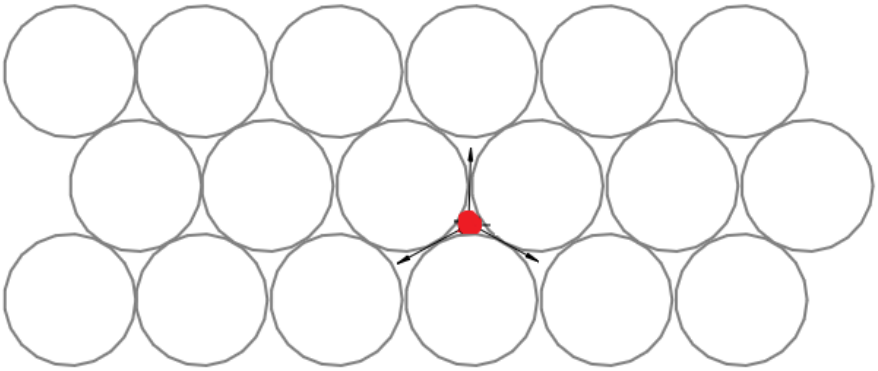

Figure 2.4 Direct interstitial jump in a close-packed system where the red atom is the interstitial atom [40]

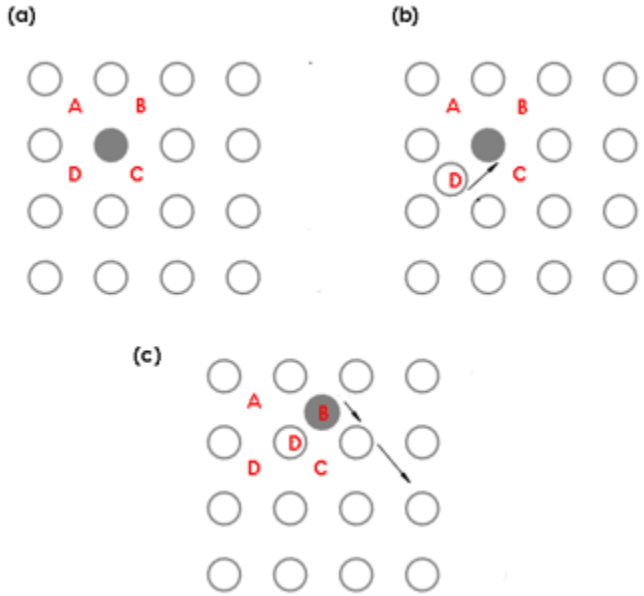

Figure 2.5 (a) Solute atom (black) surrounded by four interstitial sites, A, B, C, and D; (b) self interstitial atom moves to site D (white), the arrow show that the solute atom (black) is pushed into the B site; and (c) after being pushed into the B interstitial site, the solute atom (black) settles there [40]

including grain boundaries, surface, and interface [37] (Figure 2.6). Compared to diffusion through the bulk of the crystal, diffusion can quickly occur through these defects. These defects are the disordered regions in which atoms can migrate relatively easily (Figure 2.7). The diffusion through planar defects such as grain boundaries depends on the size of the grains and diffusion temperature [41]. As the diffusion temperature approaches the melting point Tm, the effective diffusion transforms from a predominantly grain boundary diffusion to bulk or volume diffusion, and this transformation is typically between 0.5Tm to 0.75Tm [42], [43].

After discussing the different diffusion mechanisms, the equations used to analyze, predict, and model diffusion in solids are provided in the following section.

2.4 Equations of Diffusion

The three basic equations of diffusion in binary systems developed by Adolf Fick, Albert Einstein, and Torsten Teorell are briefly reviewed in this section. The three equations are exclusively for diffusion due to concentration gradients, dilute systems, and the presence of an external field or force, respectively.

2.4.1 Fick's laws of diffusion

Adolf Fick first proposed the laws that govern diffusion. In Fick's work [1], two laws were developed to govern diffusion due to a concentration gradient. The first law relates the amount of solute diffused across a unit area with time (flux) and the concentration gradient. The first law states that the flux is directly proportional to the concentration gradient. Fick's first law for 1D

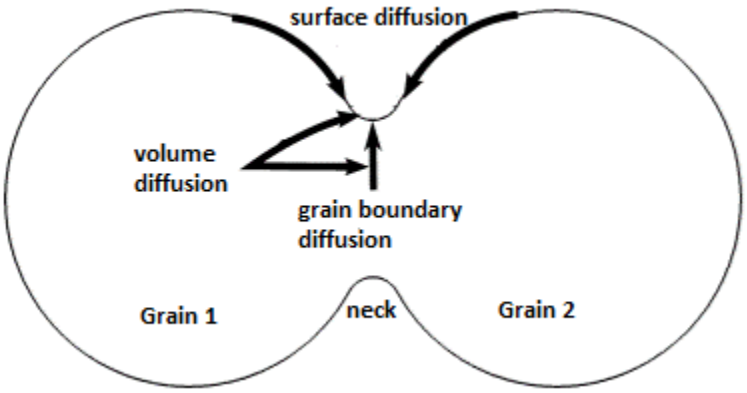

Figure 2.6 Different line diffusion routes between two grains: surface, grain boundary, and volume diffusion [44]

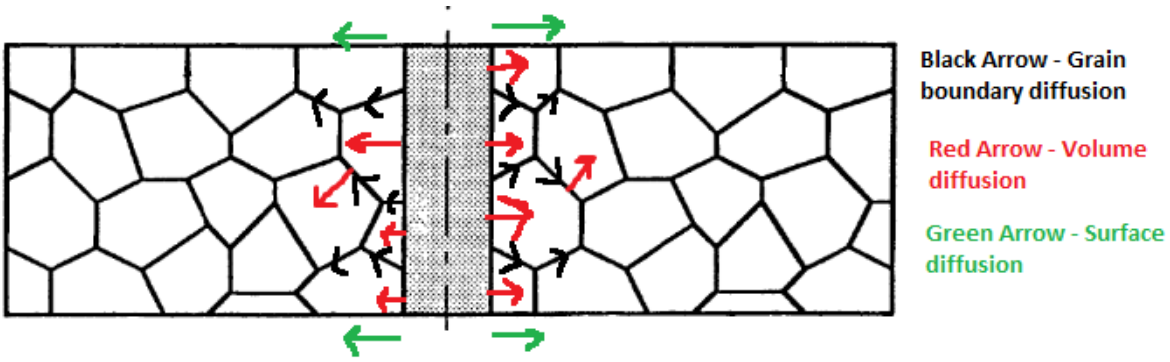

Figure 2.7 Diffusion routes in a system with multiple grains [43]

diffusion is as follows:

$$J = -D\frac{dC}{dr} \qquad 2.1$$

The negative sign in Equation 2.1 arises from the fact that solute diffuses in the direction of a negative concentration gradient.

Fick's second law is a mass conservation equation that relates the rate of solute diffusion to the spatial derivative of flux. The second law predicts how solute concentration can change with time by equating the time derivative of concentration to the negative spatial divergence of flux [2]. Fick's second law is written as:

$$\frac{dC}{dt} = -\frac{\partial J}{\partial r} = -\frac{\partial}{\partial r}\left(-D\frac{dC}{dr}\right) \qquad 2.2$$

2.4.2 Einstein's diffusion law

Einstein developed his diffusion equation [45] while developing an equation to compare the Brownian motion of particles at low liquid concentrations. Although the equation was developed for the microscopic theory of diffusion for diluted particles in a liquid [2], [46], it is relevant for the diffusion of solids at low concentrations [36]. The diffusion equation, is [2], [47]:

$$D^* = MKT \qquad 2.3$$

The Mobility, M, represents the frictional velocity per unit force [47]

2.4.3 Teorell equation of diffusion

The Teorell equation of diffusion was developed to determine the influence of external fields on diffusion, particularly electric fields. The general Teorell equation for ideal systems under isothermal conditions is [2], [46], [48]:

$$J = Ma\left(-\nabla\mu + external\ \ force\ \ per\ \ mole\right) \tag{2.4}$$

The general Teorell equation is important when external forces influence diffusion and proves that external forces or fields can influence or induce diffusion. Therefore, the following section will focus on the driving force of diffusion.

2.5 Driving Force of Diffusion

As discussed in the previous section, there is the possibility that external forces can influence diffusion and the potential driving diffusion. The diffusion potential at any given concentration is the driving force for diffusion, and several potentials can influence the diffusion rate [36]. The driving force for diffusion is defined as:

$$\vec{F}_1 = -\nabla\Phi_1 \tag{2.5}$$

This section will briefly review five potentials - chemical, electrical, thermal, stress (or pressure), and magnetic potentials. The relevant equations are presented for the first four types of potentials. Also, the influence of these potentials on effective intrinsic diffusivity will be elaborated on.

2.5.1 Chemical potential

In the absence of all fields and interfaces, when a concentration gradient is found in an isothermal material, the diffusion potential is identical to its chemical potential. In this case, the driving force can be written as:

$$\vec{F}_1 = -\nabla\Phi_1 = -\nabla\mu_1 \qquad 2.6$$

The diffusion potential μ is defined as [36]:

$$\mu_1 = \mu_1^0 + KT\ln\left(K_1 C_1\right) \qquad 2.7$$

where K_1 and μ_1^0 are constants.

$$\nabla\mu_1 = \frac{KT}{C_1}\nabla C_1 \qquad 2.8$$

The driving force is directly related to the flux by using:

$$\vec{J}_1 = L_{11}\vec{F}_1 = -L_{11}\nabla\Phi_1 = -L_{11}\nabla\mu_1 \qquad 2.9$$

$$L_{11} = M_1 c_1 \qquad 2.10$$

The mobility based on the Nernst-Einstein equation is:

$$M_1 = \frac{D_1^*}{KT} \qquad 2.11$$

Substituting Equations 2.8, 2.10 and 2.11 into Equation 2.9 yields the flux, which is the same as the Fick's first law of diffusion.

$$\vec{J}_1 = -D_1\left(\nabla C_1\right) \qquad 2.12$$

2.5.2 Electropotential

Electrostatic force is a driving force that can induce diffusion in materials, and the diffusion potential due to an electrostatic force is called electropotential. When chemical potential and electropotential generate a force that drives diffusion in a material, the resulting potential is called the electrochemical potential [49]–[51]. An example of electropotential diffusion is the electromigration of atoms during the electrolysis of metals [50], [52], [53].

The driving force for electropotential diffusion is:

$$\vec{F}_1 = -\nabla\Phi_1 = -\nabla\left(\mu_1 + Q_1\varphi_1\right) \qquad 2.13$$

Electric field $\vec{E}_1 = -\nabla\phi_1$ 2.14

$$\vec{J}_1 = L_{11}\vec{F}_1 = -L_{11}\nabla\Phi_1 = -L_{11}\nabla\left(\mu_1 + Q_1\varphi\right) = -L_{11}\left(\nabla\mu_1 + Q_1\nabla\varphi\right) \qquad 2.15$$

Combining Equations 2.8, 2.10-2.11 and 2.15, the flux is derived as:

$$\vec{J}_1 = -D_1\left(\nabla C_1 + \frac{C_1 Q_1}{KT}\nabla\varphi\right) \qquad 2.16$$

Equation 2.16 can be re-written for electromigration [36],

$$\vec{J}_1 = -D_1\left(\nabla C_1 - \frac{C_1\beta}{KT}\vec{E}_1\right) \qquad 2.17$$

where β is a constant that can be calculated using an uphill diffusion process that becomes stationary when the electrical field cancels out the concentration gradient to ensure zero flux. Thus, at zero flux:

$$\beta = \frac{\nabla C_1 KT}{C_1 \vec{E}_1} = -\frac{\nabla C_1}{\nabla \varphi}\frac{KT}{C_1} \qquad 2.18$$

Equation 2.17 can be re-written as:

$$\vec{J}_1 = -D_1\left(1+\frac{C_1\beta}{KT}\frac{\nabla\varphi}{\nabla C_1}\right)\nabla C_1 = -D_{eff}\nabla C_1 \qquad 2.19$$

The effective diffusivity, $D_{eff} = D_1\left(1+\frac{C_1\beta}{KT}\frac{\nabla\varphi}{\nabla C_1}\right)$ 2.20

Therefore, in the presence of an electrical field, the effective diffusivity can be influenced by the electrical field in the system.

2.5.3 Thermal potential

Another type of diffusion potential is thermal potential which results in thermal diffusion (the Ludwig-Soret effect) in a temperature gradient. Thermal diffusion has been studied in alloys such as gold-copper (Au-Cu), iron-carbon (Fe-C), and iron-nitrogen (Fe-N) [54]. In the presence of a thermal gradient, the flux during diffusion is given in [36] as:

$$\vec{J}_1 = -L_{11}\nabla\mu_1 - L_{1Q}\frac{\nabla T}{T} \qquad 2.21$$

The non-isothermal chemical potential depends on the concentration and temperature; hence, thermal gradients can influence the chemical potential.

$$d\mu_1(C_1,T) = \left(\frac{\partial\mu_1}{\partial C_1}\right)_T dC_1 + \left(\frac{\partial\mu_1}{\partial T}\right)_{c_1} dT \qquad 2.22$$

Defining a partial atomic entropy $\bar{s}_1$ as:

$$\bar{s}_1 = -\left(\frac{\partial \mu_1}{\partial T}\right)_{c_1} \tag{2.23}$$

$$\nabla \mu_1 = \left(\frac{\partial \mu_1}{\partial C_1}\right)_T \nabla C_1 - \bar{s}_1 \nabla T \tag{2.24}$$

From Equation 2.7, the gradient of chemical potential is:

$$\nabla \mu_1 = \frac{KT}{C_1} \nabla C_1 - \bar{s}_1 \nabla T \tag{2.25}$$

The above chemical potential gradient is different from the chemical potential gradient in Equation 2.8, which assumes no temperature gradient.

Substituting Equation 2.25 into Equation 2.21 yields:

$$\vec{J}_1 = -L_{11}\left[\left(\frac{KT}{C_1}\nabla C_1 - \bar{s}_1 \nabla T\right) - \frac{L_{1Q}}{L_{11}}\frac{\nabla T}{T}\right] \tag{2.26}$$

Substituting Equation 2.10 and 2.11 into Equation 2.26 yields:

$$\vec{J}_1 = -D_1\left(\nabla C_1 + \frac{C_1 Q_1^{Trans}}{KT^2}\nabla T\right) \tag{2.27}$$

where Q_1^{Trans} is the heat of transport, and defined as:

$$Q_1^{Trans} = \frac{L_{1Q}}{L_{11}} - T\bar{s}_1 \tag{2.28}$$

The heat of transport can be calculated by using an uphill diffusion experiment performed until the imposed temperature gradient cancels out the effect of the concentration gradient, thus resulting in a zero net flux in Equation 2.27. Hence, at zero net flux:

$$Q_1^{Trans} = \frac{KT^2 \nabla C_1}{C_1 \nabla T} \qquad 2.29$$

The heat of transport for different interstitial elements can be found in the literature [39].

$$D_T = \frac{Q_1^{Trans}}{KT^2} \qquad 2.30$$

D_T is called the thermal diffusion coefficient [54].

Equation 2.27 can be re-written as:

$$\vec{J}_1 = -D_1 \left(1 + \frac{C_1 Q_1^{Trans}}{KT^2} \frac{\nabla T}{\nabla C_1} \right) \nabla C_1 = -D_{eff} \nabla C_1 \qquad 2.31$$

$$D_{eff} = D_1 \left(1 + \frac{C_1 Q_1^{Trans}}{KT^2} \frac{\nabla T}{\nabla C_1} \right) \qquad 2.32$$

Therefore, in the presence of a temperature gradient, the effective diffusivity can be influenced by the temperature gradient in the system, and the heat of transport can be experimentally determined when a thermal gradient is applied to ensure zero flux.

2.5.4 Stress (or pressure) potential

Stress is a diffusion potential that influences the diffusion boundary conditions and atomic mobility. Stress could be external [10] or induced by diffusion [55]. Stress evolution during

diffusion contributes to the thermodynamic potential for diffusion and gives rise to elastic and plastic deformations [9]. The diffusion potential in the presence of stress is an elastochemical type of potential correction [36].

The driving force of diffusion in the presence of stress/pressure is obtained with:

$$\vec{F}_1 = -\nabla\Phi_1 = -\nabla\left(\mu_1 + V_1 P\right) \tag{2.33}$$

$$\vec{J}_1 = L_{11}\vec{F}_1 = -L_{11}\nabla\Phi_1 = -L_{11}\nabla\left(\mu_1 + V_1 P\right) \tag{2.34}$$

Combining Equations 2.8 to 2.11 and 2.34, which is the flux equation under stress, the equation for the diffusion flux in the presence of pressure is given as:

$$\vec{J}_1 = -D_1\left(\nabla C_1 + C_1\frac{V_1}{KT}\nabla P\right) \tag{2.35}$$

The above equation can be re-written as:

$$\vec{J}_1 = -D_1\left(1 + C_1\frac{V_1}{KT}\frac{\nabla P}{\nabla c_1}\right)\nabla C_1 = -D_{eff}\nabla C_1 \tag{2.36}$$

$$D_{eff} = D_1\left(1 + C_1\frac{V_1}{KT}\frac{\nabla P}{\nabla C_1}\right) \tag{2.37}$$

Therefore, in the presence of a pressure gradient, the effective diffusivity can be influenced by the external stress gradient [10] or stress gradient induced by diffusion [55] in the system. The equation for effective intrinsic diffusivity can also be found in [56].

2.5.5 Other potentials

Aside from the four described potentials of chemical, electrical, thermal, stress (or pressure) potentials, magnetic potential can also influence diffusion. Examples of diffusion in the presence of a magnetic potential studied in the literature are Al-Cu [57] and Fe-C [58], [59].

A summary of the force, flux, and effective intrinsic diffusion under various potentials is presented in Table 2.1. Thus, without a chemical potential, diffusion can proceed due to other external fields. Nevertheless, the chemical potential is the driving force for diffusion without external field potential. External and chemical potential can influence diffusion and the effective diffusion coefficient. Therefore, it is important to distinguish the different types of diffusion coefficients.

2.6 Diffusion Coefficients

The diffusion coefficient during mass transfer can be defined as the net flux of solute atoms that diffuse in the direction of a unit concentration gradient. This section discusses the common types of diffusion coefficients and the mathematical relationships between them. The four types of diffusion coefficients discussed are tracer diffusion coefficients (self and impurity tracer diffusion coefficients), intrinsic diffusion coefficients, interdiffusion coefficients, and average interdiffusion coefficients.

2.6.1 Tracer diffusion coefficients

Under certain conditions, atoms can diffuse without being driven by chemical potential. The section on the vacancy mechanism of diffusion briefly discussed diffusion without a concentration

Table 2.1: Summary of the force, flux, and effective intrinsic diffusion under various potentials

Potential	Force $\vec{F}_1 = -\nabla\Phi_1$ [36]	Flux (J) [36]	Effective intrinsic diffusivity (D_{eff})
Chemical potential	$-\nabla\mu_1$	$\vec{J}_1 = -D_1(\nabla C_1)$	$D_{eff} = D_1$
Electrical-Chemical potential (Electropotential)	$-\nabla(\mu_1 + \beta\phi_1)$ Where $q_1 \equiv \beta$	$\vec{J}_1 = -D_1\left(\nabla C_1 + \frac{C_1\beta}{KT}\nabla\varphi\right)$	$D_{eff} = D_1\left(1 + \frac{C_1\beta}{KT}\frac{\nabla\varphi}{\nabla C_1}\right)$
Thermal-Chemical potential	$-\nabla\mu_1$ $-\left(Q_1^{Trans} + T\bar{s}_1\right)\frac{\nabla T}{T}$	$\vec{J}_1 = -D_1\left(\nabla C_1 + \frac{C_1 Q_1^{Trans}}{KT^2}\nabla T\right)$ [39]	$D_{eff} = D_1\left(1 + \frac{C_1 Q_1^{Trans}}{KT^2}\frac{\nabla T}{\nabla C_1}\right)$
Pressure-Chemical potential (Elastochemical)	$-\nabla(\mu_1 + V_1 P)$	$\vec{J}_1 = -D_1\left(\nabla C_1 + \frac{C_1 V_1}{KT}\nabla P\right)$ [39]	$D_{eff} = D_1\left(1 + \frac{C_1 V_1}{KT}\frac{\nabla P}{\nabla C_1}\right)$ [56]

gradient and other external fields. In the tracer diffusion process, the isotope gradient drives the diffusion of the atoms. In tracer diffusion experiments, certain radioactive isotopes of an atom with similar chemical properties are monitored in the diffusing system.

Experimentally, a thin film of the tracer element is deposited on a base metal, and diffusion is carried out at a designed temperature and time. After diffusion, the samples are sectioned at specific lengths (r) from the initial deposition of the tracer film. The concentration of each section as a function of distance is established by using the intensity of the radioactive radiation of the section. The solution to Fick's second law for thin films with a small diffusion penetration is given as:

$$c(r,t) = \frac{C_0}{\sqrt{\pi D^* t}} \exp\left(-\frac{r^2}{4D^* t}\right) \qquad 2.38$$

Equation 2.38 can be re-written after taking the logarithm of both sides, which transforms Equation 2.38 to Equation 2.39:

$$\ln\left(c(r,t)\right) = \ln\left(\frac{C_0}{\sqrt{\pi D^* t}}\right) - \frac{r^2}{4D^* t} \qquad 2.39$$

The tracer diffusion coefficient (D^*) is the inverse of the slope of the plot of the natural logarithm of concentration against the negative of one-fourth the square of penetration divided by diffusion time, i.e., $\ln\left(c(r,t)\right)$ vs $-\frac{r^2}{4t}$. Therefore, the tracer diffusion coefficient can be determined by calculating the slope of the plot.

Two types of tracer diffusion coefficients can be obtained through tracer experiments depending on the chemical composition of the host and the isotopic tracer element. These include:

(A) Self-diffusion coefficient: This is the diffusion of species such as radioactive tracer atoms in their nonradioactive pure metal with the same chemical properties.

(B) Impurity tracer diffusion coefficient: This is the diffusion of an extremely small concentration of a tracer element in a different pure metal. At a given diffusion time, the concentration data measured by the intensity of the radioactive radiation at different points are used to calculate the impurity tracer diffusion coefficient.

2.6.2 Intrinsic diffusion coefficient

In a binary alloy system, the intrinsic diffusion coefficient is the diffusion coefficient of a component relative to the local lattice reference frame. The lattice frame of reference, also called the local C- frame or the initial origin can be traced by using a small inert marker particle. The shift in the C-frame is known as the Kirkendall effect. When an element diffuses faster than another element, vacancies are created in the region initially rich in the more rapidly diffusing element, which results in loss of mass and contraction of that region. Similarly, vacancies are destroyed in the region initially rich in the element with less mobility, thus resulting in mass gain and expansion of the region. Hence, the expansion and contraction result in mass flow which causes the movement of the marker particles.

The tracer diffusivity (D_2^*) of an element in a chemically homogeneous solution of composition C_2, is mathematically related to its intrinsic diffusivity (D_2) in a chemically inhomogeneous solution at the same concentration. The relationship is given below:

$$D_2 = D_2^*\left(1 + N_2 \frac{\partial \ln \gamma^*_2}{\partial \ln C_2}\right) = D_2^*\theta \qquad 2.40$$

$$C = cV = \frac{c}{\rho} \qquad 2.41$$

The difference between the intrinsic and tracer diffusion coefficients is due to the mass diffusion under a concentration gradient in the intrinsic condition. This implies that the random jumps of atoms are biased, and atoms move in the direction of the concentration gradient. In a binary system, the Gibbs-Duhem relation is:

$$C_2 \frac{\partial \ln \gamma^*_2}{\partial \ln C_2} = C_1 \frac{\partial \ln \gamma^*_1}{\partial \ln C_1} \qquad 2.42$$

Therefore, the ratio of the intrinsic diffusion coefficients of the component elements in a binary system is equal to the ratio of their tracer diffusion coefficients.

$$\frac{D_2}{D_1} = \frac{D_2^*}{D_1^*} \qquad 2.43$$

The ratio of intrinsic diffusivity can be estimated only at the Kirkendall marker plane by using the relation put forward by van Loo [60] for planar diffusion. This relation is expressed in Equation 2.44 and graphically [61], represented by Figure 2.8.

$$\frac{D_2}{D_1} = \frac{V_2}{V_1}\left[\frac{C_2^+ \int_{-\infty}^{r} \frac{y}{V} dr - C_2^- \int_{r}^{+\infty} \frac{1-y}{V} dr}{-C_1^+ \int_{-\infty}^{r} \frac{y}{V} dr + C_1^- \int_{r}^{+\infty} \frac{1-y}{V} dr}\right] \qquad 2.44$$

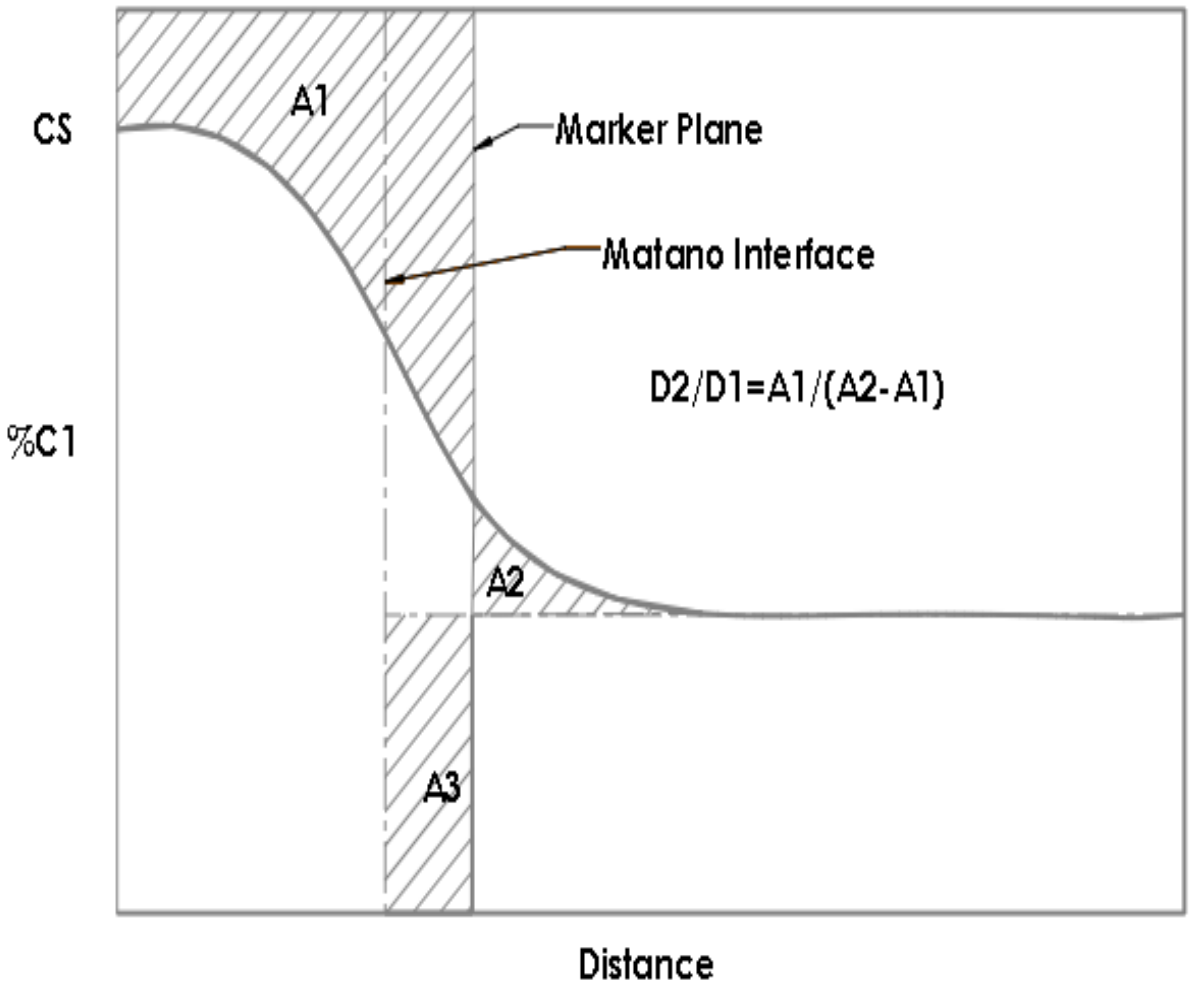

Figure 2.8 Schematic diagram for the evaluation of the ratio of intrinsic diffusion coefficients in binary systems based on the concept in the literature [61]

$$y = \frac{C - C_L}{C_R - C_L} \qquad 2.45$$

with C_R and C_L which represent the right and left boundaries of the solute composition

2.6.1 Interdiffusion coefficient

In binary systems that are undergoing diffusion in a chemically inhomogeneous system, the chemical potential is the driving force for the diffusion. The chemical potential is the concentration gradient in the absence of other external fields. Therefore, as the chemical composition changes in each concentration gradient within the diffusion zone, the diffusing elements are surrounded by different driving forces. These different driving forces of the diffusing elements at different concentrations cause the diffusion coefficients to depend on the concentration. This concentration-dependent diffusivity is called interdiffusion or a chemical diffusion coefficient [4], [5]. The interdiffusion coefficient at a given concentration is a single diffusivity that represents both components at that concentration. It is measured in the volume frame (V-frame) of reference. At the V-frame of reference, the volume flux through the plane is zero. In the interdiffusion system, the volume reference plane is the Matano plane. The interdiffusivity is, therefore, a single diffusivity in the V-frame. At the same time, in the local frame of reference, where the material flows locally at a velocity relative to the V-frame, there are two intrinsic diffusivities. The relationship between the single interdiffusion coefficient ($\tilde{D}$) and the two intrinsic diffusivities (D_1, D_2) are as follows [62]:

$$\tilde{D} = \left(D_2 C_1 + D_2 C_1\right) = \left(D_2^* C_1 + D_1^* C_2\right)\left(1 + C_2 \frac{\partial \ln \gamma^*_2}{\partial \ln C_2}\right) \qquad 2.46$$

In most cases, $\left(1+C_2\frac{\partial \ln \gamma^*_2}{\partial \ln C_2}\right)\to 1$ and the tracer diffusion coefficients become equal to the intrinsic diffusion coefficient, and from Equation 2.46, $\tilde{D}=D_2$ as $C_2\to 0$ and $\tilde{D}=D_1$ as $C_1\to 0$.

2.6.2 Average interdiffusion coefficient

The average D(C) is a single coefficient that represents the entire concentration spectrum and enhances comparisons with other diffusion coefficients at different temperatures and conditions [63], [64]. An average effective diffusivity (D_{ave}) over a given composition can be calculated by integrating the interdiffusion flux over the distance in the diffusion zone. This is equivalent to the mean value theorem for interdiffusivity against the composition.

$$D_{ave}=\frac{\int_{x_L}^{x_R} J dx}{C_L-C_R}=\frac{\int_{C_L}^{C_R} D(C)dc}{C_R-C_L} \qquad 2.47$$

2.7 Models Used in the Literature to Extract D(C) from Experimental Samples

This section will briefly discuss the models used in the literature to determine the D(C) from the experimental profiles and their limitations.

2.7.1 Methods used to determine concentration-dependent interdiffusion

The traditional techniques used to determine the diffusion coefficient in 1D systems are the Boltzmann-Matano (BM), Sauer-Freise (SF), Wagner, and Hall methods. The general limitations

of these methods are: (1) the initial condition must be a step-function assumption, which prevents in-between time and multistage analyses, and (2) the Boltzmann parameter is assumed to be constant in analytical methods, which is not the case for (i) homogenization cases, geometry analyses, etc. These methods and their specific deficiencies are briefly discussed below.

2.7.1.1 Boltzmann-Matano method

The Boltzmann-Matano (BM) method is the most widely used method to calculate D(C) from experimental profiles. The technique is usually applied in infinite systems. The BM equation is:

$$D\left[C^*\right] = -\frac{1}{2t}\frac{dr}{dC}\int_{C_L}^{C^*}\left(r - r_m\right)dC \qquad 2.48$$

The setbacks of using the BM method are D(C) with inaccuracies due to possible errors introduced when determining the position of the Matano plane, and uncertainties of the D(C) at regions close to the boundaries. The method is only applicable when the molar volume change is ideal during diffusion [65].

2.7.1.2 Sauer-Freise method

The Sauer-Freise (SF) method addresses a disadvantage of the **BM** method by eliminating the need to determine the Matano plane. The SF equation is given as:

$$D\left[C^*\right] = -\frac{1}{2t}\frac{dr}{dC}\left[\left(1 - y^*\right)\int_{-\infty}^{r^*} y\,dr + y^*\int_{r^*}^{+\infty}\left(1 - y\right)dr\right] \qquad 2.49$$

y^* is the value of y at C^*

Although this method eliminates possible errors from the need to determine the Matano interface, however, like the **BM** method, the method is limited to only infinite 1D planar systems. This can also result in uncertain diffusion coefficients at regions close to the boundaries [66].

2.7.1.3 Wagner method

The Wagner method calculates the D(C) in systems when molar volume change is not ideal [67]. This method also eliminates the need to determine the position of the Matano interface.

$$D\left[C^*\right] = -\frac{V\left(C^*\right)}{2t}\frac{dr}{dC}\bigg|_{C^*}\left[\left(1-y^*\right)\int_{-\infty}^{r^*}\frac{y}{V\left(C\right)}dr + y^*\int_{r^*}^{+\infty}\frac{\left(1-y\right)}{V\left(C\right)}dr\right] \qquad 2.50$$

However, this method also has limitations which are primarily (1) its use results in uncertain D(C) at regions close to the boundaries, (2) inaccuracy in finite systems, and (3) it is limited to 1D planar systems.

2.7.1.4 Hall method

The Hall method is commonly used to calculate impurity diffusion coefficients and D(C) in regions close to the boundaries [66], [68].

The equation for the left boundary of the concentration is:

$$D\left[C^*\right] = \frac{1}{4H_1} + \frac{K_1\sqrt{\pi}}{2H_1^2}\exp\left(U^2\right)y^* \qquad 2.51$$

The equation for the right boundary of the concentration is:

$$D\left[C^*\right] = \frac{1}{4H_2} + \frac{K_2\sqrt{\pi}}{2H_2^2}\exp\left(U^2\right)\left(1 - y^*\right) \qquad 2.52$$

Although this method is effective for regions where the BM, SF, and Wagner methods produce uncertain diffusion coefficients, it becomes less effective in areas with strong D(C) and large concentration gradients. The application of this method is also limited to 1D planar systems [30].

2.7.1.5 Forward simulation method

The **FSM** has been recently developed to address the various limitations of conventional methods. The FSM is a robust method that is used to extract both impurity and D(C) from an experimental concentration profile. The method can be used when the interdiffusion coefficient is highly or weakly dependent on the solute concentration and in both infinite and finite systems [21]–[30]. The FSM can also be used in 1D planar, 2D cylindrical, 3D spherical coordinate systems and to accurately evaluate the D(C) in systems with a significant initial solute distribution [30]. The FSM is an iterative method that accurately calculates the D(C) by utilizing the inverse proportionality between the concentration gradients and diffusion coefficients. To perform the FSM, numerical models that can solve Fick's second law in single or multi-phase systems are required. The subsequent section will review the numerical models available.

2.8 Numerical Models Used to Simulate Fick's Second Law

Generally, diffusion-controlled transformations can be in a multi-phase system with limited solubility or a single-phase system with unlimited solute solubility. Models used to solve moving boundary systems can be applied to single-phase transformations. Analytical solutions for

diffusion-controlled moving boundary problems in planar, cylindrical, and spherical coordinates have been derived for cases with constant diffusion coefficients [69]. The analytical solutions are, however, limited to only constant diffusivities. Approximate analytical solutions have been reported for variable diffusion coefficients [70], [71], and these solutions are validated with numerical solutions, which are more reliable for problems with variable diffusion coefficients.

Numerical solutions can be grouped into discretization that is fixed or variable in space. Models with spatially fixed grids use them to track the migration of interphase boundaries and interfaces. In the model developed by Nakagawa et al. [72] for fixed discretization, the interface progresses in a fixed grid with a stepwise movement. When the solute concentration of the interface differs from the equilibrium solute concentration at the diffusion temperature, the interface stops moving until the difference is eliminated. This type of interface movement is physically unrealistic and tends to introduce errors into the model. The model developed by Shinmura et al. [73] uses an explicit scheme to calculate the solute distribution while an implicit scheme is used to determine the future interface position. The calculation of the concentration near the interface is determined by using quadratic relations. In a recent model by Li et al., the position of the moving interface is obtained with the use of an implicit time integration approach [74]; however, such implicit schemes require non-trivial assumptions for variable diffusion coefficients, and the solutions might not converge.

In models with variable discretization, the size of the fixed number of grids changes as the interface advances [70]. A discretization that is variable in space can be solved directly with an explicit scheme, which uses a variable space grid to track regions with the same solute concentration [75]. Other models use Landau transformations that transform the variable grids into new fixed grids that automatically adjust to accommodate the movement of the interface [76]. This transformation

removes the errors that arise from the assumptions and approximations in the fixed grid system and ensures that the position of the interface is always on a discretization point. Heckel et al. [77] adopted the Murray-Landis variable-grid space transformation to solve diffusion-controlled moving boundary problems. Illingworth and Golosnoy [78] observed that previous models based on a Landau transformation do not conserve solute. Non-conservation of solute is an inherent problem in numerical schemes, and it is attributed to the fact that the numerical approximation used to calculate the fluxes near the interface with Fick's second law is different from the approximations used to solve Stefan's interface equation [3], [78]. Non-conservation of solutes affects the accuracy of the numerical solutions, mostly where there is a significant concentration gradient in the system. To ensure solute conservation, Illingworth et al. [3], [78] obtained the future position of the interface by equating the total amount of solute in the diffusion system in two consecutive time steps. While it is well established that diffusion coefficients depend on the concentration [70], the discretization that is variable in space in Illingworth et al. [5] mainly solves diffusion problems with constant diffusivity. Variations in the dependence of the diffusion coefficient on the concentration will produce variations in diffusion-controlled phase transformations. Applying the model in Illingworth et al. [5] to solve problems with variable diffusion coefficients uses an implicit scheme, which is very demanding in terms of computational time caused by the iterations required. Also, it involves non-trivial assumptions, which could result in the non-convergence of iterations. Hence, a new and stable explicit numerical model which conserves solutes is a major challenge for the reliable simulation of phase transformations.

CHAPTER THREE

3 METHODOLOGY

3.1 Introduction

This chapter is divided into two sections, and in each section, a theoretical model to achieve a primary goal is derived and solved. One of the primary goals of this study is to study how DIS affects D(C) theoretically; hence, the equations needed to carry out this goal are derived in the first section of this chapter. Subsequently, a numerical model is developed for extracting D(C) from experimental data. The second numerical model is required to perform the second primary goal of this work: to experimentally verify the key findings from the theoretical analysis.

3.2 Diffusion Induced Stress Equations

The equations for diffusion under the influence of the DIS are derived in this section for a binary diffusion system. The key derived equations are provided in this section, while the detailed derivations can be found in the Appendix. In this work, the theoretical solute distribution equation under DIS is derived and solved from the first principles. Similarly, the stress/pressure distribution equation is derived while incorporating Stephenson's stress generation and relaxation concept [6], [79]. The D(C) in the DIS system will also be developed in this section. In subsequent chapters, these equations will be used to study the six factors proposed to affect the D(C). Chapter 2 shows that the stress potential can influence the effective intrinsic diffusion coefficient. However, this chapter shall relate the influence of stress potential on the D(C) under DIS. Diffusion occurs across

the potential gradients, and the total potential can be expressed in composition and pressure gradients.

The intrinsic flux of each component under DIS is given as:

$$J_i = -\left(D_i^* \theta \nabla \rho_i + \frac{D_i^* \rho_i}{KT} \nabla (V_i P) \right) \tag{3.1}$$

$$\sum_{i=1}^{2} \rho_i V_i = 1 \tag{3.2}$$

$$C = \frac{\rho_1}{\rho}. \tag{3.3}$$

The equation of the thermodynamic factor (θ) which gives unity at the pure boundaries obtained from Stephenson [79] is:

$$\theta = 1 - \frac{2\alpha}{RT} C(1 - C) \tag{3.4}$$

Taking Equation 3.3 into consideration, Equation 3.1 can be re-written as:

$$J_i = -\rho \left(D_i^* \theta \nabla C_i + \frac{D_i^* C_i V_i}{KT} \nabla P \right) \tag{3.5}$$

3.2.1 Equation for pressure distribution under DIS

The derived pressure equation is given as:

$$\frac{\partial P}{\partial t} = \frac{-2E}{9(1-\upsilon)}\left[-\frac{\partial}{\partial r}\left(\left(D_1^* V_1 - D_2^* V_2\right)\theta\nabla C + \left(\frac{D_1^* C V_1 V_1}{KT} + \frac{D_2^*(1-C)V_2 V_2}{KT}\right)\frac{\partial P}{\partial r}\right) + \frac{3}{4\eta}P\right] \quad 3.6$$

$P = P(t=0)\exp\left(\frac{-Et}{6(1-\upsilon)\eta}\right)$ is the solution of Equation 3.6 if the divergences of the atomic fluxes are negligible, and this solution shows time relaxation of pressure.

When the solute distribution changes, the relative magnitude of the relaxation term and divergences of the atomic fluxes determine if the stress is relaxed or generated. For stress relaxation $\sum_{i=1}^{2} V_i \nabla J_i > \frac{3}{4\eta}P$ whereas, for stress relaxation $\sum_{i=1}^{2} V_i \nabla J_i < \frac{3}{4\eta}P$.

3.2.2 Equation for solute distribution under DIS

The derived solute distribution equation is given as:

$$\frac{\rho\partial C}{\partial t} = \frac{\partial}{\partial r}\left(\left((1-C)D_1^*\theta + CD_2^*\theta\right)\frac{\partial C}{\partial r} + \frac{C(1-C)\left(D_1^* V_1 - D_2^* V_2\right)}{KT}\frac{\rho\partial P}{\partial r}\right) \quad 3.7$$

Equation 3.7 can also be re-written as:

$$\frac{\rho\partial C}{\partial t} = \frac{\partial}{\partial r}\left(\left[\left((1-C)D_1^*\theta + CD_2^*\theta\right) + \frac{C(1-C)\left(D_1^* V_1 - D_2^* V_2\right)}{KT}\frac{\partial P}{\partial C}\right]\frac{\rho\partial C}{\partial r}\right) \quad 3.8$$

The form of Equation 3.7 avoids the indeterminate problem when $P \to 0$ and $C \to 0$.

3.2.3 Concentration-dependent interdiffusion coefficient under DIS

The equation of D(C) under DIS is:

$$\bar{D}(C) = \left((1-C)D_1^*\theta + CD_2^*\theta\right) + \frac{C(1-C)\left(D_1^*V_1 - D_2^*V_2\right)}{KT}\frac{\partial P}{\partial C} \qquad 3.9$$

The D(C) under DIS can also be re-written in terms of mobility $\left(M_i = \frac{D_i^*}{KT}\right)$ as:

$$\bar{D}(C) = \left((1-C)D_1^*\theta + CD_2^*\theta\right) + C(1-C)\left(M_1V_1 - M_2V_2\right)\frac{\partial P}{\partial C} \qquad 3.10$$

Importantly, although the stress gradients are taken to be zero at the extreme boundaries of the sample, Equation 3.9 is expected to yield a stress-free diffusion coefficient. However, close to the point of solute penetration, the impurity diffusion coefficient of very low solute concentrations can be influenced by pressure.

3.2.4 Theoretical verification of the equation for D(C) under DIS

To verify the D(C) under the influence of the DIS (Equation 3.9), it is important for the derivation approach to produce two extreme diffusion limits: the Darken limit and Nernst-Planck limit.

3.2.4.1 Darken Limit

The Darken limit assumes a stress-free system $\left(\frac{\partial P}{\partial C} = 0\right)$. The D(C) under DIS (Equation 3.9) reverts to the Darken interdiffusion coefficient presented in Equation 3.11 when the stress gradient

is zero.

$$\bar{D}_{eff} = \left((1-C)D_1^* + CD_2^*\right)\theta \tag{3.11}$$

3.2.4.2 Nernst-Planck Limit

In the Nernst-Planck limit, the Kirkendall velocity is zero. Therefore, the sum of interdiffusion fluxes with a zero Kirkendall velocity yields:

$$\bar{J}_1 + \bar{J}_2 = \frac{J_1 + J_2}{\rho} = -\left(\left(D_1^* - D_2^*\right)\theta\nabla C_1 + \frac{\left(D_1^* C_1 V_1 + D_2^* C_2 V_2\right)}{KT}\nabla P\right) = 0 \tag{3.12}$$

The pressure gradient with respect to the concentration calculated from Equation 3.12:

$$\frac{\nabla P}{\nabla C_1} = -\frac{\left(D_1^* - D_2^*\right)\theta KT}{\left(D_1^* C_1 V_1 + D_2^* C_2 V_2\right)} \tag{3.13}$$

Substituting Equation 3.13 into the D(C) under DIS (Equation 3.9) yields:

$$\bar{D}(C) = \left(C_2 D_1^*\theta + C_1 D_2^*\theta\right) + \frac{C_1 C_2\left(D_1^* V_1 - D_2^* V_2\right)}{KT}\left(-\frac{\left(D_1^* - D_2^*\right)\theta KT}{\left(D_1^* C_1 V_1 + D_2^* C_2 V_2\right)}\right) \tag{3.14}$$

Equation 3.14 can be simplified to the Nernst-Planck equation with different molar volumes:

$$\bar{D}(C) = \frac{\left(C_2 V_2 + C_1 V_1\right) D_1^* D_2^*\theta}{\left(D_1^* C_1 V_1 + D_2^* C_2 V_2\right)} \tag{3.15}$$

When the molar volumes are the same, Equation 3.15 becomes Equation 3.16, which is the commonly reported Nernst-Planck equation for constant molar volume systems.

$$\bar{D}(C) = \frac{D_1^* D_2^* \theta}{D_1^* N_1 + D_2^* N_2} \qquad 3.16$$

Therefore, the $\bar{D}(C)$ under DIS, presented in Equation 3.9, is applicable to all systems between and at the Darken and Nernst-Planck limits.

3.2.5 Dimensionless governing equations

For the theoretical analysis in this section, Equations 3.6-3.9 are transformed into dimensionless variables and parameters.

$$x' = x/L \qquad t' = tD/L^2 \qquad P' = P/E \qquad D_i^{*'} = D_i^*/D_m$$

$$\eta' = \eta D_m / EL^2 \qquad \rho' = \rho \times V_m \qquad V_i' = V_i/V_m \qquad T' = \frac{T}{\left(\frac{EV_m}{K}\right)}$$

$$\alpha' = \frac{2\alpha}{KT} = \frac{2\alpha}{T'EV_m} \qquad D(C) = \bar{D}(C)/D_m \qquad D_m = \max(D_i) \qquad V_m = V_{\max}$$

3.17

The dimensionless form of the two representations of solute distribution Equation 3.7-3.8 are:

$$\frac{\rho' \partial C}{\partial t'} = \frac{\partial}{\partial r'}\left(\left[\left(D_2^{*'} C + D_1^{*'}(1-C)\right)\theta \frac{\rho' \partial C}{\partial r'} + \frac{(1-C)C}{T'}\left(D_1^{*'} V_1' - D_2^{*'} V_2'\right)\frac{\partial P'}{\partial r'}\right]\right) \qquad 3.18$$

$$\frac{\rho' \partial C}{\partial t'} = \frac{\partial}{\partial r'}\left(\left[\left(D_2^{*'} C + D_1^{*'}(1-C)\right)\theta + \frac{(1-C)C}{T'}\left(D_1^{*'} V_1' - D_2^{*'} V_2'\right)\frac{\partial P'}{\partial C}\right]\frac{\rho' \partial C}{\partial r'}\right) \qquad 3.19$$

and the dimensionless form of the pressure distribution Equation 3.6 is:

$$\frac{dP'}{dt'} = \frac{-2}{9(1-\upsilon)}\left[\frac{\partial}{\partial r'}\left(\left(D_2^{*'}V_2' - D_1^{*'}V_1'\right)\theta\rho'\nabla C - \frac{1}{T'}\left(D_1^{*'}CV_1'V_1' + D_2^{*'}(1-C)V_2'V_2'\right)\rho'\frac{\partial P'}{\partial r'}\right) + \frac{3}{4\eta'}P'\right]$$

3.20

Similarly, the dimensionless form of the D(C) under DIS Equation 3.9 is:

$$D(C) = \left(D_2^{*'}C + D_1^{*'}(1-C)\right)\theta + \frac{(1-C)C}{T'}\left(D_1^{*'}V_1' - D_2^{*'}V_2'\right)\frac{\partial P'}{\partial C} \qquad 3.21$$

Basically, it is expected from Equation 3.21 that as the concentration and pressure gradients change, the D(C) under DIS also changes. The DIS will not influence the solute distribution when the product of stress-free intrinsic diffusivity and the molar volumes are equal (i.e., DIS will not influence the solute distribution).

3.2.6 Numerical discretization of DIS equations

This work uses a direct and explicit approach to solve a coupled set of partial differential Equations 3.18 and 3.20.

At the left boundary (i=1 node) with zero solute concentration gradient and no pressure gradients, the discretized boundary conditions for the concentration and pressure equations are:

$$\frac{C_1^{k+1} - C_1^k}{t'^{k+1} - t'^k} = \frac{2\left(D_2^{*'}\theta C_{1+1/2} + D_1^{*'}\theta(1-C_{1+1/2})\right)}{\Delta r'}\left(\frac{C_{1+1}^k - C_1^k}{\Delta r'}\right) + \frac{2\left(\frac{(1-C_{1+1/2})C_{1+1/2}}{T'}\left(D_1^{*'}V_1' - D_2^{*'}V_2'\right)\right)}{\Delta r'}\left(\frac{P_{1+1}'^k - P_1'^k}{\Delta r'}\right)$$

3.22

$$\frac{P_1'^{k+1}-P_1'^{k}}{t'^{k+1}-t'^{k}}=\frac{-2}{9(1-\upsilon)}\left(\frac{\left(V_2'D_2^{*'}\theta-V_1'D_1^{*'}\theta\right)}{\Delta r'}\left(\frac{C_{1+1}^{k}-C_1^{k}}{\Delta r'}\right)+\frac{\left(-\frac{\left(D_1^{*'}V_1'V_1'C_{1+1/2}+D_2^{*'}V_2'V_2'\left(1-C_{1+1/2}\right)\right)}{T'}\right)}{\Delta r'}\left(\frac{P_{1+1}'^{k}-P_1'^{k}}{\Delta r'}\right)+\frac{3}{4\eta'}P_1'^{k}\right)$$

3.23

In the inner nodes, the discretized boundary equations for the concentration and pressure equations are:

$$\frac{C_i^{k+1}-C_i^{k}}{t'^{k+1}-t'^{k}}=\frac{\left(D_2^{*'}\theta C_{i+1/2}+D_1^{*'}\theta\left(1-C_{i+1/2}\right)\right)}{\Delta r'}\left(\frac{C_{i+1}^{k}-C_i^{k}}{\Delta r'}\right)-\frac{\left(D_2^{*'}\theta C_{i-1/2}+D_1^{*'}\theta\left(1-C_{i-1/2}\right)\right)}{\Delta r'}\left(\frac{C_i^{k}-C_{i-1}^{k}}{\Delta r'}\right)+$$
$$\frac{\left(\frac{\left(1-C_{i+1/2}\right)C_{i+1/2}}{T'}\left(D_1^{*'}V_1'-D_2^{*'}V_2'\right)\right)}{\Delta r'}\left(\frac{P_{i+1}'^{k}-P_i'^{k}}{\Delta r'}\right)-\frac{\left(\frac{\left(1-C_{i-1/2}\right)C_{i-1/2}}{T'}\left(D_1^{*'}V_1'-D_2^{*'}V_2'\right)\right)}{\Delta r'}\left(\frac{P_i'^{k}-P_{i-1}'^{k}}{\Delta r'}\right)$$

3.24

$$\frac{P_i'^{k+1}-P_i'^{k}}{t'^{k+1}-t'^{k}}=\frac{-2}{9(1-\upsilon)}\left(\frac{\left(V_2'D_2^{*'}\theta-V_1'D_1^{*'}\theta\right)}{\Delta r'}\left(\frac{C_{i+1}^{k}-C_i^{k}}{\Delta r'}\right)-\frac{\left(V_2'D_2^{*'}\theta-V_1'D_1^{*'}\theta\right)}{\Delta r'}\left(\frac{C_i^{k}-C_{i-1}^{k}}{\Delta r'}\right)+\right.$$
$$\left.\frac{\left(-\frac{\left(D_1^{*'}V_1'V_1'C_{i+1/2}+D_2^{*'}V_2'V_2'\left(1-C_{i+1/2}\right)\right)}{T'}\right)}{\Delta r'}\left(\frac{P_{i+1}'^{k}-P_i'^{k}}{\Delta r'}\right)-\frac{\left(-\frac{\left(D_1^{*'}V_1'V_1'C_{i-1/2}+D_2^{*'}V_2'V_2'\left(1-C_{i-1/2}\right)\right)}{T'}\right)}{\Delta r'}\left(\frac{P_i'^{k}-P_{i-1}'^{k}}{\Delta r'}\right)+\frac{3}{4\eta'}P_i'^{k}\right)$$

3.25

At the right boundary (i=m+1 node) with zero solute concentration and no pressure gradients, the discretized boundary conditions for the concentration and pressure equations are:

$$\frac{C_{m+1}^{k+1}-C_{m+1}^{k}}{t'^{k+1}-t'^{k}}=-\frac{2\left(D_2^{*'}\theta C_{m+1-1/2}+D_1^{*'}\theta\left(1-C_{m+1-1/2}\right)\right)}{\Delta r'}\left(\frac{C_{m+1}^{k}-C_{m+1-1}^{k}}{\Delta r'}\right)-\frac{2\left(\frac{\left(1-C_{m+1-1/2}\right)C_{m+1-1/2}}{T'}\left(D_1^{*'}V_1'-D_2^{*'}V_2'\right)\right)}{\Delta r'}\left(\frac{P_{m+1}'^{k}-P_{m+1-1}'^{k}}{\Delta r'}\right) \tag{3.26}$$

$$\frac{P_{m+1}'^{k+1}-P_{m+1}'^{k}}{t'^{k+1}-t'^{k}}=\frac{-2}{9\left(1-\upsilon\right)}\left(\begin{array}{l}-\frac{\left(V_2'D_2^{*'}\theta-V_1'D_1^{*'}\theta\right)}{\Delta r'}\left(\frac{C_{m+1}^{k}-C_{m+1-1}^{k}}{\Delta r'}\right)-\frac{\left(-\frac{\left(D_1^{*'}V_1'V_1'C_{m+1-1/2}+D_2^{*'}V_2'V_2'\left(1-C_{m+1-1/2}\right)\right)}{T'}\right)}{\Delta r'}\left(\frac{P_{m+1}'^{k}-P_{m+1-1}'^{k}}{\Delta r'}\right)\\+\frac{3}{4\eta'}P_{m+1}'^{k}\end{array}\right) \tag{3.27}$$

3.2.7 Diffusion induced stress equations in the generalized coordinate system

The pressure equation in Stephenson [6] for coupled differential equations for diffusion in an isotropic binary system, which considers the generation and relaxation of DIS, will be extended from planar systems to cylindrical and spherical geometries to address the second objective. The general pressure equation in Stephenson [8] is:

$$\frac{\partial P}{\partial t}=-\frac{2}{9}\frac{E}{\left(1-\upsilon\right)}\left(\sum_{i=1}^{2}\left(V_i\frac{\partial}{\partial t}\rho_i\right)+\frac{3P}{4\eta}\right), \tag{3.28}$$

The pressure Equation 3.28 can be developed into Equation 3.29.

$$\frac{\partial P}{\partial t}=\frac{-2E}{9\left(1-\upsilon\right)}\left[-\frac{\partial}{r^n\partial r}\left(r^n\left(D_1^{*}-D_2^{*}\right)\theta\nabla C+r^n\left(\frac{D_1^{*}CV_1}{KT}+\frac{D_2^{*}\left(1-C\right)V_2}{KT}\right)\frac{\partial P}{\partial r}\right)+\frac{3}{4\eta}P\right] \tag{3.29}$$

Similarly, from the continuity equation, the solute distribution equation is:

$$\frac{\rho\partial C}{\partial t}=\frac{\partial}{r^n\partial r}\left(\left[\left(D_2^*\theta C+D_1^*\theta\left(1-C\right)\right)\frac{\rho\partial C}{\partial r}+\left(\frac{-D_2^*C\left(1-C\right)V_2+D_1^*\left(1-C\right)CV_1}{KT}\right)\rho\frac{\partial P}{\partial r}\right]r^n\right) \qquad 3.30$$

Equation 3.30 can be re-written as Equation 3.31.

$$\frac{\rho\partial C}{\partial t}=\frac{\partial}{r^n\partial r}\left(\left[D_2^*\theta C+D_1^*\theta\left(1-C\right)+\left(\frac{-D_2^*C\left(1-C\right)V_2+D_1^*\left(1-C\right)CV_1}{KT}\right)\frac{\partial P}{\partial C}\right]r^n\frac{\rho\partial C}{\partial r}\right) \qquad 3.31$$

The Fick's second law in the generalized coordinate system is:

$$\frac{\rho\partial C}{\partial t}=\frac{\partial}{r^n\partial r}\left(D\left(C\right)r^n\frac{\rho\partial C}{\partial r}\right) \qquad 3.32$$

Comparing Equations 3.31 and 3.32, the D(C) under DIS can be determined. The D(C) in the generalized coordinate system is given as:

$$D\left(C\right)=\left(D_2^*C+D_1^*\left(1-C\right)\right)\theta+\left(\frac{-D_2^*C\left(1-C\right)V_2+D_1^*\left(1-C\right)CV_1}{KT}\right)\frac{\partial P}{\partial C} \qquad 3.33$$

For the numerical simulation of the diffusion in a sample of length R, Equations 3.31 to 3.33 for the pressure distribution, solute distribution, and D(C) respectively are transformed using the variables in Equation 3.17 to forms that contain only dimensionless variables. The dimensionless equations for pressure, solute distributions, and effective diffusion coefficient are respectively:

$$\frac{dP'}{dt'}=\frac{-2}{9\left(1-\upsilon\right)}\left[\frac{\partial}{r'^n\partial r'}\left(r'^n\left(D_2^{*'}V_2'-D_1^{*'}V_1'\right)\theta\nabla C-\frac{r'^n}{T'}\left(D_1^{*'}CV_1'V_1'+D_2^{*'}\left(1-C\right)V_2'V_2'\right)\frac{\partial P'}{\partial r'}\right)+\frac{3}{4\eta'}P'\right]$$

3.34

$$\frac{\rho'\partial C}{\partial t'} = \frac{\partial}{r'^{n}\partial r'}\left(\left[D_2^{*'}\theta C + D_1'^{*}\theta(1-C) + \left(\frac{-D_2^{*'}C(1-C)V_2' + D_1^{*'}(1-C)CV_1'}{T'}\right)\frac{\partial P'}{\partial C}\right] r'^{n}\frac{\rho'\partial C}{\partial r'}\right) \quad 3.35$$

$$D'_{eff} = D_2'^{*'}\theta C + D_1'\theta(1-C) + \left(\frac{-D_2^{*'}C(1-C)V_2' + D_1^{*'}(1-C)CV_1'}{T'}\right)\frac{\partial P'}{\partial C} \quad 3.36$$

The discretization of Equations 3.34 to 3.36 is similar to the discretization in the 1D planar system (Equations 3.22-3.27).

3.3 Development of a New Numerical Model for Extracting Interdiffusion Coefficient from Experimental Data

FSM is a method that is advantageous over conventional methods of extracting D(C) from experimental data [21]–[30]. To use the FSM, a robust numerical model is needed. This section proposes a new numerical model to extract D(C) from experimental data. The key developed equations are provided in this section, while the detailed derivations can be found in the Appendix. In this work, the model is initially developed for two-phase systems and then applied to a single-phase system and extended to multiphase systems. This section will elaborate on the development process for two-phase systems. This approach is important because two-phase systems involve both the solute distribution and interphase equations. Then the section that follows will focus on the use of the model in single-phase systems. The next section will extend the model to multiphase systems with more than two phases, and the last section will discuss the FSM procedure and the validation of the new model. The problems of existing models, the approach used in this work to address the problems, and the targeted key features of the new model are presented in Table 3.1.

Table 3.1: Advantages of the new model over other models

Existing Models	Problem with the model	Solution	Requirement Addressed (Key features of the new model)
Planar models	Capable of tracking 1D interface migration	The generalized coordinate equations	Capable of Tracking 2D interface migration
Implicit/Explicit models with Variable grids	Non conservation of solute	Landau transformation into fixed grids	Solute Conservation
Implicit models	Non-trival assumption and non-convergence	Fully Explicit model	Accuracy for constant and variable D
Explicit models	Computational Instability	Dufort-Frankel scheme	Speed
Dufort-Frankel	Used for only fixed boundary problems	Combined Leapfrog and Dufort-Frankel schemes	Enhanced stability

Following Illingworth and Golosnoy [78], the set of equations that govern a diffusion-controlled two-phase system can be written as:

$$r^{\lambda\lambda-1}\frac{\partial C(r,t)}{\partial t}=\frac{\partial}{\partial r}\left(r^{\lambda\lambda-1}D_A\left[C(r,t)\right]\frac{\partial C(r,t)}{\partial r}\right) \qquad 0\le r\le s(t) \quad 3.37$$

$$r^{\lambda\lambda-1}\frac{\partial C(r,t)}{\partial t}=\frac{\partial}{\partial r}\left(r^{\lambda\lambda-1}D_B\left[C(r,t)\right]\frac{\partial C(r,t)}{\partial r}\right) \qquad s(t)\le r\le R \quad 3.38$$

$$D_A\left[C(r,t)\right]\frac{\partial C(r,t)}{\partial r}\bigg|_{r=s(t)^-}-D_B\left[C(r,t)\right]\frac{\partial C(r,t)}{\partial r}\bigg|_{r=s(t)^+}=\left[C_B-C_A\right]\frac{ds}{dt}, \qquad r=s(t) \quad 3.39$$

The solute distribution and diffusion in the first and second phases, A and B, respectively, are described by using Equations 3.51 and 3.52. Equation 3.53 mathematically describes the equation for the interface migration. The value of λλ defines the geometry of the system, such that λλ=1 applies to the 1D planar geometry, λλ=2 to the cylindrical geometry, and λλ=3 to the spherical geometry. Zero flux conditions are imposed at the boundaries (r=0 and r=R).

The new transformation coordinates,

$$r=su \quad \text{and} \quad r=(R-s)v+s \qquad 3.40$$

The Landau transformations of Equations 3.37 – 3.39 are given as:

$$\left[us\right]^{\lambda\lambda-1}\left(\frac{\partial p}{\partial t}-\frac{ds}{dt}\frac{u}{s}\frac{\partial p}{\partial u}\right)=\frac{\partial}{\partial u}\left(\frac{\left[us\right]^{\lambda\lambda-1}D_A(p)}{s^2}\frac{\partial p}{\partial u}\right), \quad 0\le u\le 1 \qquad 3.41$$

$$\left[\mathrm{v(R-s)+s}\right]^{\lambda\lambda-1}\left(\frac{\partial \mathrm{q}}{\partial \mathrm{t}}-\frac{\mathrm{ds}}{\mathrm{dt}}\frac{\mathrm{u}}{\mathrm{s}}\frac{\partial \mathrm{q}}{\partial \mathrm{u}}\right)=\frac{\partial}{\partial \mathrm{v}}\left(\frac{\left[\mathrm{v(R-s)+s}\right]^{\lambda\lambda-1}\mathrm{D_B(q)}}{\mathrm{(R-s)}^2}\frac{\partial \mathrm{q}}{\partial \mathrm{v}}\right), \quad 0\le \mathrm{v}\le 1 \qquad 3.42$$

$$\frac{D_A(p)}{s}\frac{\partial p}{\partial u}\bigg|_{u=1} - \frac{D_B(q)}{(R-s)}\frac{\partial q}{\partial v}\bigg|_{v=0} = [C_B - C_A]\frac{ds}{dt}, \qquad u=1, v=0 \tag{3.43}$$

To ensure solute conservation, the total amount of solute throughout the diffusion system must be the same for all diffusion times.

$$\frac{\partial}{\partial t}\left(s\int_0^1 p[us]^{\lambda\lambda-1}\,du + (R-s)\int_0^1 q\left[v(R-s)+s\right]^{\lambda\lambda-1}\,dv\right) = 0 \tag{3.44}$$

The interface migration equation is obtained by integrating Equations 3.44 over space and a time step. To ensure an explicit solution, Equations 3.41 and 3.42 are analyzed by using explicit schemes.

3.3.1 LeapFrog/Dufort-Frankel scheme

The Dufort-Frankel (**DF**) scheme is an explicit scheme that has both the stability of Crank Nicholson's scheme and the stable and faster convergence of the Euler explicit scheme. Interestingly, it is unconditionally stable, calculates explicitly, and twice as fast in convergence as Crank-Nicholson's scheme. However, the Δt is important to accurately represent physical phenomena [80]–[82]. The consistency requirement can be generally written as $\frac{\Delta t}{\Delta r} \to 0$ and this requirement is common when using a finite difference method to solve parabolic (diffusion, heat) equations [83], [84]. The **DF** scheme can also be used for constant and variable diffusion coefficient systems [81], and single-phase systems without discontinuous interface boundaries. However, Equations 3.41 and 3.42 have an advective term that represents the movement of the interface boundaries. Although the DF was developed for simple parabolic equations without a moving interface, it can also be applied to a general parabolic equation and advective-diffusive

conditions [85]. The advective component is analyzed by using the mid-level approach point in the leapfrog method, as is the case for the diffusive-advective equations in [86], [87].

Numerically integrating Equations 3.41 using a leapfrog/Dufort-Frankel algorithm gives the finite difference scheme for Phase A.

$$p_i^{k+1}\left[\frac{\left(r_{i+1/2}^{k+1}\right)^{\lambda\lambda}-\left(r_{i-1/2}^{k+1}\right)^{\lambda\lambda}}{\lambda\lambda\left(t^{k+1}-t^{k-1}\right)}-\frac{1}{2}\left(r_{i+1/2}^{k-1}\right)^{\lambda\lambda-1}\left(\dot{s}\,\alpha u_{i+1/2}-\frac{\left(D_A\right)_{i+1/2}^{k}}{s^k\left(u_{i+1}-u_i\right)}\right)+\frac{1}{2}\left(r_{i-1/2}^{k-1}\right)^{\lambda\lambda-1}\left(\dot{s}\,\beta u_{i-1/2}+\frac{\left(D_A\right)_{i-1/2}^{k}}{s^k\left(u_i-u_{i-1}\right)}\right)\right]$$

$$=p_i^{k-1}\left[\frac{\left(r_{i+1/2}^{k-1}\right)^{\lambda\lambda}-\left(r_{i-1/2}^{k-1}\right)^{\lambda\lambda}}{\lambda\lambda\left(t^{k+1}-t^{k-1}\right)}+\frac{1}{2}\left(r_{i+1/2}^{k-1}\right)^{\lambda\lambda-1}\left(\dot{s}\,\alpha u_{i+1/2}-\frac{\left(D_A\right)_{i+1/2}^{k}}{s^k\left(u_{i+1}-u_i\right)}\right)-\frac{1}{2}\left(r_{i-1/2}^{k-1}\right)^{\lambda\lambda-1}\left(\dot{s}\,\beta u_{i-1/2}+\frac{\left(D_A\right)_{i-1/2}^{k}}{s^k\left(u_i-u_{i-1}\right)}\right)\right]$$

$$+p_{i+1}^{k}\left[\left(r_{i+1/2}^{k-1}\right)^{\lambda\lambda-1}\left(\dot{s}\,\beta u_{i+1/2}+\frac{\left(D_A\right)_{i+1/2}^{k}}{s^k\left(u_{i+1}-u_i\right)}\right)\right]+p_{i-1}^{k}\left[-\left(r_{i-1/2}^{k-1}\right)^{\lambda\lambda-1}\left(\dot{s}\,\alpha u_{i-1/2}-\frac{\left(D_A\right)_{i-1/2}^{k}}{s^k\left(u_i-u_{i-1}\right)}\right)\right]$$

3.45

For the left boundary (i=1 node) with zero flux, the discretized boundary conditions for Phase A are:

$$p_1^{k+1}\left[\frac{\left(r_{1+1/2}^{k+1}\right)^{\lambda\lambda}}{\lambda\lambda\left(t^{k+1}-t^{k-1}\right)}-\frac{1}{2}\left(r_{1+1/2}^{k-1}\right)^{\lambda\lambda-1}\left(\dot{s}\,\alpha u_{1+1/2}-\frac{\left(D_A\right)_{1+1/2}^{k}}{s^k\left(u_{1+1}-u_1\right)}\right)\right]$$

$$=p_1^{k-1}\left[\frac{\left(r_{1+1/2}^{k+1}\right)^{\lambda\lambda}}{\lambda\left(t^{k+1}-t^{k-1}\right)}+\frac{1}{2}\left(r_{1+1/2}^{k-1}\right)^{\lambda\lambda-1}\left(\dot{s}\,\alpha u_{1+1/2}-\frac{\left(D_A\right)_{1+1/2}^{k}}{s^k\left(u_{1+1}-u_1\right)}\right)\right]+p_2^{k}\left[\left(r_{1+1/2}^{k-1}\right)^{\lambda\lambda-1}\left(\dot{s}\,\alpha u_{1+1/2}-\frac{\left(D_A\right)_{1+1/2}^{k}}{s^k\left(u_{1+1}-u_1\right)}\right)\right]$$

3.46

The discretized boundary equation for the interface (i=m+1) in Phase A with a constant concentration is

$$p_{m+1}^{k+1} = p_{m+1}^{k} + p_{m+1}^{k-1} = C_{AB} \qquad 3.47$$

R is the sample length, while u and v are dimensionless numbers from 0 to 1.

The above procedure is repeated in Phase B, and the discretized expression for Phase B is:

$$\begin{aligned} q_i^{k+1} & \left[\frac{\left(r_{i+1/2}^{k+1}\right)^{\lambda\lambda} - \left(r_{i-1/2}^{k+1}\right)^{\lambda\lambda}}{\lambda\lambda\left(t^{k+1}-t^{k-1}\right)} - \frac{1}{2}\left(r_{i+1/2}^{k-1}\right)^{\lambda\lambda-1}\left(\dot{s}\alpha\left(1-v_{i+1/2}\right) - \frac{\left(D_B\right)_{i+1/2}^{k}}{\left(R-s^k\right)\left(v_{i+1}-v_i\right)} \right) \right. \\ & \left. + \frac{1}{2}\left(r_{i-1/2}^{k-1}\right)^{\lambda\lambda-1}\left(\dot{s}\beta\left(1-v_{i-1/2}\right) + \frac{\left(D_B\right)_{i-1/2}^{k}}{\left(R-s^k\right)\left(v_i-v_{i-1}\right)} \right) \right] \\ = q_i^{k-1} & \left[\frac{\left(r_{i+1/2}^{k+1}\right)^{\lambda\lambda} - \left(r_{i-1/2}^{k+1}\right)^{\lambda\lambda}}{\lambda\lambda\left(t^{k+1}-t^{k-1}\right)} + \frac{1}{2}\left(r_{i+1/2}^{k-1}\right)^{\lambda\lambda-1}\left(\dot{s}\alpha\left(1-v_{i+1/2}\right) - \frac{\left(D_B\right)_{i+1/2}^{k}}{\left(R-s^k\right)\left(v_{i+1}-v_i\right)} \right) \right. \\ & \left. - \frac{1}{2}\left(r_{i-1/2}^{k-1}\right)^{\lambda\lambda-1}\left(\dot{s}\beta\left(1-v_{i-1/2}\right) + \frac{\left(D_B\right)_{i-1/2}^{k}}{\left(R-s^k\right)\left(v_i-v_{i-1}\right)} \right) \right] \\ & + q_{i+1}^{k}\left[\left(r_{i+1/2}^{k-1}\right)^{\lambda\lambda-1}\left(\dot{s}\beta\left(1-v_{i+1/2}\right) + \frac{\left(D_B\right)_{i+1/2}^{k}}{\left(R-s^k\right)\left(v_{i+1}-v_i\right)} \right) \right] + q_{i-1}^{k}\left[-\left(r_{i-1/2}^{k-1}\right)^{\lambda\lambda-1}\left(\dot{s}\alpha\left(1-v_{i-1/2}\right) - \frac{\left(D_B\right)_{i-1/2}^{k}}{\left(R-s^k\right)\left(v_i-v_{i-1}\right)} \right) \right] \end{aligned} \qquad 3.48$$

In Phase B, there is a zero flux at the right boundary (i=m+1 node) with a discretized boundary condition given as:

$$
\begin{aligned}
&q_{m+1}^{k+1}\left[\frac{(R)^{\lambda\lambda}-\left(r_{m+1/2}^{k+1}\right)^{\lambda\lambda}}{\lambda\lambda\left(t^{k+1}-t^{k-1}\right)}+\frac{1}{2}\left(r_{m+1/2}^{k-1}\right)^{\lambda\lambda-1}\left(\dot{s}\,\beta\left(1-v_{m+1/2}\right)+\frac{\left(D_B\right)_{m+1/2}^{k}}{\left(R-s^{k}\right)\left(v_{m+1}-v_{m}\right)}\right)\right]\\
&=q_{m+1}^{k-1}\left[\frac{(R)^{\lambda\lambda}-\left(r_{m+1/2}^{k+1}\right)^{\lambda\lambda}}{\lambda\lambda\left(t^{k+1}-t^{k-1}\right)}-\frac{1}{2}\left(r_{m+1/2}^{k-1}\right)^{\lambda\lambda-1}\left(\dot{s}\,\beta\left(1-v_{m+1/2}\right)+\frac{\left(D_B\right)_{m+1/2}^{k}}{\left(R-s^{k}\right)\left(v_{m+1}-v_{m}\right)}\right)\right]\\
&+q_{m}^{k}\left[-\left(r_{m+1/2}^{k-1}\right)^{\lambda\lambda-1}\left(\dot{s}\,\alpha\left(1-v_{m+1/2}\right)-\frac{\left(D_B\right)_{m+1/2}^{k}}{\left(R-s^{k}\right)\left(v_{m+1}-v_{m}\right)}\right)\right]
\end{aligned}
\qquad 3.49
$$

The discretized boundary equation for the interface (i=1) at Phase B with a constant concentration is:

$$
q_1^{k+1}=q_1^{k}=q_1^{k-1}=C_{BA} \qquad 3.50
$$

Hence, the interface equation which conserves solute is given as:

$$
\begin{aligned}
&\lambda\lambda\left(t^{k+1}-t^{k}\right)\left(r_{m+1/2}^{k}\right)^{\lambda\lambda-1}\left[\frac{\left(s^{k+1}-s^{k}\right)}{\left(t^{k+1}-t^{k}\right)}p_{m+1/2}^{k}u_{N+1/2}^{k}+\frac{\left(D_A\right)_{m+1/2}^{k}}{s^{k}}\left.\frac{\partial p}{\partial u}\right|_{m+1/2}^{k}\right]\\
&+C_A\left[\left(s^{k+1}\right)^{\lambda\lambda}-\left(s^{k}\right)^{\lambda\lambda}-\left(r_{m+1/2}^{k+1}\right)^{\lambda\lambda-1}+\left(r_{m+1/2}^{k}\right)^{\lambda\lambda-1}\right]=\\
&-C_B\left[-\left(s^{k+1}\right)^{\lambda\lambda}+\left(s^{k}\right)^{\lambda\lambda}+\left(r_{m+1/2}^{k+1}\right)^{\lambda\lambda-1}-\left(r_{m+1/2}^{k}\right)^{\lambda\lambda-1}\right]\\
&+\lambda\lambda\left(t^{k+1}-t^{k}\right)\left(r_{m+1+1/2}^{k}\right)^{\lambda\lambda-1}\left[\frac{\left(s^{k+1}-s^{k}\right)}{\left(t^{k+1}-t^{k}\right)}q_{1+1/2}^{k}\left(1-v_{1+1/2}^{k}\right)+\frac{\left(D_B\right)_{1+1/2}^{k}}{R-s^{k}}\left.\frac{\partial q}{\partial v}\right|_{1+1/2}^{k}\right]
\end{aligned}
\qquad 3.51
$$

To obtain fully explicit solutions to Equations 3.45– 3.50, the future positions must be known and calculated by using Equation 3.51. However, for non-1D planar systems, Equation 3.51 can result in higher-order polynomials with multiple roots. Iterations have been proposed to obtain the required future interface position [3], [78]. The Newton-Raphson iteration method can be used to

calculate the future interface position. In this method, the initial estimate of the future interface position is the present interface position. A computer algorithm that combines the bisection, inverse quadratic interpolation, and secant methods can calculate future interface positions. To avoid iterations and estimates, exact solutions to Equation 3.51 will therefore be derived. A generalized form of Equation 3.51, for each coordinate system, is given as follows:

$a_1 s^{k+1} + b_1 = 0$ For planar geometry

$a_2 \left(s^{k+1}\right)^2 + b_2 s^{k+1} + c_2 = 0$ For cylindrical coordinates

$a\left(s^{k+1}\right)^3 + b\left(s^{k+1}\right)^2 + cs^{k+1} + d = 0$ For spherical coordinates

Based on the data by Illingworth and Golosnoy [78], the exact solutions for the interface or Equation 3.51 can be calculated for the three coordinate systems by choosing the correct root, which satisfies the type of diffusion. The solutions are presented in Table 3.2 for two conditions, A and B. Condition A represents solute diffusion in the direction of an increasing radius of curvature. In contrast, Condition B represents solute diffusion in the direction of a reducing radius of curvature.

Hence the algorithms for diffusion problems with moving boundaries are presented below.

When k=1: The explicit numerical model has two steps.

1. Calculate the future interface position (s^2) by using Equation 3.51 and Table 3.2, and

2. Calculate p_i^2 and q_i^2.

k>1 uses a three-step explicit method based on the DF scheme:

Table 3.2: Table of future positions

Planar($\lambda\lambda = 1$)		**Cylindrical** ($\lambda\lambda = 2$)		**Spherical**($\lambda\lambda = 3$)
		Condition A	**Condition B**	**Conditions A/B**
s^{k+1} $= -b_1/a_1$	s^{k+1} $= -b_1/a_1$	s^{k+1} $= \frac{-b_2 + \sqrt{b_2^2 - 4a_2c_2}}{2a_2}$	s^{k+1} $= \frac{-b_2 - \sqrt{b_2^2 - 4a_2c_2}}{2a_2}$	$\Delta_0 = b^2 - 3ac$ $\Delta_1 = 2b^3 - 9abc + 27a^2d$ $C = \sqrt[3]{\frac{\Delta_1 + \sqrt{\Delta_1^2 - 4\Delta_0^3}}{2}}$ $C_K = \varepsilon^K C$ and $\varepsilon = -\frac{1}{2} + \frac{1}{2}\sqrt{3}i$ $x_K = -\frac{1}{3a}\left(b + \varepsilon^K C + \frac{\Delta_0}{\varepsilon^K C}\right)$ where $K = 0,1,2$ $S_1 = x_0$ $S_2 = max(x_K)$ $d = S_2 - s^k$ if $d \neq 0$ $s^{k+1} = S_2$ if $d = 0$ $s^{k+1} = S_1$

3. The future interface position (s^{k+1}) is calculated by using Equation 3.51 and Table 3.2,

4. p_i^{k+1} and q_i^{k+1} are determined by using Equations 3.45 and 3.50.

The steps above eliminate iteration or assumptions.

3.3.2 Calculation time

A timer is used to compare the relative time between the new explicit and the implicit models in systems with constant diffusivity. The calculation time of an implicit model is dependent on the grid size and convergence criteria determined by the tolerance. However, a smaller tolerance and grid size increases the accuracy of the simulation at the expense of the calculation time. In an analysis that compares the explicit and implicit models with the same grid size in a solid-solid solution in this study, the results show that the new model is about 3.4 times faster when compared to the implicit model. The explicit model is three times faster than the implicit model for two-phase solid-liquid diffusion.

3.3.3 Applying the new model to a single-phase problem

In single-phase systems, the equations for either Phase A or B can be used. For Phase B, Equations 3.48-3.50 can be used, however, with a modification of the interface equation to capture the stationary boundaries. The stationary interface discretization at the boundaries is:

$$s^{k+1} = s^k = s^{k-1} = R \text{ and } \dot{s} = 0 \qquad 3.52$$

In the single-phase systems used in this work, the total amount of solute is always conserved by zero solute migration (flux) at the boundaries. Under this condition, the boundaries of the host material act as a barrier with no migration of solute beyond the boundary. Zero solute flux at the boundary implies that solute build-up can occur there. Equation 3.50 breaks down when solute builds up because it is only applicable to systems with a fixed left boundary concentration. Therefore, the true boundary condition at the left boundary is zero flux, and applying the DF scheme will result in:

$$q_1^{k+1}\left[\frac{\left(r_{1+1/2}^{k+1}\right)^{\lambda\lambda}-(s)^{\lambda\lambda}}{\lambda\lambda\left(t^{k+1}-t^{k-1}\right)}-\frac{1}{2}\left(r_{1+1/2}^{k-1}\right)^{\lambda\lambda-1}\left(\dot{s}\,\alpha\left(1-v_{1+1/2}\right)-\frac{\left(D_B\right)_{1+1/2}^{k}}{\left(R-s^k\right)\left(v_{1+1}-v_1\right)}\right)\right]$$
$$=q_1^{k-1}\left[\frac{\left(r_{1+1/2}^{k+1}\right)^{\lambda\lambda}-(s)^{\lambda\lambda}}{\lambda\lambda\left(t^{k+1}-t^{k-1}\right)}+\frac{1}{2}\left(r_{1+1/2}^{k-1}\right)^{\lambda\lambda-1}\left(\dot{s}\,\alpha\left(1-v_{1+1/2}\right)-\frac{\left(D_B\right)_{1+1/2}^{k}}{\left(R-s^k\right)\left(v_{1+1}-v_1\right)}\right)\right]$$
$$+q_2^{k}\left[\left(r_{1+1/2}^{k-1}\right)^{\lambda\lambda-1}\left(\dot{s}\,\beta\left(1-v_{1+1/2}\right)+\frac{\left(D_B\right)_{1+1/2}^{k}}{\left(R-s^k\right)\left(v_{1+1}-v_1\right)}\right)\right] \qquad 3.53$$

Therefore, Equations 3.45-3.49, and 3.53 can be used to simulate single-phase diffusion.

3.3.4 Extending the new model to planar multi-phase systems

Single- and two-phase systems have been discussed; however, there are multiple interphases for systems with more than two phases. Unlike the two end phases, both interfaces of the inner phases have moving boundaries.

$$\frac{\partial C_1(r,t)}{\partial t}=\frac{\partial}{\partial t}\left(D_1\left[C_1(r,t)\right]\frac{\partial C_1(r,t)}{\partial t}\right) \qquad 0\le r\le s_1(t) \qquad 3.54$$

$$\frac{\partial C_{nn}(r,t)}{\partial t} = \frac{\partial}{\partial t}\left(D_{nn}\left[C_{nn}(r,t)\right]\frac{\partial C_{nn}(r,t)}{\partial t}\right) \qquad s_{nn}(t) \le r \le s_{nf-1}(t) \qquad 3.55$$

$$\frac{\partial C_{nf}(r,t)}{\partial t} = \frac{\partial}{\partial t}\left(D_{nf}\left[C_{nf}(r,t)\right]\frac{\partial C_{nf}(r,t)}{\partial t}\right) \qquad s_{nf-1}(t) \le r \le s_{nf}(t) = R \qquad 3.56$$

nn = 2… nf-1

nn is the intermediate phase, nf-1 is the right boundary phase, and the interface nf is the extreme right boundary.

Solutions to the left end phase (Equation 3.54) and right end phase (Equation 3.56) are the same as the planar case of Equations 3.45-3.47 and 3.48-3.50, respectively The Landau transformation parameter of the inner phases (Equations 3.55) is presented below.

$$w_{nn} = \frac{r - s_{nn-1}(t)}{s_{nn}(t) - s_{nn-1}(t)} \quad \text{and} \quad z(w,t) = C_{nn}(r,t) \qquad 3.57$$

The Landau transformation yields:

$$\frac{\partial\left[z(s_2 - s_1)\right]}{\partial t} = \frac{\partial}{\partial w}\left[z\left(\frac{ds_1}{dt} + w\left(\frac{ds_2}{dt} - \frac{ds_1}{dt}\right)\right) + \frac{D_E}{(s_2 - s_1)}\frac{\partial z}{\partial w}\right] \qquad 3.58$$

It is important to note that Equation 3.58 can be converted to the Phase A and B equations by applying the necessary interface condition.

The LF/DF scheme solution to Equation 3.75 is:

$$z_i^{k+1}\left[\left(s_2^{k+1}-s_1^{k+1}\right)\left(w_{i+1/2}-w_{i-1/2}\right)-\frac{1}{2}\left[\begin{array}{l}-\dfrac{D_{Ei+1/2}^{\ k}\delta t}{\left(s_2-s_1\right)\left(w_{i+1}-w_i\right)}-\dfrac{D_{Ei-1/2}^{\ k}\delta t}{\left(s_2-s_1\right)\left(w_i-w_{i-1}\right)}\\ +\alpha\left(\Delta s_1\left(1-w_{i+1/2}\right)+\Delta s_2 w_{i+1/2}\right)-\beta\left(\Delta s_1\left(1-w_{i-1/2}\right)+\Delta s_2 w_{i-1/2}\right)\end{array}\right]\right]$$
$$=z_i^{k-1}\left[\left(s_2^{k-1}-s_1^{k-1}\right)\left(w_{i+1/2}-w_{i-1/2}\right)+\frac{1}{2}\left[\begin{array}{l}-\dfrac{D_{Ei+1/2}^{\ k}\delta t}{\left(s_2-s_1\right)\left(w_{i+1}-w_i\right)}-\dfrac{D_{Ei-1/2}^{\ k}\delta t}{\left(s_2-s_1\right)\left(w_i-w_{i-1}\right)}\\ +\alpha\left(\Delta s_1\left(1-w_{i+1/2}\right)+\Delta s_2 w_{i+1/2}\right)-\beta\left(\Delta s_1\left(1-w_{i-1/2}\right)+\Delta s_2 w_{i-1/2}\right)\end{array}\right]\right]$$
$$+z_{i+1}^{k}\left[\frac{D_{Ei+1/2}^{\ k}\delta t}{\left(s_2-s_1\right)\left(w_{i+1}-w_i\right)}+\beta\left(\Delta s_1\left(1-w_{i+1/2}\right)+\Delta s_2 w_{i+1/2}\right)\right]$$
$$+z_{i-1}^{k}\left[\frac{D_{Ei-1/2}^{\ k}\delta t}{\left(s_2-s_1\right)\left(w_i-w_{i-1}\right)}-\alpha\left(\Delta s_1\left(1-w_{i-1/2}\right)+\Delta s_2 w_{i-1/2}\right)\right] \qquad 3.59$$

The boundary conditions are constant interface concentrations.

$$z_1^{k-1}=z_1^{k}=z_1^{k+1} \qquad 3.60$$

$$z_{m+1}^{k-1}=z_{m+1}^{k}=z_{m+1}^{k+1} \qquad 3.61$$

3.3.5 Solute balance in multi-phase one-dimensional planar systems

To ensure solute conservation, the total amount of solute throughout the diffusion system must be the same for all diffusion times, and by implication, the time rate of change in the total solute is zero. Therefore, consider a system with interface positions $s_0,\ s_1,\ s_2,\ldots,s_{nf-1},\ s_{nf}$. The first phase has a left boundary with zero flux, while the right boundary of the last phase has zero flux.

$$\frac{\partial}{\partial t}\left(\left(s_1-s_0\right)\int_0^1 z_1 dw_1+\left(s_2-s_1\right)\int_0^1 z_2 dw_2+\left(s_3-s_2\right)\int_0^1 z_3 dw_3+\ldots+\left(s_{nn-1}-s_{nn-2}\right)\int_0^1 z_{nn-1} dw_{nn-1}+\left(s_{nn}-s_{nn-1}\right)\int_0^1 z_{nn} dw_{nn}\right)=0 \qquad 3.62$$

The summation is done for each phase, and the equations can be solved by using a matrix:

$$\begin{bmatrix} a_1 & a_2 & & & & & \\ \mathrm{K}_{n-1} & \mathrm{K}_{nn} & \mathrm{K}_{nn+1} & & & & \\ & \cdot & \cdot & \cdot & & & \\ & & \cdot & \cdot & \cdot & & \\ & & & \cdot & \cdot & \cdot & \\ & & & & \mathrm{K}_{nf-2} & \mathrm{K}_{nf-1} \end{bmatrix} \begin{bmatrix} \Delta s_1 \\ \Delta s_{nn} \\ \cdot \\ \cdot \\ \cdot \\ \Delta s_{nf-1} \end{bmatrix} = \begin{bmatrix} b_1 \\ b_{nn} \\ \cdot \\ \cdot \\ \cdot \\ b_{nf-1} \end{bmatrix} \qquad 3.63$$

The entries in the matrix are:

$$\mathrm{K}_1 = \left(z^k_{1,m+1/2} w_{1,m+1/2} + z_{1,m+1} \left(\frac{w_{1,m+1} - w_{1,m}}{2} \right) - z^k_{2,1+1/2} \left(1 - w_{2,1+1/2} \right) - z_{2,1} \left(\frac{w_{2,2} - w_{2,1}}{2} \right) \right)$$

$$\mathrm{K}_2 = \left(-z^k_{2,1+1/2} w_{2,1+1/2} + z_{2,1} \left(\frac{w_{2,2} - w_{2,1}}{2} \right) \right)$$

$$b_1 = \frac{D^k_{2,1+1/2} \delta t}{\left(s_2 - s_1 \right)} \frac{\left(z^k_{2,2} - z^k_{2,1} \right)}{\left(w_{2,2} - w_{2,1} \right)} - \frac{D^k_{1,m+1/2} \delta t}{\left(s_1 - s_0 \right)} \frac{\left(z^k_{1,m+1} - z^k_{1,m} \right)}{\left(w_{1,m+1} - w_{1,m} \right)}$$

$$\mathrm{K}_{nn-1} = \left(z^k_{nn,m+1/2} \left(1 - w_{nn,m+1/2} \right) - z_{nn,m+1} \left(\frac{w_{nn,m+1} - w_{nn,m}}{2} \right) \right)$$

$$\mathrm{K}_{nn} = \left(z^k_{nn,m+1/2} w_{nn,m+1/2} + z_{nn,m+1} \left(\frac{w_{nn,m+1} - w_{nn,m}}{2} \right) - z^k_{nn+1,1+1/2} \left(1 - w_{nn+1,1+1/2} \right) - z_{nn+1,1} \left(\frac{w_{nn+1,2} - w_{nn+1,1}}{2} \right) \right)$$

$$\mathrm{K}_{nn+1} = \left(-z^k_{nn+1,1+1/2} w_{nn+1,1+1/2} + z_{nn+1,1} \left(\frac{w_{nn+1,2} - w_{nn+1,1}}{2} \right) \right)$$

$$b_{nn} = \frac{D^k_{nn+1,1+1/2} \delta t}{\left(s_{nn+1} - s_{nn} \right)} \frac{\left(z^k_{nn+1,2} - z^k_{nn+1,1} \right)}{\left(w_{nn+1,2} - w_{nn+1,1} \right)} - \frac{D^k_{nn,m+1/2} \delta t}{\left(s_{nn} - s_{nn-1} \right)} \frac{\left(z^k_{nn,m+1} - z^k_{nn,m} \right)}{\left(w_{nn,m+1} - w_{nn,m} \right)}$$

$$\mathrm{K}_{nf-2}=\left(z^{k}_{nf-1,m+1/2}\left(1-w_{nf-1,m+1/2}\right)-z_{nf-1,m+1}\left(\frac{w_{nf-1,m+1}-w_{nf-1,m}}{2}\right)\right)$$

$$\mathrm{K}_{nf-1}=\left(z^{k}_{nf-1,m+1/2}w_{nf-1,m+1/2}+z_{nf-1,m+1}\left(\frac{w_{nf-1,m+1}-w_{nf-1,m}}{2}\right)-z^{k}_{nf,1+1/2}\left(1-w_{nf,1+1/2}\right)-z_{nf,1}\left(\frac{w_{nf,2}-w_{nf,1}}{2}\right)\right)$$

$$b_{nf-1}=\frac{D^{k}_{nf,1+1/2}\delta t}{\left(s_{nf}-s_{nf-1}\right)}\frac{\left(z^{k}_{nf,2}-z^{k}_{nf,1}\right)}{\left(w_{nf,2}-w_{nf,1}\right)}-\frac{D^{k}_{nf,-1_{m+1/2}}\delta t}{\left(s_{nf-1}-s_{nf-2}\right)}\frac{\left(z^{k}_{nf-1,m+1}-z^{k}_{nf-1,m}\right)}{\left(w_{nf-1,m+1}-w_{nf-1,m}\right)}$$

$$s^{k+1}=\Delta s+s^{k-1}$$

In summary, to solve 1D multi-phase planar systems (γ = 1), with nf phases, the solute phase distribution at the left boundary can be solved with Equations 3.45– 3.47. The solute distribution at the right boundary can be solved with Equations 3.48 – 3.50, and the solute distribution of the inner phase can be solved with Equations 3.59-3.61. The interface is solved by using the matrix of Equation 3.63.

3.3.6 FSM procedure

To extract the D(C) from experimental data, the newly developed numerical method is coupled with the FSM, and the procedure is as follows:

Step 1. **Estimate the initial function**: The initial D(C) can be estimated or fitted by using the BM or SF method.

$$D\left(C\right)=\exp\left\{F\left(C\right)\right\} \qquad 3.64$$

where the polynomial function is F(C).

Step 2. **Simulate the numerical concentration profile**: This profile is simulated by solving Fick's second law of diffusion with the use of the experimental time, initial concentration data and D(C).

Step 3. **Compare the simulated and experimental profiles**: The experimental and simulated concentration profiles are compared by using either one of the following types of comparisons. The first type of comparison is to calculate and compare the amount of solute diffused by the simulated and experimental concentration profiles. The second approach is calculating the sum of the squared difference between the experimental and simulated concentration profiles.

Step 4: **Checking the difference calculated in Step 3 against a pre-set value:** The simulation is terminated if the difference obtained in Step 3 is lower than a pre-set value. An accurate D(C) is a function that results in matching simulated and experimental concentration profiles.

Step 5: **Adjusting the diffusion coefficient:** When Step 3 results in a difference that is greater than the pre-set tolerance value, the D(C) is adjusted by using Equation 3.65, and Steps 1-3 are repeated until the difference is a value less than the pre-set value [88].

$$D_{new} = D_{old} \frac{\left.\frac{dr}{dC}\right|_{Experiment}}{\left.\frac{dr}{dC}\right|_{Simulation}} \qquad 3.65$$

3.3.7 Experimental verification of the new numerical model

To validate the new model with the use of a diffusion couple with variable D(C), the model is coupled with the FSM to first extract the D(C) from experimental concentration profiles of α - β brass diffusion couples in the classical work of Kirkendall et al [35]. The calculated D(C) is used to simulate the migration behaviour of the interphase boundary. The simulated interface migration

is then compared to experimentally determined values by Kirkendall et al [35]. The predicted and experimentally measured interface migrations are shown in Figure 3.1. The results show that the predicted values agree with the measured experimental results, and this fully validates the newly developed model.

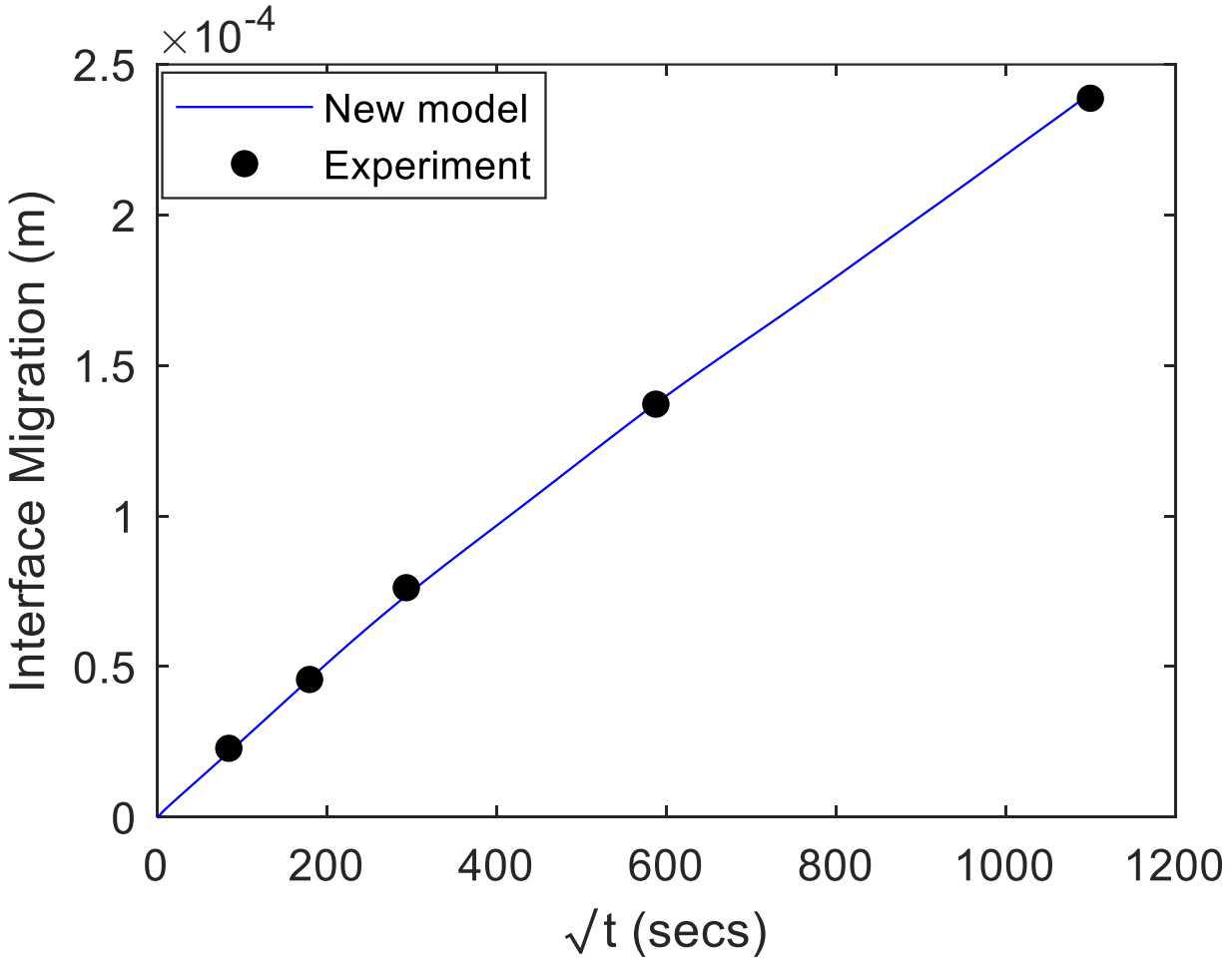

Figure 3.1 Plot of interface migration against square-root of time for Cu-Zn system at 600 ^{o}C computed from experimental concentration profiles from the literature [35]

CHAPTER FOUR

4 TIME VARIATION OF CONCENTRATION-DEPENDENT INTERDIFFUSION COEFFICIENT

4.1 Introduction

Time is an important factor during diffusion**.** In the literature, diffusion coefficients have been calculated many times by different researchers. Albeit their differences, there is the general implicit assumption that diffusion coefficients are a material constant that is time independent. Time is an important factor that changes the concentration gradient at a specific concentration, thus resulting in diffusion-induced stress changes that can alter diffusion coefficients. This chapter aims to theoretically and experimentally investigate the possibility of the effect of diffusion time on D(C). In this chapter, the D(C) will be evaluated theoretically by using the model derived in Chapter 3, which considers the possible generation and relaxation of stress during diffusion. The effective D(C) is calculated theoretically at different times to investigate the effect of time on D(C). Subsequently, the new numerical approach developed in this study will be applied to several experimental profiles at different diffusion times. The new numerical approach, which involves coupling the new model in section 3.3 and the FSM [88], will address the limitations of the common methods used to calculate the experimental reliance of the interdiffusion coefficient on concentration. Thereafter, the implication of the effect of time on D(C) in materials will be experimentally studied and discussed.

4.2 Theoretical Effect of Time on Concentration-Dependent Interdiffusion Coefficient

To study the theoretical effect of time on D(C), the discretized dimensionless Equations 3.22-3.27 are numerically solved for infinite diffusion couples by using the following input parameters. Poisson's ratio: $\upsilon = 0.3$, $\eta' = 0.000108$, $D_1^{'} = 100 D_2^{'}$, $V_1^{'} = 0.9412$, $V_2^{'} = 1.0$ and $T^{'} = 0.0052$, and dimensionless times of $t_1' = 0.0009$, $t_2' = 0.0018$, and $t_3' = 0.0054$. The concentration profiles for systems with DIS and those that do not consider DIS at different times are presented in Figure 4.1a. Similarly, the pressure gradients with respect to concentration for systems with DIS and systems that do not consider DIS at different times are shown in Figure 4.1b. The dimensionless effective D(C) for both systems are calculated by using Equation 3.21 and reported in Figure 4.2. As seen in Figure 4.1, the DIS evolves with changing concentration profiles. In Figure 4.2, the D(C) in the stress-free system does not change with time; however, during diffusion, changes in the solute concentration gradient in the crystal lattices alter the diffusion-induced strain, thus resulting in diffusion-induced stress. The results in Figure 4.2 show that theoretically, DIS can alter the D(C) as diffusion progresses with time. Hence, theoretically, the presence of DIS during diffusion, caused by a gradient of strained crystal lattices, can significantly change D(C) as diffusion time progresses. The increase in D(C) with diffusion time can be explained by using the DIS, as shown in the theoretical results reported in Figure 4.2. Therefore, theoretically, D(C) can change with the concentration gradient, which varies with concentration and time.

The next goal is to understand factors can that influence the magnitude of the effect of time. In the following subsection, understanding how other diffusion parameters influence the effect of time will be investigated. This investigation determines whether diffusion parameters enhance or reduce the effect of time on D(C). Notably, from Equation 3.21, at the same pressure and concentration

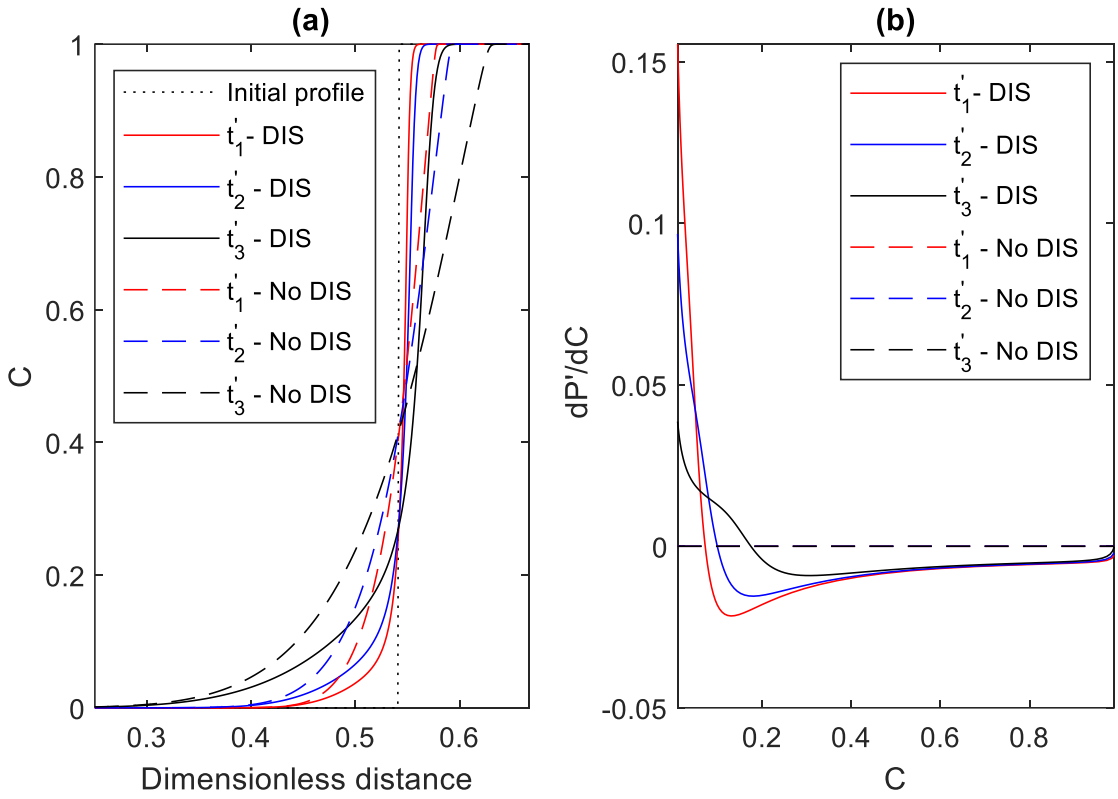

Figure 4.1 Profiles showing the effect of diffusion induced stress at different times for (a) concentration profiles and (b) Pressure gradients

(V_1' = 0.9412, V_2' = 1.0, D_1' = 1.0, D_2' = 0.01, $T^{'}$ = 0.0052, η = 0.0001083, α' = 0.8185, t_1' = 0.0009, t_2' = 0.0018, and t_3' = 0.0054)

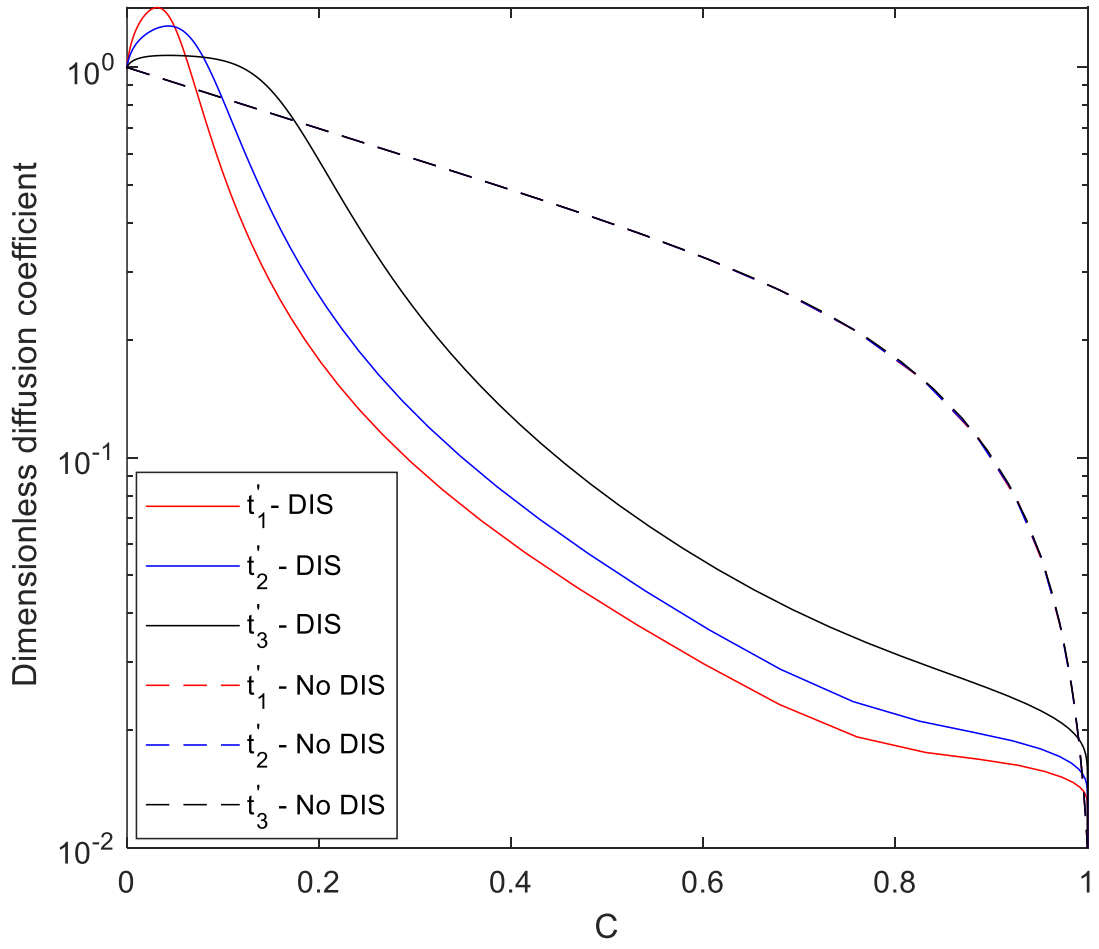

Figure 4.2 Plot of diffusion coefficient against concentration at different times for systems with diffusion induced stress and systems with the assumption of no diffusion-induced stress

(V_1 = 0.9412, V_2' = 1.0, D_1' = 1.0, D_2' = 0.01, $T^{'}$ = 0.0052, η = 0.0001083, α' = 0.8185, t_1' = 0.0009, t_2' = 0.0018, and t_3' = 0.0054)

gradients, the effect of time on the D(C) will depend on the viscosity of the system and the magnitude of the difference in the product of the mobility and molar volume $(M_i'V_i'$ or $\frac{D_i'V_i'}{RT})$. However, since the effect of time is an isothermal effect, viscosity, the stress-free tracer impurity diffusivity ratio, and the molar volume ratio shall be used to study the effect of time.

4.2.1 Influence of solid viscosity on the effect of time on D(C)

The first factor which is studied under the effect of time is viscosity. Viscosity influences plastic deformation and determines the rate of relaxation of the DIS. The Stoke-Einstein equation relates the viscosity of a system to the mobility of the slower moving component. For this study, three cases will be investigated.

Case A is a system with high viscosity, which results in only stress generation. In this system, only stress-free strain is considered. The plastic strain that relaxes the stress generated is assumed negligible due to the sluggish movement of the slow-moving diffusing component. Several studies have examined the influence of Case A on D(C) and shown that the pressure gradient per unit concentration gradient is a function of only the concentration. The concentration profiles, pressure gradients, and effective D(C) are calculated and presented in Figure 4.3. As the figure shows, there is a difference in the concentration profiles in systems with and without DIS in Case A. Figure 4.3b confirms that the pressure gradient with respect to concentration is independent of the diffusion time but a function of concentration. Figure 4.3c shows that the effective D(C) does not significantly change with time under this condition. However, while the effective D(C) does not change with time (Figure 4.3c), it is remarkably different from the condition without stress.

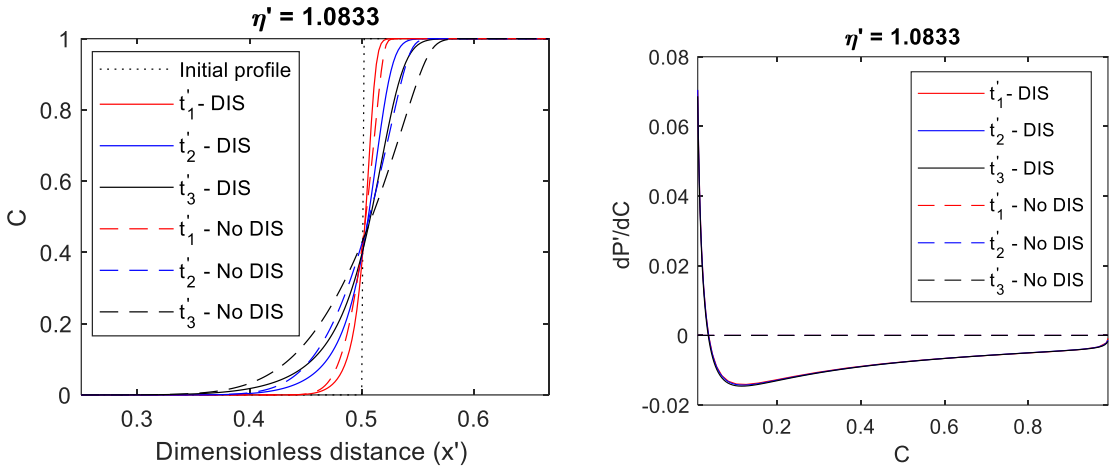

(a) (b)

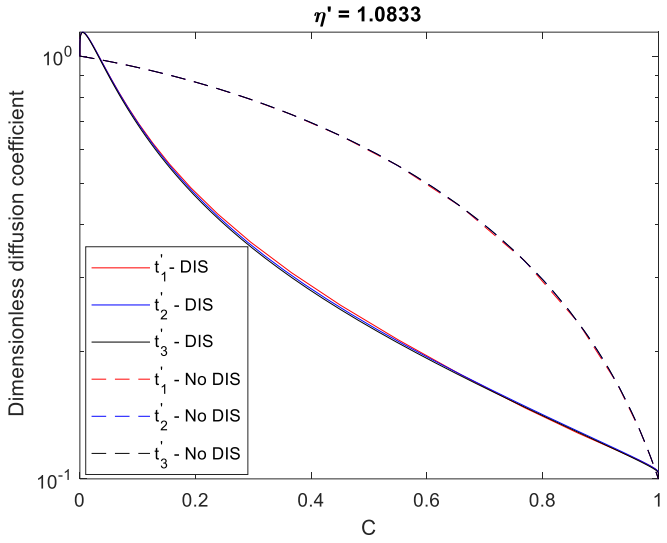

(c)

Figure 4.3 Case A effect of high viscosity on the following (a) Concentration profiles at different times (b) Pressure gradient at different times (c) Effective D(C) at different times (V_1 = 0.95, V_2' = 1.0, D_1' = 1.0, D_2' = 0.1, T’ = 0.0044, α' = -0.3638, t_1' = 0.0002, t_2' = 0.0009, and t_3' = 0.0018

Case B is a system with low viscosity, which results in a correspondingly rapid rate of stress relaxation. This implies that any DIS generated is quickly relaxed. Hence, the changes in the stress should be negligible. For this case, the concentration profiles, pressure gradients, and effective D(C) are calculated and presented in Figure 4.4. For all diffusion times, the DIS has no significant effect on the concentration (Figure 4.4a), the resulting stress gradient distributions are negligible (Figure 4.4b), and the effective D(C) is approximately the same as the function in an unstressed system.

Case C is a system with moderate viscosity. In this system, the DIS is generated and relaxed with time, resulting in different concentration profiles in the stressed and unstressed systems (Figure 4.5a). Most importantly, as the stress gradient with respect to the concentration changes with time (Figure 4.5b), the effective D(C) also changes with time (Figure 4.5c). Case C is a more accurate representation of real systems with simultaneous generation and relaxation of the DIS [8], [14], [16], [17], [89].

The solute penetrations of the three cases were then investigated. The solute penetration in Cases A and B follows a parabolic relationship (Figure 4.6). It is observed that, with time, the solute penetration in Case B coincides with the penetration of the stress-free system, due to the rapid rate of relaxation of any DIS generated. The penetration rate in Case C deviates from the rate in Case A towards Case B. Thus, a system with very low viscosity does not cause time to have a significant effect during diffusion; a low rate of relaxation of the DIS due to a high viscosity, results in a different effective D(C) which does not change with time. In contrast, a moderate viscosity causes time to have a significant effect on the effective D(C).

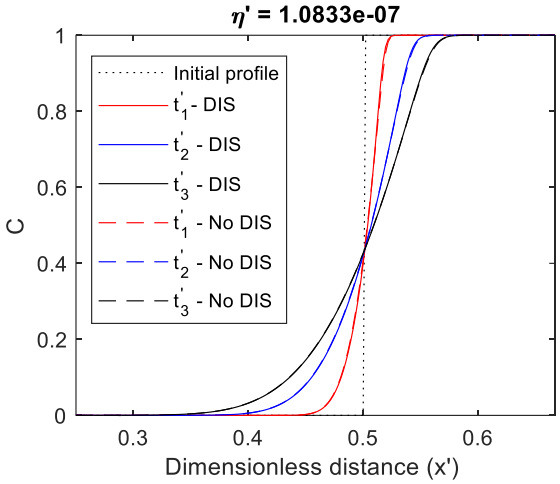

(a)

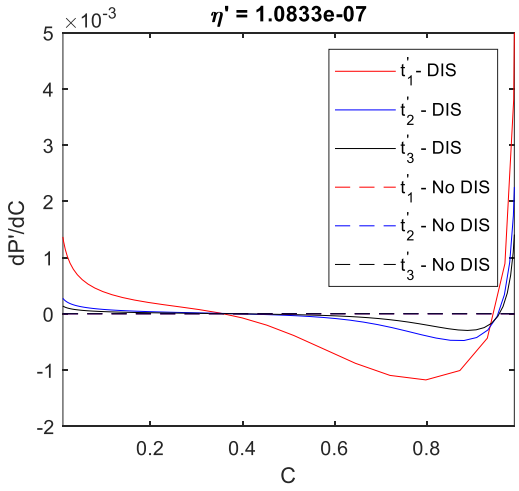

(b)

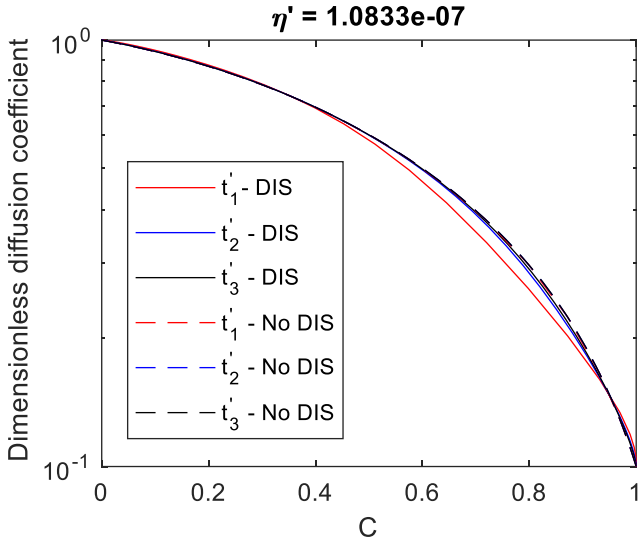

(c)

Figure 4.4 Case B effect of low viscosity on the following (a) Concentration profiles at different times (b) Pressure gradient at different times (c) Effective D(C) at different times ($V_1 = 0.95$, $V_2' = 1.0$, $D_1' = 1.0$, $D_2' = 0.1$, $T' = 0.0044$, $\alpha' = -0.3638$, $t_1' = 0.0002$, $t_2' = 0.0009$, and $t_3' = 0.0018$)

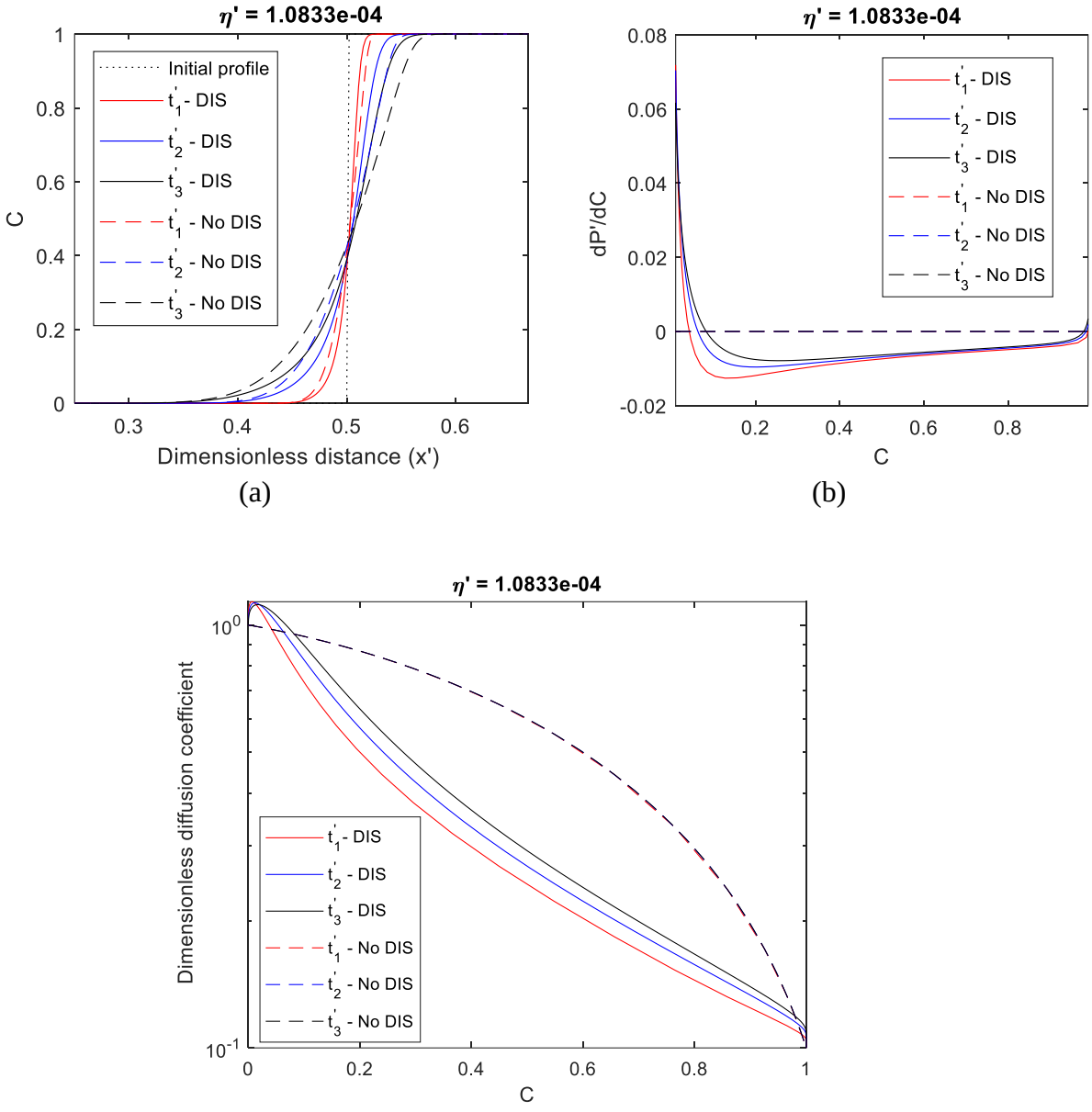

Figure 4.5 Case C effect of intermediate viscosity on the following (a) Concentration profiles at different times (b) Pressure gradient at different times (c) Effective D(C) at different times (V_1 = 0.95, V_2' = 1.0, D_1' = 1.0, D_2' = 0.1, T' = 0.0044, α' = -0.3638, t_1' = 0.0002, t_2' = 0.0009, and t_3' = 0.0018)

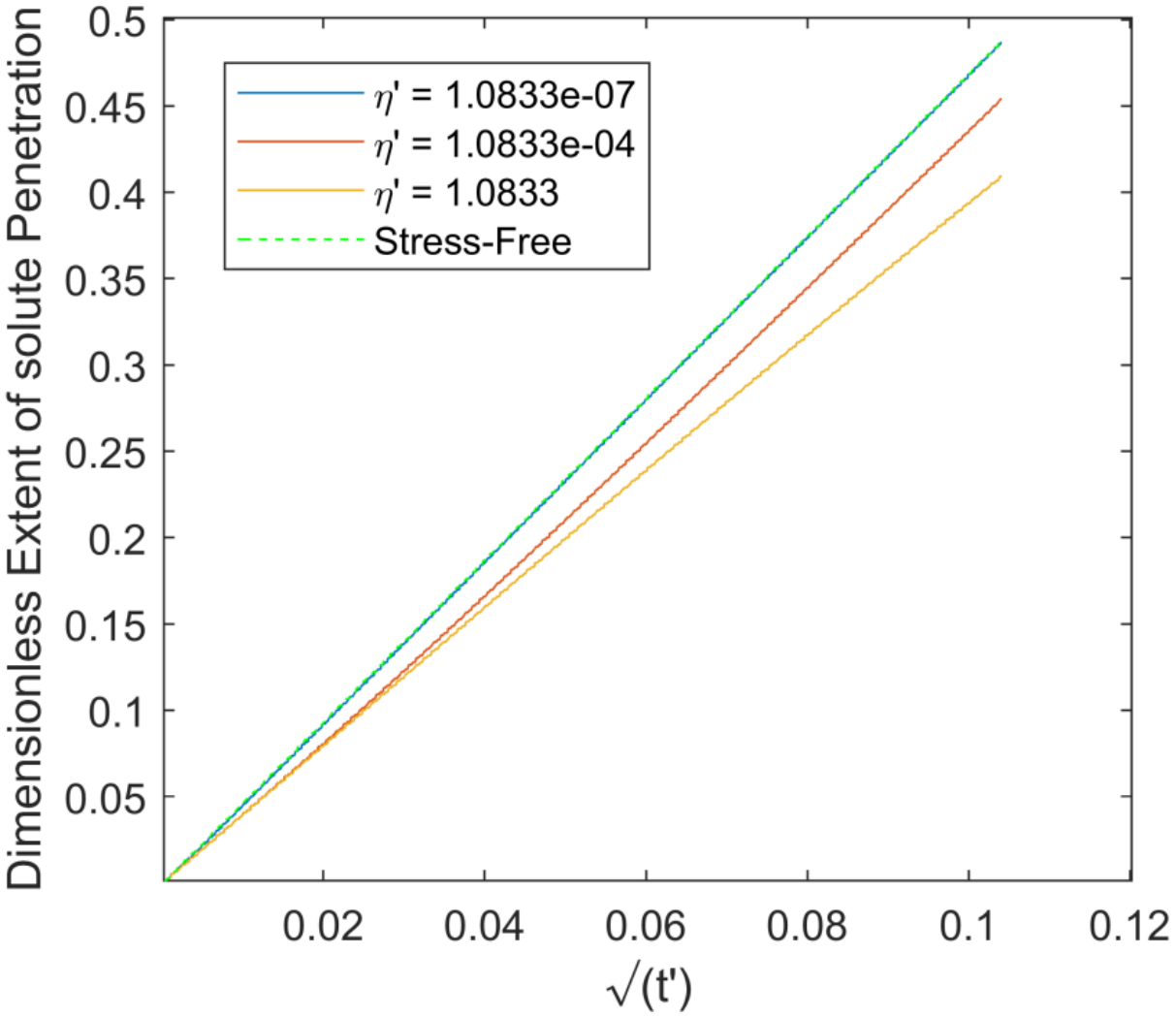

Figure 4.6 Penetration against square-root of time for different viscosities ($V_1 = 0.95$, $V_2' = 1.0$, $D_1' = 1.0$, $D_2' = 0.1$, $T' = 0.0044$, $\alpha' = -0.3638$, $t_3' = 0.0108$)

4.2.2 Influence of molar volume ratio on the effect of time on D(C)

The influence of the molar volume ratio on the effect of time on the effective D(C) will be investigated here—diffusion couples at the same temperature with different stress-free impurity diffusivity ratios and molar volumes are investigated. Four cases of molar volume variations are analyzed. For the first three cases, the molar volume of the more rapidly moving component is equal, 0.7, and 0.3 times the molar volume of the slower moving component, respectively. For the fourth case, the molar volume ratio of the rapid to slow moving component is equal to the inverse of the rapid to slow stress-free impurity diffusivity ratio. The effective D(C) for the three cases are presented in Figure 4.7, which shows that the effect of time on D(C) is more pronounced in a system with different impurity diffusivities when the two components have equal molar volumes. A very negligible effect of time is observed when the ratio of the molar volume of the rapidly to slow-moving component is equal to the inverse ratio of fast to slow diffusivity. Therefore, isothermal systems with different stress-free impurity diffusivities and a close molar volume will significantly affect the effect of time on effective D(C).

4.2.1 Influence of stress-free impurity diffusivity ratio on the effect of time on D(C)

This section investigates the influence of the stress-free impurity diffusivity ratio under isothermal conditions on the effect of time on D(C). This analysis is for diffusion couples at the same temperature with two components with different molar volumes and stress-free impurity diffusivity ratios. Three different stress-free impurity diffusivity ratios are investigated as three cases. For the first two cases, the stress-free impurity diffusivity of the slow-moving component is equal and 0.7 times the stress-free impurity diffusivity of the more rapidly moving component. For the last case, the stress-free impurity diffusivity of the slow to rapid-moving component is

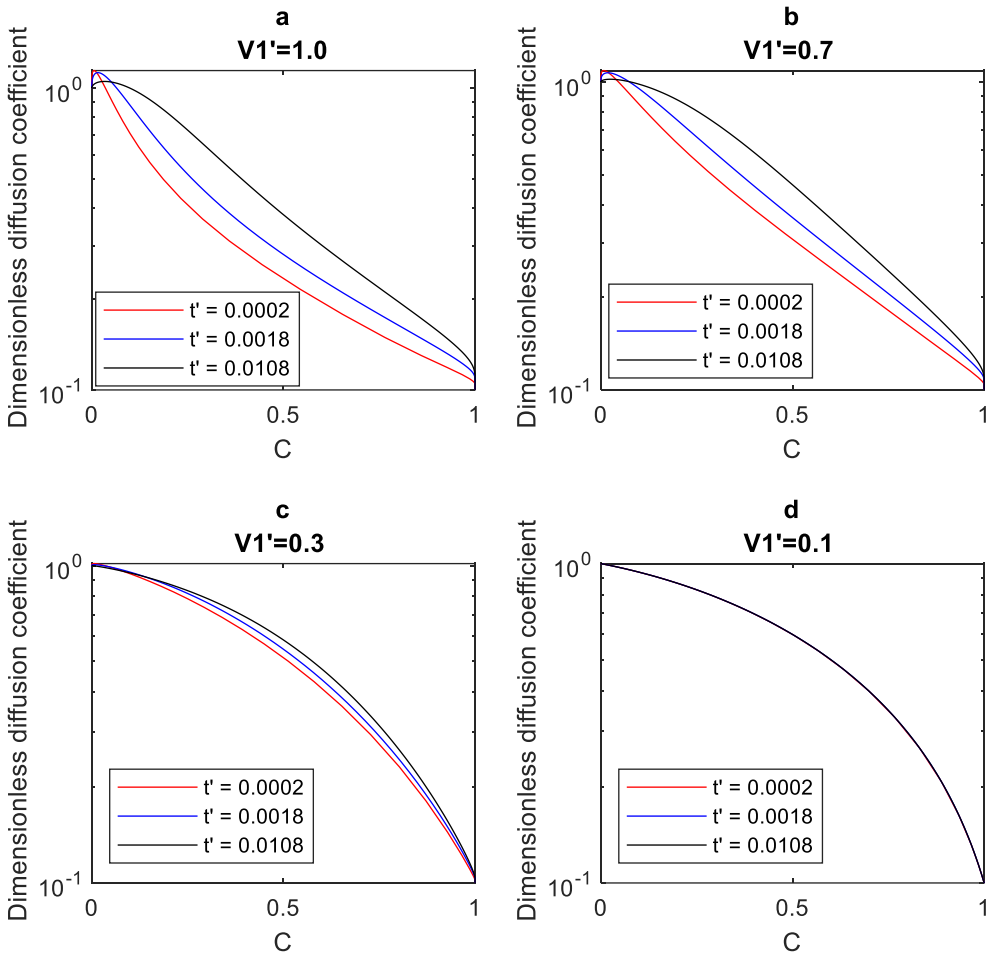

Figure 4.7 Effect of several molar volume ratios at different times (V_2' = 1.0, D_1' = 1.0, D_2' = 0.1, T’ = 0.0044, α' = -0.3638, t_1' = 0.0002, t_2' = 0.0018, and t_3' = 0.0108

equal to the ratio of the molar volumes of the rapid to slow-moving component. The effective D(C) for the three cases are reported in Figure 4.8, which shows that the effect of time is more pronounced as the stress-free impurity diffusivity ratio of the slow to rapidly moving component becomes smaller. The effect of time is very negligible when the stress-free intrinsic diffusivity ratio of the slow to the rapidly moving component is equal to the inverse ratio of their molar volumes. Therefore, time has the greatest effect on the effective D(C) in isothermal systems with different molar volumes but close stress-free impurity diffusivities.

The next goal is to experimentally verify the key theoretical findings observed in this section.

4.3 Experimental Verification of Effect of Time on Concentration-Dependent Interdiffusion Coefficient

Two different types of binary alloy systems are used to study the effect of diffusion time on D(C) at a given concentration. The systems are single-phase and two-phase diffusion systems. Solid-liquid diffusion couples are a reliable way to determine D(C) in a two-phase system [22]. Hence, a two-phase solid-liquid silver (Ag)-copper (Cu) system with limited solubility is used to study the effect of time in a two-phase system. In contrast, a Cu-Ni diffusion couple with unlimited solute solubility is used to study the effect of time in a single-phase system. The Ni-Cu diffusion couples were made by electroplating Ni on Cu substrates. Subsequently, the Ni-Cu diffusion couples were subjected to interdiffusion heat treatments at $600\,^{o}C$ for durations of 1, 10, 25, and 72 hrs in an electric furnace under purified argon. For the Ag-Cu solid-liquid diffusion couple, the copper foil was sandwiched between two Ag plates, where the Ag plates acted as the solid substrate. The assembled couples were then subjected to diffusion heat treatments in a vacuum at $820\,^{o}C$ for

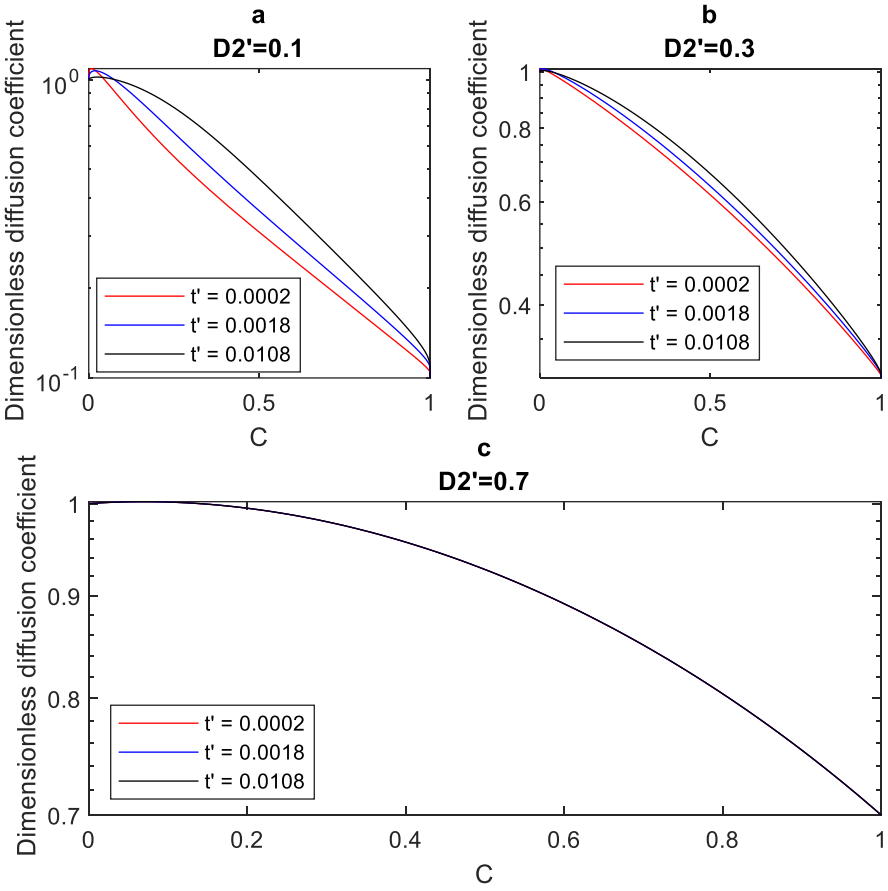

Figure 4.8 Effect of several stress-free impurity diffusivity ratios at different times (V_1' = 0.7, V_2' = 1.0, D_1' = 1.0, T' = 0.0044, α' = -0.3638, t_1' = 0.0002, t_2' = 0.0018, and t_3' = 0.0108)

durations of 1, 5, 25, 72, and 96 hrs. Other studies have reported a similar solid-liquid approach to provide an accurate D(C) by using a solid-liquid diffusion couple [21], [23]. Microanalyses by using X-ray energy and wavelength dispersive spectroscopy techniques were done to acquire the concentration profiles of each sample after the interdiffusion heat treatments. A minimum of five concentration profiles were extracted from each sample for each diffusion time, and the average profile from five profiles was determined. The FSM coupled with the new model in section 3.3 was used to extract the D(C) from the average experimental profiles. The experiments were repeated three times for each diffusion time to obtain three average profiles. The standard deviation of the error bars for each concentration was determined from the three average profiles. Also, the concentration averaged diffusivity for each of the three profiles was determined by using Equation 2.47 obtained from [63], [64]. In this study, the statistical variation of the concentration-average diffusion coefficient (D_{ave}) at a given time is less than 10% and 12% for the Cu-Ni and Ag-Cu systems, respectively. The statistical variations obtained in this work are comparable to that of the 10% found in the literature [67], [90]–[92].

4.3.1 Occurrence of time variation of concentration dependence of interdiffusion coefficient

The experimental concentration profiles in the Cu-Ni and Ag-Cu diffusion couples are presented in Figures 4.9a and 4.9b, respectively. The D(C) are calculated from the experimental profiles at 1 hr and 72 hrs in the Ag-Cu system at $820\,^{o}C$ by using the numerical model in section 3.3 and the FSM. The average D(C) plots at specific concentrations and their corresponding standard errors are shown in Figure 4.10. The average diffusivity for the full concentration range is 2.14×10^{-13} m^2/s at 1 hr and 1.25×10^{-13} m^2/s at 72 hrs.

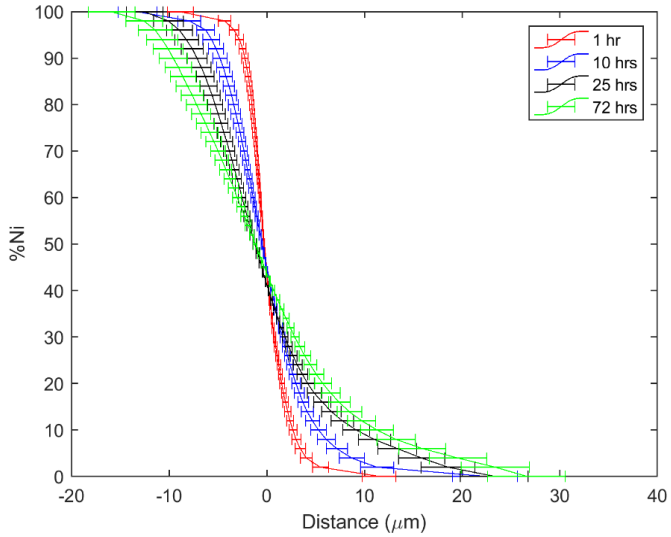

(a)

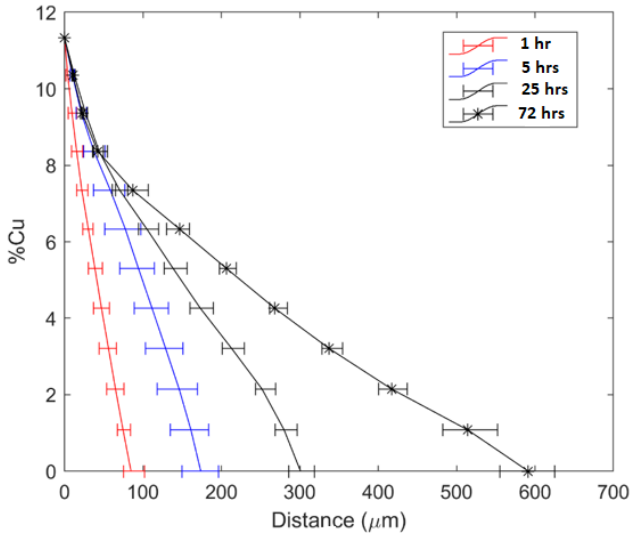

(b)

Figure 4.9 Concentration profiles in (a) Cu-Ni diffusion couples at 600 ^{o}C , and (b) Ag-Cu diffusion couples in the solid phase at 820 ^{o}C

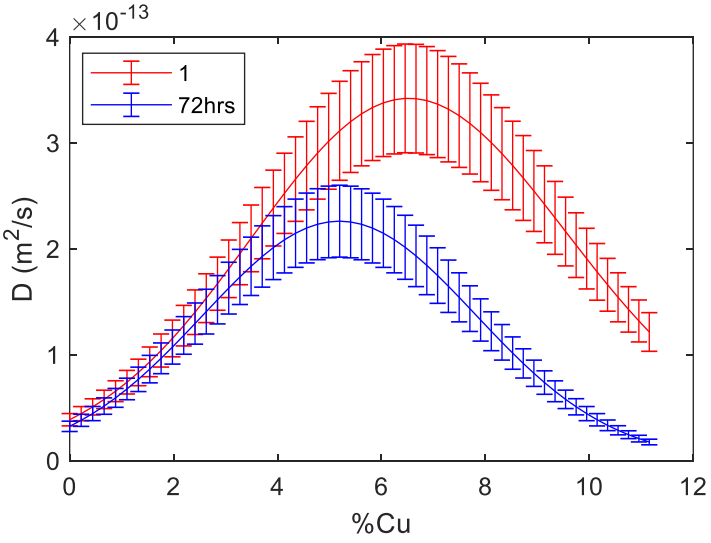

Figure 4.10: Time Variation of the D(C) at 1 hr and 72 hrs in two-phase Ag-Cu couple at 820 ^{o}C

The average diffusivity difference is a 37% reduction in the diffusion coefficient, which is larger than the acceptable statistical change of 12%. The error bars do not overlap, and a lower average D(C) indicates a change in the D(C) between 1 hr and 72 hrs.

Analyses were further performed to experimentally substantiate the effect of time on the D(C) operative between 1 hr and 72 hrs and remove any possible errors caused by pre-diffusion processes. The D(C) required to numerically re-produce the 5, 25, and 72 hrs experimental concentration profiles, when the pre-existing solute profiles in the material are the average experimental concentration distributions at 1, 5, and 25 hrs after diffusion, respectively, are calculated. The calculation process uses the numerical model in section 3.3 and the FSM. This approach of eliminating potential errors due to the non-uniform initial solute profile is not possible using conventional methods that are often used to calculate the D(C). The resulting D(C) calculated using the FSM and the new numerical model are presented in Figure 4.11 for the D(C) operative between diffusion times of 1 - 5 hrs, 5 - 25 hrs, and 25 - 72 hrs. The error bars that do not overlap in Figure 4.11, show that the D(C) changes between the time intervals. The D_{ave} over the full range of concentration profiles is calculated and presented in Table 4.1. The table shows that the average D(C) is reduced by 57% between 1-5 hrs and 5-25 hrs but increased by 41% between 5-25 hrs and 25-72 hrs. Similarly, as illustrated by the error bars in Figures 4.12 and 4.13 and Table 4.2, the time variation of the D(C) is also observed in the single-phase system of the Cu-Ni diffusion couple at $600^{\circ}C$. When compared with the average D(C) in the Cu-Ni system, there is a reduction of about 65% in the average diffusivity between 1-10 hrs and 25-72 hrs. The experimental results from the Ag-Cu and Cu-Ni diffusion systems experimentally validate the time variation of D(C). The use of the initial profiles produced through diffusion shows that the time variation of the D(C) cannot be attributed to errors potentially caused by pre-diffusion concentration profiles.

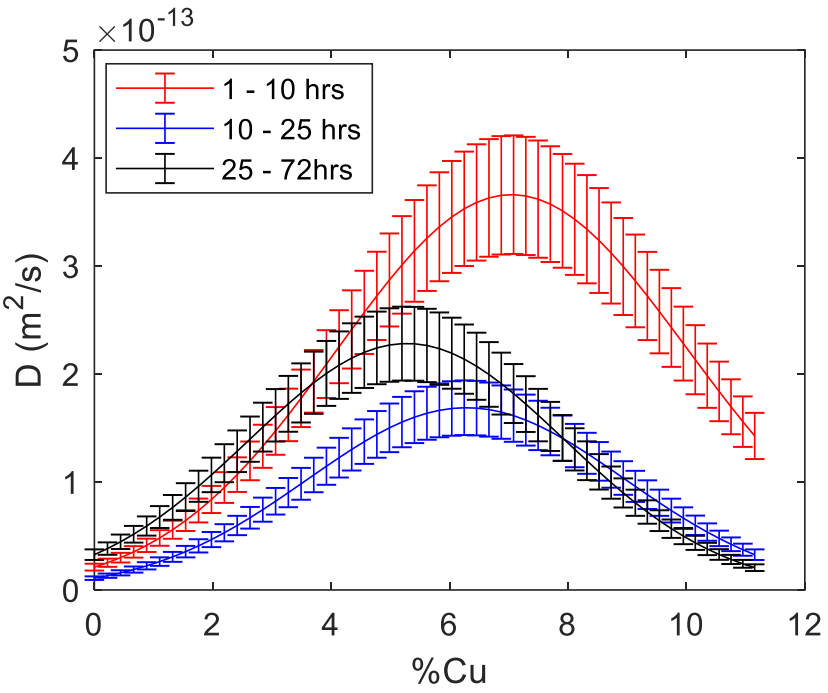

Figure 4.11: Different time interval variation of the D(C) in Ag-Cu diffusion couple at 820 ^{o}C

Table 4.1: Concentration-average diffusivity at different times for Ag-Cu system

Time (hrs)	Concentration-average diffusivity (m^2/s) (10^{-13})	% Change of D_{ave} from 1-5 hrs	% Change of D_{ave} from 5 - 25 hrs
25-72	1.29	41%	37%
5-25	0.94	57%	--
1-5	2.19	--	133%

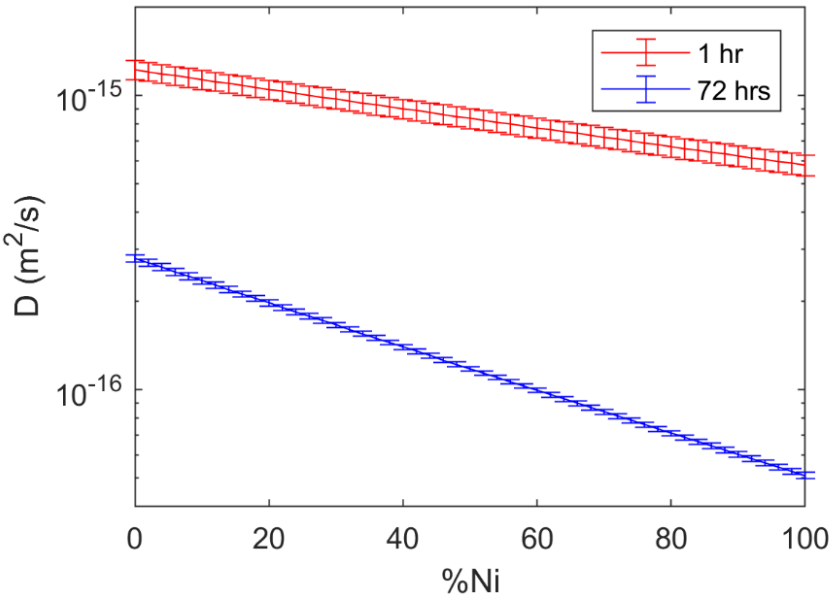

Figure 4.12: Time variation of the D(C) at 1 hr and 72 hrs in Cu-Ni diffusion couple at 600 ^{o}C

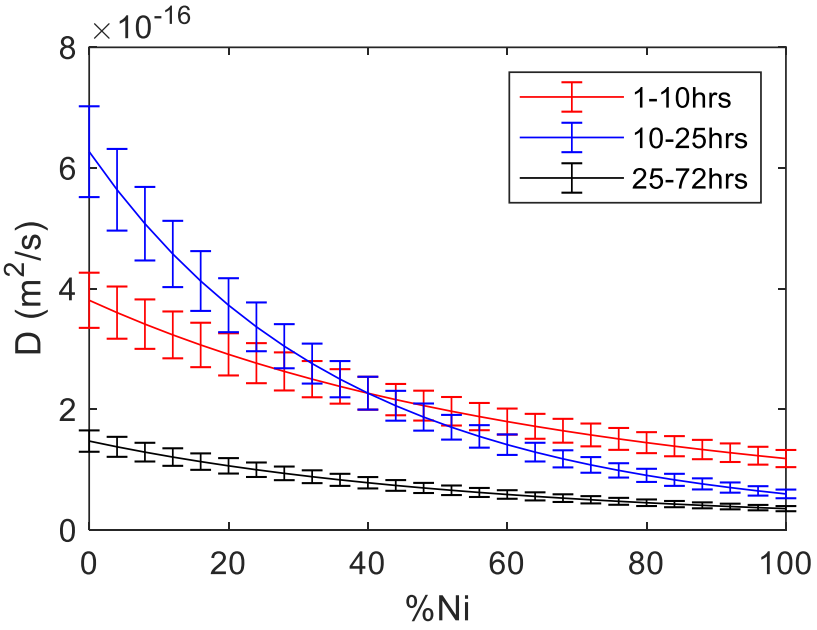

Figure 4.13: Different time interval variation of the D(C) in Cu-Ni diffusion couple at 600 ^{o}C

Table 4.2: Concentration-average diffusivity at different times for Cu-Ni system

Time (hrs)	Concentration-average diffusivity (m^2/s) (10^{-16})	% Change of D_{ave} from 1 - 10 hrs	% Change of D_{ave} from 10 - 25 hrs
25-72	0. 81	65%	68%
10-25	2.50	7%	--
1-10	2.33	--	7%

Other possible causes of the time variation in the D(C) are (i) the presence of residual stress in the material prior to the diffusion process and (ii) grain growth during diffusion, and for the following reasons, these factors are not responsible for the observed time variation in D(C). The time variation of D(C) is not due to grain growth because the Ag-Cu and Cu-Ni samples subjected to 1 hr and 72 hrs of diffusion heat treatments showed no significant grain growth under microstructural examination. The average grain size of the Cu substrate in the Cu-Ni diffusion couple, after 1 hr and 72 hrs, is 30 μm and 32 μm, respectively. Likewise, in the Ag-Cu system, the average grain size of the Ag substrate is 582 μm and 586 μm, respectively, after 1 hr and 72 hrs of diffusion. Similarly, residual stress in the material prior to the diffusion process cannot be attributed to the time variation of D(C) because prior to the diffusion heat treatments, the materials were not subjected to any form of mechanical loading that could have generated the residual stress. The diffusion temperatures in both systems are above the stress relief temperatures of the Ag substrate in the liquid-solid couple and the Cu and Ni solids in the solid-solid diffusion couple. Also, possible errors due to the profiles prior to diffusion, grain growth, and the presence of residual stress cannot account for an increase in the concentration-averaged diffusion coefficient. Therefore, these three factors cannot explain the observed time variation of D(C) in this work. Although grain growth and residual stress cannot explain the observed variation in the concentration dependence of interdiffusion coefficient with time, the behavior can nonetheless be related to the concept of DIS [6]–[9]. Considering that strain affects diffusion coefficient coefficients [10]–[15], and the magnitude of strain induced by interdiffusion is dependent on concentration gradient [8], it is logical that D(C) can change with concentration gradient, which varies with both concentration and time. Therefore, it is conceivable that D(C) could change with both concentration and time.

4.4 Implications of time variation of concentration dependence of interdiffusion coefficient

In a binary alloy system with a constant surface concentration (SC) and no solute build-up at the boundary of the substrate, the migration of a specific amount of concentration is typically linearly dependent on the square root of time; this is called the parabolic law. In the literature, phase change processes are reportedly exclusively controlled by diffusion when they follow the parabolic rule [93]–[96]. Deviation from the parabolic rule is assumed to result from an interfacial reaction, grain growth, or a combination of diffusion and other processes. Solutions of Fick's second law show that the parabolic law is only valid when the D(C) does not change; however, in this work, D(C) is time-dependent during diffusion, and there is no significant difference in grain size and no interfacial reaction. To investigate the implication of the time variation of D(C) and how it affects the parabolic law, a constant D(C) obtained between 1-5 hrs in the Ag-Cu system and 1-10 hrs in the Cu-Ni system are used to simulate the diffusion process between 1 hr and 72 hrs. Also, the D(C,t) obtained by fitting the D(C) at various time intervals, shown in Figures 4.5 and 4.7, is used to simulate the diffusion process between 1 hr and 72 hrs. The migration of the penetrating solute with 0% Ni and 0% Cu in the Cu-Ni and Ag-Cu systems is plotted against the square root of the diffusion time for the experiment and simulations obtained with D(C) and D(C,t) functions. The plotted simulated penetration, experimental penetration of the solute, and theoretically derived migration of the penetrating solute from a previous theoretical analysis are presented in Figure 4.14. The values reported in Figures 14a and 14b, and 14c are for the Ag-Cu system, Cu-Ni system, and a theoretical system with DIS, respectively. The results show that the prediction using a constant D(C) obeys the parabolic law but is erroneous when compared to the experimental results. In contrast, the simulations that use D(C,t) deviate from the parabolic law and are in excellent

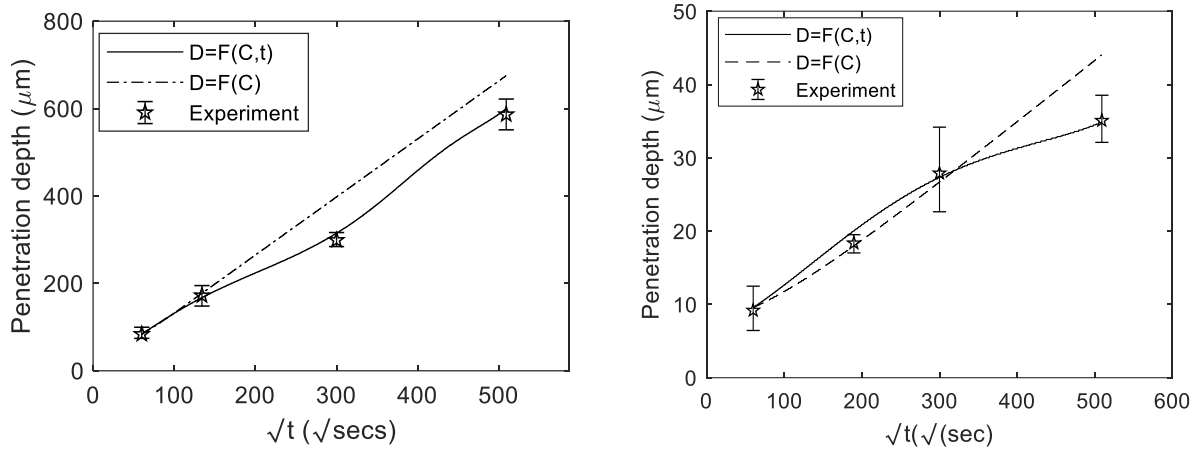

(a) (b)

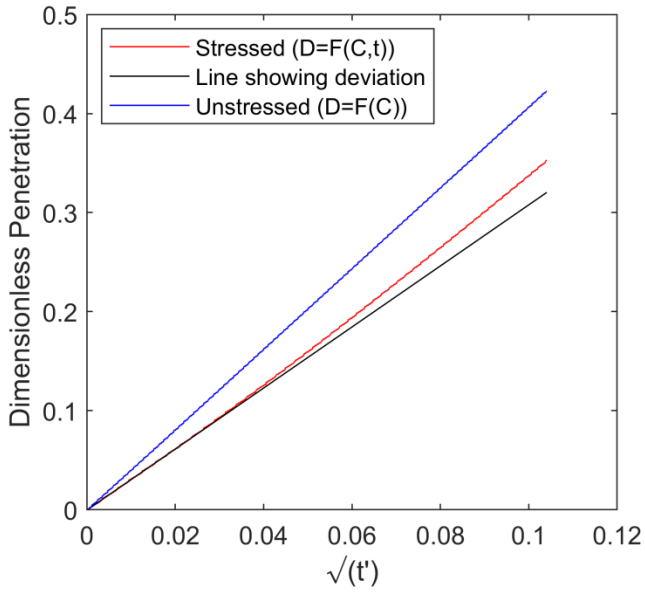

(c)

Figure 4.14: Solute penetration depth vs square-root of time for (a) Experimental Ag-Cu at 820 ^{o}C, (b) Experimental Cu-Ni at 600 ^{o}C, and (c) Theoretical computation (same data used to produce Figure 4.1 but a longer diffusion time of t' = 0.0108)

agreement with the experimental results. Therefore, the results show that it is possible for a solute transport event, with boundary conditions of a constant surface concentration (**SC**) and no solute build-up to be exclusively diffusion-controlled and not follow the parabolic law. Therefore, the time variation of D(C) can help to re-interpret the mechanism phase transformations because it is possible that systems exclusively controlled by volume diffusion do not obey the expected parabolic law.

The second implication of the time variation of D(C) is the possibility of a significant error in theoretical model predictions. To illustrate this point, the depth of the solute penetration for 72 hrs, which is predicted by using the constant D(C) obtained between 1-5 hrs in the Ag-Cu diffusion system, and experimentally are 600 μm and 675 μm, respectively (Figure 4.14a). Also, in terms of the diffusion time required to attain the same extent of solute penetration obtained experimentally after 72 hrs, the D(C) predicts 57 hrs, which is a difference of 15 hrs. Similarly, in the Cu-Ni system, the extent of solute penetration predicted by the D(C) for 72 hrs obtained between 1-10 hrs is 44 μm, while the experimentally obtained depth of penetration is 35 μm (Figure 4.14b). The same significant error in the theoretical model predictions was observed in the theoretical calculations in the Ag-Cu system (Figure 4.14c). Interestingly, in both the Ag-Cu and Cu-Ni diffusion systems, the D(C,t) accurately predicted the solute penetration. A second prediction error that can arise from using a constant D(C) is a theoretical solute distribution that is erroneous, which can affect the material property predictions. To further show this, the constant D(C) obtained at 1-10 hrs and 1-5 hrs in the Cu-Ni and Ag-Cu diffusion couples, respectively, along with the D(C,t) in both systems, are used to predict the solute profile after 72 hrs of diffusion. The simulated and experimentally obtained solute distributions are presented in Figure 4.15. The results for the Ag-

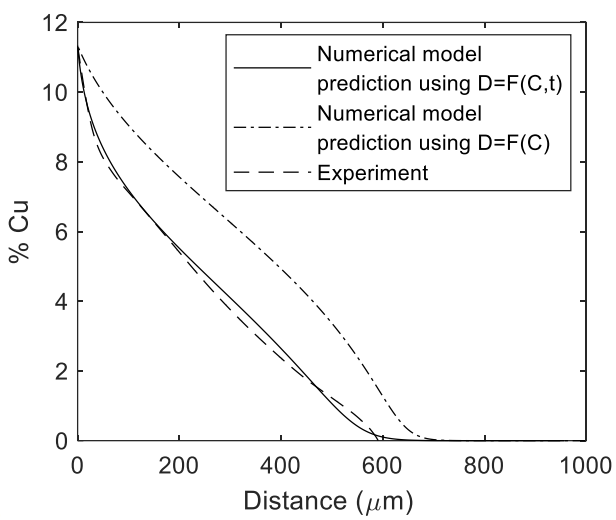

(a)

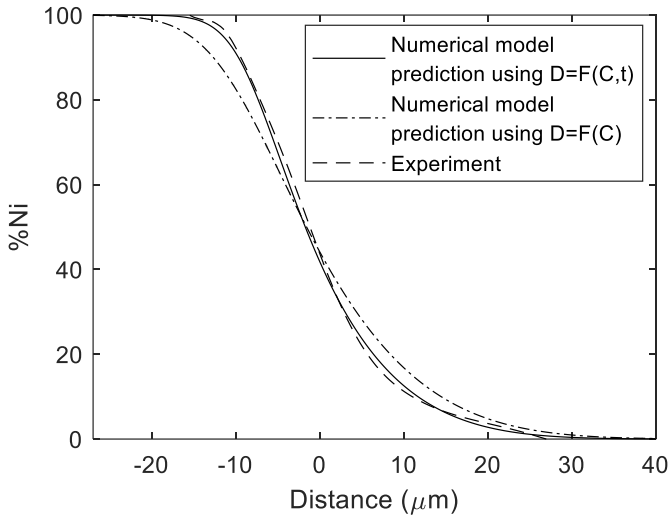

(b)

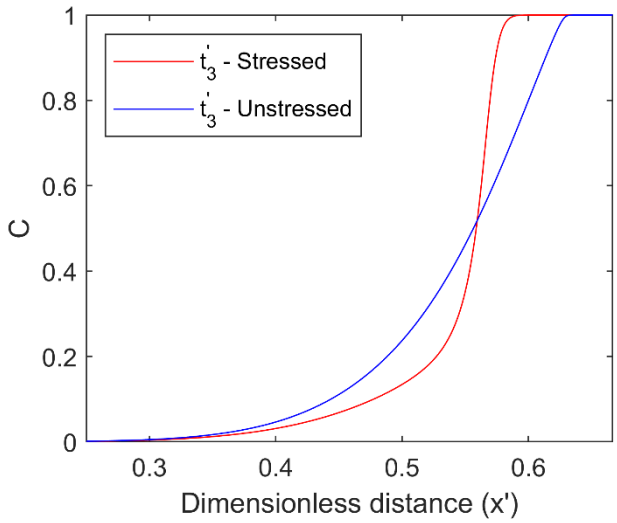

(c)

Figure 4.15 Concentration distribution at 72 hrs for (a) Ag-Cu at 820 ^{o}C and (b) Cu-Ni at 600 ^{o}C (c) Theoretical computation (same data used to produce Figure 4.1)

Cu system are presented in Figure 4.15a, the Cu-Ni system in Figure 4.15b, and theoretical simulations in Figure 4.15c. Figure 4.15 shows that when the profiles predicted with a constant D(C) are compared with the actual solute distribution, there are substantial errors in the theoretical model prediction of the solute profile. On the other hand, for simulations that use D(C,t), there is a good agreement between the experimentally obtained and theoretically predicted concentration profiles (Figures 4.15a and 4.15b). This experimental implication is also theoretically investigated, where the constant D(C) from DIS-free systems is compared to the DIS conditions where the effective D(C) is time-dependent. There are also large errors between the profiles obtained using a constant D(C) in a DIS-free systems and profiles from DIS system at the final diffusion time (Figure 4.15c). Therefore, neglecting the time variation of D(C) can lead to erroneous theoretical predictions and misidentification of the mechanism of microstructural changes caused by phase transformation reactions.

CHAPTER FIVE

5 EFFECT OF TEMPERATURE ON CONCENTRATION-DEPENDENT INTERDIFFUSION COEFFICIENT

5.1 Introduction

The Arrhenius equation is generally used in the literature to describe the functional relationship between D(C) and temperature. Two key parameters are used in the Arrhenius equation to evaluate the D(C) at any given temperature, and these are the concentration-dependent activation energy (**Q(C)**) and pre-exponential factor (**D_0(C)**). Interestingly, when the D(C) at different temperatures are known, the Q(C) and D_0(C) can be determined. The literature generally assumes that Q(C) and D_0(C) in the Arrhenius equation methodically vary only with concentration as the interdiffusion coefficient changes with concentration [4]. Hence, Q(C) and D_0(C) are considered to be time independent [97]. The assumption of a constant Q(C) and D_0(C) neglects the DIS which changes the D(C) as diffusion progresses with time. As shown in Chapter 4 of this thesis, D(C) that are used to evaluate the Q(C) and D_0(C), can change with diffusion time. Considering that Q(C) and D_0(C) are calculated from D(C) data, it is important to study how changes in temperature influences the time dependent DIS, and the concomitant influence on the D(C), Q(C), and D_0(C). Therefore, the aims in this chapter are to carry out a theoretical study and an experimental verification of the effect of temperature on D(C). To do so, the possible time variations of Q(C) and D_0(C), which are used to calculate the D(C) at different temperatures, will be studied theoretically by using the numerical model developed in section 3.2. The theoretical findings will

be experimentally verified by coupling the FSM [88] and the new numerical model developed in section 3.3 to extract accurate interdiffusion coefficients from experimental data.

5.2 Theoretical Study of The Effect of Temperature on D(C)

5.2.1 Time variation in Q(C) and D_0(C) at different temperatures

The pressure equation, presented in Equation 3.6, shows that there is a simultaneous generation and relaxation of DIS during diffusion. The stress relaxation results in the Kirkendall effect or the movement of the diffusing interface. Taking into consideration the dynamic nature of the DIS, it is important to theoretically study how the DIS can theoretically influence interdiffusion coefficients, activation energy, and frequency factors at different times. The theoretical equations for solute distribution and pressure under DIS, presented in Chapter 3, will be used here. The relationship between stress-free impurity diffusivities and temperatures will be assumed to follow the Arrhenius equation for accurate simulation purposes. Based on the Stokes-Einstein relationship (Equation A.11), the viscosity is expected to follow an inverse relationship with the minimum stress-free impurity diffusivity and a direct relationship with temperature. The table of dimensionless data for simulation is presented in Table 5.1. To further show the validity of the stress-free impurity diffusion coefficients, an Arrhenius plot of the natural logarithm of stress-free tracer diffusion coefficients against the inverse of temperature is plotted and presented in Figure 5.1. Also, the viscosity values in the tables obey the Stokes-Einstein relationship among viscosity, temperature, and minimum stress-free intrinsic diffusivity, which is $\eta' D_2^{*'} / T'$ = constant. As seen in the dimensionless groups in Chapter 3, the α' term in the thermodynamic constant is related to

Table 5.1: Diffusion parameters for the theoretical study of Time variation in Q(C) and $D_0(C)$

T'	$D_1^{*'}$	$D_2^{*'}$	V_1'	V_2'	η'	α'
0.0027	1	0.05	0.6875	1	0.2708e-04	-4.5
0.0036	2	0.075	0.6875	1	0.2347e-04	-3.4615
0.0110	9.5	0.1868	0.6875	1	0.2900e-04	-1.125

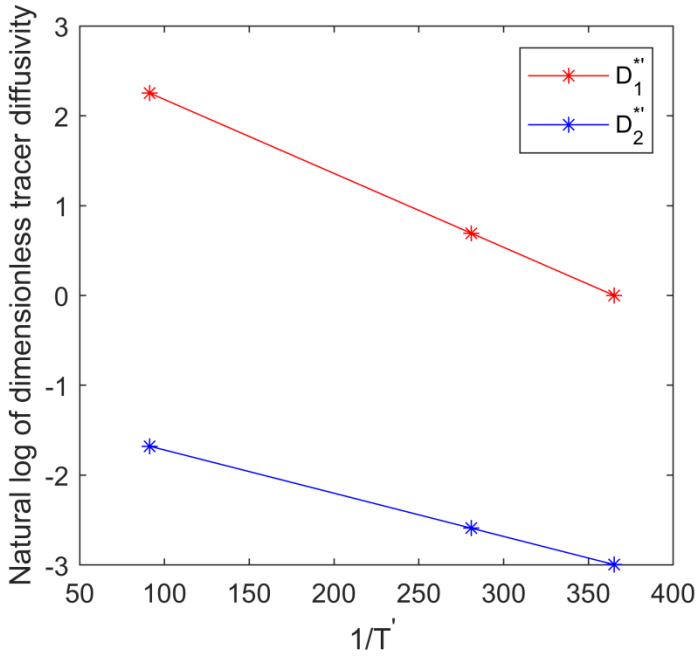

Figure 5.1: Arrhenius plot of the natural logarithm of dimensionless stress-free tracer diffusion coefficients against the inverse of dimensionless temperature

the temperature with the relationship $\alpha' T'$ = constant.

The concentration profiles at the different dimensionless diffusion times of 0.000135, 0.000903, and 0.0027 are calculated for each temperature. The concentration profiles for dimensionless temperatures of 0.0027, 0.0036, and 0.0110 are shown in Figures 5.2a, 5.2c, and 5.2e, respectively. Similarly, the pressure gradients are presented in Figures 5.2b, 5.2d, and 5.2f for dimensionless temperatures of 0.0027, 0.0036, and 0.0110, respectively. The effective D(C) of each profile and corresponding pressure gradients is calculated using Equation 3.21 and presented in Figures 5.3a, 5.3b, and 5.3c for dimensionless diffusion times of 0.000135, 0.000903, and 0.0027, respectively. The figures reported in Figure 5.3 show that the effective D(C) can change independently with time at different temperatures. By implication, the rate of stress generation and relaxation with time is different at different temperatures. These results convincingly show that the effective isothermal D(C) changes with time independently at different diffusion temperatures.

5.2.2 Theoretical concentration-dependent activation energy and frequency factor

The Arrhenius law defines the relationship between interdiffusion coefficients and temperature. The general form of the Arrhenius equation is [4]:

$$D_{eff}(C) = D_0(C)\exp\left(-\frac{Q(C)}{KT}\right) \qquad 5.1$$

From the definition of dimensionless parameters,

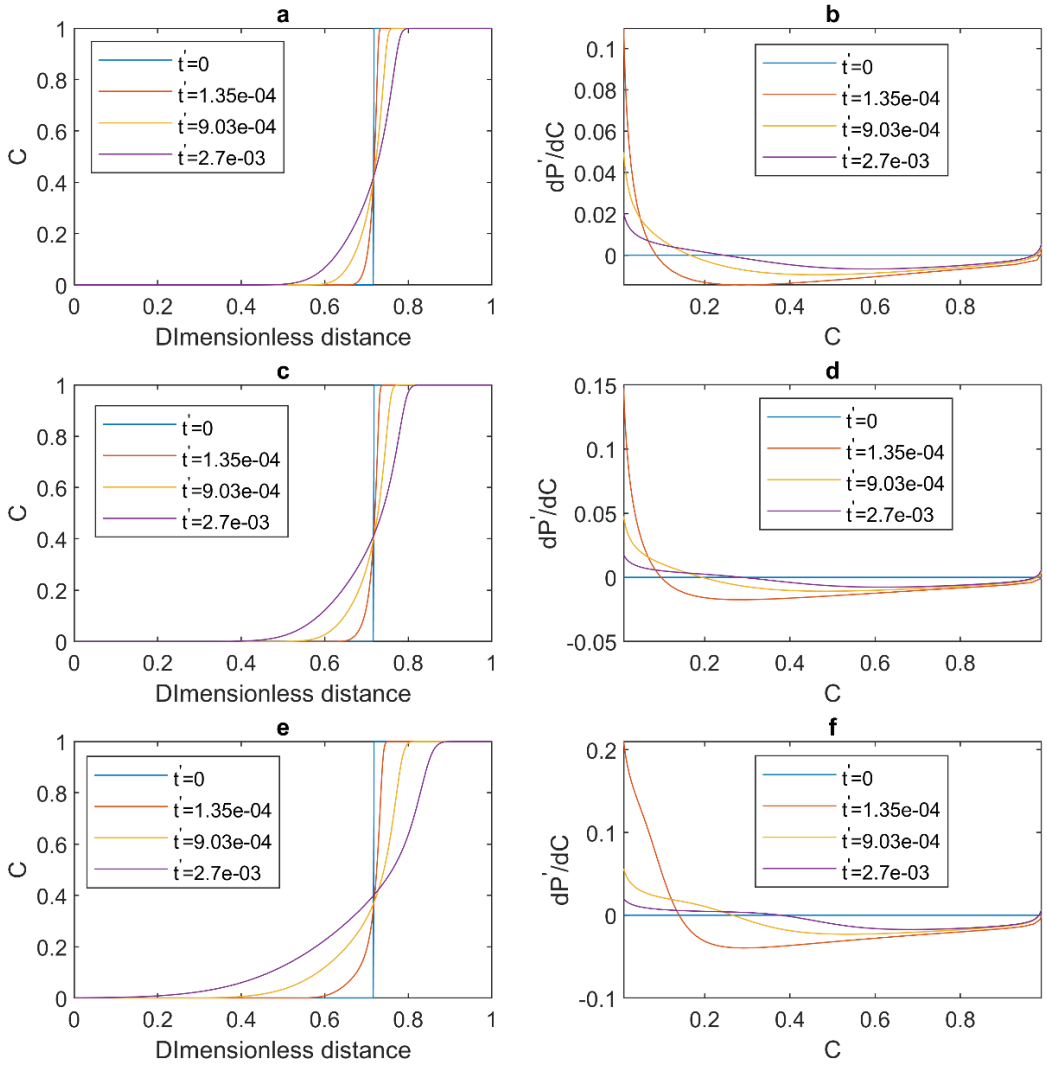

Figure 5.2: Theoretical concentration dependence of the dimensionless concentration profiles at different dimensionless diffusion times and dimensionless temperatures of (a) concentration profiles at T'=0.0027, (b) pressure gradients at T'=0.0027, (c) concentration profiles at T'=0.0036, (d) pressure gradients at T'=0.0036, (e) concentration profiles at T'=0.0110, and (f) pressure gradients at T'=0.0110

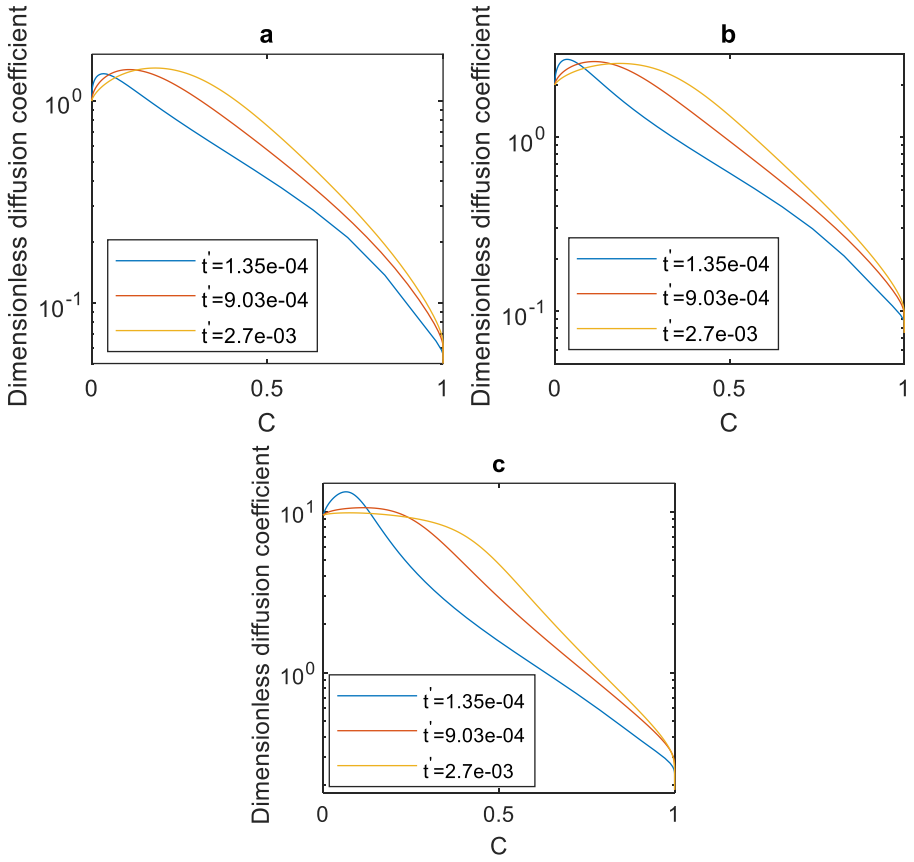

Figure 5.3 Theoretical concentration dependence of the interdiffusion coefficient at different dimensionless diffusion time and dimensionless temperatures of (a) T'=0.0027, (b) T'=0.0036, and (c) T'=0.0110

Therefore $Q'(C) = \frac{Q(C)}{EV_m}$

$$T' = \frac{T}{\left(\frac{EV_m}{K}\right)} \qquad D'_{eff}(C) = D_{eff}(C)/D_m \qquad D'_0(C) = D'_0(C)/D_m$$

Therefore, the dimensionless form of the Arrhenius equation (Equation 5.1), can be written as:

$$D'_{eff}(C) = D'_0(C)\exp\left(-\frac{Q'(C)}{T'}\right) \qquad 5.2$$

where Q' is the dimensionless activation energy and D'_0 is the dimensionless frequency factor or pre-exponential factor

The dimensionless concentration-dependent activation energy ($Q'(C)$) and dimensionless concentration-dependent frequency factor ($D'_0(C)$) can be calculated from the interdiffusion coefficients in Figure 5.3. To verify the Arrhenius equation, the natural logarithm plots of the interdiffusion coefficient against the inverse of temperature at a dimensionless time of 0.000135 and specific compositions of 0.20, 0.40, 0.60, and 0.80 are plotted in Figure 5.4. The figure shows that at the dimensionless time of 0.000135, the Arrhenius plots that are stress-free and the plots subjected to stress differ due to the DIS. The Arrhenius plots for other dimensionless diffusion times of 0.000903 and 0.0027 are plotted in Figures 5.5 and 5.6. These plots show changes with concentration but not with time in a stress-free system (versus Figures 5.4a, 5.5a, and 5.6a). The Arrhenius plots for the same composition in a DIS considered system (Figure 5.7) show that the slope changes with time. The slope in Figures 5.6 and 5.7 represents the dimensionless $Q'(C)$, and

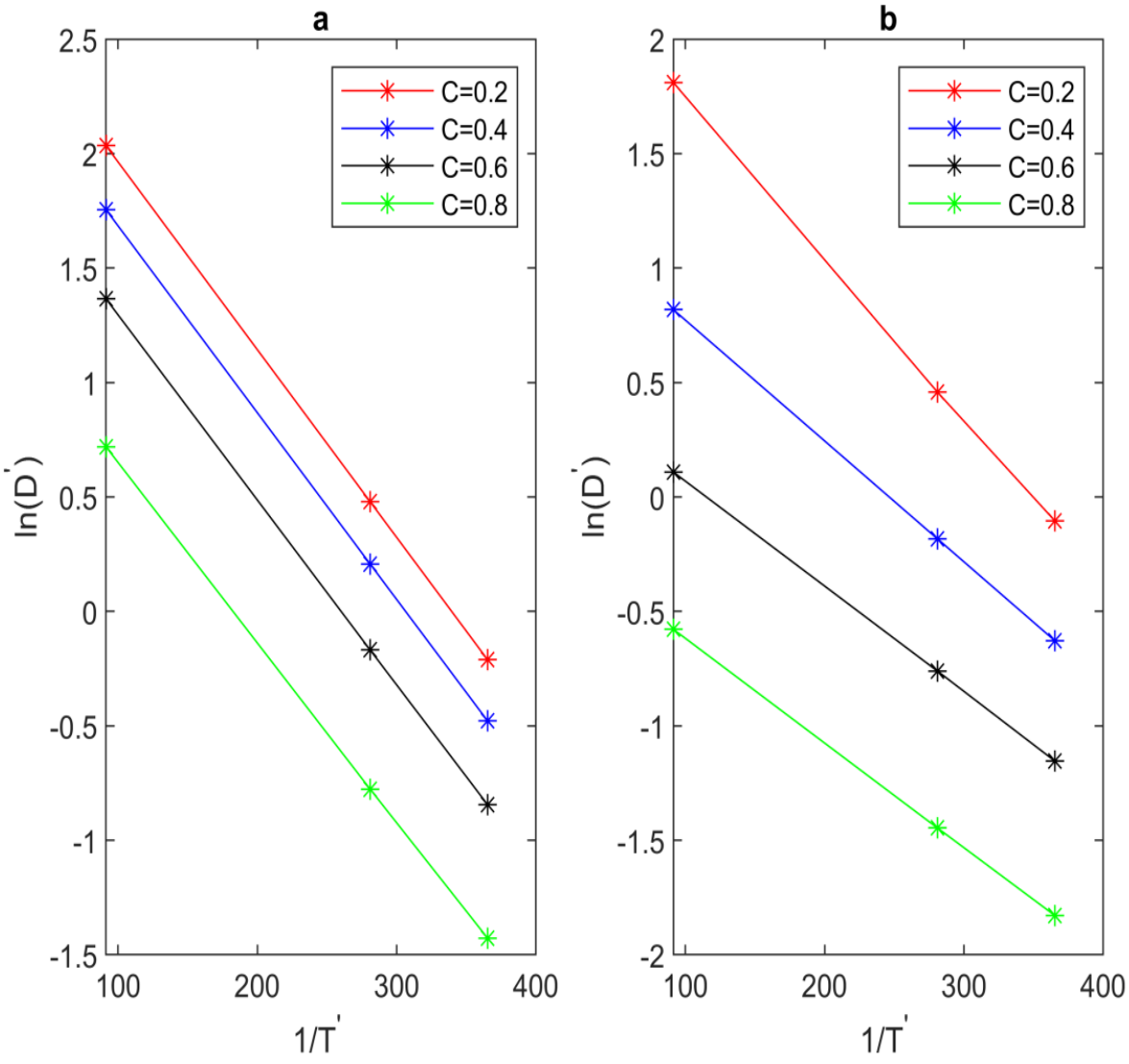

Figure 5.4 Theoretical dimensionless temperature dependence of the interdiffusion coefficients at dimensionless time of 0.000135 for (a) stress-free (b) DIS influenced

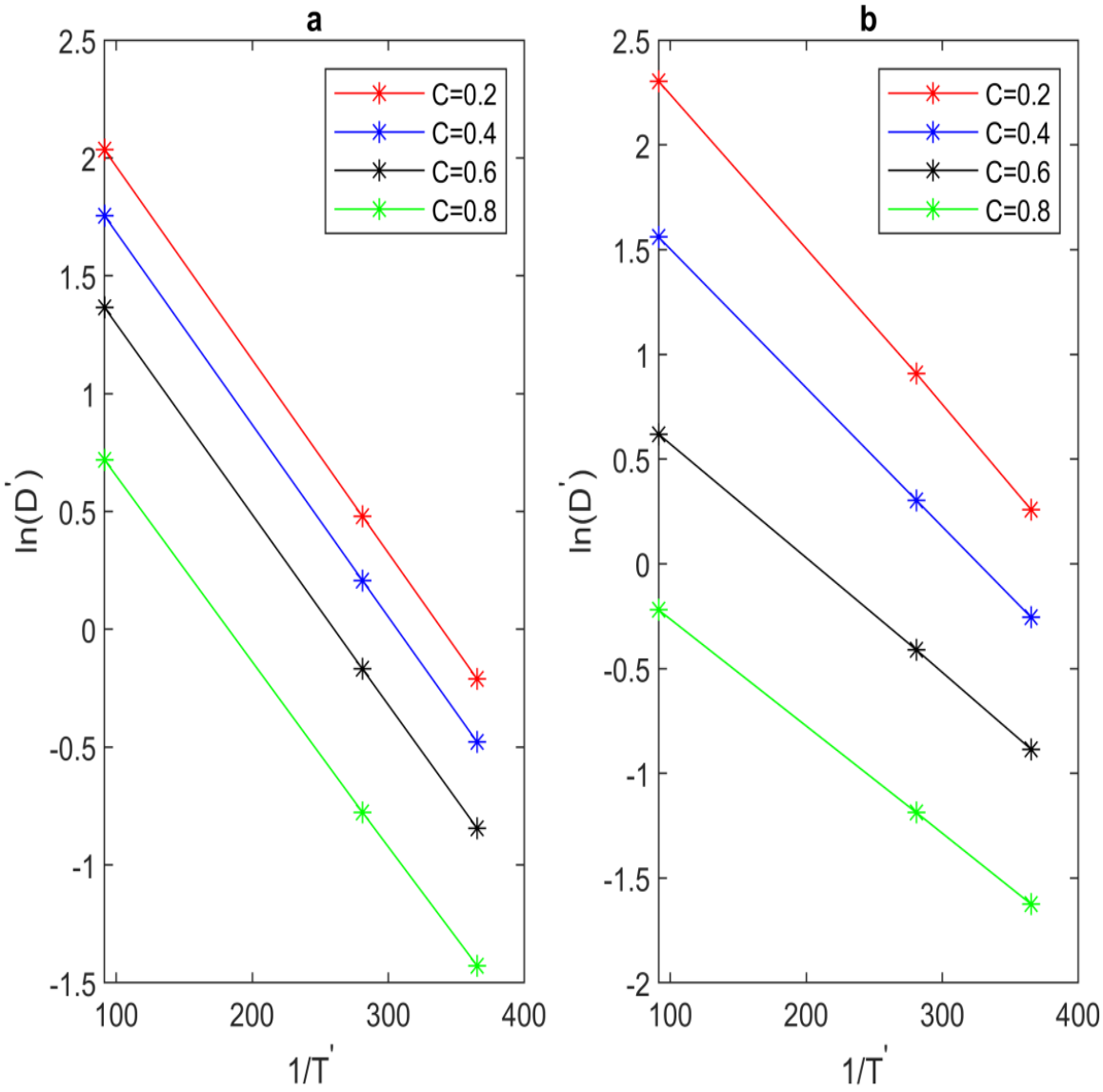

Figure 5.5 Theoretical dimensionless temperature dependence of the interdiffusion coefficients at dimensionless time of 0.000903 for (a) stress-free (b) DIS influenced

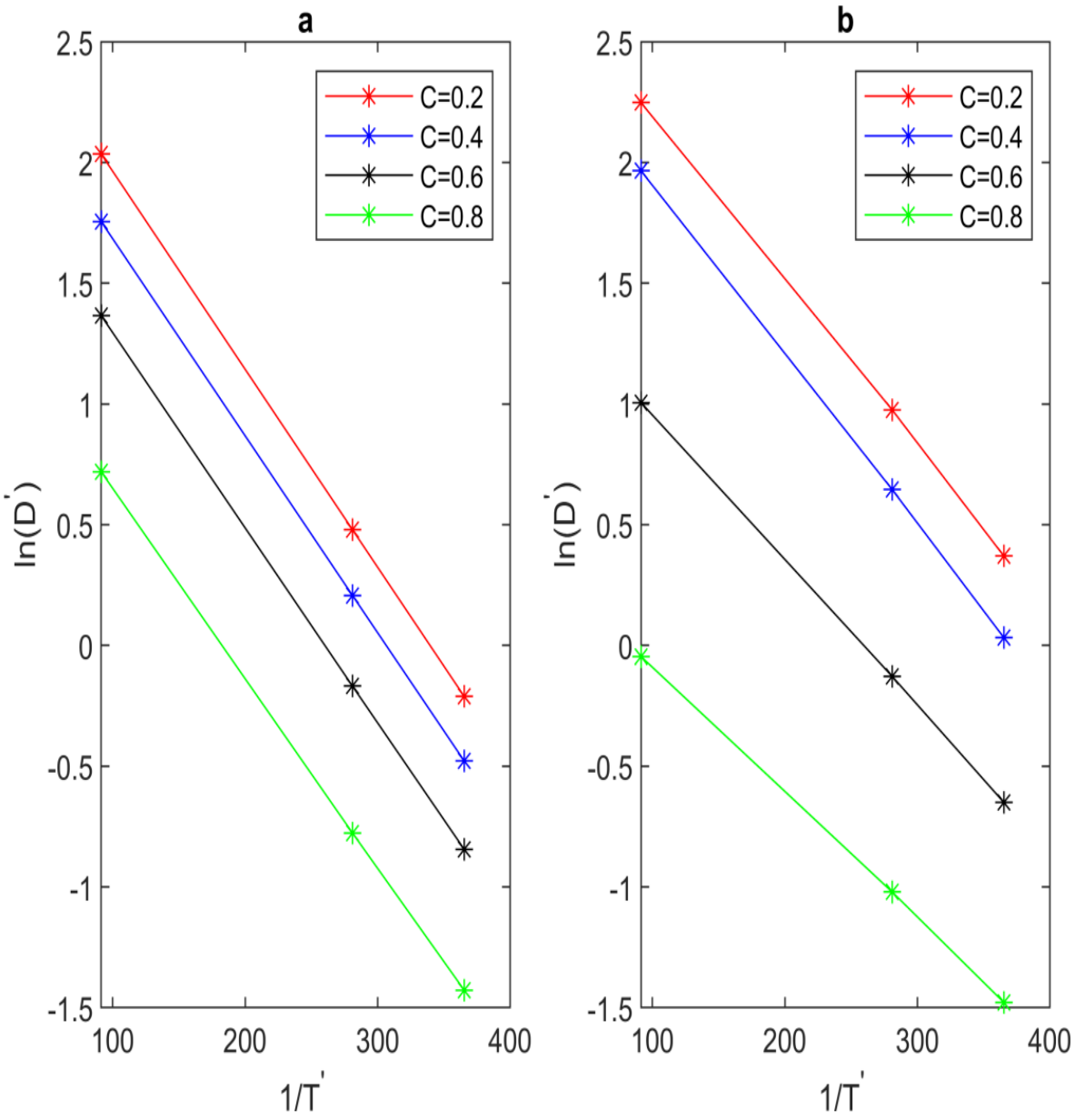

Figure 5.6 Theoretical dimensionless temperature dependence of the interdiffusion coefficients at dimensionless time of 0.0027 for (a) stress-free (b) DIS influenced

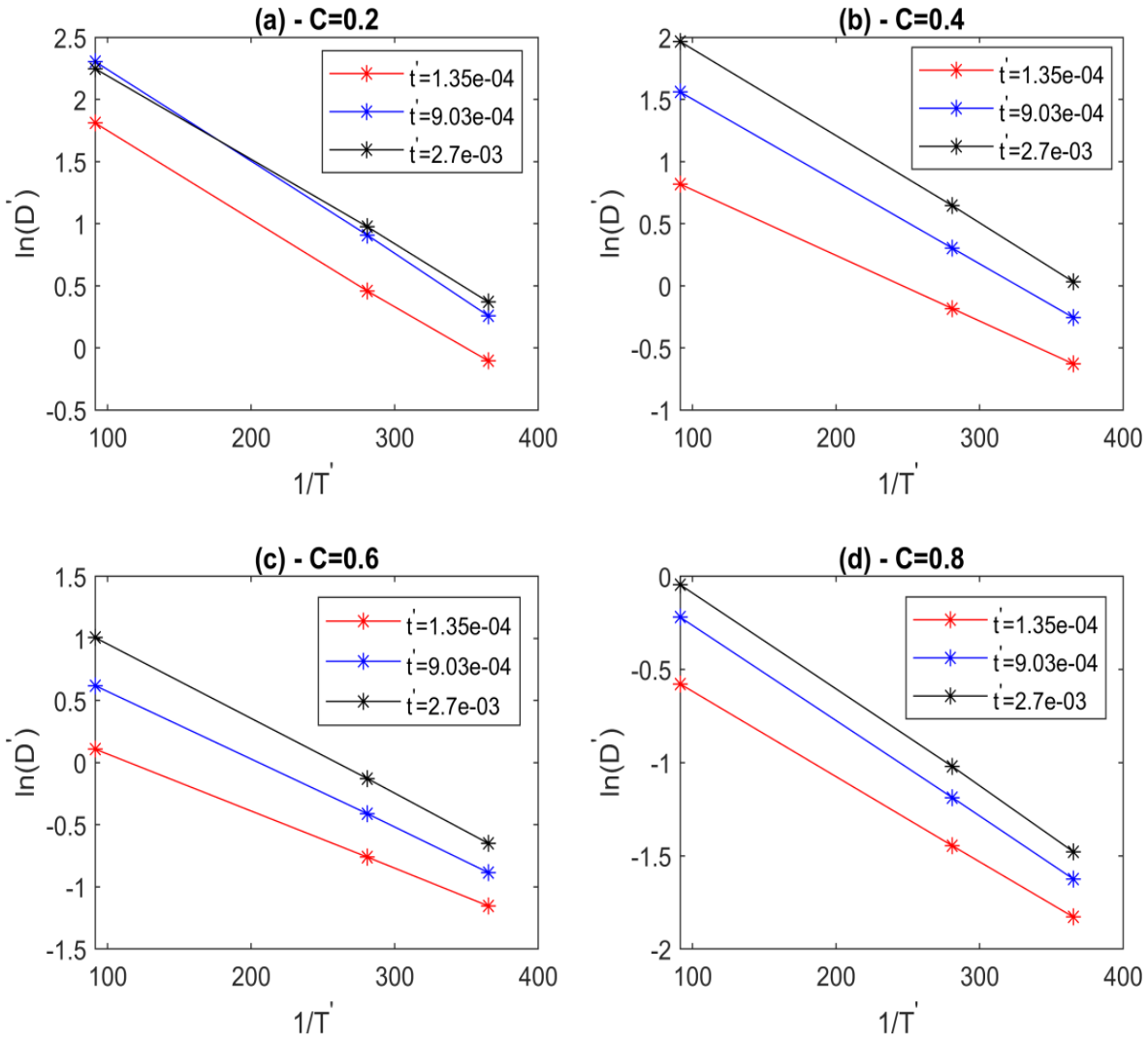

Figure 5.7 Theoretical dimensionless temperature dependence of the interdiffusion coefficients at different diffusion times for concentrations of (a) C=0.2 (b) C=0.4 (c) C=0.6 (d) C=0.8

the vertical intercept of the plot is the dimensionless $D_0'(C)$. The $Q'(C)$ and $D_0'(C)$ for different compositions and at different times are calculated. The dependence of the activation energy and frequency factor is illustrated in Figures 5.8 and 5.9, respectively. They show that the activation energy and frequency factor change with the composition in both systems that are subjected to either stress or without stress conditions. While the activation energy and frequency factor change with the composition, the plots at different times show that when the DIS is neglected, $Q'(C)$ and $D_0'(C)$ are time independent. In contrast, when DIS is considered, $Q'(C)$ and $D_0'(C)$ change with time.

5.2.3 Effect of temperature on concentration-dependent interdiffusion coefficient

To theoretically study the effect of temperature on the interdiffusion coefficient at a particular diffusion time, the dimensionless equations; that is, Equations 3.22-3.27, were solved numerically for diffusion couples with the input parameters; see Table 5.2. For these simulations, the viscosities are related to the temperature using Stokes' law (Equation A.11), and the constant (α') in the thermodynamic factor is related to temperature using the thermodynamic equation. The simulated concentration profiles and pressure gradients are presented in Figures 5.10a and 5.10b, respectively. The calculated dimensionless D(C) for a system with diffusion-induced stress for each diffusion time were calculated using Equation 3.21 and presented in Figure 5.10c for each diffusion temperature. The figure shows that it is theoretically possible for a certain range of concentration to have a higher interdiffusion coefficient at a lower temperature when compared to the interdiffusion coefficient at a higher temperature. This anomalous behaviour has not been previously reported in the literature and it is attributable to the occurrence of DIS.

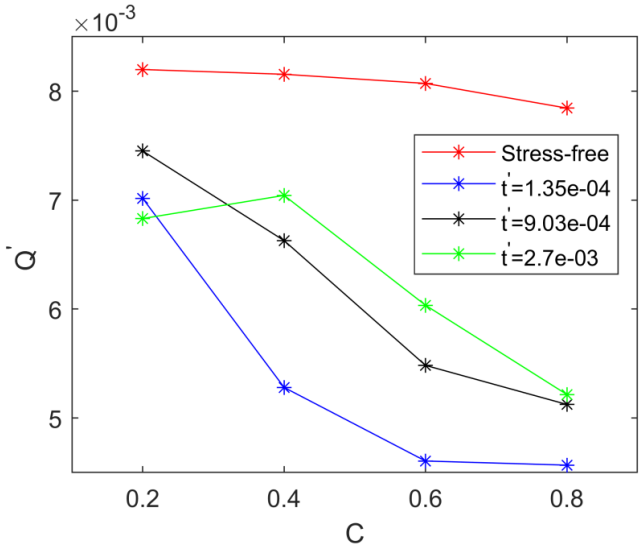

Figure 5.8: Theoretical stressed and unstressed concentration dependence of activation energy at different dimensionless diffusion times

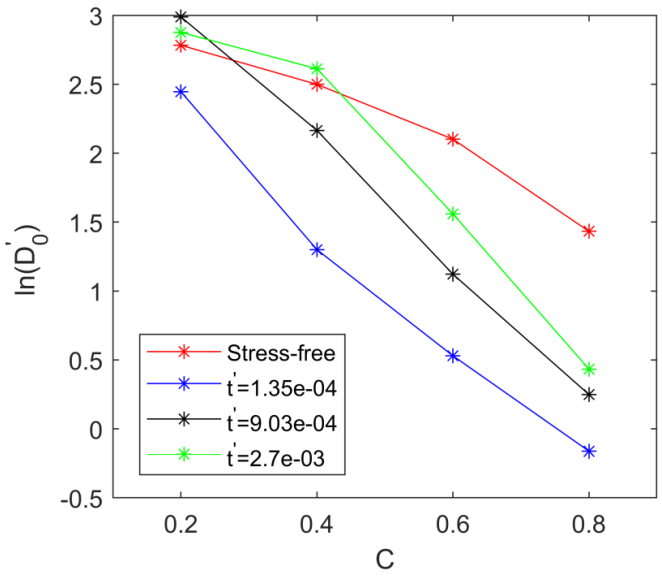

Figure 5.9: Theoretical stressed and unstressed concentration dependence of frequency factor at different dimensionless diffusion times

Table 5.2: Diffusion parameters for anomalous diffusivity

T'	$D_1^{*'}$	$D_2^{*'}$	V_1'	V_2'	η'	α'	t'
0.004	1	0.05	0.9091	1	0.9028e-4	-8.4825	0.0045
0.0096	1.2	0.2	0.9091	1	0.5417e-4	-3.5344	0.0045
0.0159	1.26	0.297	0.9091	1	0.6075e-4	-2.1206	0.0045

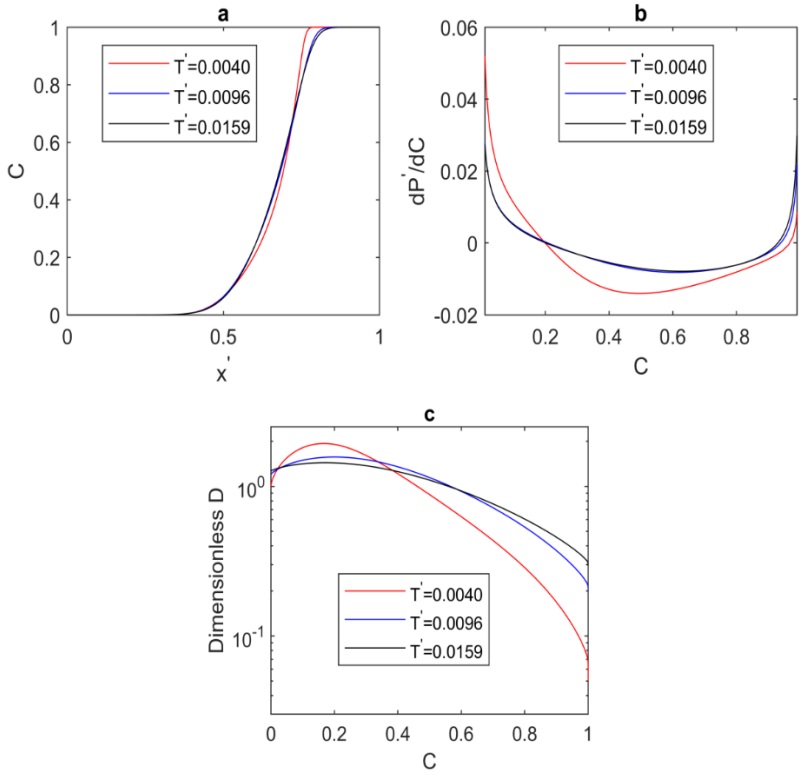

Figure 5.10: Theoretical simulation of anomalous diffusion at the same dimensionless diffusion time with (a) concentration profiles, (b) pressure gradients, and (c) D(C)

5.3 Experimental Verification

A two-phase solid-liquid Ag-Cu system with limited solubility is used to study the effect of temperature on D(C) at different times in a two-phase binary system. On the other hand, the Cu-Ni diffusion couple with unlimited solute solubility is used for the study in a single-phase binary system. The Ag-Cu solid-liquid diffusion couple, made using copper foil sandwiched between two solid Ag substrates, was subjected to diffusion heat treatment in vacuum at $790\,^{o}C, 820\,^{o}C,$ and $850\,^{o}C$ for durations of 1, 5, 25, 72, and 96 hrs. Similarly, the Cu-Ni diffusion couples made by electroplating Ni on Cu substrates were subjected to interdiffusion heat treatments at $550\,^{o}C, 580\,^{o}C,$ and $600\,^{o}C$ for durations of 1, 10, 25, and 72 hrs. The Cu-Ni diffusion heat treatment was carried out in an electric furnace under purified argon gas. Microanalyses by using X-ray energy and wavelength dispersive spectroscopy techniques were used to acquire the concentration profiles from each sample after the interdiffusion heat treatment. At least five concentration profiles were obtained from each sample, and the average profile per sample was calculated. The new numerical model in section 3.3, coupled with the FSM was used to extract the D(C) from the average experimental profiles. For each diffusion time and temperature, the experiments were repeated three times to obtain three average profiles, and the standard deviation of the error bars of diffusivity at each concentration was determined from the three average experimental profiles. Also, the concentration averaged diffusivity for each of the three average profiles was determined. In this investigation, the statistical variation of the concentration-average interdiffusion coefficient at a given time is less than 10% in the Cu-Ni system and 12% in the Ag-Cu system. The statistical variations obtained in this work are comparable to the statistical variation of 10% found in the literature [67], [90]–[92].

5.3.1 Concentration dependence of interdiffusion coefficient

The calculated average and standard deviation of the interdiffusion coefficient at a given concentration in the Ag-Cu system are plotted against the concentration in Figure 5.11. Similarly, the interdiffusion coefficient results for the Cu-Ni systems are shown in Figure 5.12.

Experimental concentration profiles were used as a reference profile to calculate D(C), removing any possible errors due to initial solute distribution before diffusion heat treatment. Hence, D(C) is calculated between the reference profile and experimental profiles obtained at a longer diffusion time. This approach of eliminating possible errors due to the presence of the initial solute is not possible by using conventional methods, such as the BM and SF methods that are often used to calculate D(C). However, by combining the FSM and the new numerical model in section 3.3, possible errors due to the presence of a non-uniform initial solute distribution can be eliminated. Therefore, the concentration profile at 1 hr is used as the common reference profile for each temperature in this study. This implies that the average concentration profiles at 1 hr are used as the initial condition. The D(C) that can simulate the final experimental concentration profile at the longer diffusion time, using the profile at 1 hr as the initial condition is calculated. This approach is used to calculate the D(C) between 1 and 10 hrs; 1 and 25 hrs; and 1 and 72 hrs in the Cu-Ni system. The calculated D(C) plots at various time intervals are presented in Figure 5.13. Similarly, the diffusion profile at 1 hr is also used as the reference profile in the Ag-Cu system. The D(C) is calculated between 1 and 5 hrs; 1 and 25 hrs; and 1 and 72 hrs, and the results are reported in Figure 5.14. The non-overlapping error bars for both Ag-Cu and Cu-Ni diffusion couples, in Figures 5.11-5.14, convincingly show that experimentally, the isothermal D(C) changes with time at different temperatures.

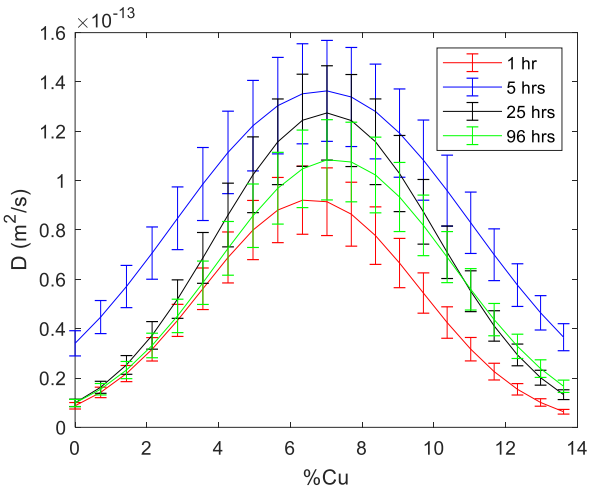

(a)

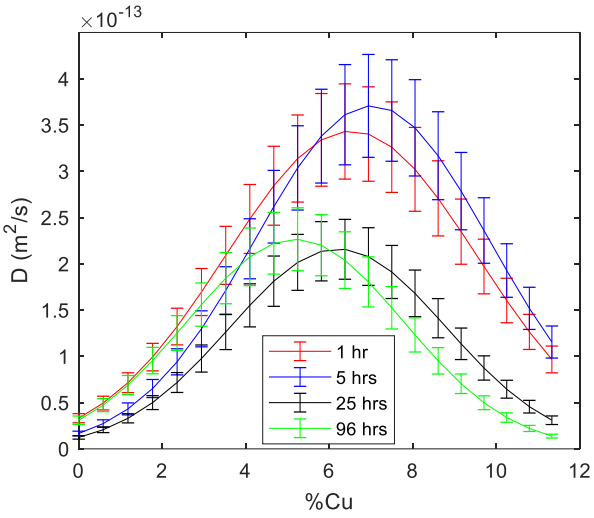

(b)

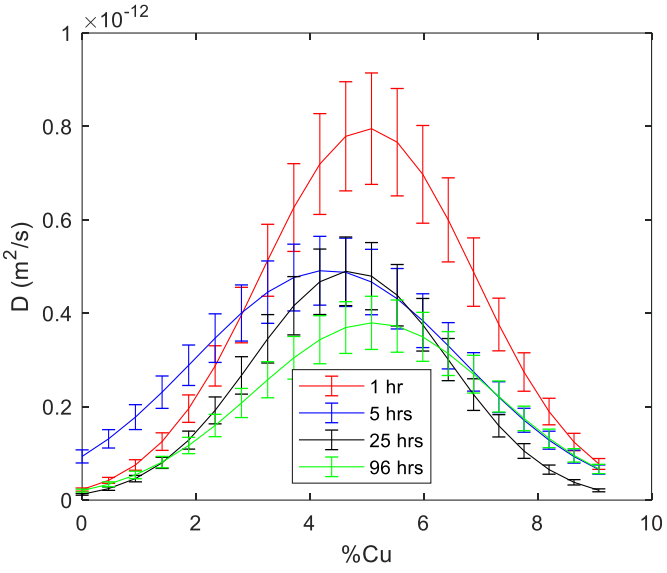

(c)

Figure 5.11: Concentration dependence of the interdiffusion coefficient of Ag-Cu interdiffusion couple at different diffusion times and temperatures (a) 790 ^{o}C (b) 820 ^{o}C (c) 850 ^{o}C

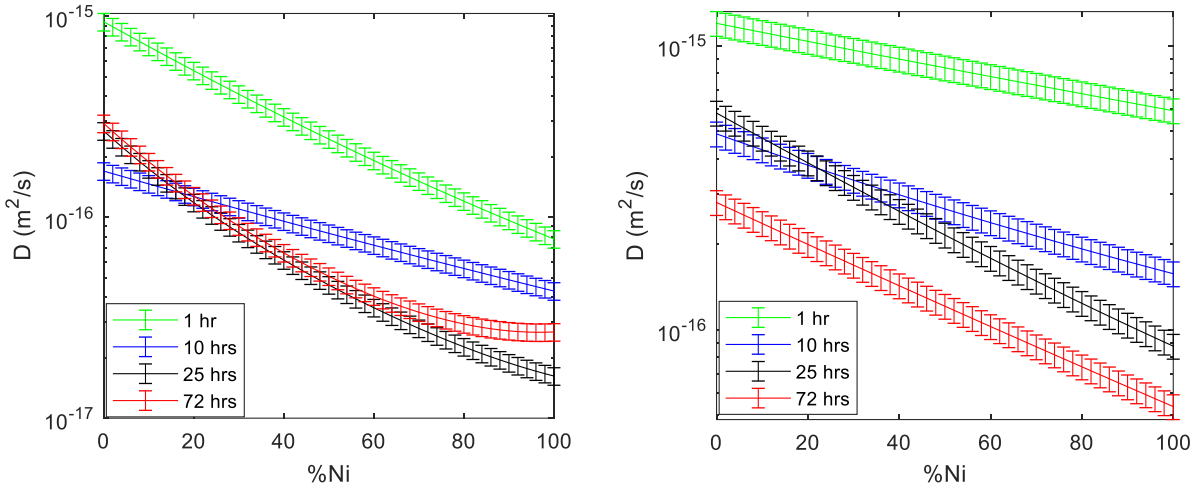

(a)

(b)

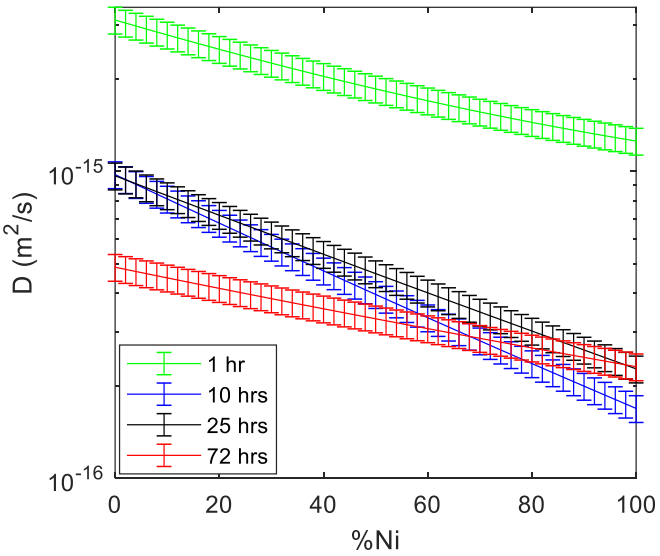

(c)

Figure 5.12: Cu-Ni Concentration dependence of the interdiffusion coefficient at different diffusion times and temperatures (a) 550 ^oC (b) 600 ^oC (c) 630 ^oC

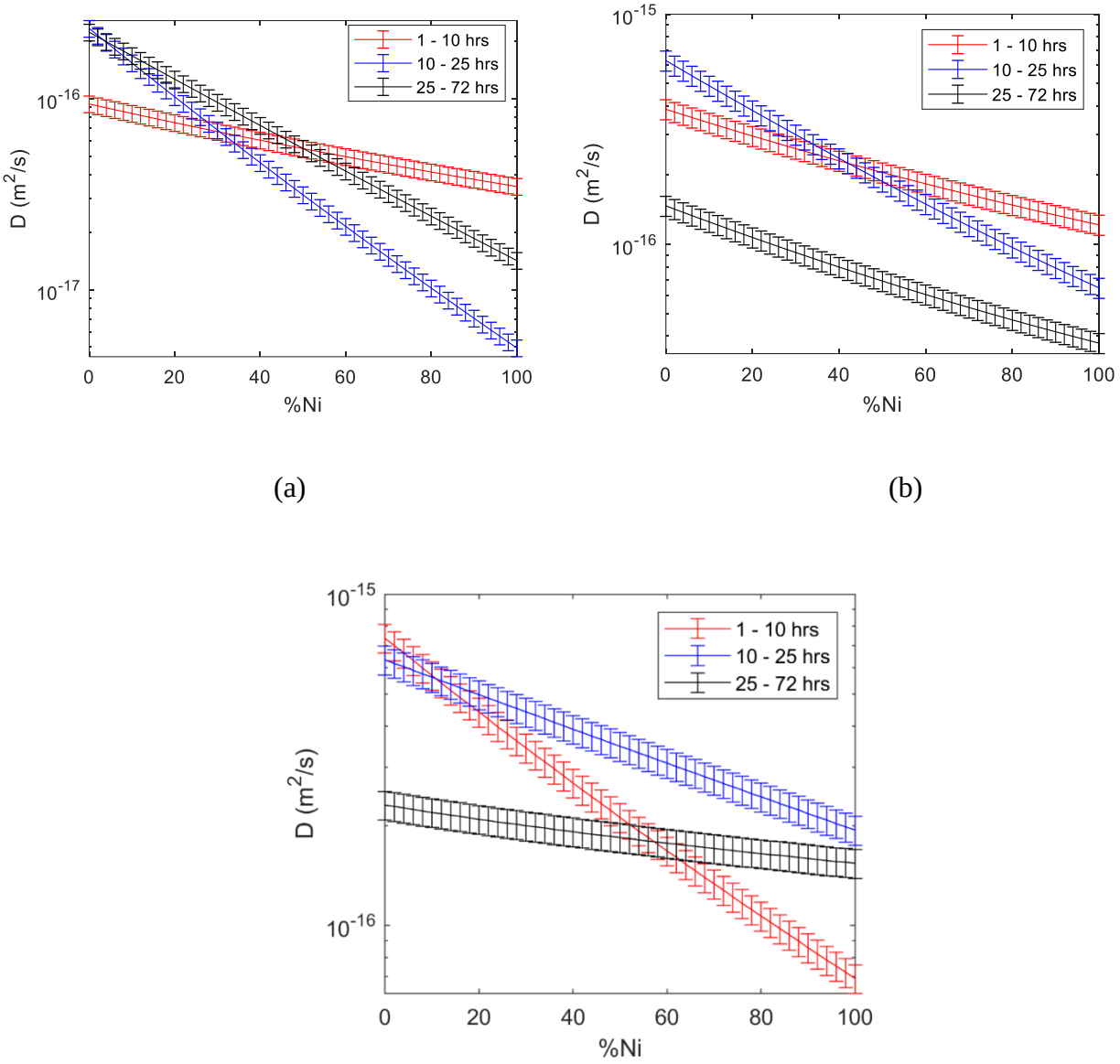

Figure 5.13: Cu-Ni concentration dependence of the interdiffusion coefficient operative in-between interdiffusion times and at temperatures of (a) 550 ^{o}C (b) 600 ^{o}C (c) 630 ^{o}C

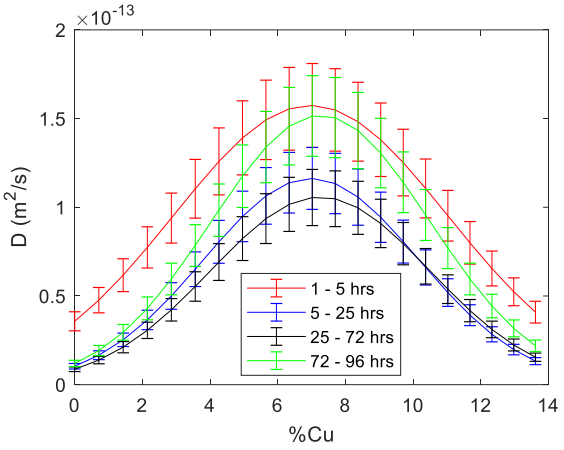

(a)

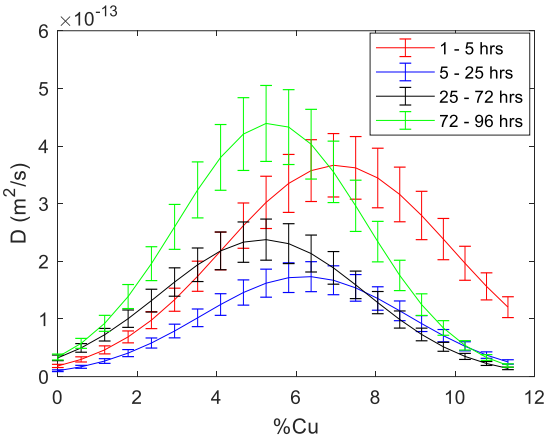

(b)

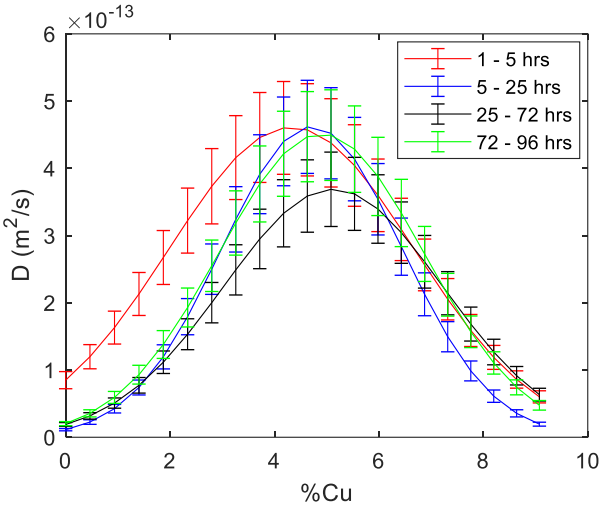

(c)

Figure 5.14: Concentration dependence of the interdiffusion coefficient of Ag-Cu interdiffusion couple operative in-between interdiffusion times and at temperatures of (a) 790 ^{o}C (b) 820 ^{o}C (c) 850 ^{o}C

5.3.2 Concentration-dependent activation energy and frequency factor

The Arrhenius law defines the relationship between the interdiffusion coefficients and temperature (see Equation 5.3). The Q(C) and D_0(C) can be calculated from the interdiffusion coefficients previously determined at various temperatures and diffusion times (Figures 5.11-5.14). To verify the Arrhenius equation, the natural logarithm of the interdiffusion coefficient against the inverse of temperature (Kelvin) at specific concentrations and a diffusion time at 25 hrs is plotted in Figure 5.15. The D_0(C) ranges between 4.6×10^{-9} m^2/s and $1.5\times10^{-4} m^2/s$, while the Q(C) ranges from 98kJ/mol-K to 204kJ/mol-K, which are consistent with the activation energy reported data in Wang et al. [4].

$$D(C) = D_0(C)\exp\left(-\frac{Q(C)}{N_A KT}\right) \qquad 5.3$$

The activation energy and frequency factors are also calculated for diffusion times of 1 hr and 10 hrs and the results are presented in Figures 5.16 and 5.17. The figures show that the concentration dependence of the activation energy and frequency factor in Cu-Ni diffusion systems change with time. Similarly, the Q(C) and D_0(C) in the Ag-Cu diffusion couple are also calculated for different diffusion times and the calculated values are presented in Table 5.3. The results of the two binary alloy systems, Cu-Ni and Ag-Cu, show the time variation in Q(C) and D_0(C). Similarly, the D(C), which removes any possible errors due to a variable initial solute concentration in the material before diffusion (Figures 5.13-5.14), is utilized to calculate the Q(C) and D_0(C). For the Cu-Ni diffusion system, the Arrhenius plots of the natural log of the diffusion coefficient against the inverse of temperature for 1-25 hrs are shown in Figure 5.18. The activation energy and frequency factors are calculated from the Arrhenius plots, and this repeated for other diffusion times. The Q(C) and D_0(C) in the Cu-Ni system are plotted for various times in Figures 5.19 and 5.20,

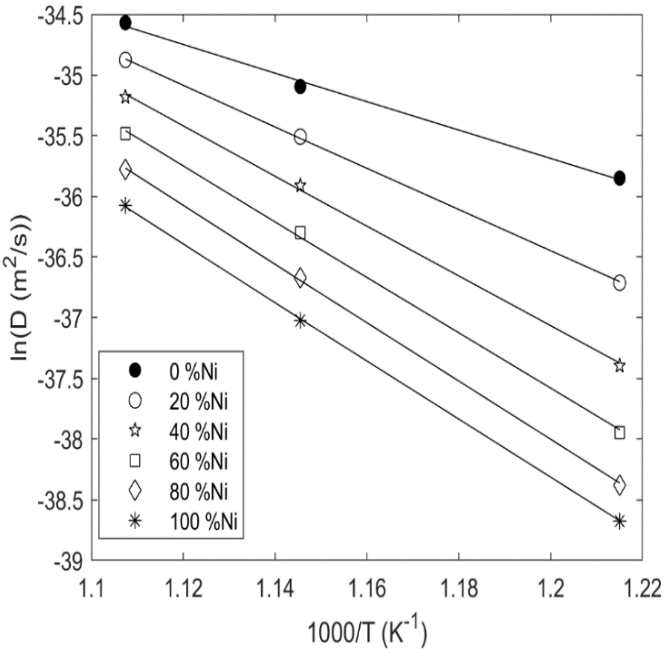

Figure 5.15: Temperature dependence of the interdiffusion coefficients at 25hrs diffusion time and 20 % interval of Ni

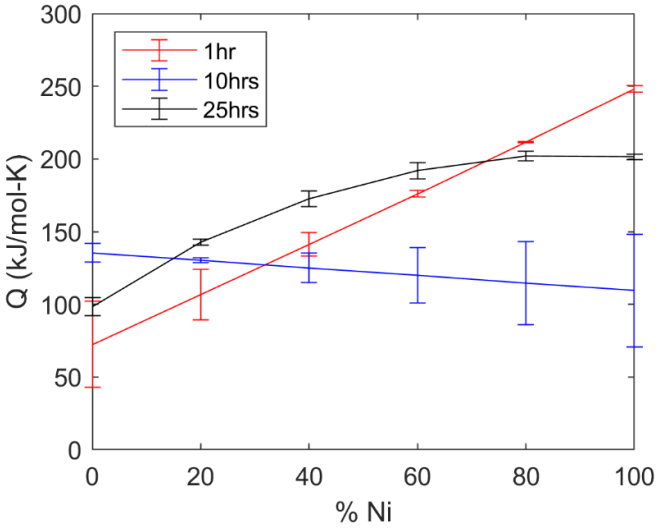

Figure 5.16: Concentration dependence of activation energy for interdiffusion of Cu-Ni diffusion couple.

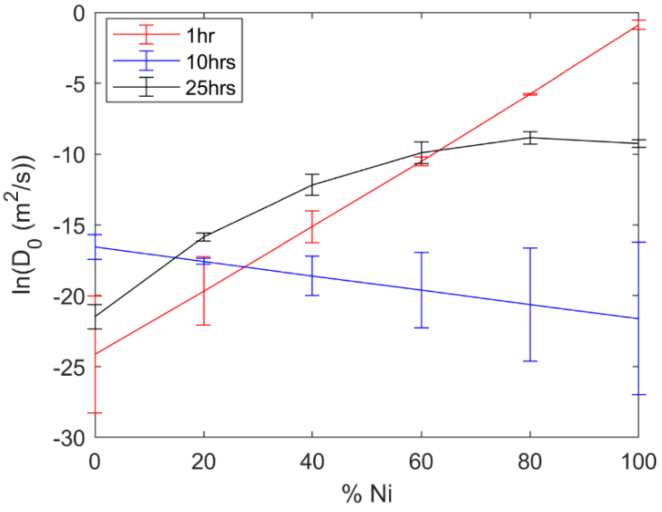

Figure 5.17: Concentration dependence of the frequency factor for interdiffusion of Cu-Ni diffusion couple.

Table 5.3: Average activation energy (Q(kJ/mol-K)) and natural logarithm of frequency factor (D_0 (m^2/s)) values at various concentrations and diffusion times.

%Cu	1hr		5 hrs		25 hrs		72 hrs	
	ln(D0)	Q	ln(D0)	Q	ln(D0)	Q	ln(D0)	Q
0	-12.9	169	-12.3	168	-26.7	48	-17	130
1	-2.1	260	-6.6	215	-14.1	155	-9.9	190
2	6.6	332	-2.6	247	-4.6	236	-4.2	240
3	12.0	377	-0.9	259	1.1	280	-1.02	260
4	14.1	392	-1.5	251	2.1	286	-0.4	263
5	12.8	379	-4.4	223	-1.1	254	-2.3	244
6	8.2	337	-9.7	175	-8.7	186	-6.7	204

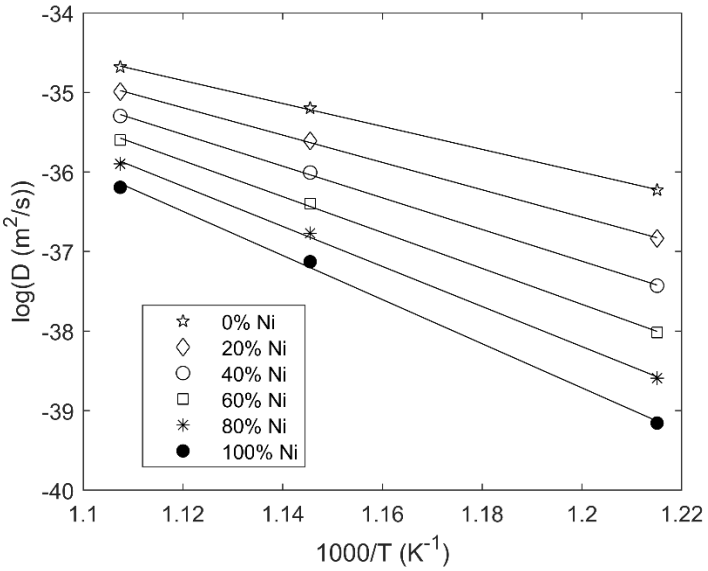

Figure 5.18: Temperature dependence of the interdiffusion coefficients at 1-25hrs diffusion time for Cu-Ni diffusion system

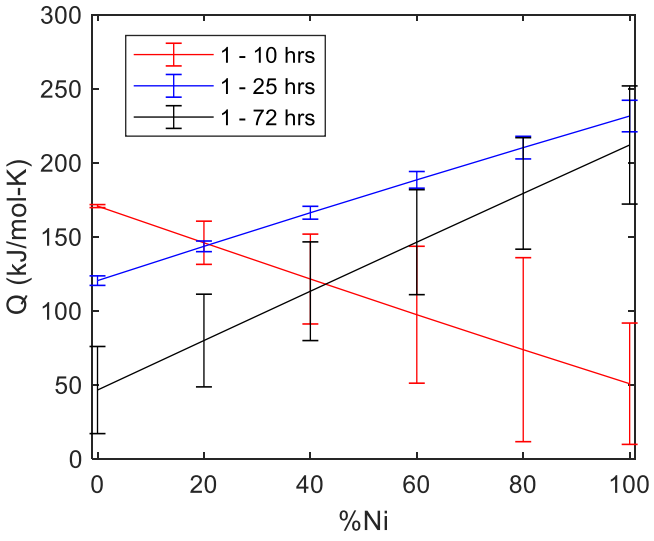

Figure 5.19: Concentration dependence of activation energy for interdiffusion in Cu-Ni diffusion couple

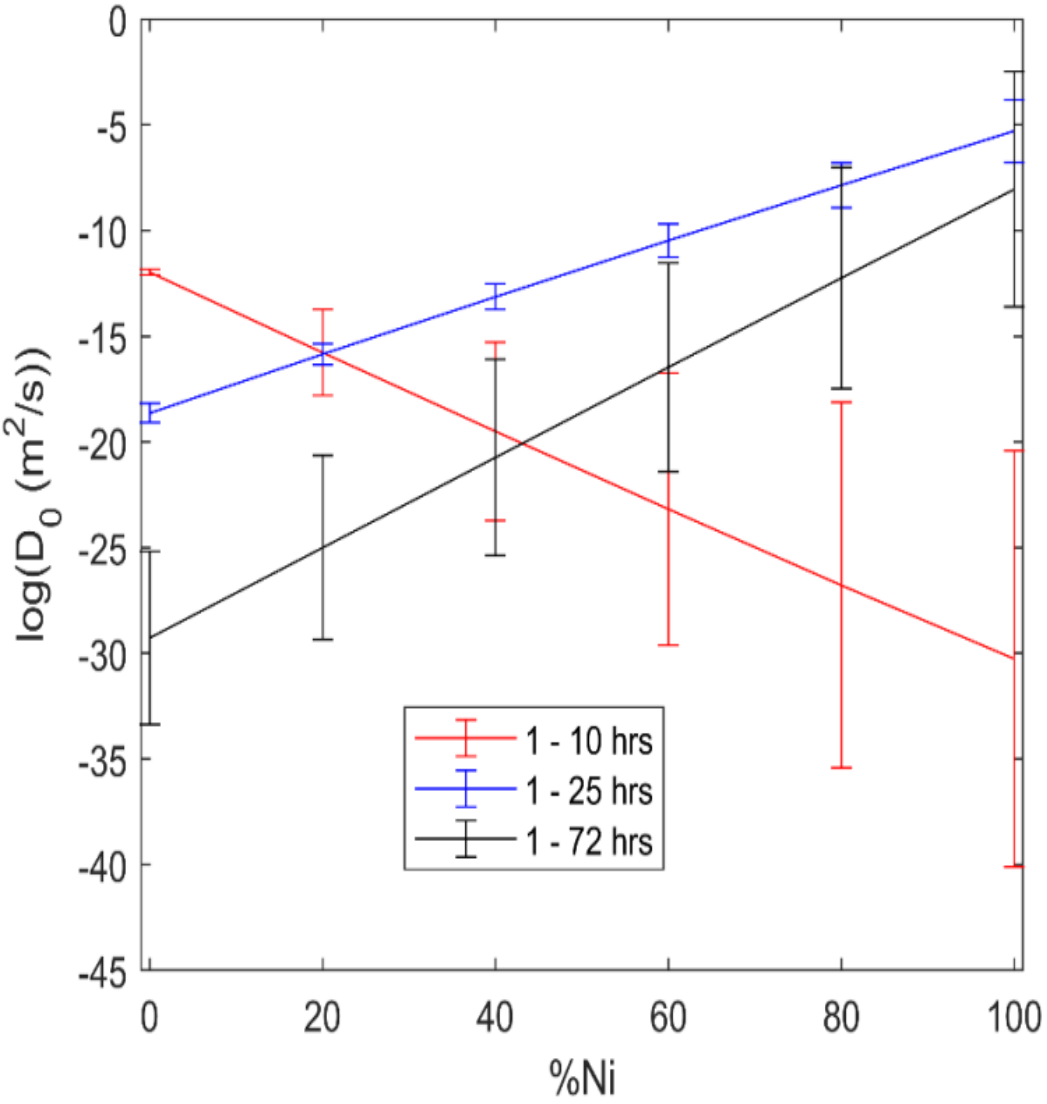

Figure 5.20: Concentration dependence of frequency factor for interdiffusion in Cu-Ni diffusion couple

respectively. Similarly, using D(C) which eliminates errors due to the presence of initial concentration gradients prior to diffusion (Figure 5.14), the values of Q(C) and D_0(C) at different diffusion times in the Ag-Cu system are calculated and presented in Table 5.4. The results obtained in the Cu-Ni and Ag-Cu diffusion couples clearly show that both the Q(C) and D_0(C) change with diffusion time. However, the change cannot be attributed to errors due to the presence of an initial solute distribution, nor a change in the underlying mechanism at a critical temperature [98]–[100]. The time variation of Q(C) and D_0(C) is attributable to time variations in the interdiffusion coefficients at various temperatures caused by diffusion-induced strain. These results, therefore, experimentally validate the time variation of the activation energy and frequency factor.

5.4 Implications of Time Variation of Concentration-Dependent Activation Energy and Frequency Factor

To illustrate the implications of the time variation of Q(C) and D_0(C) on the theoretical predictions of diffusion processes, the Q(C) and D_0(C) obtained at $820^{o}C$ for 1-5 hrs in the Ag-Cu diffusion couple are used to calculate a constant D(C). The diffusion process from 1 hr to 96 hrs is simulated with the constant D(C) obtained with the use of Q(C) and D_0(C) obtained at $820^{o}C$ for 1-5 hrs. The simulated concentration and the experimental profiles are presented and compared in Figure 5.21. The result of the simulation, when compared to the actual experiment (Figure 5.21), shows that there can be a significant error in the theoretically predicted solute distribution when Q(C) and D_0(C) vary with time. Furthermore, as previously established, D(C) is time-dependent at any given temperature. Also, the time variation of an isothermal D(C) is different at various temperatures (Figures 5.10-5.13), which can cause an abnormal condition in which at a certain range of

Table 5.4: Average activation energy (Q(kJ/mol-K)) and frequency factor ($D_0(m^2/s)$) values at various concentrations and diffusion times.

%Cu	1-5hrs		1-25hrs		1-72hrs	
	$\ln(D_0)$	Q	$\ln(D_0)$	Q	$\ln(D_0)$	Q
0	-12.0	169	-26.6	48	-17.6	130
1	-6.4	215	-14.0	154	-9.8	190
2	-2.4	247	-4.3	236	-4.2	236
3	-0.7	259	1.1	280	-1.0	261
4	-1.3	250	2.2	286	-0.4	264
5	-4.2	223	-1.1	254	-2.3	245
6	-9.4	175	-8.6	186	-6.7	205

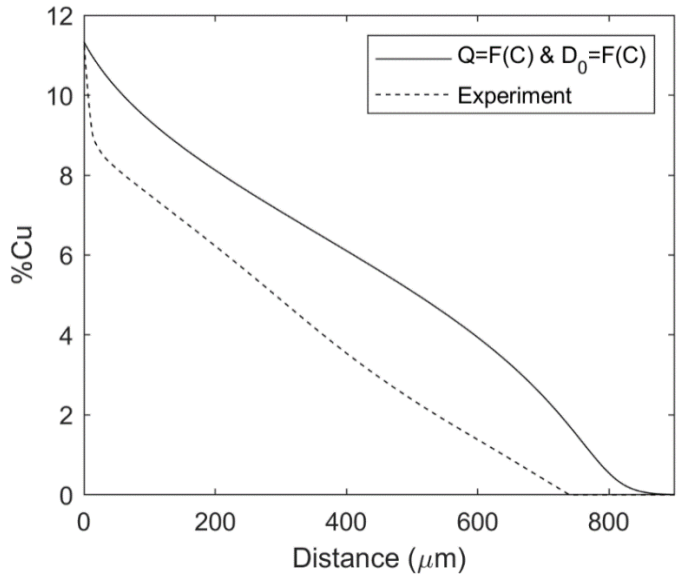

Figure 5.21: Predicted and experimental concentration profiles of Ag-Cu diffusion couple at 96hrs and 820 ^{o}C

concentration and time, the interdiffusion coefficient at a lower temperature will be higher than the values at a higher temperature. This results in a higher diffusion rate at lower temperatures compared to that at higher temperatures. This behavior can be observed between 0-32% at a duration of 25-72 hrs in the Cu-Ni diffusion couple at $550\,^{o}C$ and $600\,^{o}C$ in this study (Figure 5.22a), and between $600\,^{o}C$ and $650\,^{o}C$ as reported in Schwarz et al. [97]. This anomalous behavior is also observed in the Ag-Cu system (Figure 5.22b), where at concentrations higher than 6.4% Cu, and duration of 72 - 96 hrs, the interdiffusion coefficient is larger at a lower temperature of $820\,^{o}C$ compared to the values at a higher temperature of $850\,^{o}C$ (Figure 5.22b). Similarly, a careful review of the literature shows that this unusual observation is found in alloy systems such as Cu-Ni [101], Cu-Zn [102], and Ni-Nb [103]. This behaviour can result in a situation where for a given time duration, there is less diffusion and the diffusion kinetics are lower at a higher temperature, which is contrary to expectations. To illustrate this, the extent of diffusion obtained from the experimental concentration profiles in the Ag-Cu system for 72-96 hrs is observed to be 149 μm at $820\,^{o}C$, which is considerably higher than that of 113 μm at a higher temperature of $850\,^{o}C$. A similar occurrence can be observed between 25-72 hrs in the Cu-Ni diffusion system, where within the same period of time, the extent of diffusion at a lower temperature of $550\,^{o}C$ is 12.6 μm. In contrast, the same duration only resulted in a depth of 7.4 μm of solute penetration at a higher temperature of $600\,^{o}C$.

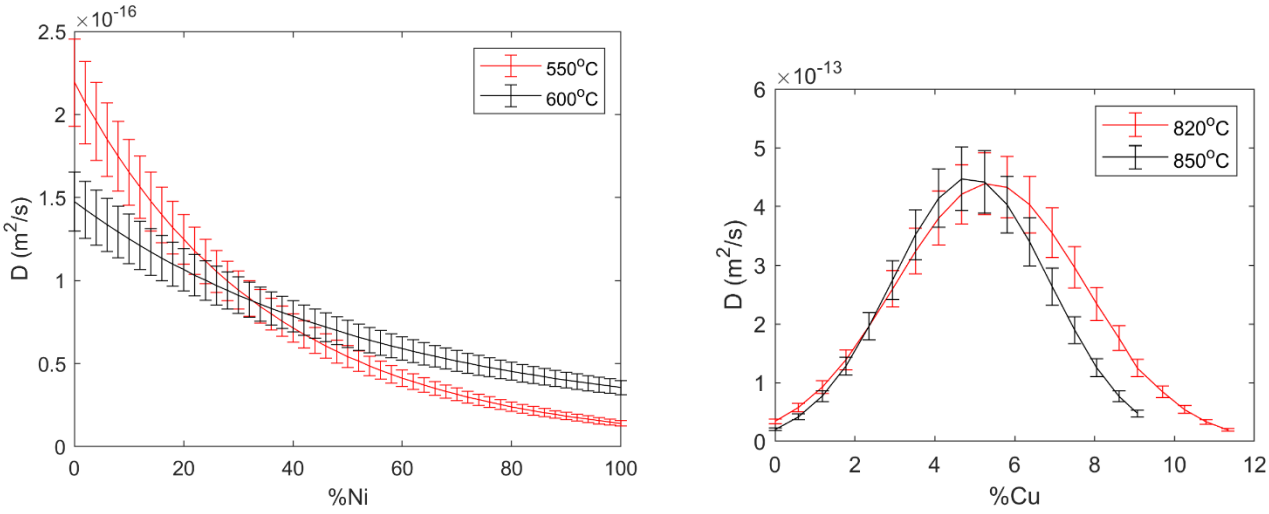

(a) (b)

Figure 5.22: Concentration dependence of the interdiffusion coefficient in (a) Cu-Ni system, between 25 and 72 hrs (b) Ag-Cu system between 72 and 96 hr

CHAPTER SIX

6 ANALYSIS OF CONCENTRATION DEPENDENT INTERDIFFUSION COEFFICIENT UNDER THE CONDITION OF PRE-EXISTING NON-UNIFORM SOLUTE DISTRIBUTION

6.1 Introduction

A number of material processes use different temperatures instead of a single temperature in multiple consecutive heat treatments for diffusion. Examples of such processes are diffusion brazing [43], diffusion coating [104], sintering [105], age-hardening [106], and other types of heat treatments [107]. During these processes, there is non-uniform distribution of the solutes produced in the material through diffusion into the substrate at the first stage before other subsequent stages of diffusion. Interestingly, several researchers who worked on single-stage diffusion have also reported significantly non-uniform initial solute distribution during metal coupling prior to diffusion heat treatment. Examples of common pre-diffusion stage metal coupling methods with reported significant non-uniform initial solute distribution are forced contact [108], [109], hot isostatic pressing (HIP) [30], electro spark deposition [110], and electroplating [52], [53]. In diffusion processes with multiple steps or stages, the D(C) used to model or analyze the diffusion behaviour at each stage are generally obtained by applying a standard condition in which basically a non-uniform initial solute distribution at a specific temperature does not exist. The single-stage processes often assume that the solute concentration is a step function in space. Hence, standard approaches such as the **BM**, **SF**, Hall, and Wagner methods, which are derived only for systems with a uniform initial solute state, are used to extract the standard interdiffusion coefficients from such systems [65]–[68], [105], [111]. Nevertheless, these commonly used methods are based on the standard condition that the material basically has a uniform solute state prior to the diffusion

process. It is generally assumed that the standard diffusion coefficients obtained from the single-stage processes would work reliably in diffusion processes with multiple stages, regardless of whether a non-uniform solute distribution is already found on the material prior to the subsequent diffusion stage. This is based on the assumption that the D(C) does not depend on the initial composition gradients prior to the diffusion process. However, as previously stated, several studies have shown that the concentration gradient of the solutes in a crystal is a factor that affects diffusion-induced strain/stress [6]–[9], and other studies have shown that diffusion-induced strain/stress influences the diffusion coefficients [8], [10]–[15]. These assumptions can be investigated theoretically by using the numerical model developed in section 3.2 for DIS analysis. For the experimental verification, the traditional methods used to extract the D(C) from experiments cannot be used when there is a pre-existing non-uniform solute distribution prior to diffusion. A method that is not based on the standard condition of a step function will be used to extract reliable D(C) values from experimental methods. Interestingly, numerical inverse methods, including the FSM discussed in Chapters 2 and 3 can be used to handle diffusion cases with pre-existing solute distributions [30]. Therefore, the goal of this chapter is to theoretically investigate the possible influence of initial solute distribution on DIS, its effect on the D(C), and experimentally verify the theoretical findings by using the FSM and the new numerical method presented in section 3.3. This chapter verifies the validity of the common assumption that the standard diffusion coefficients obtained from a single-step diffusion process are reliable for analyzing diffusion in material processes that involve multiple stages such as sintering, brazing, coating, and heat other types of heat treatments, with pre-existing non-uniform solute distributions. The chapter will start with a theoretical study of the assumptions made in the literature, followed

by a study of the factors that can influence the effect of non-uniform solute distribution on the D(C), then an experimental verification, and concludes with providing the practical implications.

6.2 Theoretical effect of pre-existing non-uniform solute distributions on D(C)

The influence of pre-existing initial solute distributions prior to diffusion and their corresponding pressure distributions on the effective D(C) is studied theoretically in this section. Concentration profiles, pressure distributions, and D(C) under DIS were theoretically simulated and studied with the use of two cases. The two cases are: (i) a two-stage diffusion process with a non-uniform initial solute distribution prior to diffusion, and (ii) a single-stage diffusion process without a non-uniform initial solute distribution prior to diffusion. To study the cases, the diffusion parameters for the conditions prior to diffusion and main diffusion are presented in Table 6.1. The initial concentration and pressure distributions in the two-stage diffusion process are simulated by using the parameters for the process prior to the diffusion. Subsequently, the solute and pressure distributions of the process prior to the diffusion coupled with the diffusion parameters of the final diffusion, are used as the initial conditions to simulate the final solute and pressure distributions. The final solute and pressure distributions in the two-stage diffusion process are used to determine the D(C) under DIS in the final step of the two-stage diffusion process. Similarly, for the single-stage diffusion process, the final concentration and pressure distributions are directly calculated by using the final diffusion parameters without an initial solute and pressure distribution. The final concentration and pressure distributions in this single-stage diffusion system are used to calculate the D(C) under DIS in a single-stage diffusion system. The calculated D(C) under DIS in the one and two stage diffusion process systems are compared to investigate the possible effects of non-

Table 6.1: Diffusion parameters for influence of non-uniform initial solute distribution

Diffusion Condition	T'	$D_1^{*'}$	$D_2^{*'}$	V_1'	V_2'	η'	θ	t'
Initial step Parameters for two-stage process	0.0029	1.0	0.0125	0.9091	1.0	2.39×10^{-4}	1	0.0072
Final diffusion Parameters for both cases	0.0022	0.5	0.0063	0.9091	1.0	3.61×10^{-4}	1	0.0036

uniform initial solute distribution. The initial solute concentration profiles for the one- and two stage processes are presented in Figures 6.1a and 6.1b, respectively. Similarly, the final solute concentration profiles for both processes are shown in Figures 6.2a and 6.2b, respectively. The corresponding pressure distributions determined for the initial and final one- and two stages processes are illustrated in Figure 6.3. The solute and pressure distributions are calculated by using Equations 3.22-3.27. The stress distribution shows that the final stress gradients are different in the one- and two-stage diffusion processes with and without a non-uniform initial solute distribution, respectively. The effective diffusion coefficients for the final diffusion times of both processes are calculated by using Equation 3.21 and compared in Figure 6.4. This theoretical study shows that the D(C) is dependent on the initial solute distribution in diffusion systems.

This section will subsequently evaluate some of the diffusion parameters that can influence the effect of the initial solute distribution on the D(C). They are: (i) the amount of initial solute, and (ii) final diffusion time.

6.2.1 Influence of amount of initial solute on the effect of pre-existing non-uniform solute distributions on D(C)

The time prior to the diffusion is a major factor that influences the amount of non-uniform initial solute. Differences in time prior to diffusion are expected to influence the initial solute distribution prior to the final diffusion process. As previously established, the difference in the initial solute distributions can affect the pressure distribution in a system. In Equation 3.21, differences in the pressure distribution can be observed to influence the D(C). To confirm this possibility, the effective diffusion coefficient in a one-stage diffusion process will be compared to that in three

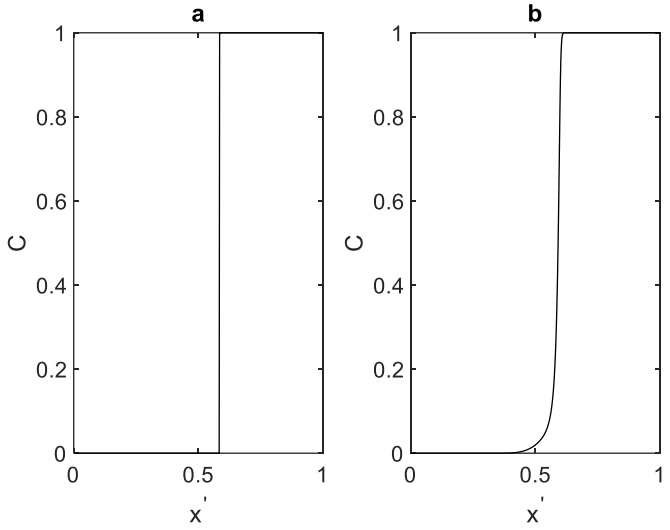

Figure 6.1: Theoretical concentration profiles at $t' = 0$ for the final diffusion process. (a) Represents the initial concentration profiles for one-stage diffusion process (b) Represents the simulated initial concentration profiles for two-stage diffusion process.

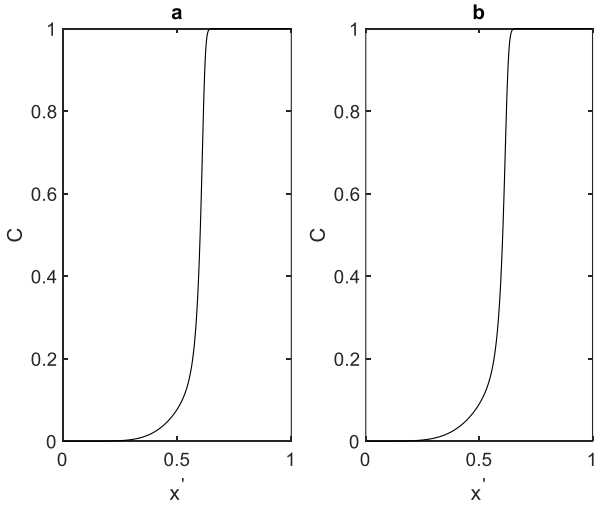

Figure 6.2: Theoretical concentration profiles at $t' = 0.0036$ at the final diffusion process. (a) Represents the simulated final concentration profiles for one-stage diffusion process (b) Represents the simulated final concentration profiles for two-stage diffusion process.

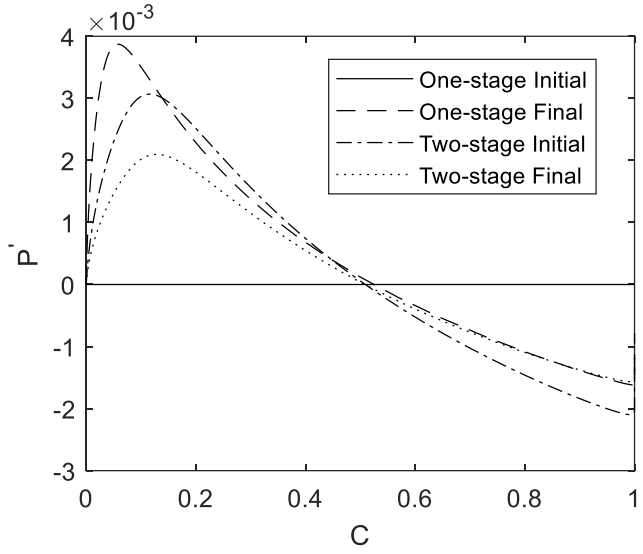

Figure 6.3 Theoretical pressure distributions at the initial and final diffusion times for the one-stage and two-stage diffusion processes

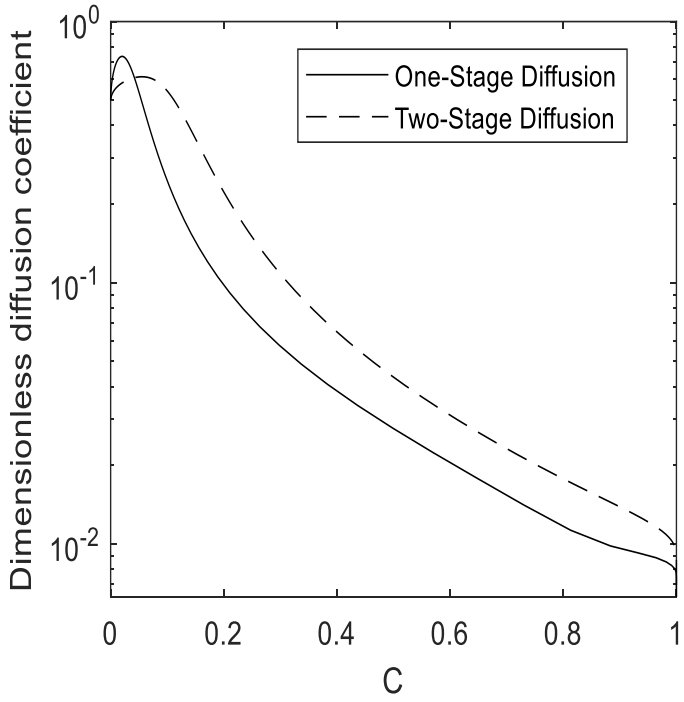

Figure 6.4 Theoretical comparison between the D(C) at the final diffusion times for both one-stage and two-stage diffusion processes

two-stage diffusion processes with varying amounts of non-uniform initial solute distribution. Three pre-diffusion times are used coupled with the other parameters in Table 6.1 to achieve three two-stage diffusion processes with varying quantities of non-uniform initial solute. The pre-diffusion times prior to the final diffusion duration are: $t' = 0.0036$, $t' = 0.0072$, and $t' = 0.0506$. The simulations before the final diffusion are carried out by using Equations 3.22-3.27 for the three different lengths of times. The final diffusion processes are determined using the final diffusion parameters in Table 6.1, for the three two-stage diffusion processes, and the one-stage diffusion process with a dimensionless diffusion time of 0.0072. The initial and final non-uniform distributions are presented in Figure 6.5a for the one-stage diffusion process, and the three two-stage processes are shown in Figures 6.5a-6.5d. The plots in Figure 6.5 show that increasing the amount of initial solute changes the concentration gradient in the diffusion system. The stress gradients are calculated and presented in Figure 6.6. The D(C) for each case is calculated from the final composition (Figure 6.5) and pressure gradients (Figure 6.6) and presented in Figure 6.7. The results in Figure 6.7 illustrate that increasing the non-uniform initial solute distribution in a two-stage diffusion process increases the difference between the D(C) in a one- and two-stage diffusion process. Therefore, increasing the initial amount of solute amplifies the effect of non-uniform initial solute distribution on the D(C).

6.2.2 Influence of final diffusion time on the effect of pre-existing non-uniform solute distributions on D(C)

A second factor that can influence the magnitude of the effect of a non-uniform initial solute distribution is the final diffusion time in the one- and two-stage diffusion systems. In this section,

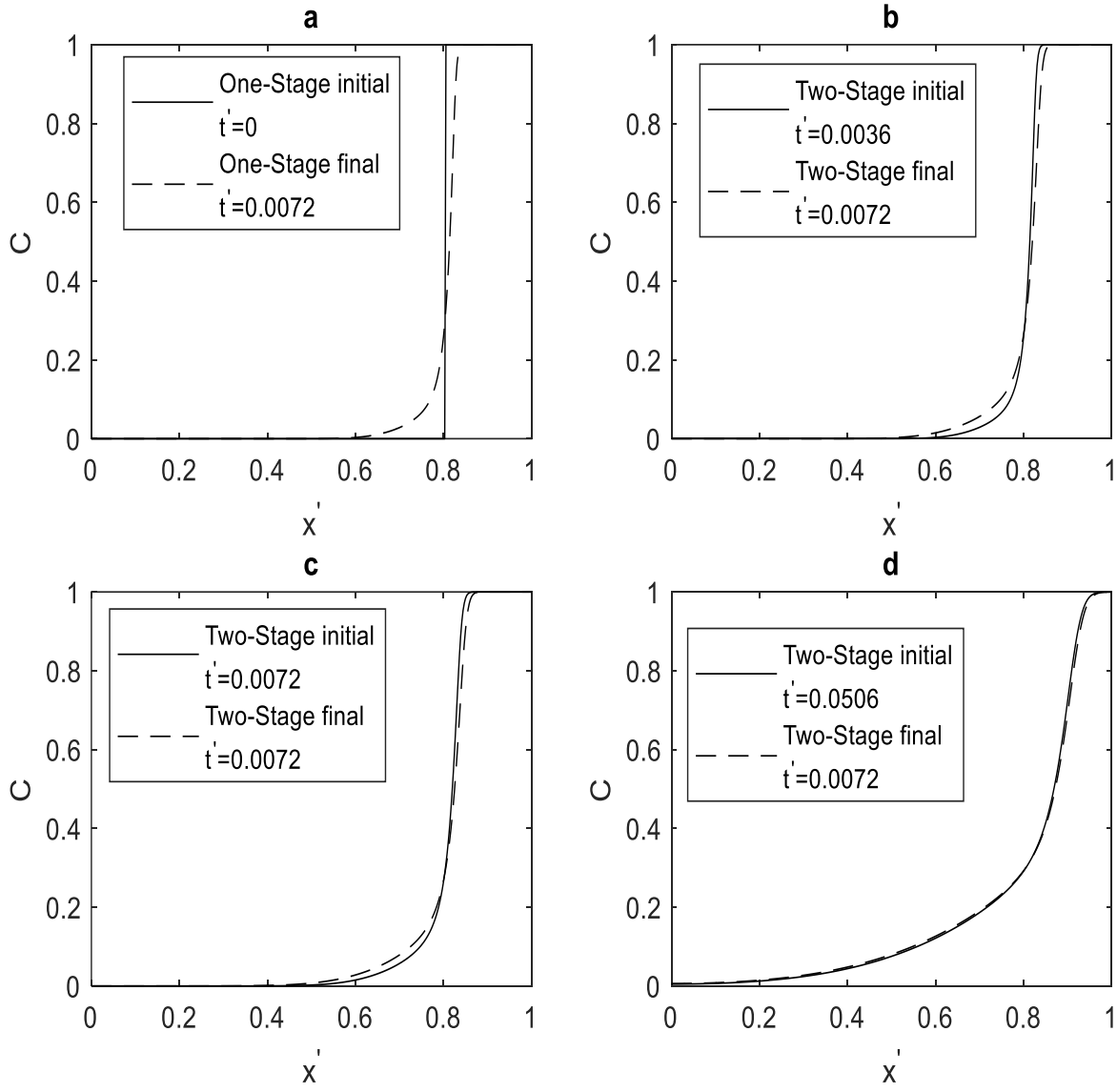

Figure 6.5: Simulated initial and final concentration profiles for (a) an one-stage diffusion process, (b) a two-stage process with an initial pre-diffusion time of 0.0036, (c) a two-stage process with an initial pre-diffusion time of 0.0072, and (d) a two-stage process with an initial pre-diffusion time of 0.0506

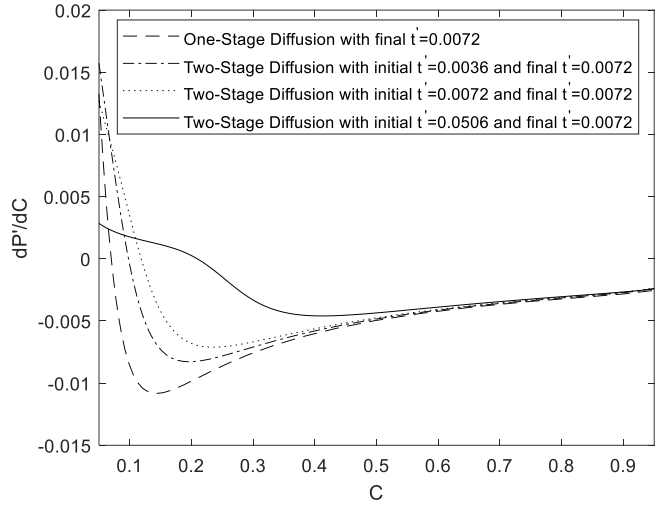

Figure 6.6: Simulated pressure gradients for one-stage diffusion process and the three two-stage diffusion processes with varying pre-diffusion times.

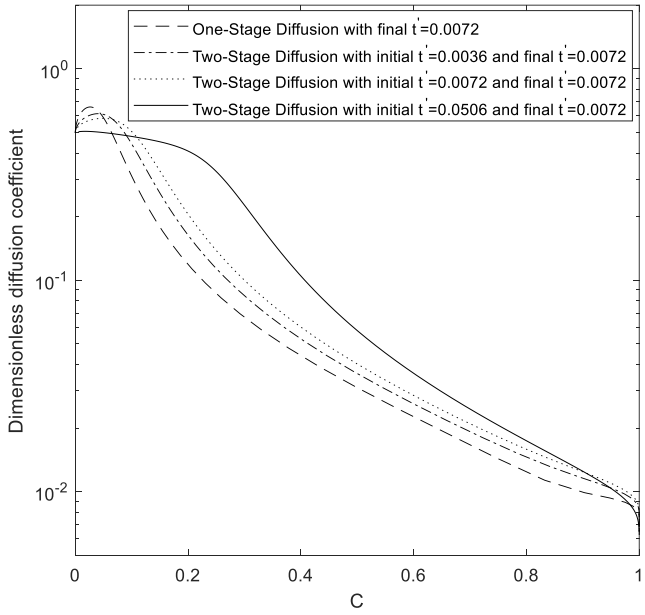

Figure 6.7 Simulated D(C) under DIS for one-stage diffusion process and the three-two step diffusion processes with varying pre-diffusion times.

the D(C) under DIS in a one-stage diffusion process will be compared to the data in two-stage diffusion processes at different final diffusion times. The purpose of this investigation is to understand the influence of the final diffusion time on the effect of a non-uniform initial solute distribution on the D(C). To achieve this, the one-stage diffusion process is simulated by using Equations 3.22-3.27, the final diffusion parameters in Table 6.1, and the final diffusion times of $t' = 0.0036$, $t' = 0.0072$, and $t' = 0.0506$. For the two-stage process, the process prior to diffusion is simulated by using Equation 3.22-3.27 and the related parameters are listed in Table 6.1. The final diffusion stage of the two-stage processes are also simulated by using Equations 3.22-3.27, and the final diffusion parameters in Table 6.1 with final diffusion times of $t' = 0.0036$, $t' = 0.0072$, and $t' = 0.0506$. The initial and final non-uniform distributions are presented in Figure 6.8 for both the one- and two-stage diffusion processes for the three final diffusion times. Figure 6.8 shows that increasing the final diffusion time also increases the final amount of solute in the systems. With longer final diffusion times, the one- and two-stage diffusion processes tend towards each other. The final pressure gradients for the systems are presented in Figure 6.9, which shows that the stress gradients become increasingly equal with time. The D(C) for each case is calculated from the final composition and pressure profiles by using Equation 3.21. The D(C) are reported in Figure 6.10. The results in Figure 6.10 show that increasing the final diffusion time decreases the effect of the non-uniform initial solute distribution.

At the same final diffusion time, there are generally three types of two-stage diffusion processes, including:

1. The process in which the main diffusion temperature is higher than that before the main diffusion takes place. For example, mechanically joining metals at high-temperatures before

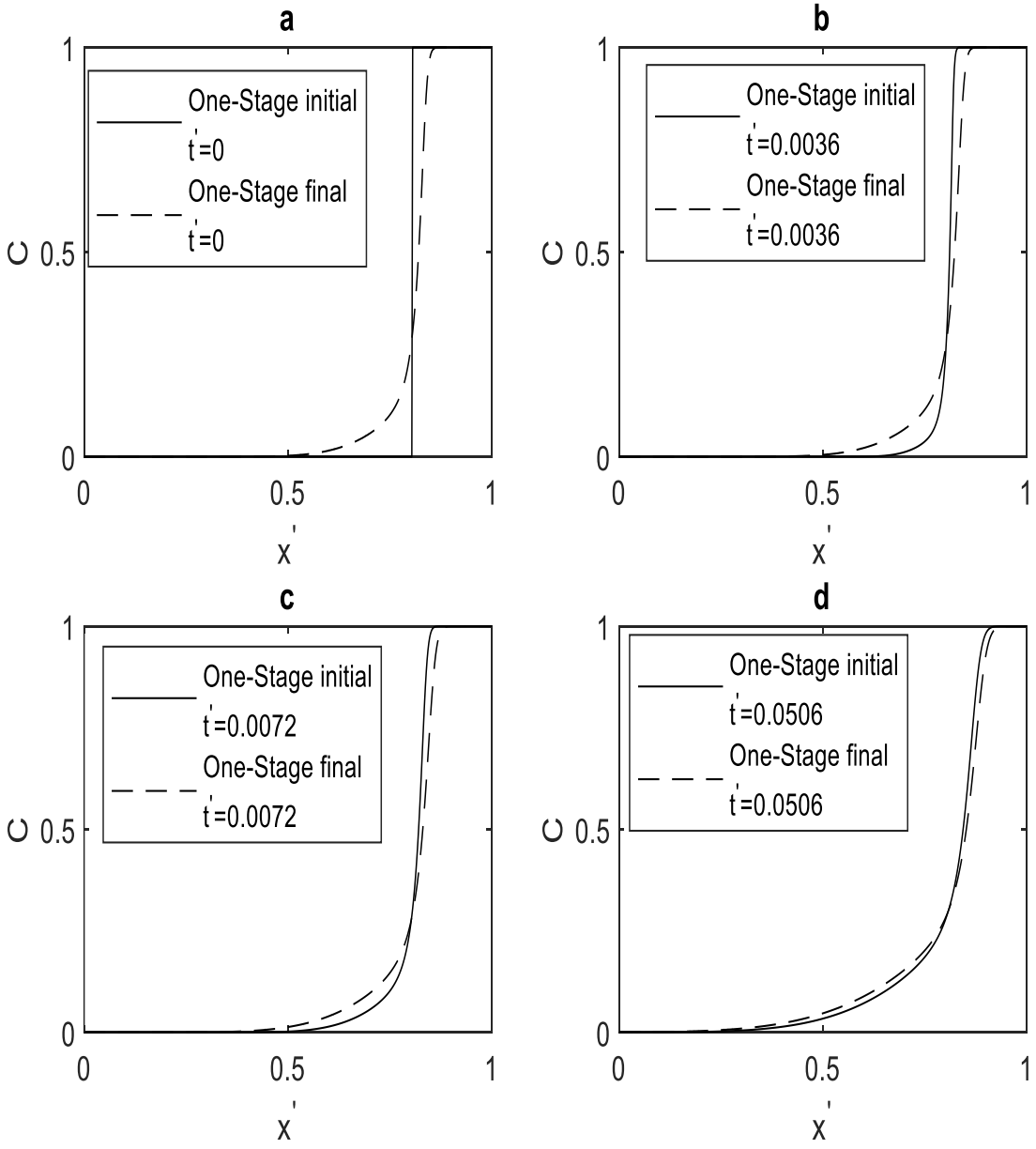

Figure 6.8: Simulated concentration profiles for one-stage and two-stage diffusion processes at different diffusion times (A) $t' = 0$ (B) $t' = 0.0036$, (C) $t' = 0.0072$, (D) $t' = 0.0506$.

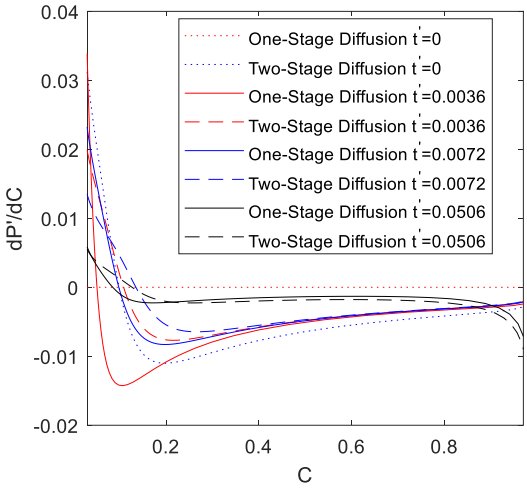

Figure 6.9: Simulated Pressure gradient for one-stage and two-stage diffusion processes at different diffusion times

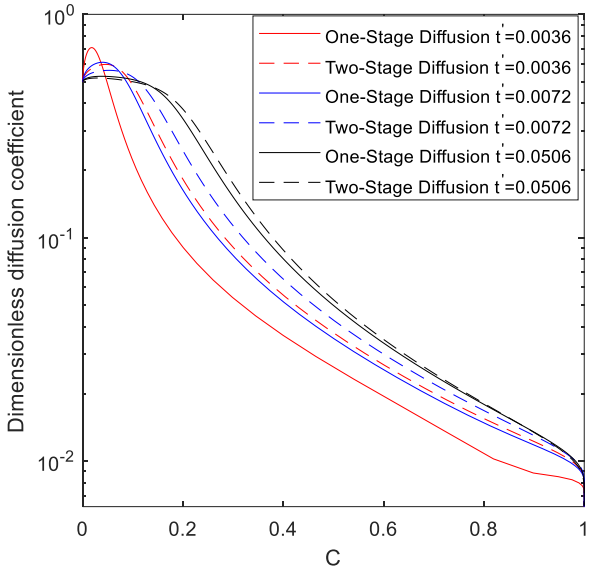

Figure 6.10 Simulated D(C) under DIS for one-stage diffusion process and the three-two step diffusion processes showing increasing final diffusion times decreases the effect of initial non-uniform solute distribution

the final diffusion at a much lower temperature [109].

2. The main diffusion temperature equals the temperature before the main diffusion. For example, the base metal dissolution stage and isothermal solidification stage in TLP bonding are both at the same temperature [43].
3. The main diffusion temperature is lower than the temperature before the main diffusion process. For example, age-hardening treatment [106].

With the same diffusion duration, the three cases presented can have different influences on the effect of non-uniform solute distributions on the D(C). Thus, these three cases will be theoretically investigated here. The diffusion parameters used to investigate the cases are presented in Table 6.2. The initial concentration profiles are shown in Figure 6.11a for both one- and two-stage diffusion. The final one- and two-stage diffusion profiles for Cases 1, 2, and 3 are presented in Figures 6.11b - 6.11e, respectively. The corresponding pressure gradients obtained at each concentration profile are shown in Figure 6.12. The effective D(C) at the final profiles are calculated by using Equation 3.21 and presented in Figure 6.13. As illustrated in Figure 6.13, the initial solute state has a greater effect when the final diffusion process is slower than the rate before the main diffusion started. Interestingly, Figure 6.13a shows that when a diffusion process proceeds from a high-temperature to a low-temperature (Case 1), the effect of the non-uniform initial solute distribution on the D(C) increases. Therefore, inducing a significant amount of non-uniform initial solute relative to the final solute distribution will significantly affect the effective D(C) if the final diffusion process takes place for a short time or at a slow rate of diffusion.

Table 6.2: Diffusion parameters for the three cases on the influence of diffusivity on non-uniform initial solute distribution

Diffusion Condition	T'	$D_1^{*'}$	$D_2^{*'}$	V_1'	V_2'	η'	θ	t'
Initial step Parameters for two-stage process	0.0050	1.20	0.050	0.9091	1.0	1.81×10^{-4}	0	0.0072
Final diffusion Parameters for Case 1	0.0025	1.0	0.0125	0.9091	1.0	3.61×10^{-4}	0	0.0072
Final diffusion Parameters for Case 2	0.0050	1.2	0.050	0.9091	1.0	1.81×10^{-4}	0	0.0072
Final diffusion Parameters for Case 3	0.0075	1.2752	0.0794	0.9091	1.0	1.71×10^{-4}	0	0.0072

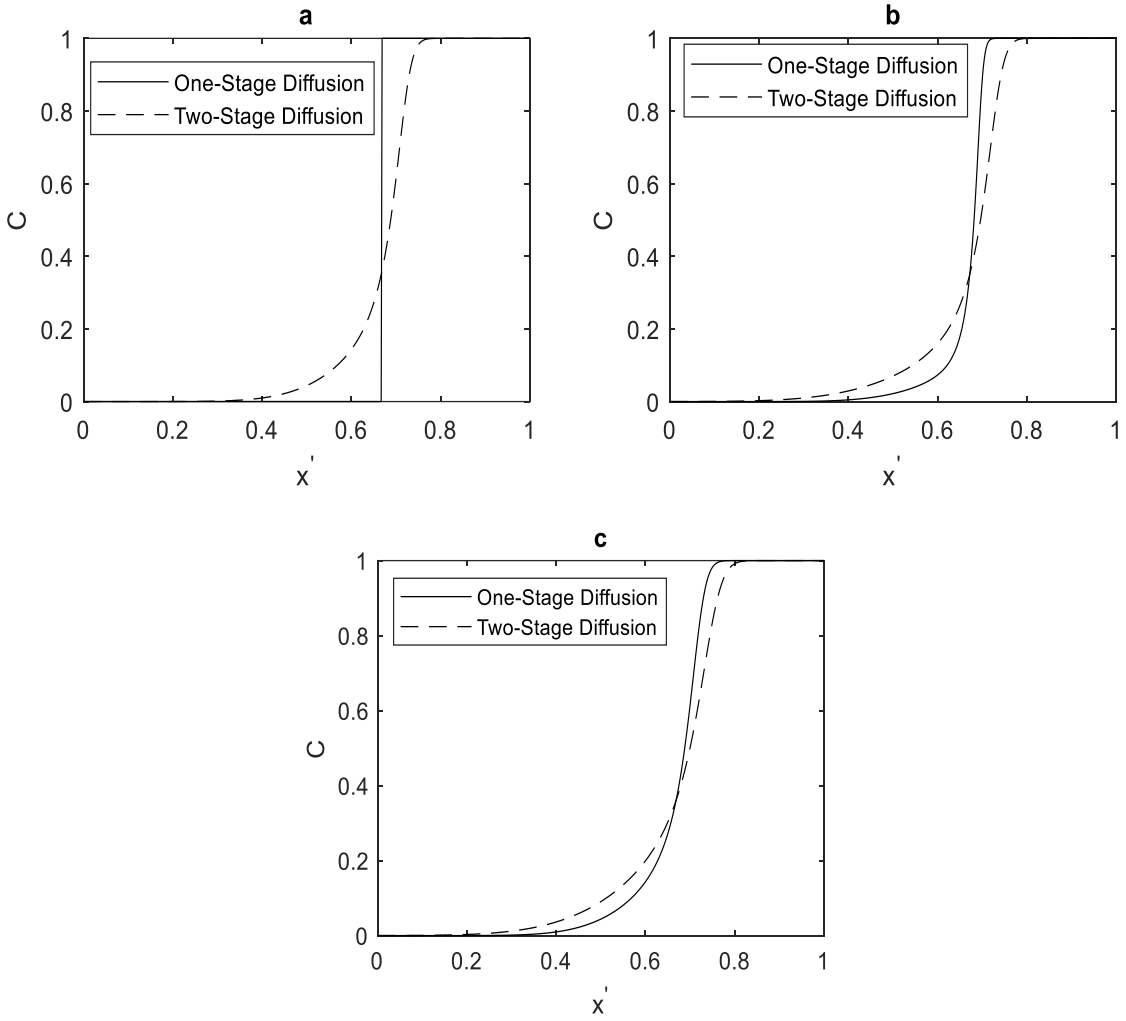

Figure 6.11 Simulated concentration profiles for (a) Initial profiles for one-stage and two-stage diffusion (b) One-stage and two- stage diffusion final profiles for case 1, (c) One-stage and two- stage diffusion final profiles for Case 2 (d) One-stage and two-stage diffusion final profiles for Case 3

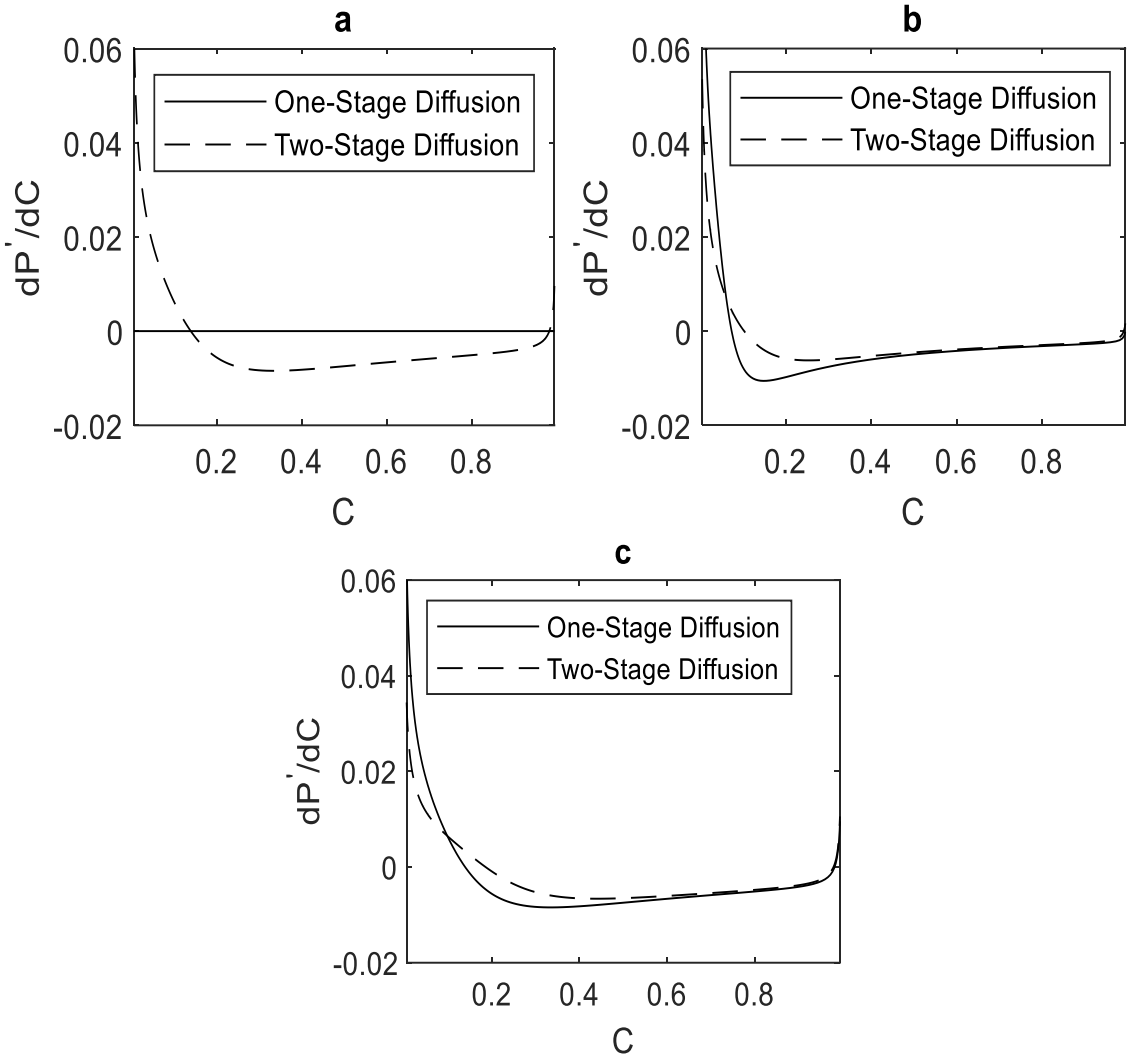

Figure 6.12 Simulated pressure gradients for (a) Initial profiles for one-stage and two-stage diffusion, (b) One-stage and two-stage diffusion final profiles for case 1, (c) One-stage and two-stage diffusion final profiles for Case 2, (d) One-stage and two-stage diffusion final profiles for Case 3

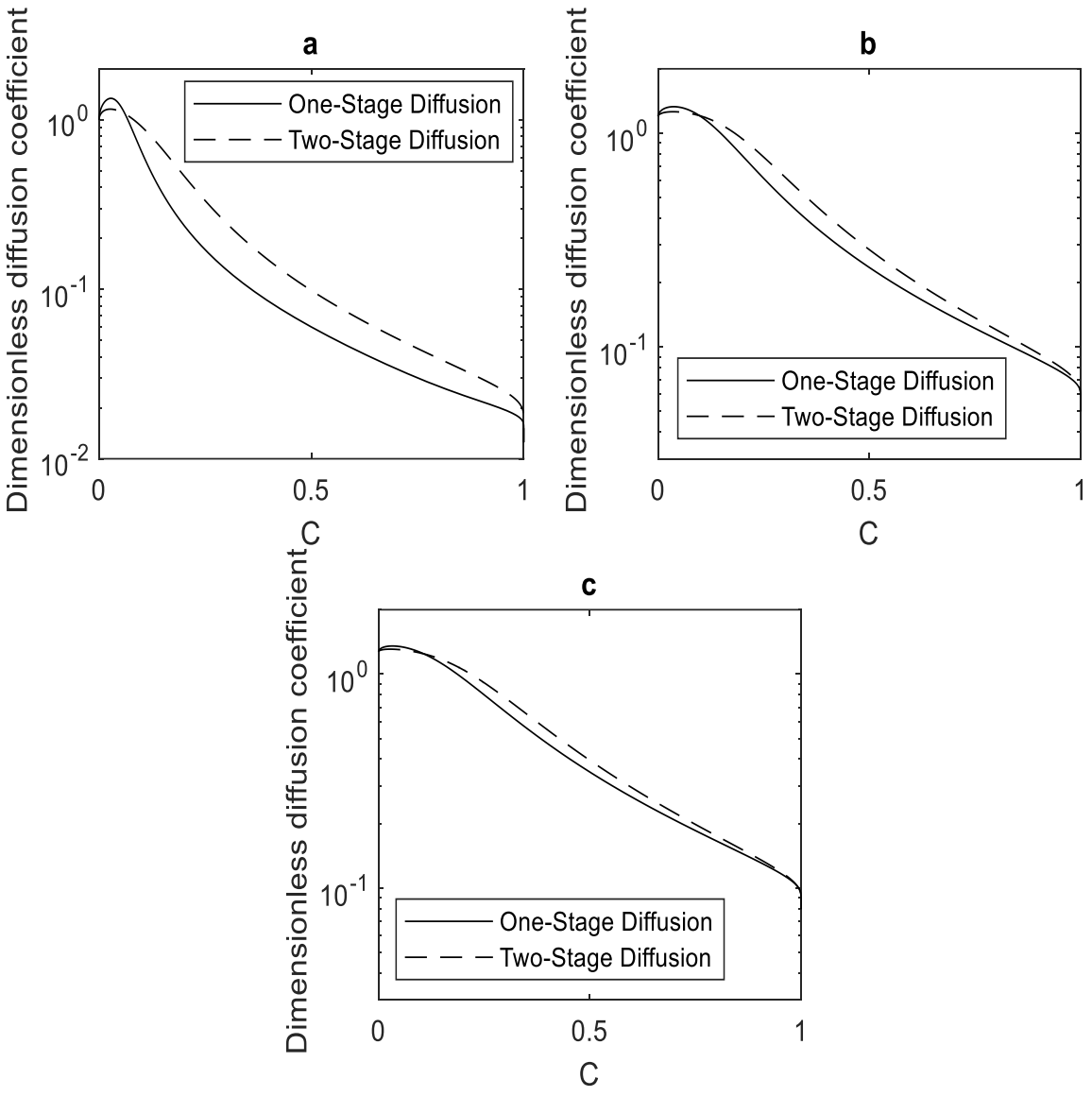

Figure 6.13 One-stage and two-stage diffusion D(C) against concentration for (a) Case 1, (b) Case 2 (c) Case 3

6.3 Experimental Verification of the Theoretical Findings

This section presents the experimental procedure for verifying the effect of a non-uniform initial solute distribution. Subsequently, the determination of when a system can be considered "effectively free" of a pre-existing non-uniform solute distribution shall be discussed, followed by the concept of an experimental "calculation-error free" D(C). A comparison between the experimental D(C) of the one- and two-stage diffusion processes shall be discussed in this section.

6.3.1 Experimental procedure

The experimental procedure is presented below:

1. The homogeneity of alpha brass samples with a flat surface and dimensions of 10 mm by 10 mm with a thickness of 1.4 mm was first validated through microanalysis.
2. Eight alpha brass samples were then polished, placed in a sealed quartz tube backfilled with high purity argon, and heated at 600^{o}C for 1 hr to grow the grains and relieve the residual stresses that could interfere with diffusion at lower temperatures.
3. Subsequently, the alpha brass samples were chemically cleaned. They were:
    a. heated for 20 minutes in a boiling solution of sodium hydroxide, sodium phosphate, and sodium carbonate,
    b. rinsed with distilled water before immersed for 10 minutes in a 30% hydrochloric acid (HCl) solution at room temperature,
    c. rinsed with distilled water before heated for 5 minutes in a boiling 10% sulphuric acid solution, and
    d. rinsed with distilled water before heated for 5 minutes in a 5% sulphuric acid solution at room temperature.

Copper was deposited on the chemically cleaned and rinsed samples at a current density of 4 mA/cm^2 until reaching a deposition thickness of 120 microns. The samples were grouped into two sets. One set was placed in a sealed quartz tube backfilled with high purity argon and subjected to a one-stage diffusion heat treatment at 400^oC for 30 and 55 hrs. The second set of samples were subjected to a two-stage diffusion process. They were placed in a sealed quartz tube backfilled with high purity argon and then subjected to a heat treatment at 455^oC for 25 hrs, before being subjected to a second and final heat treatment at 400^oC for 30 and 55 hrs, respectively. The diffusion samples were sectioned using Electro Discharge Machining (EDM) and then mounted, grounded, and polished using standard metallography sample preparation techniques. Microanalyses on the two sets of samples were performed by using X-ray and wavelength dispersive spectroscopy techniques. The composition profiles were measured in a perpendicular direction to the interface. To determine the extent of the uncertainty in the experimental work, the following steps were carried out:

(a) Three individual samples with the initial condition were subjected to the same diffusion condition.

(b) At least five different concentration profiles were obtained from each of the three (3) samples to calculate the average dependence of the interdiffusivity on the concentration in each sample. This process reduces the sample-to-sample variation in the concentration profiles used to extract the D(C).

(c) Subsequently, the FSM was used to extract the **D(C)** from the experimental composition results.

(d) The concentration-averaged diffusion coefficient (D_{ave}) for each sample was calculated by using the average dependence of the interdiffusivity on the concentration for each sample.

(e) The variations from the average dependence of interdiffusivity on the concentration in each of the three (3) samples were analyzed to determine the extent of the uncertainty due to experimental errors.

(f) Two criteria were used to determine the extent of uncertainty in the experimental data: percentage change in concentration-averaged diffusion coefficient (D_{ave}) and standard deviation in the plot of the three average interdiffusion coefficients against concentration.

(g) The three D_{ave} for the condition variations were analyzed for the D_{ave} criteria to determine the extent of uncertainty due to experimental errors for each diffusion condition. This was done by calculating the maximum percentage change in the D_{ave} for each condition. In this study, the maximum variation in D_{ave} from the three samples falls below 12%, which is consistent with the <15% reported in the literature for two interdiffusion coefficients considered statistically similar [12], [67], [90], [112], [113].

(h) For the second criteria, regions with no overlap between the error bars of the three average interdiffusion coefficients against concentration in the one- and two-stage diffusion processes indicate a change in the D(C).

6.3.2 System "effectively free" of pre-existing non-uniform solute distribution and "calculation-error free" D(C)

The diffusion couples used to determine the experimental D(C) by using analytical methods such as the BM, SF, and Hall methods are often assumed to be free of a pre-existing initial solute state. However, it has been established that non-uniform solute distribution is often generated in diffusion couples during the metal joining process prior to diffusion. The electroplating process used to join Cu to the Cu-Ni alloy before heat treatment results in the electromigration of the solute

atoms, which establishes a non-uniform solute distribution in the diffusion couples [52], [53]. The diffusion potential from electromigration has been briefly discussed in Chapter 2. Standard analytical methods used to extract the D(C) from experimental couples result in erroneous D(C) values when the non-uniform initial solute state is significant compared to the final profile. However, when the extent of the non-uniform initial solute is insignificant compared to the final profile, the initial profile can be effectively assumed to be a step function in space. Hence, the D(C) calculated by using a standard analytical method is reliable with minimal errors when the non-uniform initial profile is negligible. The FSM is a numerical method that has been reported to calculate interdiffusion coefficients accurately for two modes: (i) when the pre-existing solute distribution is neglected and (ii) when the pre-existing solute distribution is not neglected. The mode of calculation that assumes no pre-existing solute distribution, and the FSM for this first condition will hereafter be referred to as **FSM-1**. In contrast, the second mode of calculation uses the actual pre-existing solute distribution as the initial condition and will hereafter be referred to as **FSM-2**. When the D(C) from FSM-1 is comparable to the D(C) from FSM-2, the diffusion couple can be considered to be "effectively free" of a pre-existing non-uniform solute distribution. This approach will be used to determine whether the one- and two-stage diffusion processes can be defined as samples that are "effectively free" of a pre-existing initial solute state. The average concentration profiles with error bars are presented in Figures 6.14-6.16 for the concentration profiles at 0, 30, and 55 hrs, respectively, for the final stage of diffusion in the one- and two-stage diffusion processes. The 0 hr profile for the one-stage diffusion process is introduced due to the electrodeposition process, while the 0 hr profile for the two-stage diffusion process is due to the first stage of diffusion at $455^{o}C$ for 25 hrs. FSM-1 and FSM-2 are used to determine the D(C) in the two-stage diffusion process to determine whether the non-uniform profiles prior to the final

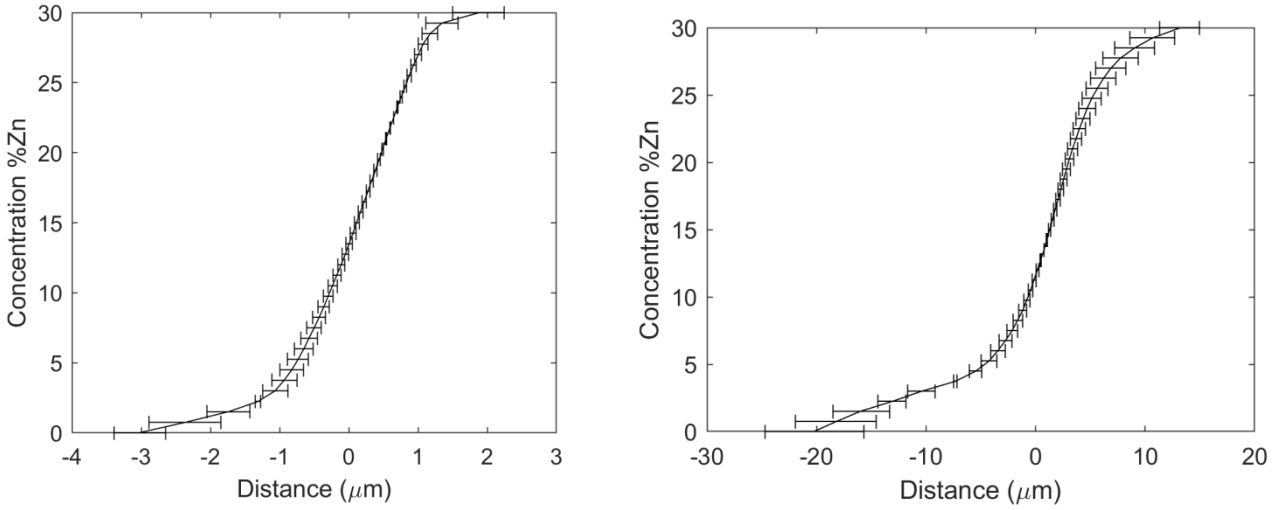

a b

Figure 6.14 Cu-Zn concentration profiles at 0 hrs (a) Represents the concentration profile after electrodeposition (b) Represents the concentration profile after electrodeposition and diffusion at $455\,^{o}C$ for 25 hrs.

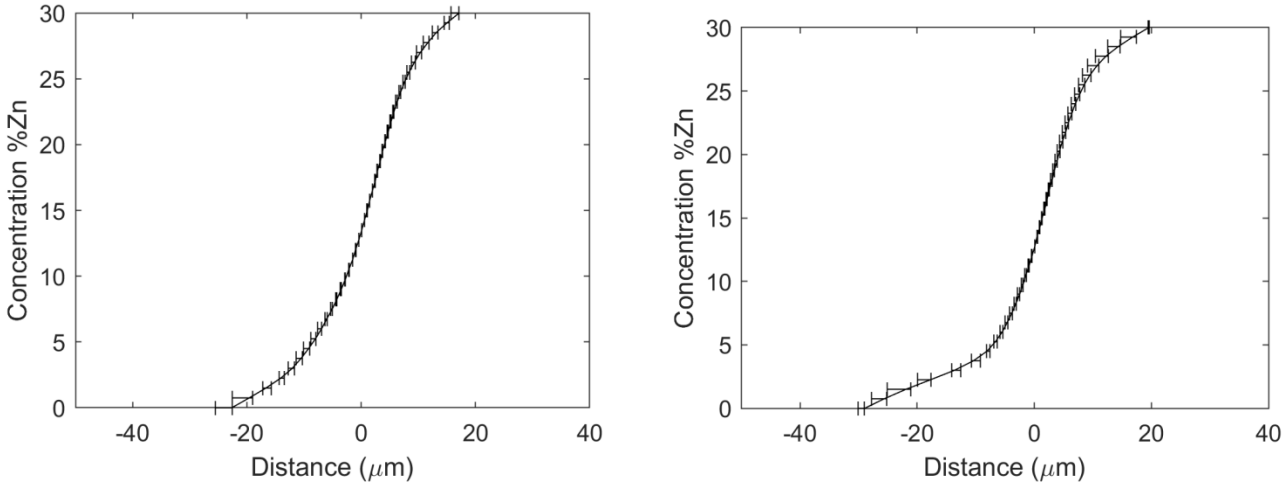

a b

Figure 6.15 Cu-Zn concentration profiles at 30 hrs (a) Single-step diffusion (b) Two-stage diffusion

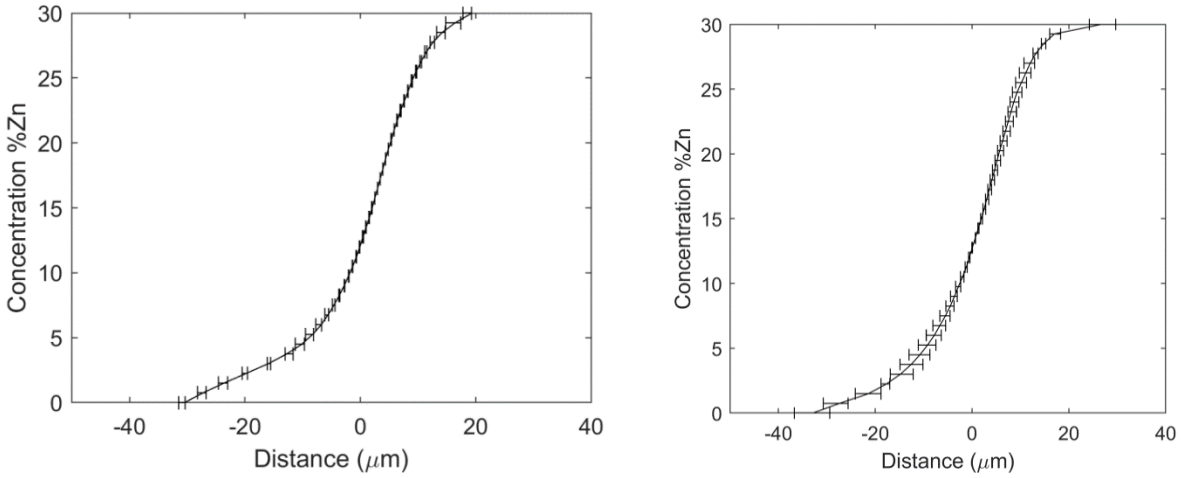

a b

Figure 6.16 Cu-Zn concentration profiles at 55hrs (a) Single-step diffusion (b) Two-stage diffusion

stage of diffusion are significant. In this task, the FSM-1 procedure is used to calculate the D(C) between the assumption of the absence of a non-uniform initial solute distribution and the final profiles after 30 and 55 hrs of diffusion. At the same time, the FSM-2 procedure is used to calculate the D(C) between the actual initial solute distribution obtained after diffusion at $455\,^{o}C$ for 25 hrs and the final profiles of a subsequent 30 and 55 hrs of diffusion at $400\,^{o}C$. The results of the FSM-1 and FSM-2 procedures are presented in Figure 6.17. The results show that the D(C) from FSM-1 and FSM-2 are significantly different for the two-stage process. Hence, the two-stage diffusion samples cannot be considered to be "effectively free" of pre-existing non-uniform solute distributions. The deviation between the D(C) of FSM-1 and FSM-2 in the two-stage diffusion process is due to the calculation errors in FSM-1, which neglects the actual significant pre-existing non-uniform solute distribution. In contrast, FSM-2 takes into consideration the actual pre-existing non-uniform solute distribution. The same approach is used in the one-stage diffusion process. In this case, the initial condition for FSM-2 is the initial solute concentration profile after electrodeposition (Figure 6.14a). The D(C) results from FSM-1 and FSM-2 are presented in Figure 6.18. The plots in Figure 6.18 show that the D(C) of FSM-1 and FSM-2 are statistically comparable in the one-stage diffusion process. Hence, the samples subjected to the one-stage diffusion process can be considered "effectively free" of a pre-existing non-uniform solute distribution. In addition, FSM-2 calculates a reliable "calculation error-free" D(C) as it incorporates the actual initial profiles of the materials before the final diffusion process.

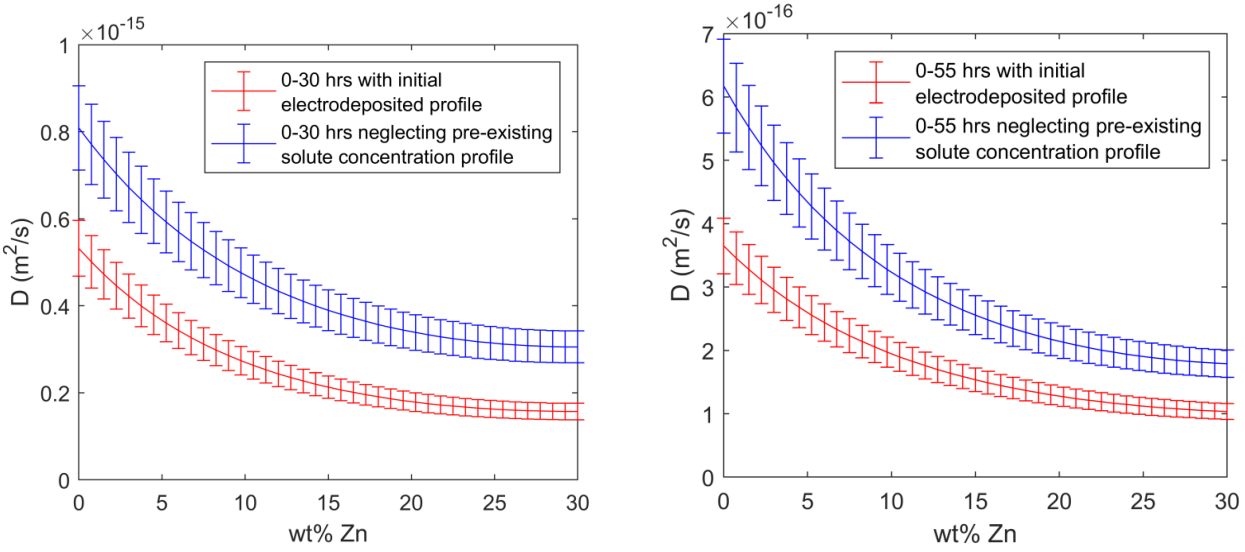

a b

Figure 6.17 Cu-Zn concentration dependence of the D(C) calculated using FSM-1 and FSM-2 for the Single-step diffusion between (a) 0-30 hrs and (b) 0-55hrs

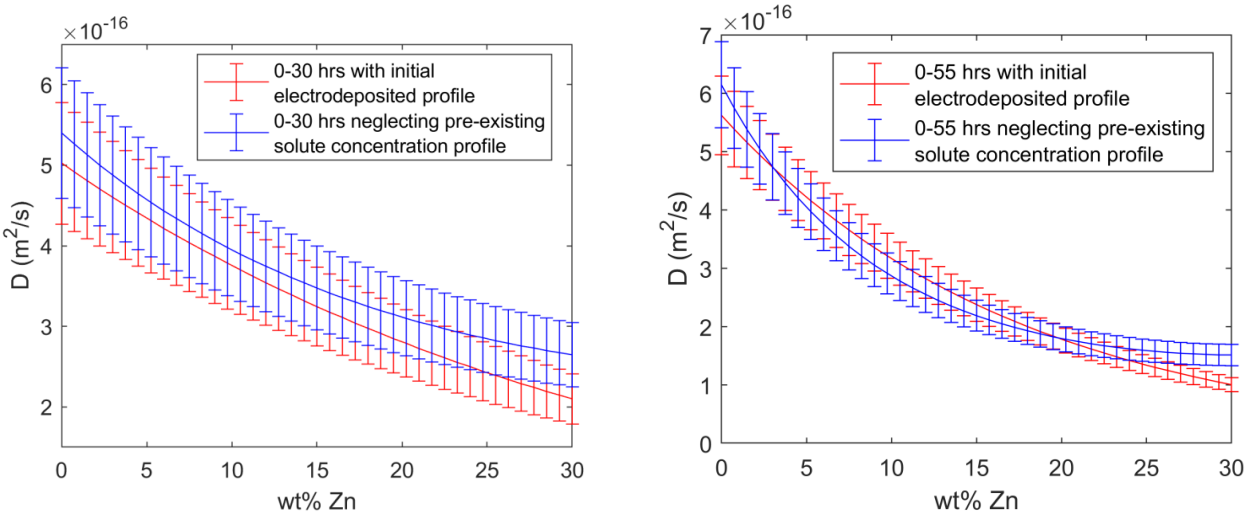

a b

Figure 6.18 Cu-Zn concentration dependence of the D(C) calculated using FSM-1 and FSM-2 for the Single-step diffusion between (a) 0-30 hrs and (b) 0-55hrs

6.3.1 Effect of pre-existing non-uniform solute distribution on ‘‘calculation-error-free’’ concentration dependence of interdiffusion coefficient

The focus in this section is to determine the effect of a pre-existing non-uniform solute distribution on "a calculation-error-free" D(C). This is achieved by comparing the D(C) calculated by using the FSM-2 for the one- and two-stage diffusion samples. The D(C) operative between 0-30 hrs, 0-55 hrs, and 30-55 hrs are calculated for the one- and two-stage diffusion processes and presented in Figures 6.19a, 6.19b, and 6.19c, respectively. The results presented in Figure 6.19 show that the experimental "calculation-error-free" D(C) under the one-stage and two-stage diffusion processes differ significantly at the same temperature and diffusion time. In addition, applying Equation 2.47, the concentration-averaged diffusivity (D_{ave}) is calculated by using "the calculation-error-free" D(C) under the one-stage and two-stage diffusion processes at each diffusion interval. The D_{ave} from the two-stage diffusion process differs from the values calculated in the one-stage diffusion process by 24%, 33%, and 62% for diffusion intervals of 0-30 hrs, 0-55 hrs, and 30-55 hrs, respectively. The percentage difference in D_{ave} is greater than the maximum 12% change in D_{ave} from samples under the same diffusion condition. D_{ave} further confirms that the calculation error-free D(C) from the one-stage diffusion process significantly differs from the values obtained in the two-stage diffusion process. The two systems were subjected to the same final diffusion process of 400^{o}C and the same final diffusion process but different pre-existing initial solute distributions. The difference in the "calculation-error-free" D(C) between the one-stage and two-stage diffusion processes is not due to errors that arise from assuming that there is no pre-existing solute distribution with the FSM-1. The disparity is attributed to the significantly different pre-existing non-uniform solute distribution before the final diffusion process in the one- and two-

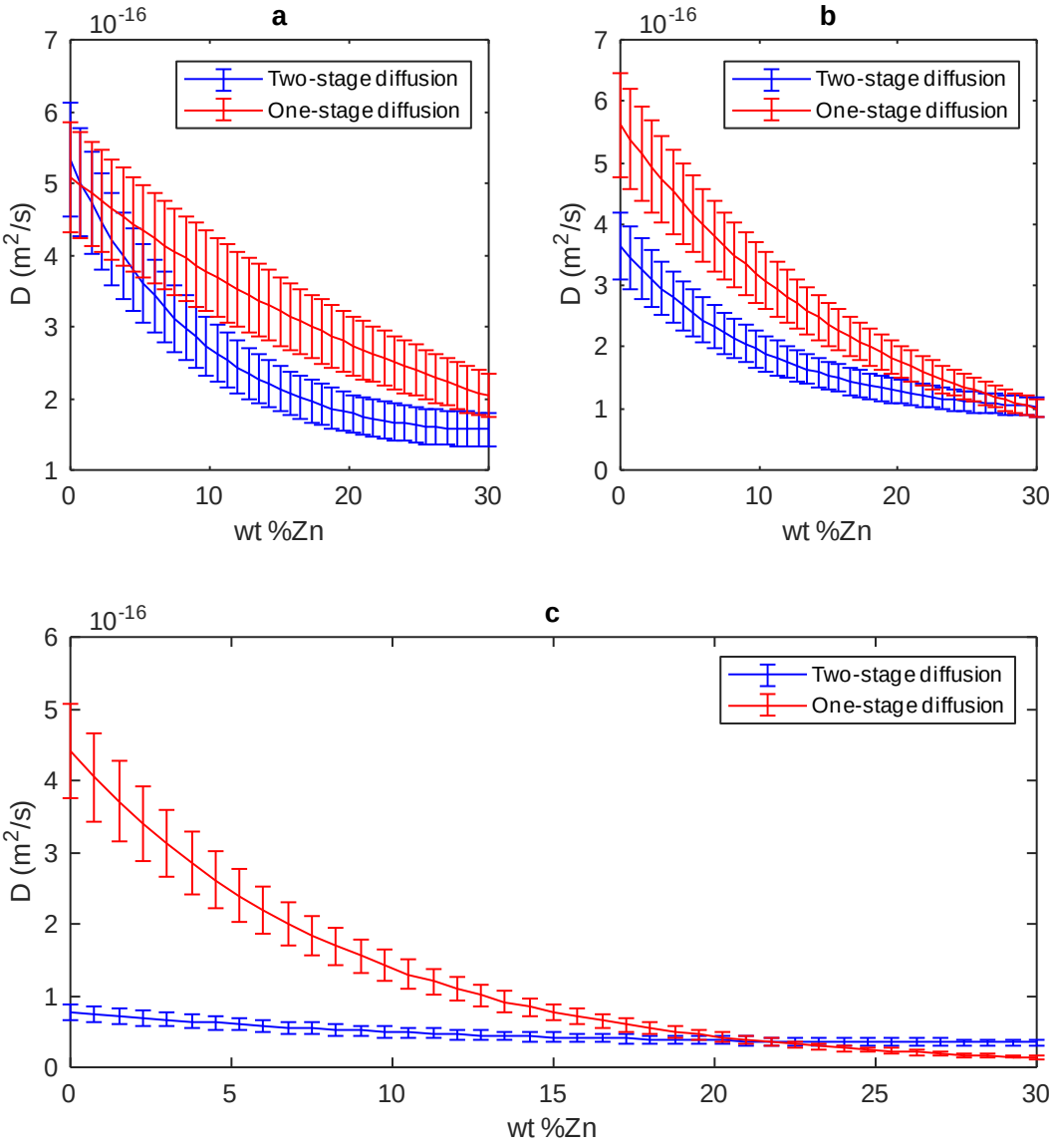

Figure 6.19 Comparison of concentration dependence of interdiffusion coefficient in Single-step and Two-stage Diffusion Conditions (a) 0-30 hrs (b) 0-55 hrs (c) 30-55 hrs

stage diffusion processes. Therefore, these results experimentally confirm that pre-existing non-uniform solute distribution can significantly alter the D(C) in experimental diffusion systems.

6.4 Implications of the Effect of Non-Uniform Initial Solute Distribution on D(C)

In the literature, there is a common practice of using the D(C) obtained from a one-stage diffusion process to simulate two-stage diffusion processes. To analyze a possible consequence of this practice, the D(C) calculated from a one-stage diffusion process, which basically does not have a pre-existing non-uniform solute distribution, will be used to predict a two-stage diffusion process. The D(C) of the sample from the one-stage diffusion, which was subjected to a diffusion process for 55 hrs at 400°C, was used to predict the final concentration profile of a sample subjected to a two-stage diffusion process for 55 hrs at 400°C. The predicted and experimental profiles of the two-stage diffusion process at 400°C for 55 hrs are presented in Figure 6.20. The concentration profiles in Figure 6.20 show that the practice of using the D(C) calculated under the condition where basically a non-uniform initial solute distribution does not exist to predict diffusion processes in a system with a significant pre-existing non-uniform solute distribution can lead to considerable errors. However, when the D(C) calculated by using FSM-2 is used to predict diffusion processes in a system with a significant pre-existing non-uniform solute distribution, there is a good agreement between the predicted and experimental profiles (Figure 6.20). Therefore, the D(C) calculated by using standard techniques without an initial solute gradient, such as the BM, SF, Hall, and Wagner methods, can result in inaccurate predictions during material diffusion processes with multiple stages like coating, age-hardening, diffusion brazing, and sintering treatments.

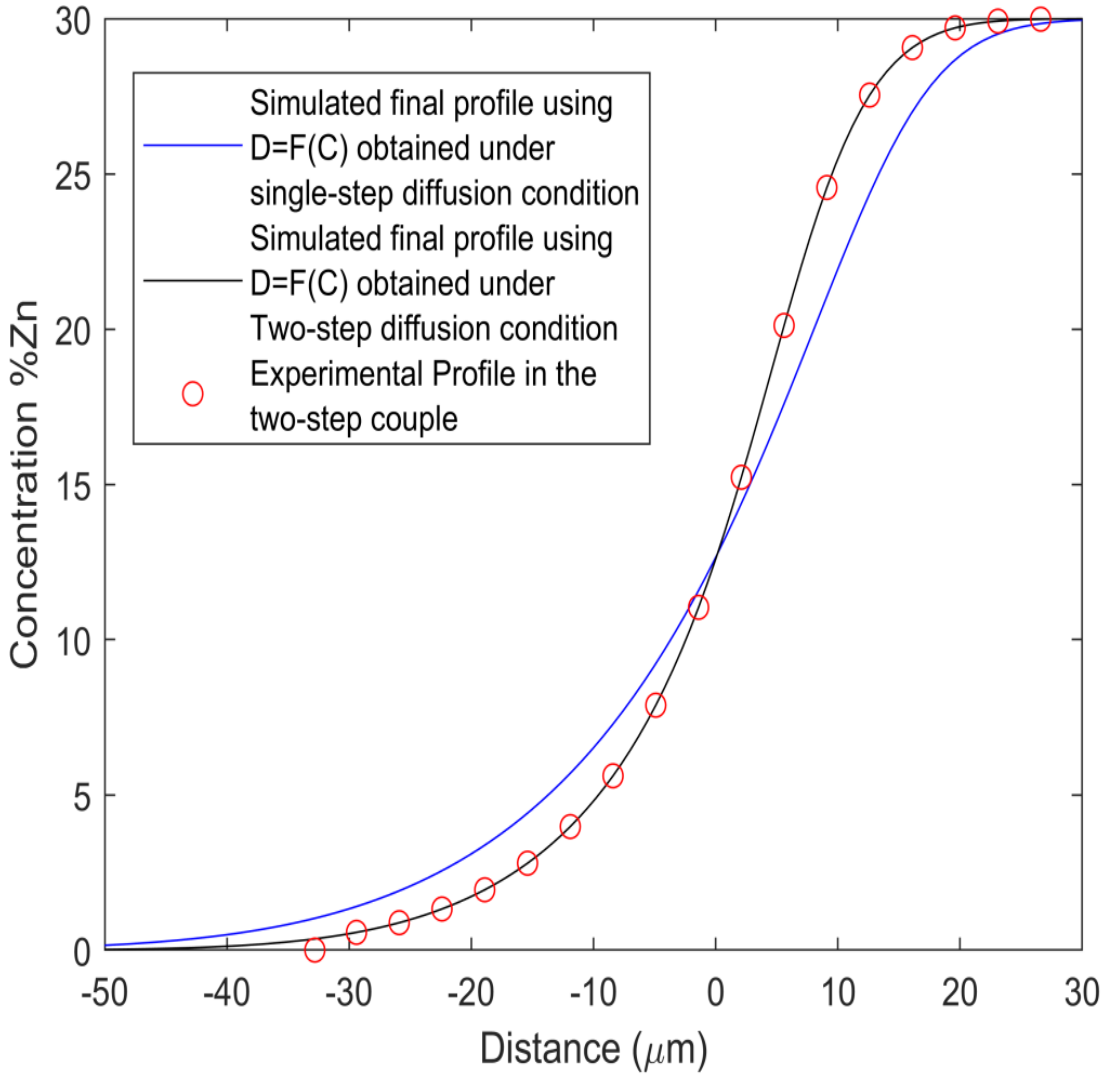

Figure 6.20 Experimental and predicted concentration profiles showing the significant error in predicting two-step diffusion processes using the D(C) obtained from the single-step diffusion, under the condition of "effectively no initial non-uniform solute distribution." Excellent agreement exists between the Experimental and predicted concentration profiles of the two-step diffusion process when the D(C) obtained from the two-step diffusion process is used.

CHAPTER SEVEN

7 ANALYSIS OF CONCENTRATION DEPENDENCE OF INTERDIFFUSION COEFFICIENT UNDER THE CONDITION OF A TIME-VARYING SURFACE CONCENTRATION

7.1 Introduction

D(C) are essential for the analysis and understanding of several diffusion-controlled phase transformation reactions and for simulating diffusion-based material processing methods such as sintering, coating, brazing, etc. Generally, standard analytical methods are used to compute D(C), and these methods include Boltzmann-Matano (**BM**), Sauer- Freise (**SF**), Hall, and Wagner method [114]–[118]. Fundamentally, from the derivation of the standard methods, the D(C) obtained by these methods are based on the assumption that the solute concentration is dependent on a single variable, λ, where λ is the ratio of distance to the square-root of time $\left(\lambda = r/\sqrt{t}\right)$, known as the Boltzmann's parameter. This assumption is valid provided the surface/boundary concentrations remain constant throughout the diffusion process. However, this is not the case for several practical diffusion processes, such as during homogenization heat treatments after the dissolution of a secondary phase, casting, sintering, diffusion brazing, or surface alloying and coating by diffusion. During these processes, at least one of the surface concentrations (**SC**) changes with time, which invalidates the use of Boltzmann's parameter. Hence, the standard analytical methods like the **BM**, **SF**, and Wagner methods cannot be used to calculate the D(C) under the condition of a time-varying surface concentration. The usual practice is that the D(C) obtained by the standard analytical methods, under the condition of constant surface

concentrations, is assumed to be valid for conditions where surface concentration changes with time. This crucial assumption, however, needs to be appropriately verified both experimentally, and theoretically. To experimentally verify this vital assumption, an appropriate method for computing D(C), which does not rely on the assumption that solute concentration is a function of a single variable, λ, is required. It has been established that numerical inverse methods, which do not rely on the assumption that solute concentration is a function of a single variable, can be used to overcome the limitations of the standard analytical methods for computing accurate D(C) [30], [119]. Therefore, the main goal of this chapter is to verify the assumption that the D(C) obtained from constant surface conditions are reliable enough to analyze diffusion in time-varying SC processes. This investigation will involve a theoretical study using the DIS influenced model to simulate theoretical concentration profiles and calculate their effective D(C). In the experimental verification, numerical inverse methods, which do not rely on the assumption of a parabolic relationship, will be used to overcome the limitations of the standard analytical methods to calculate accurate D(C) [22], [120]. The FSM is an appropriate numerical inverse method that can calculate the D(C) with a time-varying SC. This chapter thus starts with a theoretical study of the assumption, followed by the experimental verification of the theoretical results. The chapter concludes with a discussion of the implications of the findings in this chapter.

7.2 Theoretical Study of the Effect of Time-Varying Surface Concentration on D(C)

The effect of time-varying SC on the interdiffusion coefficient is theoretically studied in this section. The concentration profiles, pressure distributions, and D(C) under DIS were theoretically simulated by using the numerical model developed in section 3.2. To understand the effect, the effective D(C) is compared in a system with time-varying SC and a system without solute build

up. To do so, all the parameters are held constant while the initial thickness of the solute source is varied to realize either a time-varying SC or a constant SC. The numerical model developed in section 3.2 is applied to the two solute source thicknesses to simulate the final concentration and pressure distributions for time-varying SC and constant SC conditions. The thicker sample produces a constant solute SC system, while the less thick sample gives the time-varying SC system. The final solute and pressure distributions are used to calculate the effective D(C) for time-varying and constant SC conditions.

The dimensionless parameters are: $V_1' = 1.0,\ V_2' = 0.9091,\ D_1^{*'} = 0.01,\ D_2^{*'} = 1.0,$

$\eta' = 0.0001872,\ T' = 0.0034,\ t' = 0.0208,$ and $\alpha' = 0.$

The dimensionless solute source thickness for time-varying SC is 0.0117, whereas that for the constant SC is 0.6817. The data are used to theoretically simulate the concentration profiles and pressure distributions by using Equations 3.45-3.50. The simulated concentration profiles for the time-varying SC are presented in Figure 7.1a. Similarly, the theoretically simulated concentration profile for the constant SC system is reported in Figure 7.1b. The profiles show that changing the solute source thickness can result in either a time-varying or a constant SC with a different concentration gradient. The pressure gradients for the constant SC and time-varying SC are presented in Figure 7.2, and the plot shows the change in pressure gradient when SC changes with time. Figure 7.2 shows that pressure/stress distribution due to DIS varies as the SC changes with time. The effective dimensionless D(C) in both systems is calculated by using Equation 3.21, and the results are presented in Figure 7.3 for both time-varying and constant SC cases. Figure 7.3 illustrates a theoretical change in the D(C) under DIS between systems with constant and time-

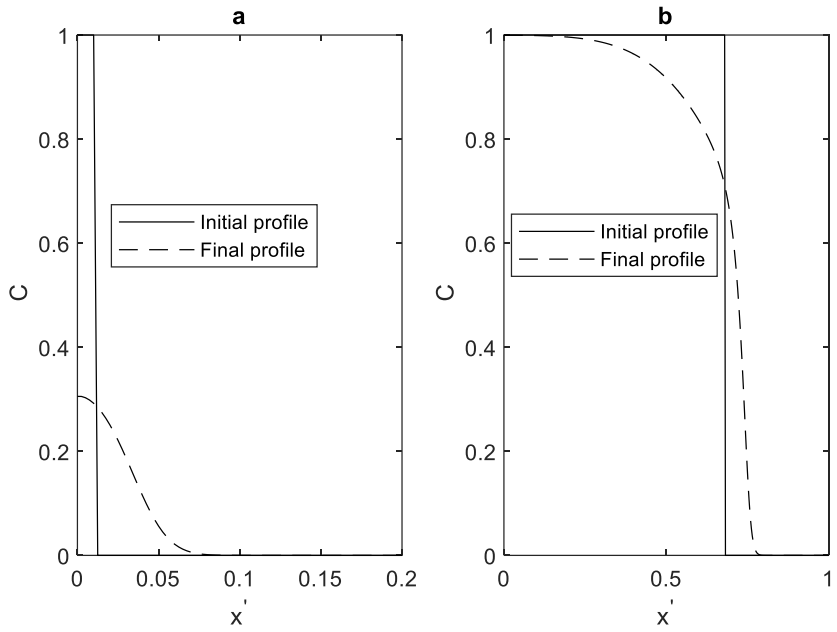

Figure 7.1 Theoretically simulated concentration profiles for (a) Time-varying concentration diffusion process (b) Constant surface concentration diffusion process

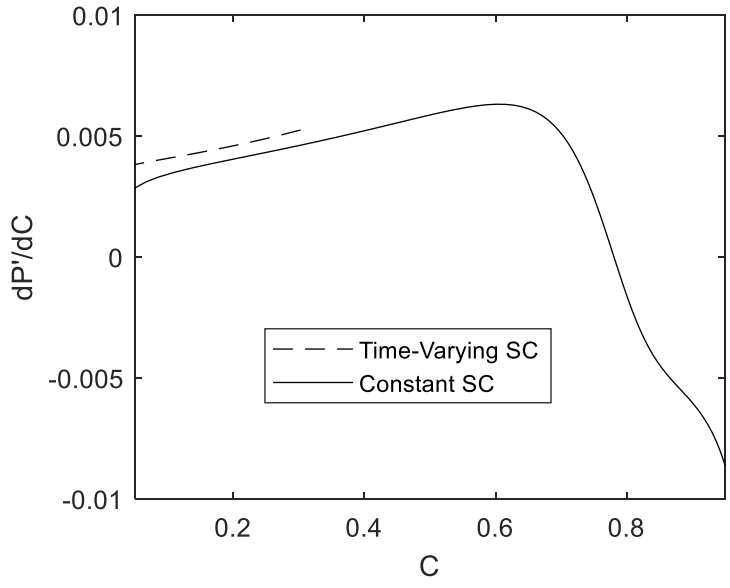

Figure 7.2 Theoretical pressure distributions for both the time-varying and constant surface concentration diffusion process

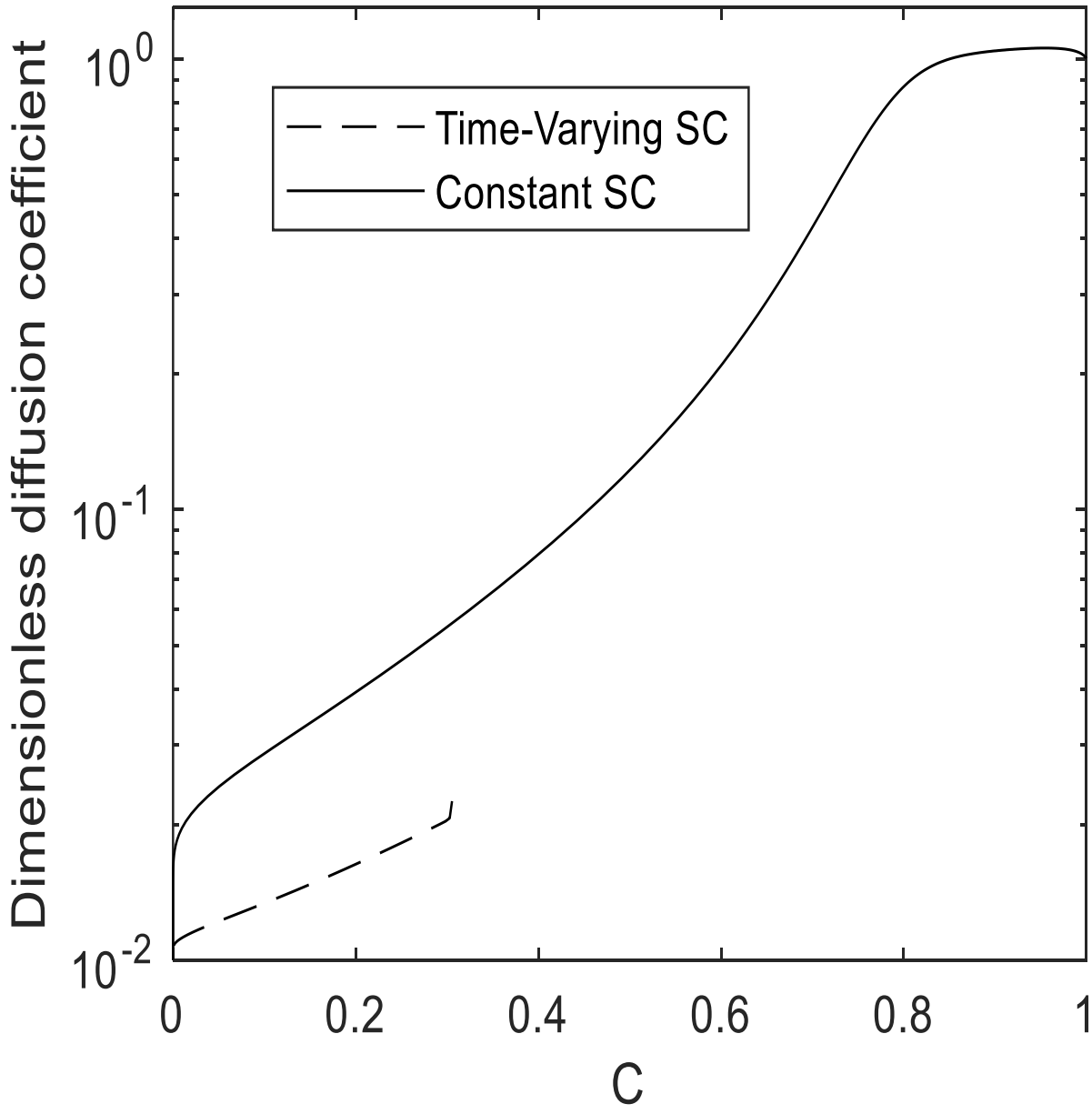

Figure 7.3 Theoretical effective D(C) for both the time-varying and constant surface concentration diffusion process

varying SC. It is generally known that the presence of stress/strain in a crystal lattice can significantly influence diffusivity [8], [10]–[15]; hence, it is conceivable that the D(C) can change as the SC changes with time due to the influence of the **DIS**. Therefore, theoretically, when the DIS in a system is considered, the D(C), which satisfies Fick's second law of diffusion, can be significantly altered when a system changes from a constant SC to a time-varying SC.

7.3 Experimental Verification

This section will present the experimental procedure for verifying the effect of time-varying SC on the D(C). A comparison between the experimental time-varying and constant SC was made by depositing Cu of two different thicknesses on a Ni-Cu alloy with a chemical composition of 90% Cu and 10% Ni.

7.3.1 Experimental procedure

. The experimental procedure is as follows:

1. The homogeneity of the samples with a flat surface and dimensions of 100 mm by 100 mm with a thickness of 1.4 mm was first validated through a microanalysis.
2. The alloy samples were polished, placed in a sealed quartz tube backfilled with high purity argon, and heated at 950°C for 24 hrs to grow the grains and relieve the residual stresses that could interfere with diffusion at lower temperatures.
3. Subsequently, the Ni-Cu alloy was chemically cleaned. The alloy was:
   a) heated for 20 minutes in a boiling solution of sodium hydroxide, sodium phosphate, and sodium carbonate,

b) rinsed with distilled water before immersed for 10 minutes in a 30% HCl solution at room temperature,

c) rinsed with distilled water before heated for 5 minutes in a boiling 10% sulphuric acid solution, and

d) rinsed with distilled water before heated for 5 minutes in a 5% sulphuric acid solution at room temperature.

The samples were divided into two sets. Copper was deposited on the first set of samples, which were chemically cleaned at a current density of 4 mA/cm^2 until reaching a deposition thickness of 30 microns. Similarly, Cu was also deposited on the second set of samples until they reached a thickness of 200 microns. The former are henceforth referred to as the 30Th samples, while the latter are the 200Th samples. The two sets of samples were placed in a sealed quartz tube backfilled with high purity argon and subjected to diffusion heat treatment at 780^{o}C for 5, 35, and 135 hrs. The diffusion samples were sectioned using EDM, then mounted, grounded, and polished using standard metallography sample preparation techniques. Microanalyses of the two sets of samples were performed by using X-ray and wavelength dispersive spectroscopy techniques. The composition profiles were measured in the perpendicular direction to the interface. To determine the uncertainties in the experiment, the following steps were carried out:

a) Three separate samples with the same thickness of deposited Cu were subjected to the same diffusion temperature and time.

b) At least five different concentration profiles were taken from each of the three (3) samples to calculate the average dependence of the interdiffusivity on the concentration in each sample. This averaging process for each sample reduces the sample-to-sample variation in the concentration profiles used to extract the D(C).

c) Subsequently, the FSM coupled with the new model was used to extract the D(C) from the experimental composition results.

d) The concentration-averaged diffusion coefficient (D_{ave}) for each sample was calculated by using the average dependence of the interdiffusivity on the concentration in each sample.

e) The variations from the average dependence of the interdiffusivity on the concentration in each of the three (3) samples were analyzed to determine the extent of uncertainty due to experimental errors.

f) Two criteria were used to determine the extent of uncertainty in the experimental data. These are the percentage change in concentration-averaged diffusion coefficient (D_{ave}) and the standard deviation plot of the three average interdiffusion coefficients against concentration.

g) The three D_{ave} for the condition variations were analyzed for the D_{ave} criteria to determine the extent of uncertainty in the experimental errors for each diffusion condition. This was done by calculating the maximum percentage change in the D_{ave} for each condition. In this study, the maximum variation in D_{ave} from the three samples falls below 15%, which is consistent with the uncertainty reported in the literature for two interdiffusion coefficients considered statistically similar [12], [67], [90], [112], [113].

h) For the second criteria, regions with no overlap between the error bars of the three average interdiffusion coefficients against concentration in the one- and two-stage diffusion processes indicate a change in the D(C).

The concentration profiles in the 30Th and 200Th samples at 0, 5, 35, and 135 hrs are presented

in Figures 7.4a and 7.4b, respectively. Electromigration introduces the 0 hr profiles during the electrodeposition process [52], [53]. As illustrated in Figure 7.4, the diffusion process between 0 – 5 hrs take place at a constant SC in both the 30Th and 200Th samples. In contrast, between 35–135 hrs of diffusion, the SC is constant in the 200Th sample and changes with time in the 30Th samples. The standard analytical methods such as BM, SF, and Hall methods that are often used to calculate the D(C) from experimental concentration profiles cannot be used when the SC changes with time. Standard analytical methods result in erroneous D(C) under these conditions. The FSM coupled with the new numerical model in this study can accurately calculate the D(C) by an iterative process. An excellent agreement between the experimental and simulated profiles indicates an accurate D(C). This numerical method eliminates calculation errors due to the consideration of a non-uniform solute distribution that exists before the main diffusion by incorporating the initial solute into the calculation system. The D(C) operable in the 30Th and 200Th samples will be compared and discussed in the subsequent sections.

7.3.2 Comparison of the D(C) operative in the 30Th and 200Th samples with constant surface concentration

The FSM, coupled with the new numerical model in section 3.3, is used to calculate the D(C) operative between 0 - 5 hrs in the 30Th and 200Th samples. This procedure establishes if the samples with different thicknesses are effectively the same under constant SC. The profiles at 0 hr are used as the initial profile at 0 hr. The D(C) that reproduces the experimental results at 5 hrs of diffusion is iteratively determined for the 30Th samples. Similarly, the process is also repeated for the 200Th samples. The simulated and experimental profiles are presented in Figures 7.5a and 7.5b

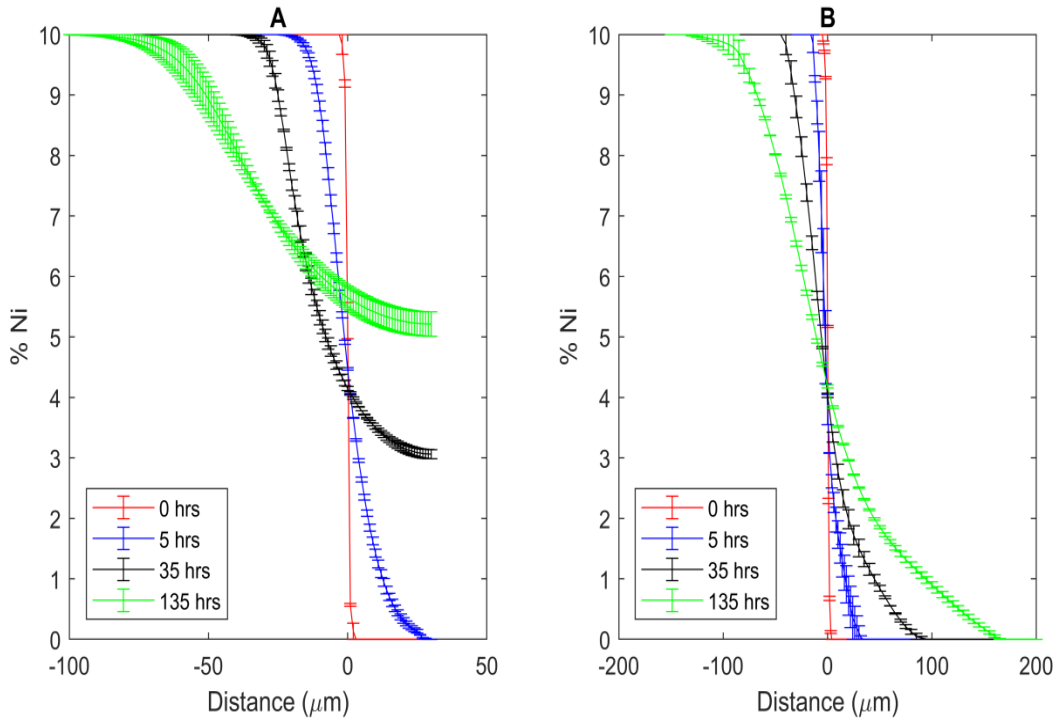

Figure 7.4 Experimental concentration profiles for (a) 30Th samples, and (b) 200Th sample

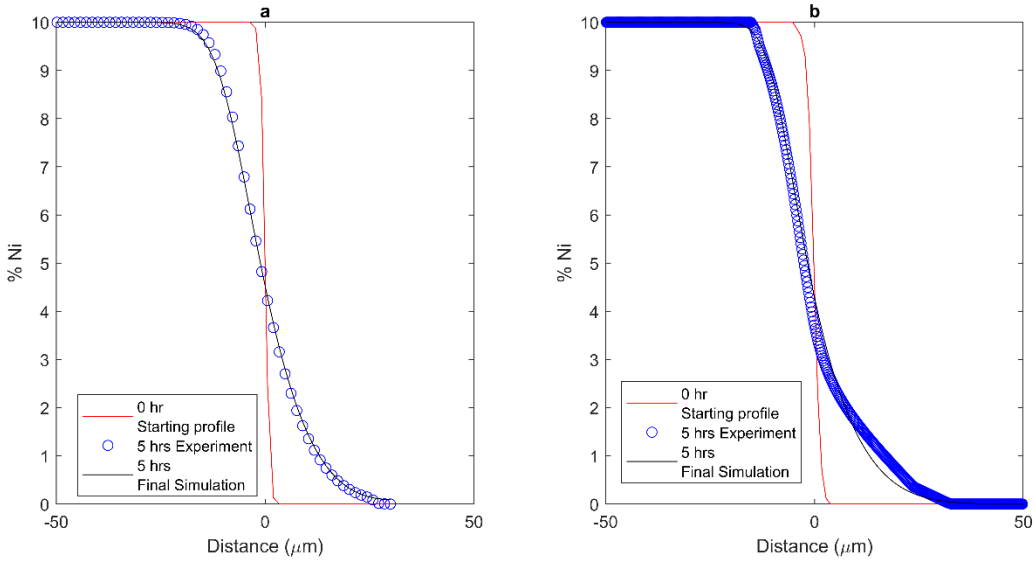

Figure 7.5 Comparison between the simulated and actual experimental concentration profiles for (a) 30Th samples and (b) 200Th samples

for the 30Th and 200Th samples, respectively. The agreement between the experimental and simulated profiles indicates that the calculated D(C) is reliable. The calculated D(C) of the 30Th and 200Th samples are presented in Figures 7.6, respectively. The error bars in Figures 7.6 show that the D(C) in both samples are statistically the same. The D_{ave} is also calculated and determined to be $0.2549\times10^{-14} m^2/s$ and $0.2552\times10^{-14} m^2/s$ in the 30Th and 200Th samples, respectively, between 0 – 5 hrs of diffusion. This is a difference of less than 1% and insignificant when compared to the maximum sample-to-sample variation of 15%. Therefore, the error bars of the D(C) and percentage change in the D_{ave} in the 30Th and 200Th samples show that both sets of samples are similar under constant SC conditions.

7.3.3 Comparison of D(C) operative in the 30Th and 200Th samples with constant and time-varying surface concentrations

The FSM coupled with the new numerical model in section 3.3 was also used to calculate the D(C) in the 200Th and 30Th samples to determine whether the D(C) in both systems are effectively the same under constant and time-varying SC, respectively. The concentration profile at 35 hrs was used as the initial profile to determine the D(C) that reproduces the experimental results at 135 hrs of diffusion in the 30Th samples. Under this condition, the SC changes with diffusion time. Similarly, the process is also repeated for the 200Th samples, with a constant SC. The simulated and experimental profiles are presented in Figures 7.7a and 7.7b for the 30Th and 200Th samples, respectively. The agreement between the experimental and simulated profiles indicates that the calculated D(C) are reliable. The calculated D(C) in both samples are presented in Figures 7.8. The error bars in Figure 7.8 prove that the D(C) in both samples are statistically different. The D(C) under a time-varying SC is smaller than that under a constant SC. The D_{ave} between the same

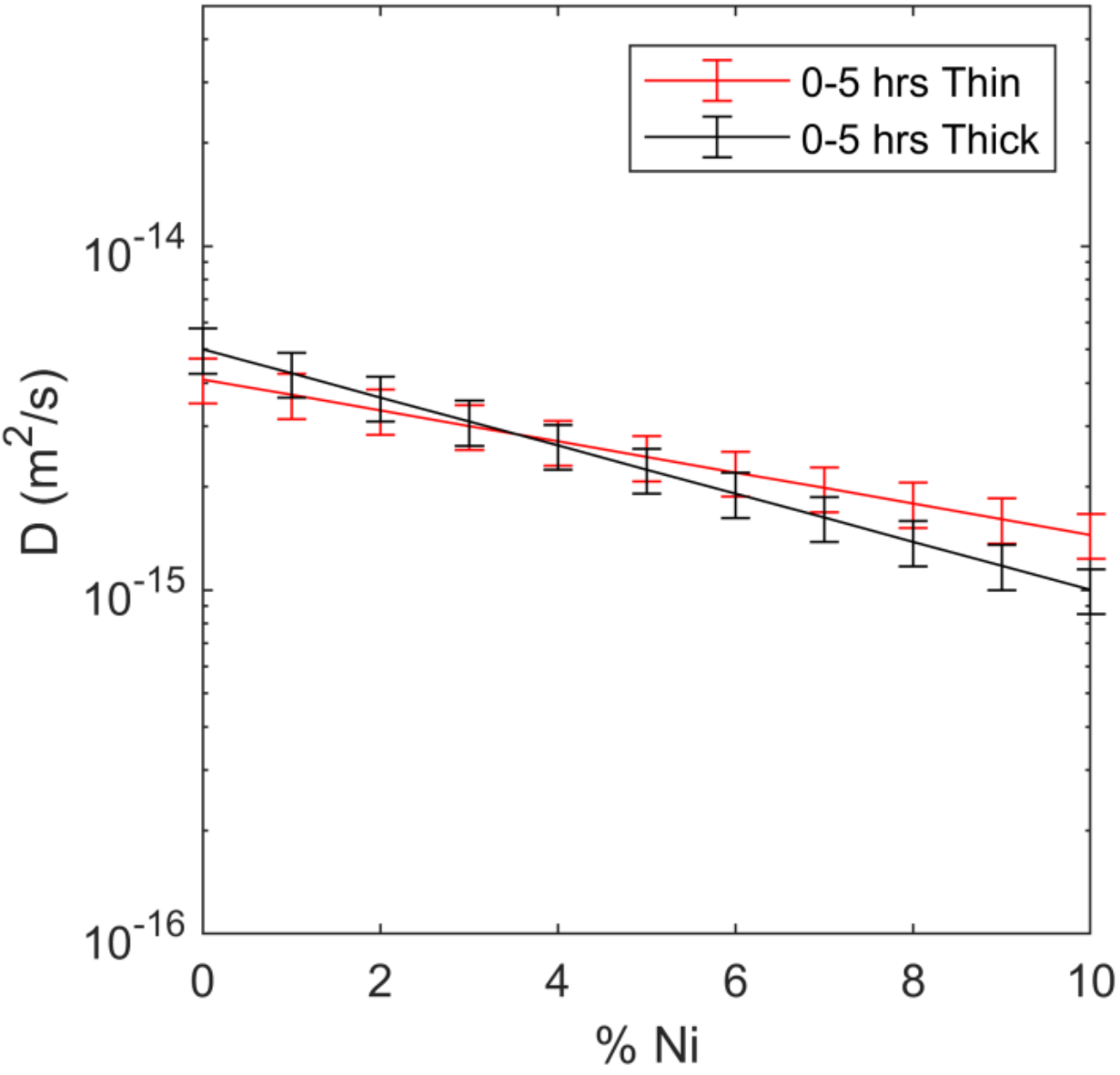

Figure 7.6 D vs C in 30Th and 200Th samples with constant surface concentration

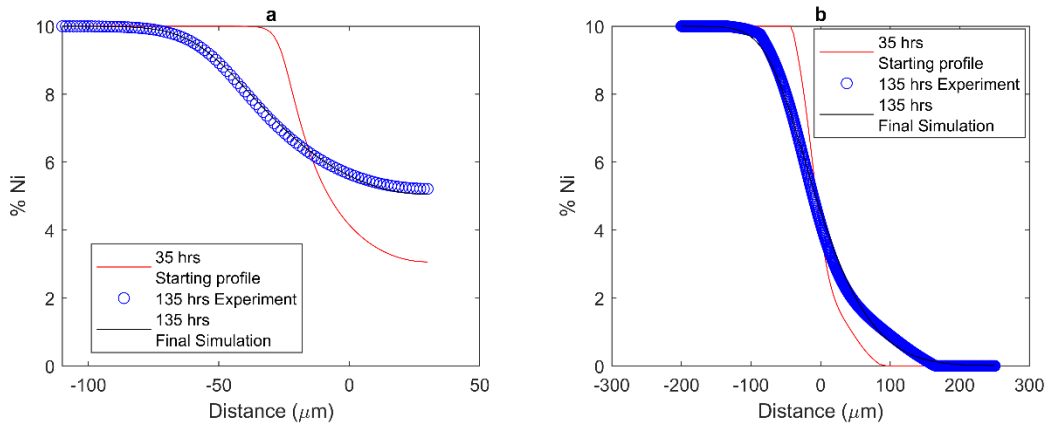

Figure 7.7 Simulated concentration profiles produced by using the D(C) computed by the numerical inverse forward simulation method, in comparison with actual experimental concentration profiles for (A) 30Th sample with time-varying surface concentration, and (B) 200Th sample with constant surface concentration

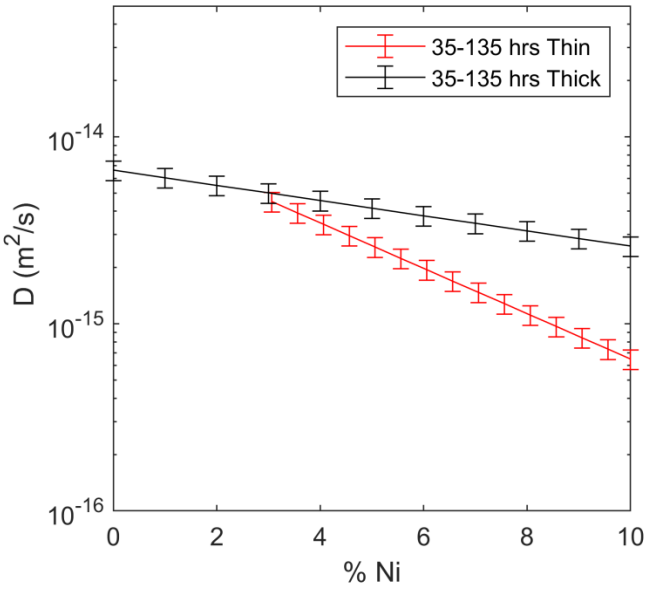

Figure 7.8 Disparity between the D vs C in both 30Th and 200Th samples with constant surface concentration and time-varying surface concentrations

concentration range is also calculated and reported in Table 7.1. The difference in the D_{ave} between the time-varying and constant SC systems is about 52%, which is significantly higher than the maximum sample-to-sample variation of 15%. Therefore, the results in this section confirm that experimentally, when the SC changes, the D(C) changes from the D(C) under a constant SC with the same conditions.

7.4 Implication of The Effect of Time-Varying Surface Concentration

The experimental and theoretical investigations done in this study have revealed that the D(C) from a constant SC differs from the effective D(C) from a time-varying SC. Hence, the common use of D(C) from a constant SC to simulate and analyze processes with time-varying SC may lead to significant errors. The possibility of errors is investigated by using the experimental D(C) for 35-135 hrs under constant SC to simulate the concentration profile expected in the same time duration under time-varying SC. The simulation result and experimental data are presented and compared in Figure 7.9. The error for the solute penetration is about 40%, and the simulated profile is well beyond the experimental error range. These results show that using a D(C) obtained under constant SC to simulate concentration profiles under time-varying SC produces an erroneous result (Figure 7.9). This result contrasts with the previous result, which shows that the experimental D(C) obtained under a time-varying SC can accurately predict the experimental profiles under the same condition (Figure 7.7b). This result is relevant in diffusion processes where at least one surface has solute build-up or depletion. Therefore, due consideration of the potential differences between a D(C) operative with a constant SC and when at least a SC changes with time is crucial for reliable diffusion analyses with solute build-up or depletion.

Table 7.1: Concentration-averaged interdiffusion coefficient at different diffusion time intervals

Sample	Condition	Time interval (hrs)	D_{ave} (m^2/s) 10^{-14}	% change in D_{ave} from the constant surface concentration (0-5 hrs)	% change in D_{ave} from the constant surface concentration (35-135 hrs)
30Th sample	Constant surface concentration	0-5	0.26	-	40%
200Th sample	Constant surface concentration	0-5	0.26	0%	40%
30Th sample	Time varying concentration	35-135	0.20	53%	53%
200Th sample	Constant surface concentration	35-135	0.43	65%	-

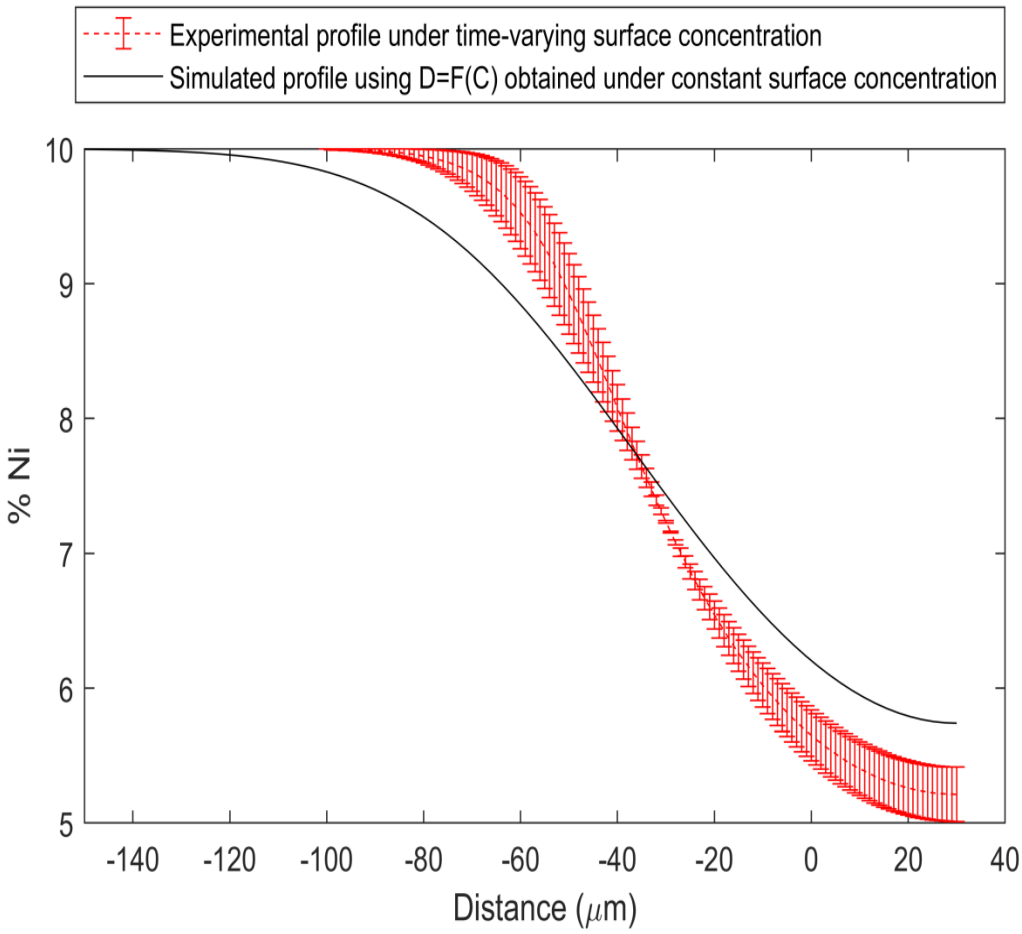

Figure 7.9 Comparison of the experimental profile under time-varying surface concentration and the theoretical profile prediction using the D(C) from a diffusion system with constant surface concentration

CHAPTER EIGHT

8 EFFECT OF SOLUTE-SOURCE COMPOSITION ON COMPOSITION-DEPENDENT INTERDIFFUSION COEFFICIENT

8.1 Introduction

Binary alloy systems are a convenient means of examining diffusion phenomena in metal systems. Therefore, the previous chapters in this thesis have investigated whether the assumption that the D(C) extracted from pure-metal/pure-metal diffusion couples can be applied to other systems with different conditions holds true. Another important boundary condition during diffusion is the value of the constant solute source (Cs). Pure-metal/pure-metal couples have a solute source composition that tends towards unity and zero sink composition. However, apart from pure-metal/pure-metal couples, it is common for industries to use pure-metal/alloy diffusion couples with a solute source composition that is not unity or sink concentrations that are not zero. In the literature, the D(C) from pure-metal/pure-metal couples are often used to analyze pure-metal/alloy diffusion couples. Nevertheless, when two systems have the same solute sink concentration, the composition gradient during diffusion can be altered by the solute-source composition (Cs) [121], [122]. Hence, different surface compositions (**SC**) can have different concentration gradients at the same concentration. A change in concentration gradient at the same concentration changes the DIS [7], [10]–[15], which then influences the D(C) [14], [15], [17], [18]. Theoretical and experimental comparisons between the D(C) from a pure-metal/pure-metal couple and a pure-metal/alloy couple are largely absent in the literature. In response to this deficiency, the goal of the chapter is to study the effect of the value of solute source concentration on D(C). The developed numerical model for

DIS-influenced diffusion will be used to investigate the effect of the magnitude of the solute source concentration on D(C). The experimental analyses will be performed by coupling the FSM and the new numerical model in section 3.3 of this study. Each of these objectives will be discussed in detail in the following sections.

8.2 Theoretical Study of The Effect of Surface Concentration on D(C)

The dimensionless composition and pressure equations in section 3.2 are solved simultaneously to simulate the concentration and pressure distribution in the diffusion systems. The equations are applied to two infinite diffusion couples with the following input parameters: Poisson's ratio: ν = $0.3, \eta' = 0.0001872$, $D_1^{*'} = 0.01$, $D_2^{*'} = 1.0$, $v_1' = 1.0$, $v_2' = 0.9091$, $T' = 0.0034$, and $t_1' = 0.0062$. The first diffusion couple is a pure-metal/pure-metal diffusion couple, with a solute source composition that tends towards unity and zero sink composition. In contrast, the second diffusion couple is a pure-metal/alloy diffusion couple with a 0.1 solute source composition and zero sink composition. The calculated concentration profiles for both systems under diffusion-induced stress are presented in Figure 8.1. Similarly, the calculated pressure gradients with respect to concentration gradients are also presented in Figure 8.2. From the profiles in Figure 8.1, it is evident that the concentration gradients for the same concentration are different. The differences in concentration gradients result in a pressure gradient disparity (Figure 8.2). The concentration profile and pressure gradients were used to calculate the effective D(C) in both systems, and the dimensionless effective D(C) are presented in Figure 8.3. The values in Figure 8.3 show the theoretical disparity between the D(C) when solute source concentration changes from 1 to 0.1. Therefore, the theoretical result shows that the D(C) in diffusion couples can significantly vary when the source concentration is different.

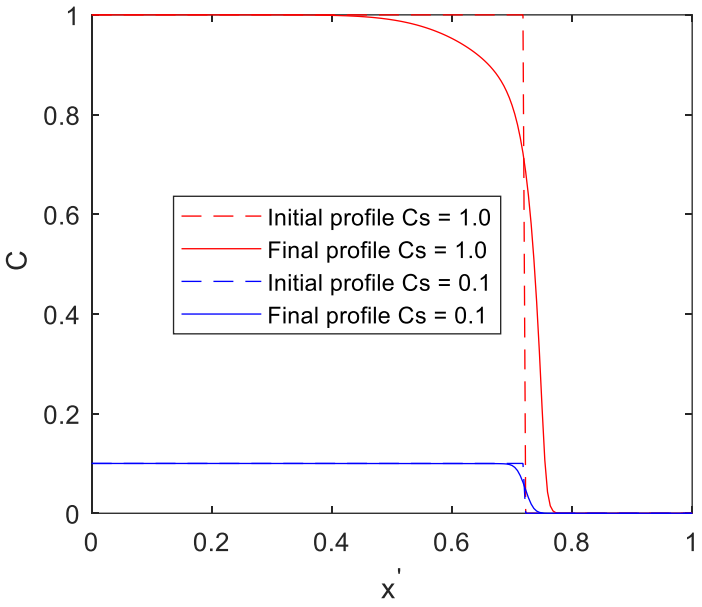

Figure 8.1 Theoretically simulated concentration profiles for different solute source concentrations

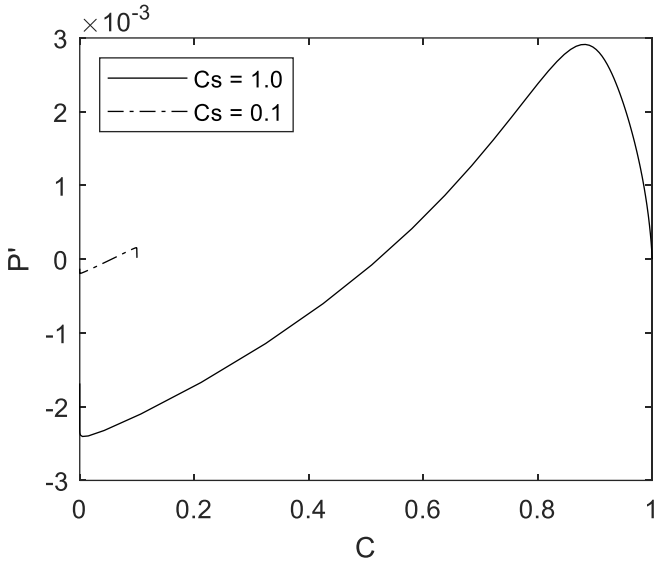

Figure 8.2 Theoretically simulated pressure gradients for different solute source concentrations

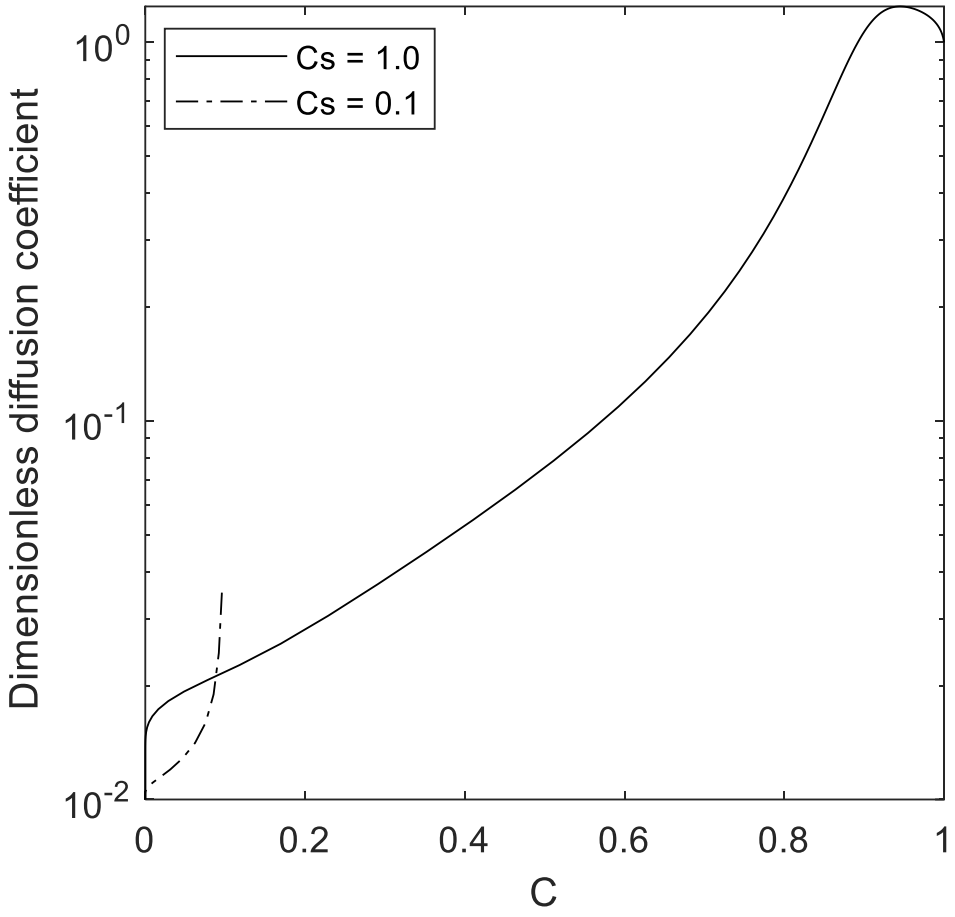

Figure 8.3 Theoretically calculated D(C) for different solute source concentrations

8.3 Experimental Verification of The Effect of Source Concentration On D(C)

This section will present the experimental procedure for verifying the effect of the solute source concentration on the D(C). The different experimental solute source concentrations will be compared by depositing Cu on pure metals and alloys, which produces pure-metal/pure-metal and pure-metal/alloy diffusion couples, respectively. In this investigation, the pure-metal/pure-metal diffusion couple is a Cu/Ni system, while the pure-metal/alloy diffusion couple is the Cu/Ni-Cu alloy. The systems are used because an experimental study in Opposits et al. has confirmed the presence of DIS in a Ni/Cu system [17].

8.3.1 Experimental procedure

The experimental procedure is as follows:

1. The homogeneity of pure 100% Ni and Ni-Cu alloy with a chemical composition (at%) of 10% Ni and 90% Cu, both with a thickness of 1 mm, was first validated through microanalysis.
2. The samples were polished, placed in a sealed quartz tube backfilled with high purity argon, and heated at 950°C for 24 hrs to grow the grains and relieve the residual stresses that could interfere with diffusion at lower temperatures. It is important to note that this process was performed prior to the electrodeposition of Cu onto the samples.
3. Subsequently, the pure Ni and Ni-Cu alloys were chemically cleaned. They were:

a) heated for 20 minutes in a boiling solution of sodium hydroxide, sodium phosphate, and sodium carbonate,

b) rinsed with distilled water before immersed for 10 minutes in a 30% hydrochloric acid (HCl) solution at room temperature,
c) rinsed with distilled water before heated for 5 minutes in a boiling 10% sulphuric acid solution, and
d) rinsed with distilled water before heated for 5 minutes in a 5% sulphuric acid solution at room temperature.

Copper was deposited on the chemically cleaned samples at a current density of 4 mA/cm^2 until reaching a deposition thickness of 180 microns. The two sets of samples were placed in a sealed quartz tube backfilled with high purity argon and subjected to a diffusion heat treatment at 800^oC for 60 hrs. The diffusion samples were sectioned by using EDM, and then mounted, grounded, and polished by using standard metallography sample preparation techniques. Microanalyses on the two sets of samples were performed by using X-ray and wavelength dispersive spectroscopy techniques. The composition profiles were measured in a perpendicular direction to the interface. The process was repeated for the other two samples.

To determine the uncertainties in the experiment, the following steps were carried out:

a) Three identical samples were subjected to the same diffusion temperature and time.
b) At least five different concentration profiles were obtained from each of the three (3) samples and used to calculate the average dependence of the interdiffusivity on the concentration in each sample. This process reduces the sample-to-sample variation in the concentration profiles used to extract the D(C).
c) Subsequently, the FSM coupled with the model in section 3.3 was used to extract the D(C) from the experimental composition results.

d) The concentration-averaged diffusion coefficient (D_{ave}) for each sample was calculated by using the average dependence of the interdiffusivity on the concentration for each sample.

e) The variations from the average dependence of interdiffusivity on the concentration in each of the three (3) samples were analyzed to determine the extent of the uncertainty due to experimental errors.

f) Two criteria were used to determine the extent of uncertainty in the experimental data. These are the percentage change in concentration-averaged diffusion coefficient (D_{ave}), and standard deviation of the three average interdiffusion coefficients plotted against concentration.

g) The three D_{ave} for the condition variations were analyzed for the D_{ave} criteria to determine the extent of uncertainty in the experimental errors for each diffusion condition. This was done by calculating the maximum percentage change in the D_{ave} for each condition. In this study, the maximum variation in D_{ave} from the three samples falls below 15%, which is consistent with the uncertainty reported in the literature for two interdiffusion coefficients considered statistically similar [12], [67], [90], [112], [113].

h) For the second criteria, regions with no overlap between the error bars of the three average interdiffusion coefficients against concentration in the pure-metal/pure-metal and pure-metal/alloy diffusion couples indicate a change in the D(C).

i) For the second criteria, regions of no overlap between the error bar plots of the three average interdiffusion coefficients against concentration in the pure-metal/pure-metal and pure-metal/alloy diffusion couples indicate a change in D(C).

8.3.2 Comparison of D(C): pure-metal/pure-metal diffusion couple vs. pure-metal/alloy diffusion couple

The average experimental composition results from the pure-metal/pure-metal diffusion and pure-metal/alloy diffusion couples are presented in Figure 8.4. The '0 hr' composition profiles are the initial condition prior to diffusion, which resulted from electromigration during the electrodeposition process. Similarly, the composition profiles at 60 hrs are also reported for both systems (Figure 8.4). The FSM is coupled with the new numerical model in section 3.3 to extract a reliable D(C) from the experimental system. Interestingly, the good agreement between the numerically simulated and experimental profiles, as presented in Figure 8.5, confirms the reliability of the new approach and accuracy of the D(C) data. The calculated D(C), along with the standard deviation of errors for the pure-metal/pure-metal and pure-metal/alloy diffusion couples, are presented in Figure 8.6. The results in Figure 8.6 illustrate the experimental difference between the D(C) in a pure-metal/pure-metal diffusion system versus the D(C) in a pure-metal/alloy diffusion system. Furthermore, the D_{ave} is calculated for the same composition range of 0-0.1 in each diffusion system. The D_{ave} between compositions of 0 - 0.10 is 0.208×10^{-14} m^2/s for Cs=0.1, and 0.859×10^{-14} m^2/s for Cs=1.0. The % change of D_{ave} of the pure-metal/alloy diffusion system vs. that of the pure-metal/pure-metal diffusion system is about 76%, which is higher than the highest uncertainty of 15% found experimentally. The experimental results thus confirm that changing the constant SC in systems can result in a significant change in the D(C), as variations in constant SC change the concentration gradient distribution [121], [122], which alters the DIS[7], [10]–[15] and this is known to influence the D(C) [14], [15], [17], [18].

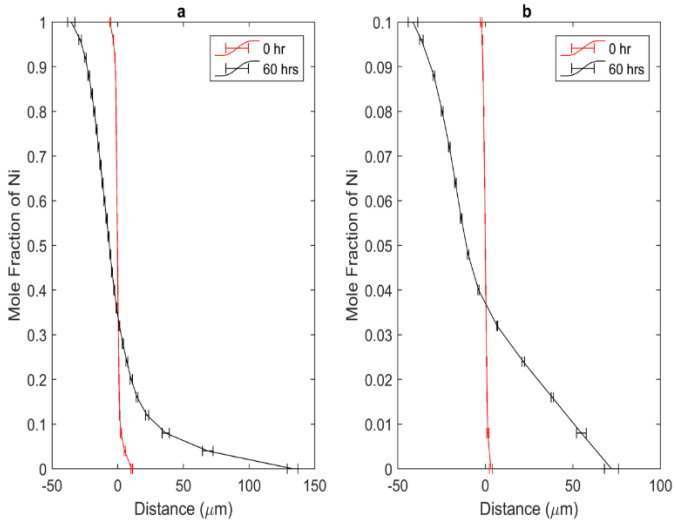

Figure 8.4 Experimental composition profiles for (a) pure-metal/pure-metal diffusion couple with Cs=1 at "0" hr and 60 hrs diffusion time and (b) pure-metal/alloy diffusion couple with Cs=0.1 at "0" hr and 60 hrs diffusion times

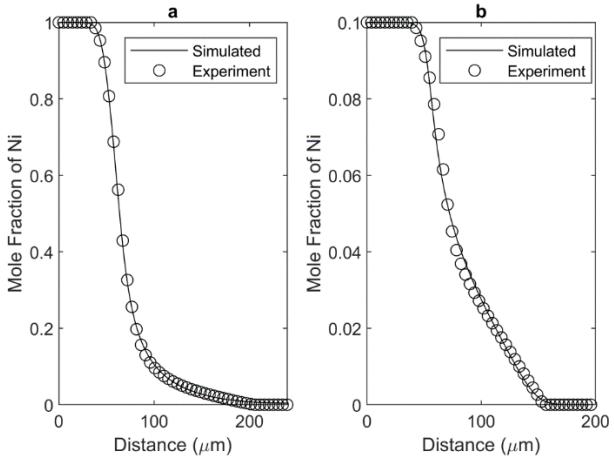

Figure 8.5 Comparison of the experimental and numerical concentration profiles for (a) pure-metal/pure-metal diffusion couple with Cs=1 and (b) pure-metal/alloy diffusion couple with Cs=0.1

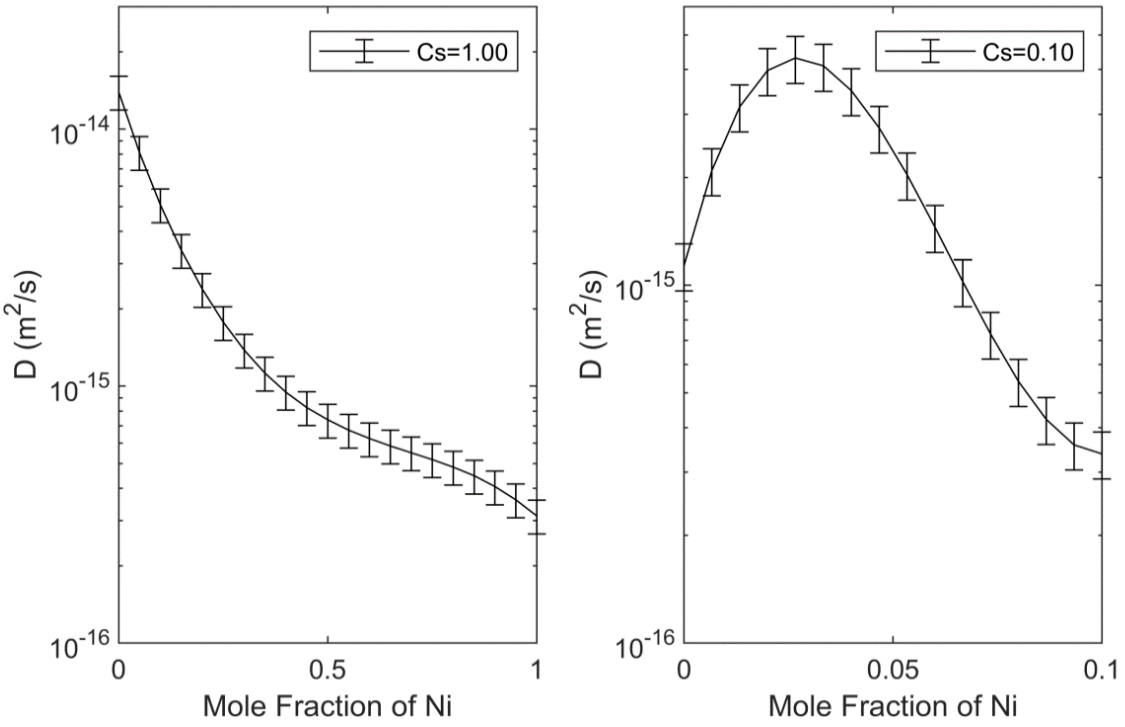

(a) (b)

Figure 8.6 Plots of D vs C in (a) pure-metal/pure-metal diffusion couple and (b) pure-metal/alloy diffusion couple

8.4 Implication of Effect of Surface Concentration on Concentration-Dependent Interdiffusion Coefficient

The previous sections have identified and discussed the effect of an SC on the D(C). However, it is crucial to understand the implication of this effect on diffusion analyses. To do so, the general expectation that the D(C) from a pure-metal/pure-metal diffusion couple can be used to simulate the diffusion process in a diffusion couple with an alloy will be analyzed. Hence, the experimental D(C) from the pure-metal/pure-metal diffusion sample at 60 hrs is used to simulate the diffusion process for 60 hrs in the experimental pure-metal/pure-alloy diffusion couple. The simulated composition and experimental profiles at the final diffusion time, in both pure-metal/pure-metal and pure-metal/alloy diffusion couples, are presented in Figure 8.7. Based on the composition profile in the pure-metal/alloy diffusion couple, the predicted diffusion affected zone is 350 μm, whereas the actual diffusion affected zone is 113 μm. The percentage difference in the error between the predicted and actual diffusion affected zone is 210%. Interestingly, using the D(C) from the pure-metal/pure metal diffusion couple to predict the diffusion zone of 113 μm after 60 hrs in a pure-metal/alloy diffusion couple will require a diffusion time of only 7.5 hrs. The difference in error of diffusion time is 52.5 hrs. Aside from the error in predicting the diffusion zone, another significant implication of using the D(C) from a pure-metal/pure metal diffusion couple to predict diffusion in a pure-metal/alloy system is an erroneous solute distribution. The large discrepancy in the solute distribution can be observed in Figure 8.7. Therefore, the common practice of using the D(C) from a pure-metal/pure-metal diffusion couple to predict and analyze diffusion in a pure-metal/alloy or alloy/alloy diffusion couple can result in a significant error in theoretical predictions. This analysis is critical in diffusion processes such as solid-solid diffusion couples and vapour-solid diffusion couples with different surface compositions.

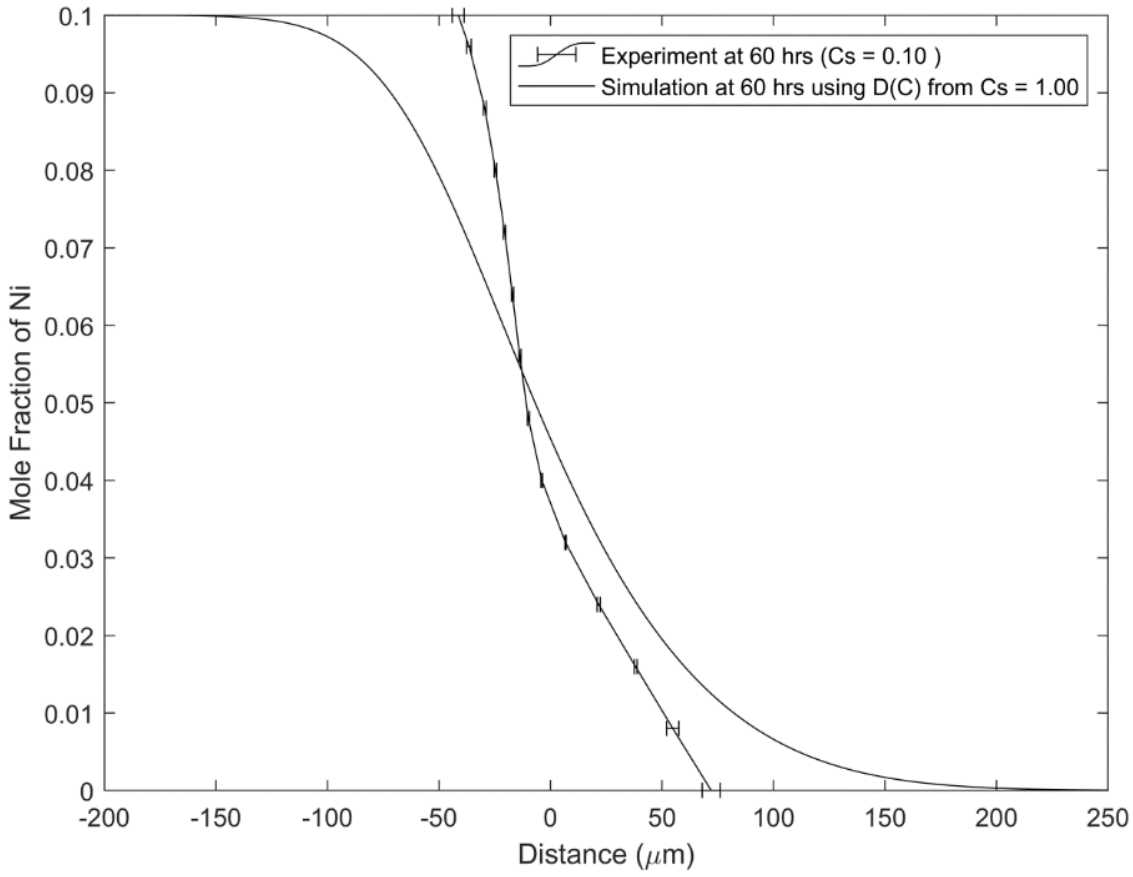

Figure 8.7 Comparison between the predicted composition profile in a pure-metal/alloy diffusion couple (Cs=0.1), computed using the D(C) in a pure-metal/pure-metal diffusion couple (Cs=1.0), and the actual experimental diffusion couple at the same diffusion time of 60 hrs.

CHAPTER NINE

9 EFFECT OF 1D AND 2D MIGRATION OF DIFFUSION INTERFACE ON CONCENTRATION-DEPENDENT INTERDIFFUSION COEFFICIENT

9.1 Introduction

There are several common types of diffusion processes found in non-planar geometries. Examples of these non-planar applications are sintering, coating, and repairing. In 2D planar diffusion systems, 1D diffusion causes the interface between solids to migrate in one direction, whereas, in diffusion couples with a non-planar interface, the interface between two solids can migrate in two directions (thus 2D diffusion). Notably, in the literature, the D(C) is considered an isothermally constant material parameter in both planar and non-planar geometries, regardless of the direction of the interface migration. Two crucial procedures arise from assuming a constant D(C) in planar/non-planar diffusion system analyses, including wire and plate experiments. The procedures are: (i) the common use of standard planar analytical models to extract the D(C) in non-planar systems such as wires and cylindrical holes, and (ii) the use of D(C) from planar systems to analyze diffusion in non-planar systems. The two procedures are issues of concern because they ignore two essentially relevant factors. First, the governing equation for diffusion that involves the migration of a 1D interface is different from that of 2D and 3D interfaces. Secondly, the diffusion geometry has been reported to influence the DIS during diffusion [7], [14]. A review of the literature shows that the comparison of the D(C) in diffusion systems with 1D migration of the interface and the function when diffusion proceeds in 2D has not been experimentally verified. This research gap is because commonly used methods, including the BM,

SF, and Hall methods, which are used to extract the D(C) from experimental data, can only be applied to a 1D planar geometry and do not apply to a 2D cylindrical geometry [114]–[118], [123], [124]. The analytical methods also assume that a non-uniform initial solute state does not exist in the system, and solute concentration depends on Boltzmann's parameter $\left(\lambda = r/\sqrt{t}\right)$. Notably, the Boltzmann parameter is not applicable when the interface migrates in a 2D cylindrical geometry [122]. Therefore, this chapter has two major objectives that address the two procedural issues raised. The first objective is to determine whether 1D planar methods can be used to extract reliable D(C) profiles from non-planar diffusion systems. The second objective is to theoretically investigate the D(C) in 1D and 2D migrations of interfaces under DIS conditions and experimentally verify the finding. The next section of this chapter will investigate the accuracy of the D(C) calculated from non-planar systems using 1D planar methods. The second section will study the assumption that D(C) is an isothermal material constant that is independent of the dimension of the migrating interface during diffusion and the sample geometry.

9.2 The Reliability of using 1D Interface Migration Models to Extract D(C) from Diffusion Systems With 2D and 3D Migration of Interface

In the literature, it has been noted that the use of planar methods to extract D(C) in non-planar experiments can be erroneous [18,19]. Nevertheless, this procedure is common in diffusion analyses because it is assumed that the diffusion in non-planar systems with 1D migration of the interface is the same as the diffusion in certain diffusion couples with 2D migration of the interface. This section investigates the first objective of this work by using numerical models to generate composition profiles in non-planar systems before subsequently using planar methods to extract

the D(C). Therefore, two possible factors that can affect the reliability of the assumption associated with using non-planar systems to extract D(C) in such non-planar systems will be investigated. The two factors are: (i) the initial interface position and (ii) diffusion duration. Concentration profiles in non-planar diffusion systems with 2D and 3D migration of the interface will be produced to carry out this task. Subsequently, the planar FSM coupled with a planar solution of Fick's diffusion law will extract the D(C) from the profiles. The extracted D(C) will be compared to the actual D(C) used to simulate the concentration profiles. The possible disparity between the calculated and actual D(C) will determine factors that increase the unreliability of this approach.

9.2.1 Initial interface position

An important parameter in 1D or 2D diffusion is the initial distance between the position of the interface and the center of a radial diffusion. The practical initial interface position is the diameter of the wires, holes, and balls prior to the welding stage of diffusion heat treatment. To investigate the influence of the position of the initial interface on the reliability of the D(C) extracted from diffusion systems, a stress-free D(C) will be used to simulate the diffusion process in a stress-free system. The new model in section 3.2, stress-free D(C), and three dimensionless initial interface positions are used for each geometry.

The simulation parameters are: $\nu = 0.3,\ \eta' = 0.0001872,\ D_1^{*'} = 0.01,\ D_2^{*'} = 1.0,\ v_1' = 1.0,\ v_2' = 1,$ $T' = 0.0038,\ \frac{\partial P'}{\partial r'} = 0,$ and $t_1' = 0.0031.$

In this section, 1D migration of the interface followed by 2D and 3D migration of the interface are considered. For the system with 1D migration of the interface, the concentration profiles are simulated for each interface position (Figure 9.1). The D(C) operative between the diffusion times

is calculated using the FSM coupled with the new numerical model in section 3.3 for planar systems. The calculated and actual D(C) are presented in Figure 9.1, and the results show that the initial interface position does not influence the reliability of D(C) from profiles generated and calculated in planar systems. A similar procedure is performed for diffusion with 2D migration of the interface, and the three concentration profiles are presented in Figure 9.2a. The 1D planar FSM coupled with the new numerical model in section 3.3 extracts the D(C) from the concentration profiles obtained in the system with the 2D migration of the interface. The D(C) extracted by using the 1D planar FSM and the actual D(C) used to simulate the profiles are compared; see Figure 9.2b. The results show that using the 1D planar FSM approach becomes less reliable as the initial interface position shifts to the centre of the diffusion, in the system with 2D migration of the interface. Similarly, the procedure is performed in a system with 3D migration of the interface. The simulated concentration profiles for the three initial interface positions are shown in Figure 9.3a; the actual and the calculated D(C) that use the 1D planar FSM are presented in Figure 9.3b. The results in Figure 9.3b also show that the D(C) error obtained by using the 1D planar FSM increases as the initial interface position shifts to the centre of the diffusion. Therefore, this result shows that an erroneous D(C) can be extracted by using planar methods when the diffusion is a non-planar diffusion experiment, and the error increases with a decreasing initial interface position such as the diameter of wires, holes, and balls prior to the welding stage of diffusion heat treatment.

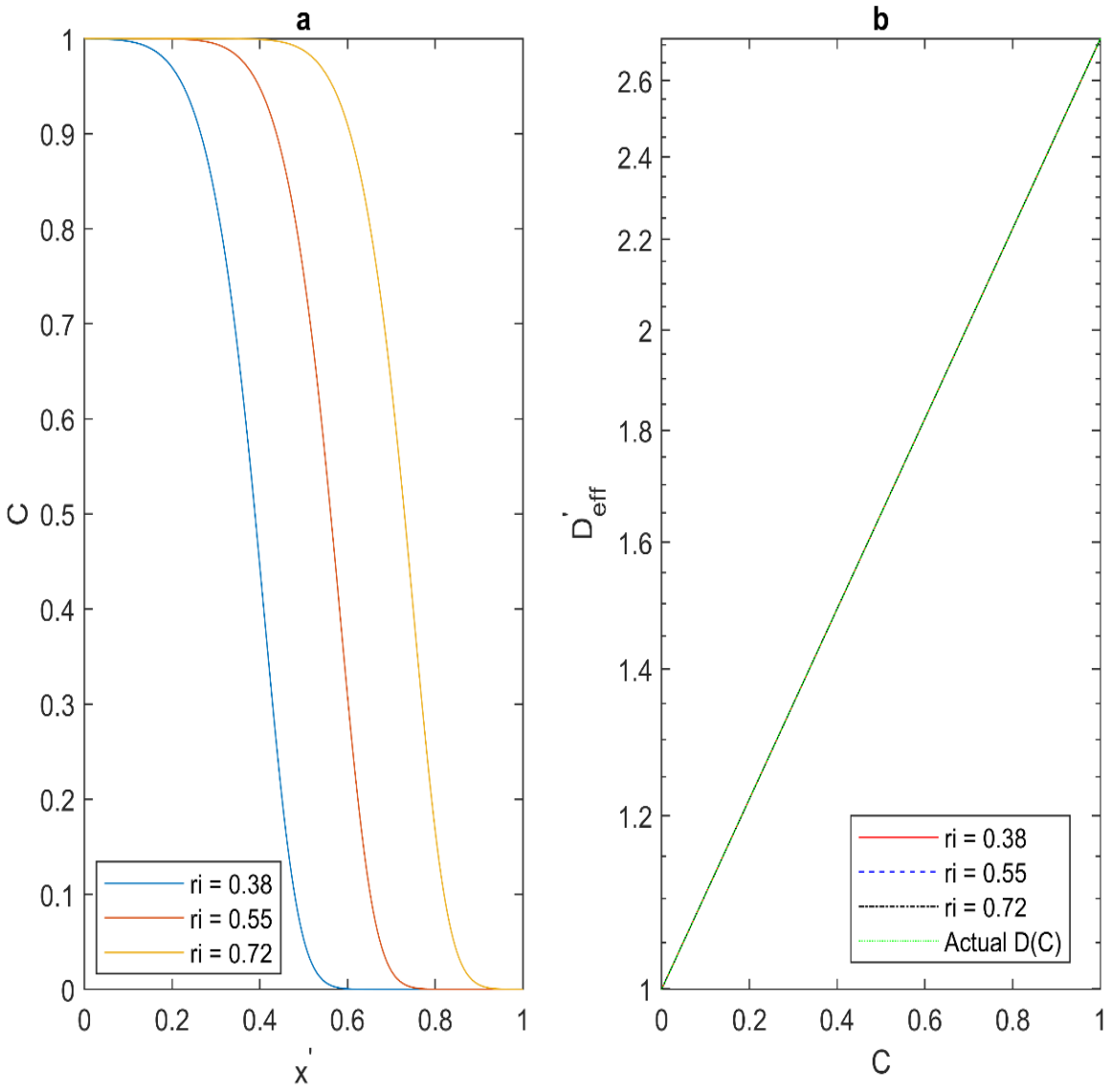

Figure 9.1 Stress-free 1D interface migration simulations for different initial interface positions (X_i) (a) Concentration profiles (b) Actual and 1D planar FSM computed D vs C for each initial interface positions

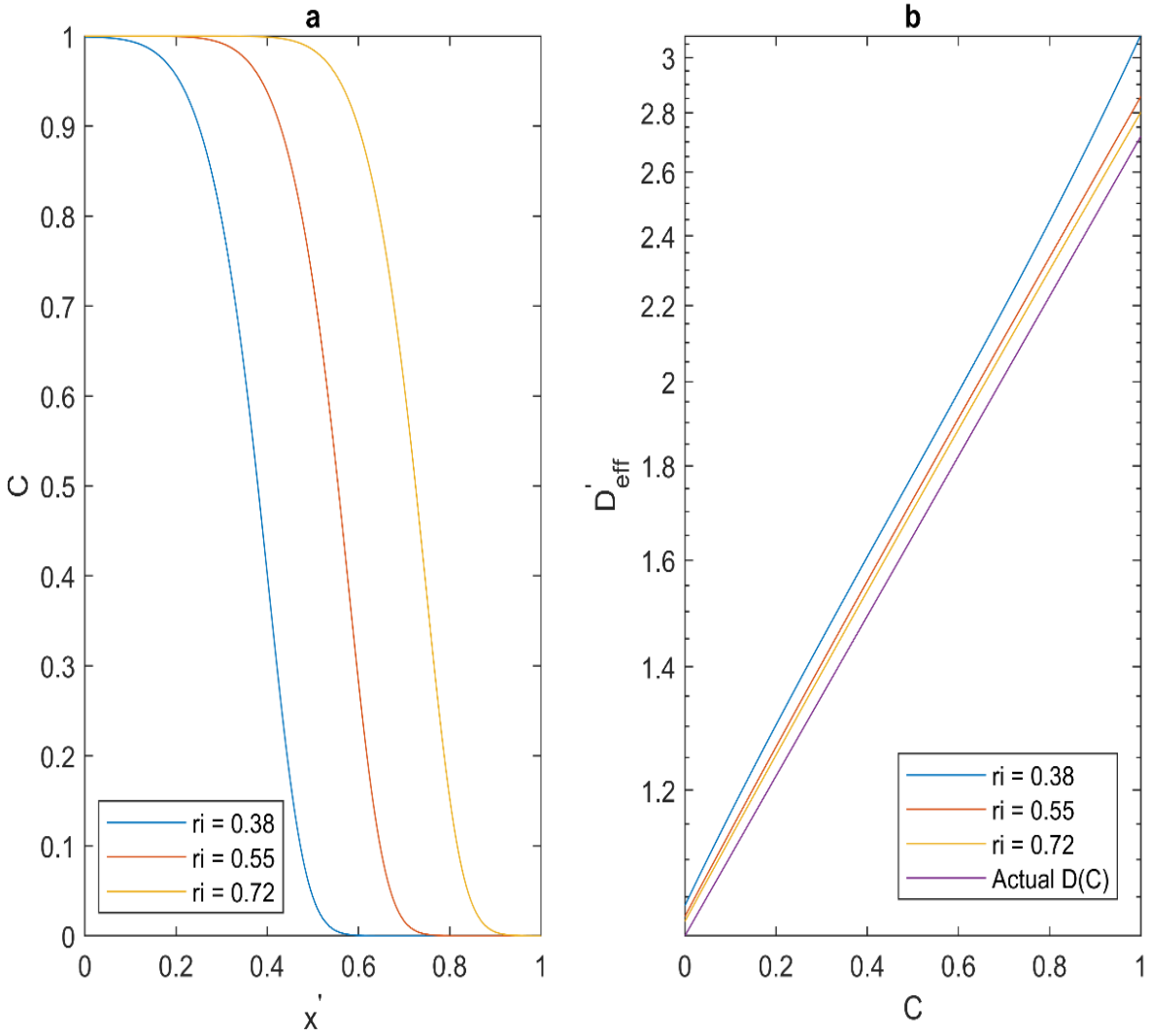

Figure 9.2: Stress-free 2D interface migration simulations for different initial interface positions (X_i) (a) Concentration profiles (b) Actual and 1D planar FSM computed D vs C for each initial interface positions

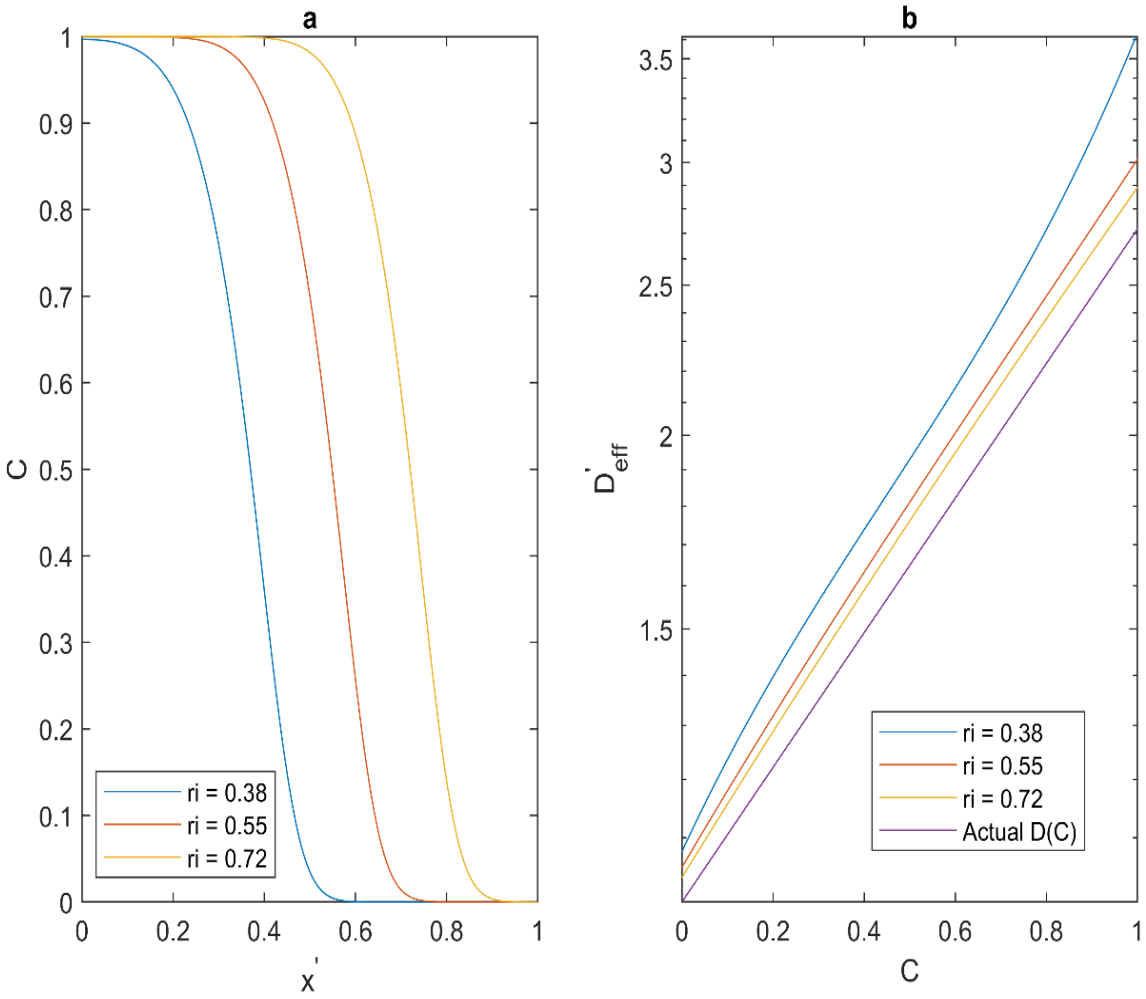

Figure 9.3: Stress-free 3D interface migration simulations for different initial interface positions (X_i) (a) Concentration profiles (b) Actual and 1D planar FSM computed D vs C for each initial interface positions

9.2.2 Diffusion duration

Another factor that can influence the reliability of using a 1D planar method to extract the D(C) from a non-planar experiment is the diffusion duration or the corresponding amount of solute diffusion. In this section, the reliability of using 1D models to extract D(C) in non-planar systems will be investigated at a given initial interface position with different durations of diffusion. The diffusion parameters for this simulation are:

$$\nu = 0.3,\ \ \eta' = 0.0001872,\ D_1^{*'} = 0.01,\ \ D_2^{*'} = 1.0,\ \ \ v_1{}' = 1.0,\ v_2{}' = 1,\ \ T' = 0.0038,\ \ \frac{\partial P'}{\partial x'} = 0,$$

and $t_1' = 0.0031$

The simulations are performed by using a stress-free D(C) for different times and diffusion that involves 1D, 2D, and 3D interfaces. The concentration profiles for 1D diffusion with various durations of diffusion are presented in Figure 9.4a. At the same time, the D(C) extracted with the FSM and planar model are reported in Figure 9.4b. The results reported in the latter further validate that in a stress-free system, the D(C) does not change with time when planar methods are used to extract the D(C) from diffusion systems with 1D migration of the interface. Similarly, the process is repeated for diffusion with the migration of the 2D interface. The concentration profiles produced at different diffusion times are presented in Figure 9.5a. FSM coupled with a planar 1D interface model is used to extract the D(C) between zero and the final time. The comparison between the actual D(C) used to simulate the concentration profile in a diffusion system with 2D migration and the D(C) extracted by using the FSM coupled with a planar model 1D interface are shown in Figure 9.5b. The results show that the common use of planar models with the migration

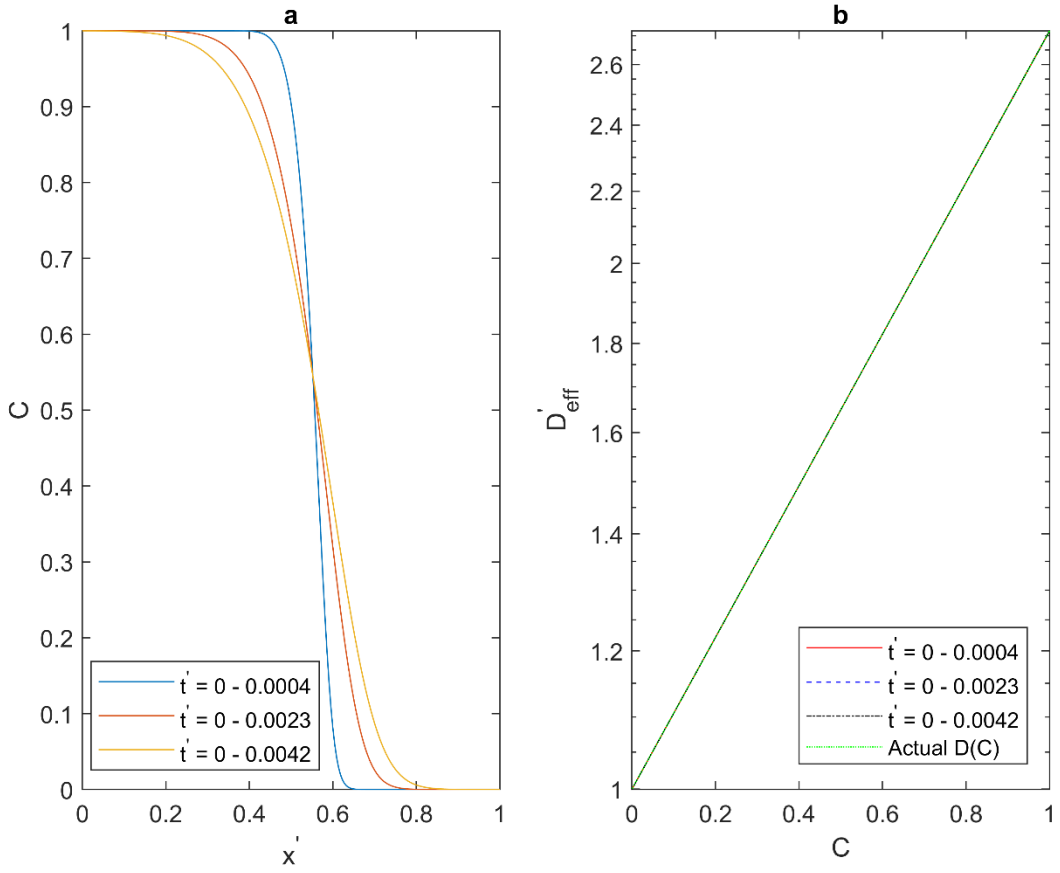

Figure 9.4: Stress-free 1D interface migration simulations for different durations of diffusion (a) Concentration profiles (b) Actual and 1D planar FSM computed D vs C for each diffusion times

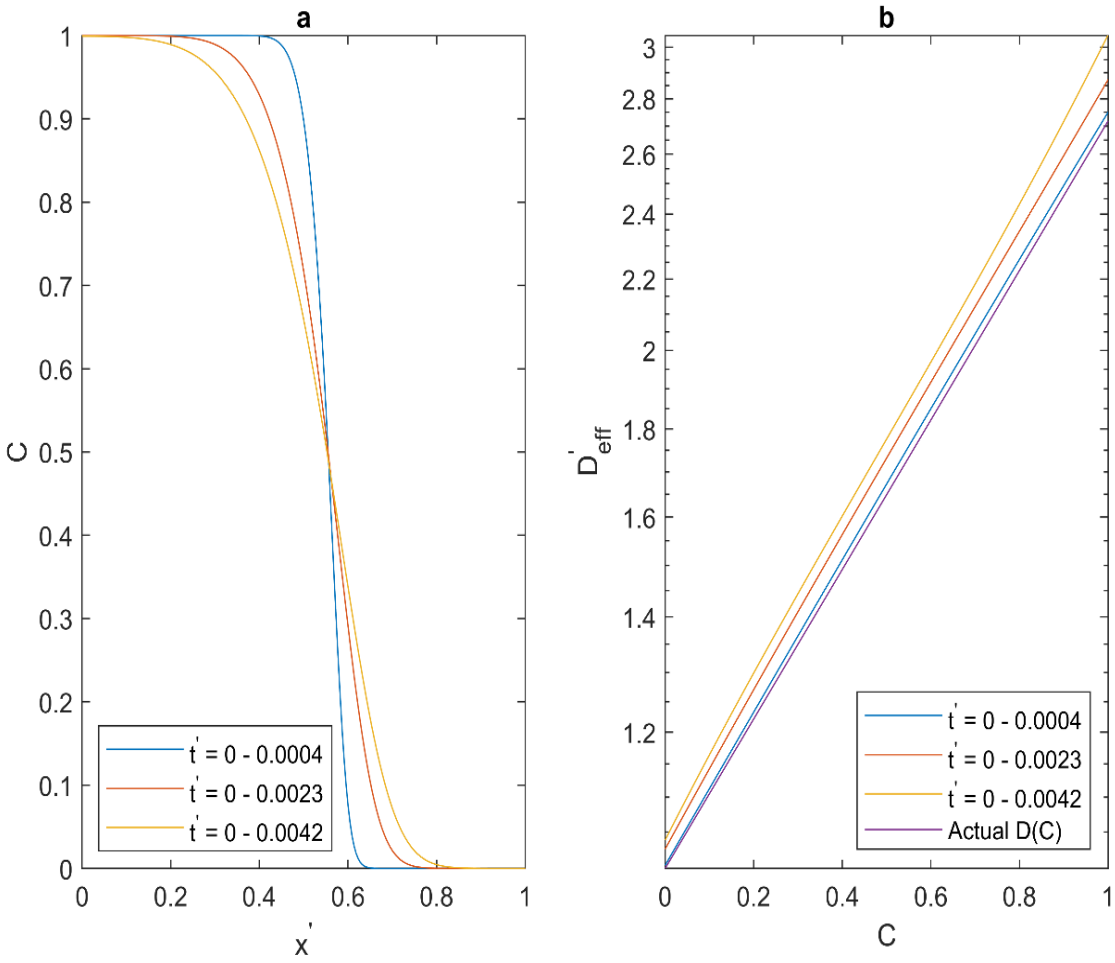

Figure 9.5: Stress-free 2D interface migration simulations for different durations of diffusion (a) Concentration profiles (b) Actual and 1D planar FSM computed D vs C for each diffusion times

unreliable as the duration of diffusion increases. The reliability of using planar models with the migration of the 1D interface to extract D(C) from diffusion with the migration of the 3D interface is also investigated. The concentration profiles simulated by using a stress-free D(C) at different diffusion times are presented in Figure 9.6a. Also, the D(C) is extracted by using the FSM coupled with a planar 1D interface model, and the results for each time interval are presented in Figure 9.6b. The results reported in Figure 9.6b also show that the common use of planar models with 1D migration of the interface to extract the D(C) from diffusion with 3D migration of the interface becomes increasingly unreliable as the duration of the diffusion increases. Therefore, increasing the diffusion time reduces the reliability of the D(C) calculated by using planar methods with 1D migration of interface.

9.3 New Method of Calculating Initial Interface Position

Simulation results from the present study have shown that the generalized equation for the interface position (r_m) of planar, cylindrical, and spherical geometries with diffusion in the radial direction and constant molar volume can be represented with Equation 9.1. The equation becomes the Matano interface position when n=0, for planar systems.

$$r_m^{n+1} = \frac{\int_{C_L}^{C_R} r^{n+1} dC}{C_R - C_L} \qquad 9.1$$

Although Equation 9.1 is new, it can easily be verified by using the numerically simulated profiles in section 9.2.1. To validate Equation 9.1, the new equation is used to calculate the initial position of the concentration profiles in Figures 9.1-9.3. Table 9.1 compares the calculated initial interface

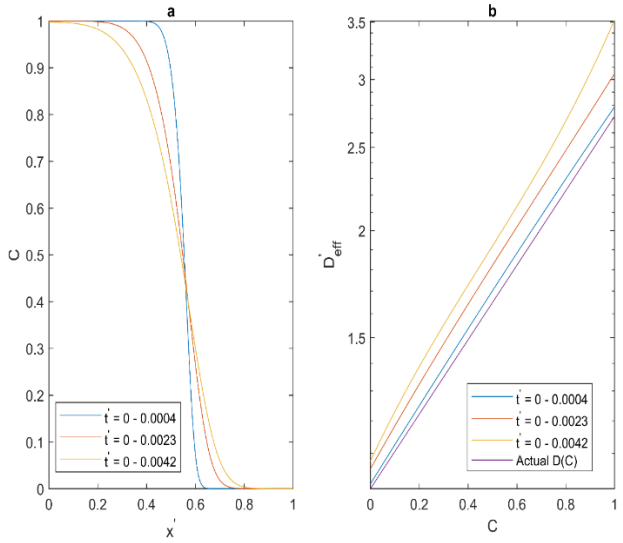

Figure 9.6 Stress-free 3D interface migration simulations for different durations of diffusion (a) Concentration profiles (b) Actual and 1D planar FSM computed D vs C for each diffusion time

Table 9.1: Comparison between the actual and calculated initial interface position

Geometry	n	Profile	Actual r_m	Calculated r_m using Equation 9.1
Planar	0	Figure 9.1	0.38	0.38
			0.55	0.55
			0.72	0.72
Cylindrical	1	Figure 9.2	0.38	0.38
			0.55	0.55
			0.72	0.72
Spherical	2	Figure 9.3	0.38	0.38
			0.55	0.55
			0.72	0.72

position and the actual interface positions. The accuracy of the initial interface position in planar, cylindrical, and spherical geometries calculated by using Equation 9.1 validates the Equation. The new Equation 9.1 is significant because it is useful when calculating the D(C) required to reproduce an experimental result when the diffusion is non-planar.

9.4 Effect of Geometry on D(C)

This section investigates the second objective of this chapter, which studies the effect of 2D and 3D migration of the interface on the D(C). A theoretical model is used to compare the effective D(C) when stress is considered in diffusion with 1D, 2D, and 3D migration of the interface. Subsequently, the theoretical results are experimentally verified.

9.4.1 Theoretical investigation of the effect of geometry on D(C)

The dimensionless forms of Equations 3.34 and 3.35 are used to simultaneously simulate the pressure and solute distributions for the planar and cylindrical geometries. These simulations ensure that the influence of DIS during diffusion in all geometries is considered. The calculated solute distributions for both the planar and cylindrical geometries are presented in Figure 9.7a. The concentration profiles in Figure 9.7a show that the solute distribution in a planar and cylindrical diffusion system can be different with the same diffusion parameters. The pressure distributions in both systems are presented in Figure 9.7b, while the pressure gradients in both systems are presented in Figure 9.7c. The plotted pressure gradients show the difference in pressure gradient with respect to concentration when the geometry changes from planar diffusion to cylindrical

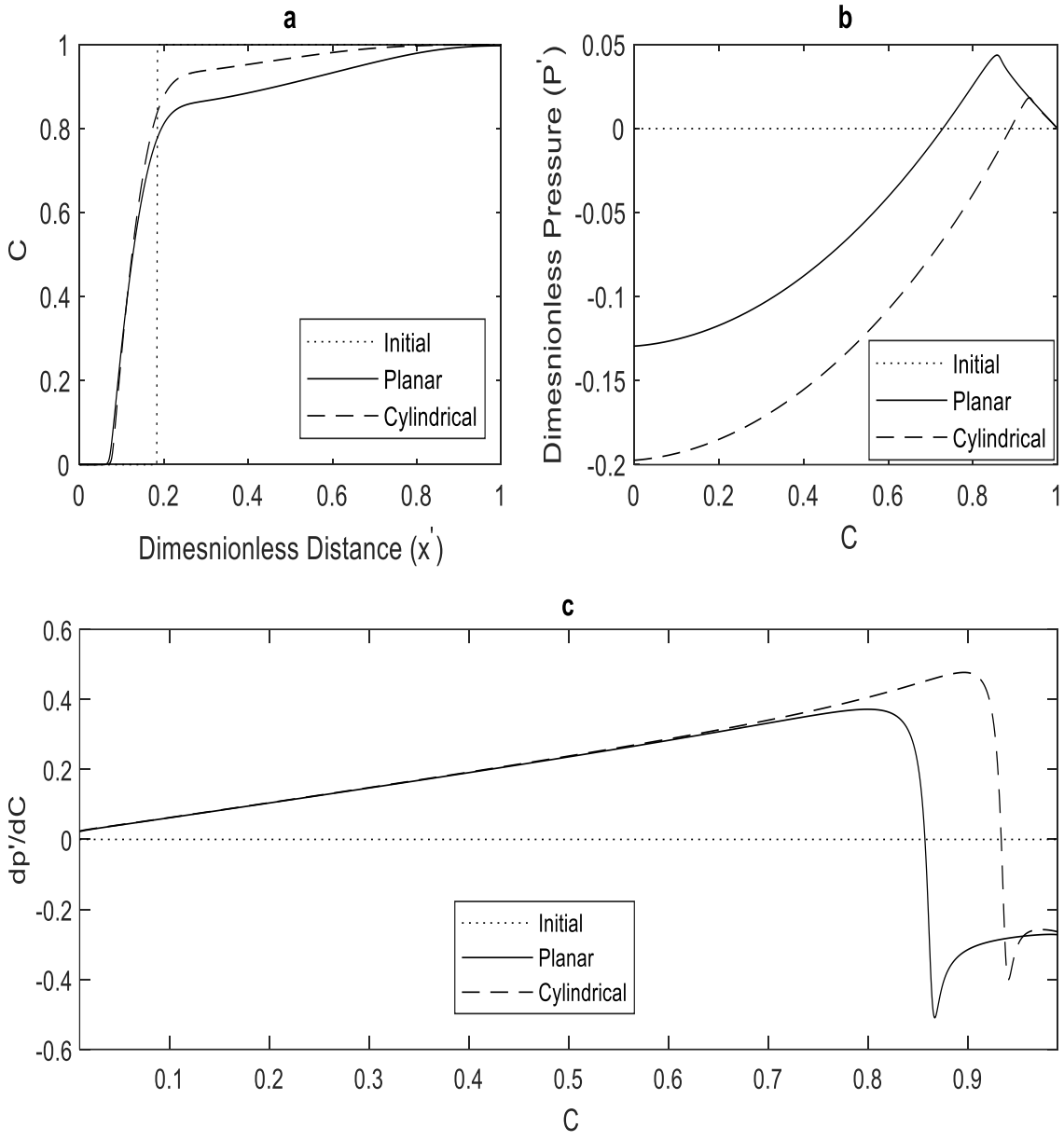

Figure 9.7 Data comparison of a diffusion in planar and cylindrical systems (a) composition profiles (b) Stress vs concentration and (c) Stress gradient with respect to concentration

diffusion. This is significant because an effective D(C) depends on the pressure gradients in the system. The effective D(C) at the final time of diffusion is calculated for each diffusion geometry by using Equation 3.36, and the data for each geometry are reported in Figure 9.8. The figure shows that the effective D(C) in both geometries is different, with a greater D(C) in the system with 1D migration of the interface in comparison to the 2D diffusion system. This, therefore, shows that theoretically, the D(C) in diffusion systems with planar geometries can be different from the diffusion in cylindrical systems due to the changes in concentration and stress gradients in both systems.

9.5 Experimental Verification

This part of the study experimentally verifies the theoretical findings in the previous section. The diffusion in a cylindrical system with 2D migration of the interface does not follow the parabolic relationship in Chapter 4. By implication, the BM, SF, Hall methods, and planar numerical methods [114]–[118], [123], [124] used to extract the D(C) can be erroneous. The error when using planar methods to extract the D(C) from non-planar systems has been investigated in section 9.1. Interestingly as noted in Chapter 2, the FSM [88] can be used to reproduce the experimental result by calculating the D(C), which satisfies the relevant Fick's law of diffusion. The FSM, however, requires a numerical solution model for the generalized coordinate system, and these equations have been developed in Chapter 3. This approach eliminates the errors in using standard analytical methods in non-planar geometries, including the assumption of 1D planar diffusion and that a non-uniform initial solute state does not exist.

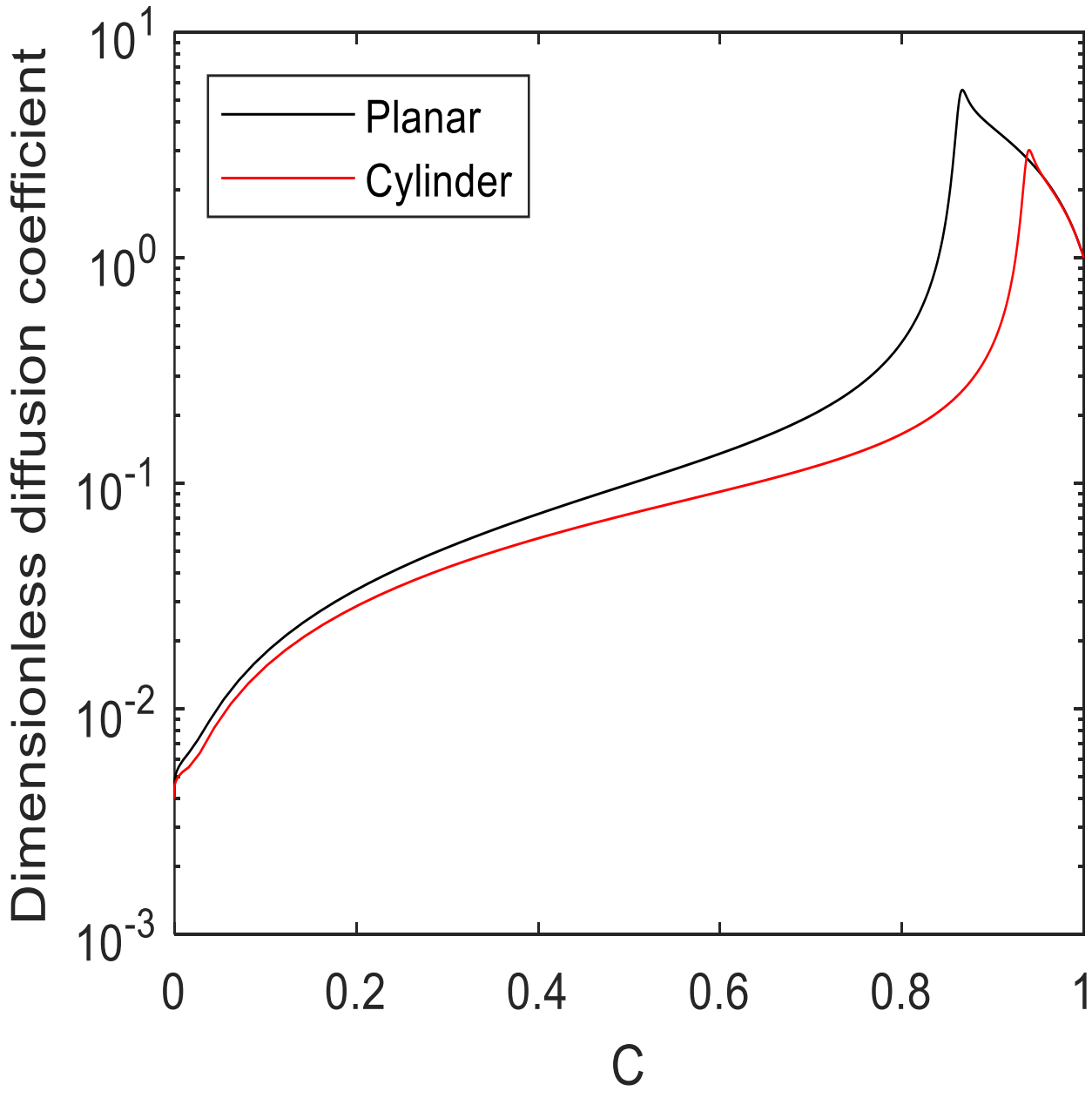

Figure 9.8 Theoretical D(C) in both planar and cylindrical geometries

9.5.1 Experimental procedure

Two alloy systems with different geometries were used to experimentally verify the influence of the geometry on the D(C) at a given concentration. Single-phase solid-solid diffusion couples are a reliable way to determine the interdiffusion coefficient. Hence, the Cu-Ni diffusion couple with unlimited solute solubility was used to study the effect of geometry on the D(C) in a single-phase system. The experimental procedures are as follows:

A plate of 100% pure Cu with a thickness of 1 mm, and 100% pure Cu wire with a diameter of 0.5 mm were cut to a length of 10 mm. The plates and wires were placed in a sealed quartz tube, backfilled with high purity argon, and heated at 950°C for 24 hrs to grow the grains and relieve the residual stresses that could interfere with diffusion at lower temperatures. It is important to note that this process was performed before the electrodeposition of Ni on the plates and wires. Subsequently, the pure Cu wire and plates were chemically cleaned. They were:

a) heated for 20 minutes in a boiling solution of sodium hydroxide, sodium phosphate, and sodium carbonate,
b) rinsed with distilled water before immersed for 10 minutes in a 30% HCl solution at room temperature,
c) rinsed with distilled water before heated for 5 minutes in a boiling 10% sulphuric acid solution, and
d) rinsed with distilled water before heated for 5 minutes in a 5% sulphuric acid solution at room temperature.

Copper was deposited on the chemically cleaned samples until reaching a deposition thickness of 240 μm. The electroplated wire and plate samples were placed in a sealed quartz tube backfilled with high purity argon and subjected to a diffusion heat treatment at 900°C for the same duration

of 75 hrs. The diffusion samples were sectioned by using EDM, and then mounted, grounded, and polished by using standard metallography sample preparation techniques. Microanalyses on the two sets of samples were performed by using X-ray and wavelength dispersive spectroscopy techniques. The composition profiles were measured in the perpendicular direction to the interface. The process was repeated for the two other samples. To identify the uncertainties in the experiment, the following steps were carried out:

a) Three separate samples with the same thickness of deposited Ni were subjected to the same diffusion temperature and time.
b) At least five different concentration profiles were taken from each of the three (3) samples to calculate the average dependence of the interdiffusivity on the concentration in each sample. This averaging process for each sample reduces the sample-to-sample variation in the concentration profiles used to extract the D(C).
c) Subsequently, the FSM was used to extract the D(C) from the experimental composition results.
d) The concentration-averaged diffusion coefficient (D_{ave}) for each sample was calculated by using the average dependence of the interdiffusivity on the concentration in each sample.
e) The variations from the average dependence of the interdiffusivity on the concentration in each of the three (3) samples were analyzed to determine the extent of uncertainty due to experimental errors.
f) For the second criteria, regions with no overlap between the error bars of the three average interdiffusion coefficients against concentration in the wire and plate diffusion couples indicate a change in the D(C).

g) The three D_{ave} for the condition variations were analyzed for the D_{ave} criteria to determine the extent of uncertainty in the experimental errors for each diffusion condition. This was done by calculating the maximum percentage change in the D_{ave} for each condition. In this study, the maximum variation in D_{ave} from the three samples falls below 15%, which is consistent with the uncertainty reported in the literature for two interdiffusion coefficients considered statistically similar [12], [67], [90], [112], [113].

9.5.2 Results and discussion

Experimental concentration profiles are reported in Figure 9.9 for the wires and plates. The profiles at 0 hr are the initial profiles produced as a result of electrodeposition. In contrast, the final profiles are generated after diffusion heat treatment at 900°C with a holding time of 75 hrs. The FSM coupled with the generalized numerical model extracts the D(C) from the experimental composition profiles in the wire and plate samples. This approach ensures that the appropriate diffusion equations are used, and the initial profile at 0 hr can be used as the initial condition, while the final profiles are used as the final condition during the time of the diffusion. The D(C) is iterated until a function is obtained to reproduce the experimental concentration results in the plates and wires (Figure 9.10). The D(C), which produces the same experimental results, is a reliable function. The D(C) from the three average concentration profiles are used to calculate the experimental deviation for each concentration. The error bar plots are presented in Figure 9.11. Also, the concentration-averaged diffusivity (D_{ave}_i) is calculated for each sample. The mean D_{ave}_i for the three sample geometry is the D_{ave} of the wire and plate experiments are reported in Table 9.2. Two criteria are experimentally assessed to determine if the D(C) in both geometries is

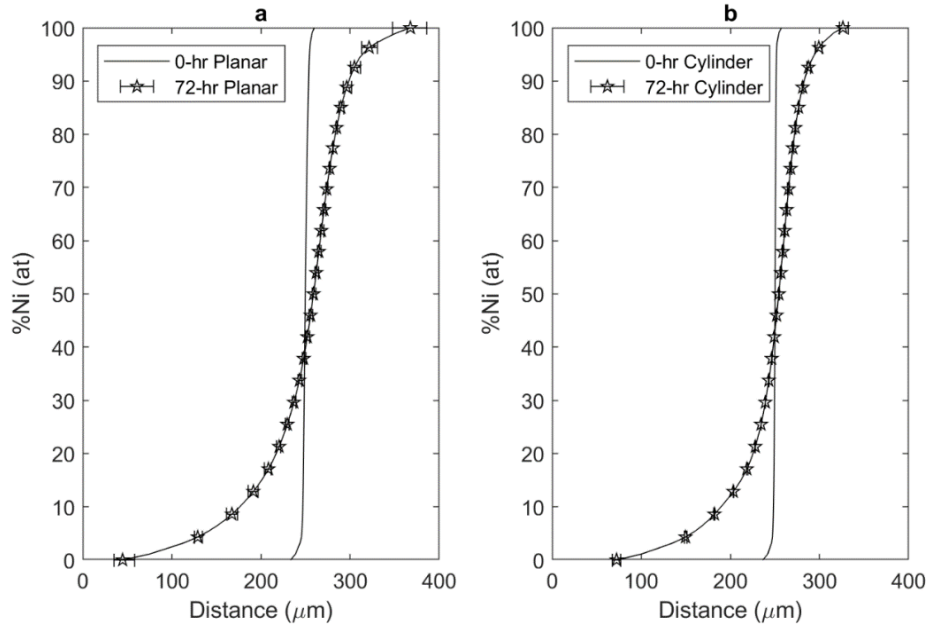

Figure 9.9 Average experimental Cu-Ni compositional profiles in (a) Planar geometry (b) Cylindrical geometry

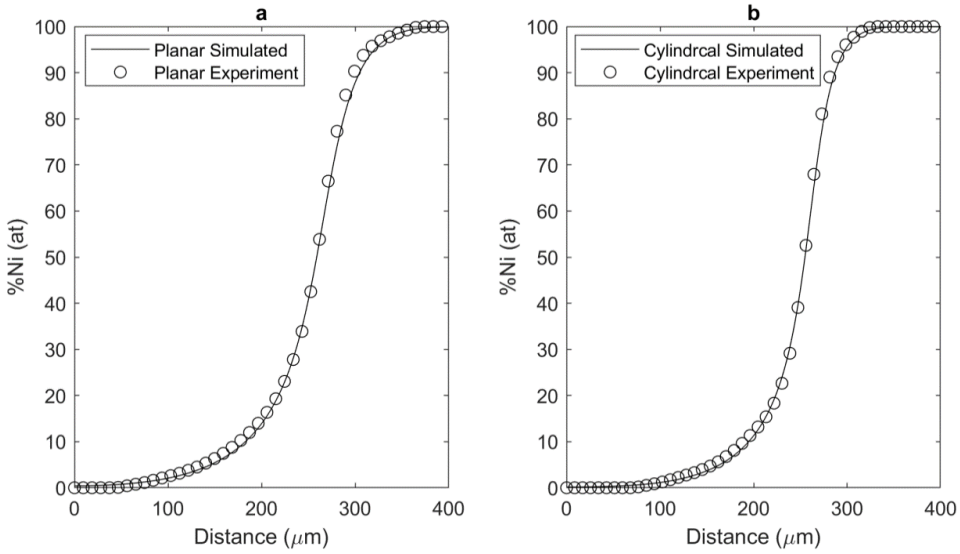

Figure 9.10: simulated and experimental concentration profiles in both 1D planar and 2D cylindrical geometries samples in (a) Planar geometry (b) Cylindrical geometry

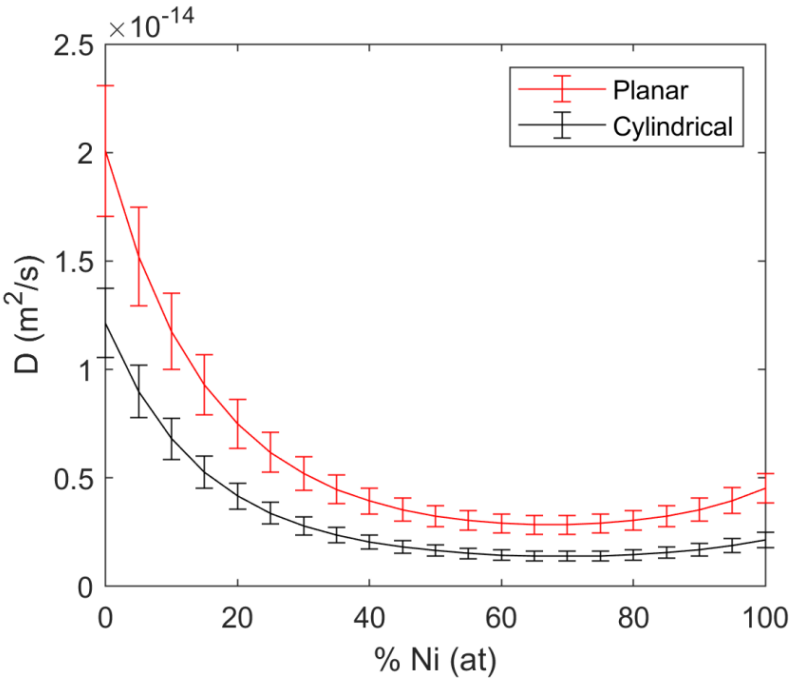

Figure 9.11: D(C) obtained for both 1D planar and 2D cylindrical geometries

Table 9.2: Concentration-average diffusivity in planar and cylindrical systems

Geometry	Sample 1 $D_{ave}\_1 \times 10^{-15}$ (m^2/s)	Sample 2 $D_{ave}\_2 \times 10^{-15}$ (m^2/s)	Sample 3 $D_{ave}\_3 \times 10^{-15}$ (m^2/s)	Max % change in D_{ave}_1 to D_{ave}_3 for the same geometry	Geometry $D_{ave} \times 10^{-15}$ (m^2/s)	% change of Cylindrical sample from Planar geometry
Planar	5.68	6.39	5.54	15%	5.87	45%
Cylinder	3.06	3.24	3.32	8%	3.21	

beyond uncertainty. The first criterion is the percentage difference in D_{ave}, while the second criterion is the deviation in the error bar plot for each concentration. The maximum D_{ave} calculated for the same diffusion condition is 15% (Table 9.2), which is comparable to the maximum percentage difference reported in the literature [12], [67], [90], [112], [113]. The second criterion is the error bar plot. At a given concentration, regions with no overlap between the maximum and minimum diffusivities of different diffusion geometries indicate an experimental disparity in the D(C). For the first criterion, the observed percentage difference in the wire and plate samples is calculated and found to be 45%, which is larger than the maximum 15% in the same diffusion geometry. Similarly, as shown in Figure 9.11, the error bar plots show that the D(C) in the planar and cylindrical diffusion systems with 1D and 2D migration of the planar and cylindrical interfaces can be significantly different. This difference experimentally confirms the theoretical finding that the difference in the DIS in diffusion systems with cylindrical and planar geometries can result in an experimentally different D(C). This study confirms that the D(C) can be isothermally different with different diffusion geometries.

The results in this section show that the common use of D(C) reported for planar geometry to analyze or predict diffusion in non-planar systems such as cylindrical and spherical geometries can result in inaccurate predictions. This finding can be used to analyze or predict the diffusion process of diffusion-controlled phase transformations in cylindrical and spherical coordinates, such as those found in sintering or bonding of solids with spherical, cylindrical, and other geometries.

CHAPTER TEN

10 A NEW ANALYTICAL METHOD FOR COMPUTING CONCENTRATION-DEPENDENT INTERDIFFUSION COEFFICIENT IN BINARY SYSTEMS WITH PRE- EXISTING SOLUTE CONCENTRATION GRADIENT

10.1 INTRODUCTION

An accurate mathematical description of a diffusion process is important for providing a reliable solution to diffusion problems. Generally, the mathematical description of processes requires four key components: (1) a proper model equation, (2) the initial condition, (3) boundary conditions, and (4) the final condition. The proper model equation commonly used for diffusion is Fick's laws of diffusion (Equations 2.1 and 2.2) with the crucially important D(C). When the key components 1-4 are obtained from experiments, the unknown parameter is the D(C). Any solution to the D(C), using the proper model, that does not adequately consider the three conditions of the system (key components 2-4) is less reliable and inaccurate in most cases. Hence, a proper application of conditions 2-4 is necessary for accurate solutions. Most of the means of calculating the D(C) in Fick's first and second laws of diffusion are analytical. The BM [88] method is the most common analytical method. Others are the SF [125], Wagner [126] and Hall [68], [127] methods. These analytical methods discussed in Chapter 2 of this thesis have a common limitation. The fundamental limitation of these methods is the derivational assumption that a non-uniform initial solute state does not exist, which implies a concentration that is a step-function in space. However, as discussed in Chapter 6, pre-diffusion metal joining processes produce non-uniform initial solute distribution in diffusion systems. As shown in Chapter 6 of this study, numerical methods can be accurately used to extract the D(C) from the final diffusion stage. Nevertheless, analytical methods

are straightforward procedures that yield an accurate solution without costly computational space and skills. A review of literature provides a graphical method in Kirkendall et al., which was used to calculate the average constant diffusivity operative between two profiles [35], [128], [129]. However, Kirkendall's approach does not produce the D(C) required to reliably analyze or predict actual diffusion processes. Therefore, a new analytical method to determine the concentration dependence of an interdiffusion coefficient operative between isothermal concentration profiles is developed in this study. The new method can be used when there is a pre-existing solute distribution before the final diffusion process and between isothermal profiles when the pre-existing distribution is unknown. The key concept used to develop the new method is validated with experimental data from the literature. Subsequently, a numerical experimental procedure is carried out to produce composition results for both single-phase and two-phase systems. The third section of this chapter will analyze the composition profiles using the SF and new methods. The D(C) extracted using both methods will be compared to the true data used to produce the concentration results, and the errors will be quantified. The final section of this chapter will use the new method to analyze an experimental binary diffusion system.

10.2 Derivation of the New Analytical Method for Unidirectional Diffusion

In a unidirectional diffusion system, the stripped region in Figure 10.1 is given as:

$$dA_C = \left(r_f - r_i\right)dC \qquad 10.1$$

dA_C is the area of the shaded portion, r is the position, c is the concentration, and the subscripts i and f indicate the initial and final concentration profiles, respectively. From Equation 2.41 and the

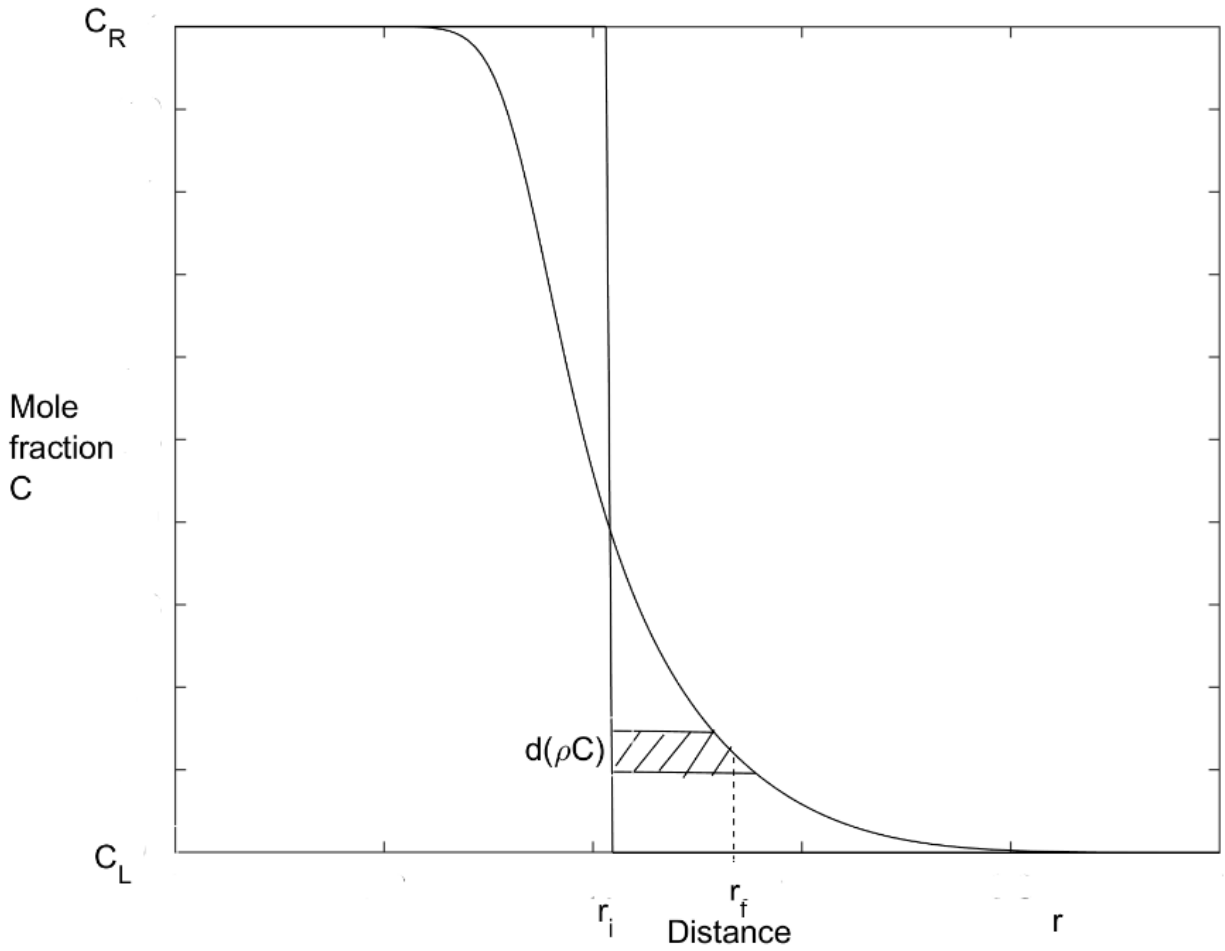

Figure 10.1 Planar concentration profile for a unidirectional diffusion couple

definition of concentration ρC as the amount (Ms) of solute diffused in a given volume (V) [67].

$$c = \rho C = \frac{Ms}{Vo} \tag{10.2}$$

The stripped region in Figure 10.1 has a length of $\left(r_f - r_i\right)$. For a cross-sectional area (A) and length $\left(r_f - r_i\right)$, the volume (Vo) is given as:

$$Vo = A\left(r_f - r_i\right) \tag{10.3}$$

The concentration change (d(ρC)) in the stripped region can be determined from Equations 10.2 and 10.3.

$$d\left(\rho C\right) = \frac{dMs}{Vo} = \frac{dMs}{A\left(r_f - r_i\right)} \tag{10.4}$$

Substituting Equation 10.4 into Equation 10.1 in a constant molar volume system gets

$$dA_C = \left(r_f - r_i\right) d\left(\rho C\right) = \frac{\left(r_f - r_i\right) dMs}{A\left(r_f - r_i\right)} = \frac{dMs}{A} \tag{10.5}$$

Therefore, the stripped region is the change in solute quantity diffused for a cross-sectional area. Integrating Equation 10.5 and dividing by the duration of the diffusion gives the total quantity of solute diffused at the concentration in a cross-sectional area for each diffusion time. This is given in Equation 10.6, which is the graphical area between the concentration and profile for a unit time interval of diffusion [32]–[35].

$$\frac{A_C}{\Delta t} = \frac{1}{\Delta t}\int_{C_R}^{C^*} \left(r_f - r_i\right) d\left(\rho C\right) = \frac{1}{\Delta t}\int_{C_R}^{C^*} \frac{dMs}{A} = \frac{Ms}{A\Delta t} \tag{10.6}$$

The flux in the direction of a concentration gradient can be described as the quantity of solute that diffuses per cross-sectional area with time.

This definition can be expressed by using the mathematical equation of flux given as [32]:

$$J = \frac{Ms}{A\Delta t} \tag{10.7}$$

Equations 10.6 and 10.7 are equal and can be equated to give Equation 10.8.

$$J = \frac{Ms}{A\Delta t} = \frac{1}{\Delta t}\int_{C_R}^{C^*}\left(r_f - r_i\right)d\left(\rho C\right) \tag{10.8}$$

Equation 10.8 is the flux, J, defined as the quantity of solute atoms diffused per cross-sectional area with time. This is the area bounded by a composition profile divided by the diffusion time [32]–[35].

Equating Equations 2.1 (Fick's first law) and 10.8 gives Equation 10.9.

$$J = \frac{\Delta Ms}{A\Delta t} = \frac{1}{\Delta t}\int_{C_R}^{C}\left(r_f - r_i\right)d\left(\rho C\right) = -D\overline{\frac{d\left(\rho C\right)}{dr}} \tag{10.9}$$

Therefore, the flux in Fick's first law of diffusion is the area bounded by the composition curve for each duration of diffusion. Equation 10.9 can be found in the literature [35], [128], [129]. For a constant molar density system or constant molar density $\left(\rho\right)$, the D(C) can be calculated by using Equation 10.9, and the equation is reported in Equation 10.10.

$$D[C] = -\frac{\overline{\frac{dr}{dC}}\int_{C_R}^{C}\left(r_f - r_i\right)dC}{\Delta t} \tag{10.10}$$

When the initial time is zero $(t_i = 0)$, the BM solution D(C) from Fick's second law is:

$$D[C] = -\frac{1}{2t}\frac{dr}{dC}\int_{C_R}^{C}(r_f - r_m)dC \qquad 10.11$$

$\frac{dr}{dC}$ is the inverse concentration gradient of each concentration profile.

Equating the D(C)from Fick's first (Equation 10.10) and second (Equation 10.11) equations yields:

$$\overline{\frac{dr}{dC}} = \frac{1}{2}\frac{dr}{dC} \qquad 10.12$$

Therefore, the inverse concentration gradient at a given concentration in Fick's first law is the average inverse gradient at a given concentration. In a diffusion system with an initial concentration profile defined as a step function in space, as shown in Figure 10.1, there is no initial inverse concentration gradient$\left(\frac{dr}{dC_i} = 0\right)$; however, Equation 10.12 is also valid when the initial solute distribution is not uniform in the system. In such systems, the average inverse concentration gradient is defined as Equation 10.13, which is a new key concept in this derivation:

$$\overline{\frac{dr}{dC}} = \frac{1}{2}\left(\frac{dr}{dC_i} + \frac{dr}{dC_f}\right) \qquad 10.13$$

The new method to calculate the D(C) between two profiles can be obtained by substituting Equation 10.13 into Equation 10.10.

$$D[C] = -\frac{1}{2}\left(\frac{dr}{dC_i} + \frac{dr}{dC_f}\right)\frac{\int_{C_R}^{C}(r_f - r_i)dC}{\Delta t} \qquad 10.14a$$

Equation 10.14 applies to situations where both profiles have the same Matano plane. The approach used to derive the SF method in Equation 2.43 can be used to eliminate the requirement of the Matano plane; this is done by using the normalized concentration (y). The modified form of Equation 10.14 becomes:

$$D[y^*] = -\frac{1}{2}\left(\frac{dr}{dy_i} + \frac{dr}{dy_f}\right)\frac{\left[\left((1-y^*)\int_{-\infty}^{r^*} y dr_f + y^*\int_{r^*}^{+\infty}(1-y)dr_f\right) - \left((1-y^*)\int_{-\infty}^{r_i^*} y dr_i + y^*\int_{r_i^*}^{+\infty}(1-y)dr_i\right)\right]}{\Delta t} \qquad 10.14b$$

In situations where the concentration is represented in atomic fraction (C) per molar volume (V) or mole, Equation 10.14 can be further modified to account for the molar volume. The form of Equation 10.14 which accounts for molar volumes is:

$$D[y^*] = -\frac{1}{2}\left(\frac{dr}{dy_i} + \frac{dr}{dy_f}\right)V^*\frac{\left[\left((1-y^*)\int_{-\infty}^{r^*}\frac{y}{V}dr_f + y^*\int_{r^*}^{+\infty}\frac{(1-y)}{V}dr_f\right) - \left((1-y^*)\int_{-\infty}^{r_i^*}\frac{y}{V}dr_i + y^*\int_{r_i^*}^{+\infty}\frac{(1-y)}{V}dr_i\right)\right]}{\Delta t} \qquad 10.14c$$

In cases where the starting profiles are negligible compared to the final profile, the initial inverse concentration gradients are also negligible compared to the final inverse concentration gradient. By implication, in these cases, the initial inverse gradient tends to zero as the final inverse gradient increases. In such situations, Equation 10.14a tends to the standard BM method (Equation 2.48).

The derivation of Equation 10.14 shows that the D(C) between two isothermal profiles in Fick's first law is the product of the total amount of solute diffused per unit time and the mean inverse concentration gradient. This approach has not been previously reported.

10.2.1 Validation of the key concept in the new model

The key concept in Equation 10.13 will be validated by using the experimental data in [35], [128]. In their work, the mean inverse gradient between two concentration profiles is graphically determined by using both concentration profiles. The mean inverse gradient between two concentration profiles was graphically evaluated as the common inverse gradient, which diffuses the same amount of solute. Hence, the mean gradients between two concentration gradients, which Kirkendall graphically determined, are presented in Tables 10.1-10.3 for different diffusion temperatures of Cu-Zn. Similarly, the mean inverse gradients between profiles are calculated using Equation 10.13, and the values are reported in Tables 10.1-10.3 for the different diffusion temperatures of Cu-Zn. The calculated values and the graphically obtained values are compared in Tables 10.1-10.3 for temperatures of $600^{o}C$, $655^{o}C$, and $720^{o}C$ see Figure 10.2. The good correlation between the graphical values by Kirkendall, and the values calculated by using Equation 10.13 at three different temperatures, validates the use of Equation 10.13 for calculating the mean inverse gradients between two concentration profiles.

The validity of the new method will be investigated by using both single and two-phase binary diffusion systems in the subsequent sections. The investigation commenced with numerical simulation experiments, followed by using the new method to analyze actual experimental data in the literature.

Table 10.1: Mean concentration gradients from the experimental Cu-Zn system at $600\,^{\circ}C$

Diffusion Time (hrs)	dC/dr (%wt per inch) [35]	Time interval between profiles (hrs)	Graphically calculated mean dC/dr (%wt per inch) [35]	Theoretically calculated mean dC/dr (%wt per inch) from Equation 10.13
2	29650	2-9	19700	19771
9	14830	9-24	11050	11124
24	8900	24-96	6350	6353
96	4940	96-339	3630	3607
339	2840			

Table 10.2: Mean concentration gradients from the experimental Cu-Zn system at $655^{o}C$

Diffusion Time (hrs)	dC/dr (%wt per inch) [35]	Time interval between profiles (hrs)	Graphically calculated mean dC/dr (%wt per inch) [35]	Theoretically calculated mean dC/dr (%wt per inch) from Equation 10.13
1	23200	1-4	15000	14961
4	11040	4-10	8950	9093
10	7730	10-24	5950	5945
24	4830	24-96	3250	3180
96	2370			

Table 10.3: Mean concentration gradients from the experimental Cu-Zn system at $720^{\circ}C$

Diffusion Time (hrs)	dC/dr (%wt per inch) [35]	Time interval between profiles (hrs)	Graphically calculated mean dC/dr (%wt per inch) [35]	Theoretically calculated mean dC/dr (%wt per inch) from Equation 10.13
1	12500	1-3	9050	9089
3	7140	3-8	5260	5265
8	4170	8-16	3380	3421
16	2900	16-24	2510	2578
24	2320			

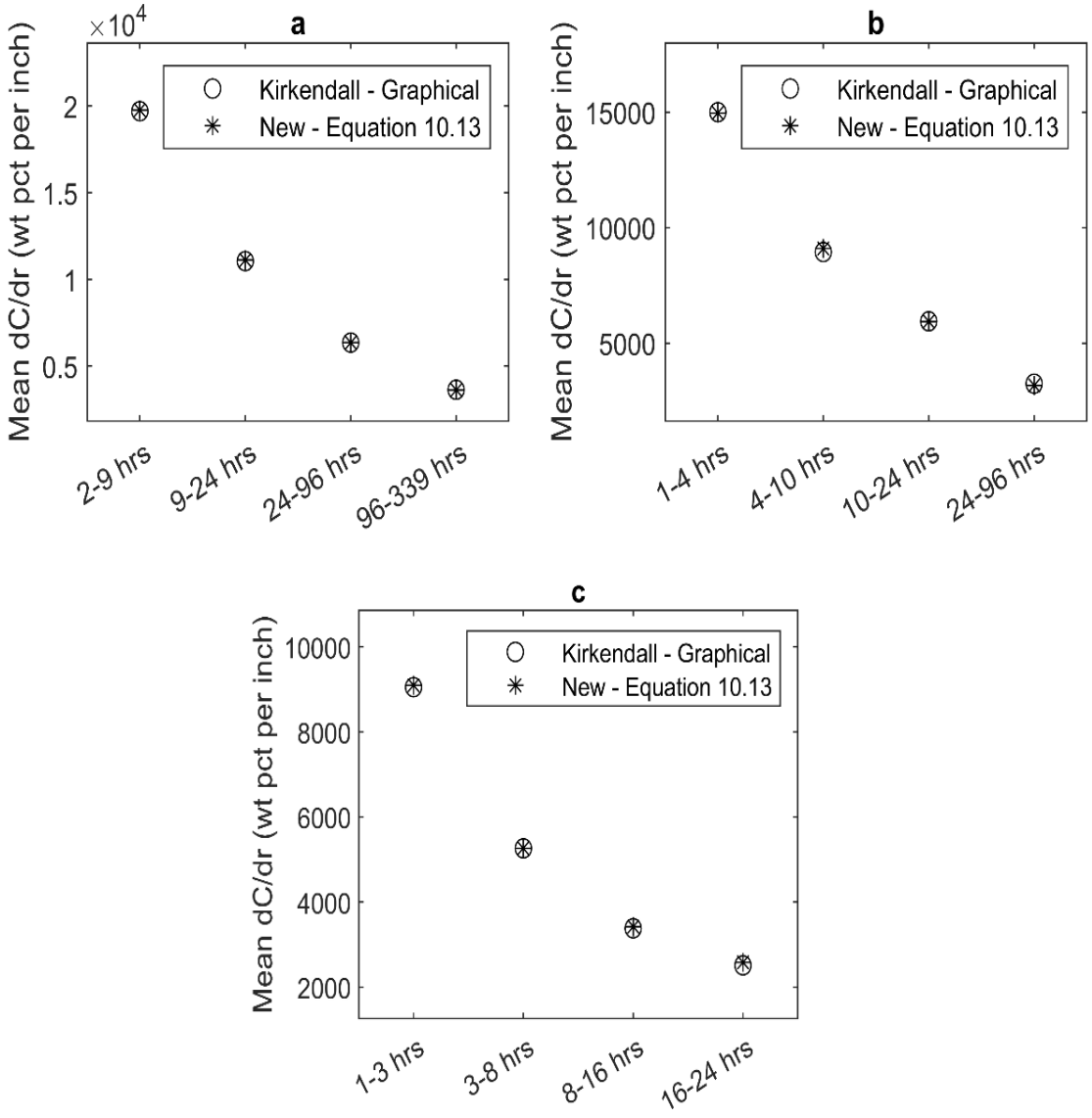

Figure 10.2 Comparison between the mean gradients of two concentration profiles using Kirkendall graphical approach and the new method of Equation 10.13 for (a) 600^{o}C (b) 655^{o}C and (c) 720^{o}C

10.3 Numerical Simulation Experiments

Numerical experiments are performed in binary single-phase and two-phase systems. For the experiment, a known D(C) function numerically simulates concentration profiles in both phases. Two cases are considered; the first case is a system without a pre-existing non-uniform solute distribution, while the second case has a non-uniform initial solute distribution. Three common D(C) types will be considered: constant, non-linear, and linear interdiffusion coefficient dependence on concentration. The three functions are presented in Equations 10.15 – 10.16, while the three functions are plotted in Figure 10.3.

Function 1 - A constant D(C)

$$D[C] = 38.242 \times 10^{-17} \qquad 10.15$$

Function 2 - A non-linear D(C)

$$D[C] = \left(1.714 \times 10^{-15}\right) \times \exp\left(9.9 \times 10^{-4} C^2 - 1.1 \times 10^{-1} C\right) \qquad 10.16$$

Function 3 - A linear D(C)

$$D[C] = \left(1.714 \times 10^{-15}\right) \times \exp\left(-0.0069\ C\right) \qquad 10.17$$

The simulations are performed with the new model for both planar single-phase and two-phase systems. For the simulations, s is the interface position, and I(x) is the initial conditions. The initial and boundary conditions of the simulations are presented in Tables 10.4 and 10.5. In the binary systems with a pre-existing non-uniform solute distribution, the third function (Equation 10.17) is

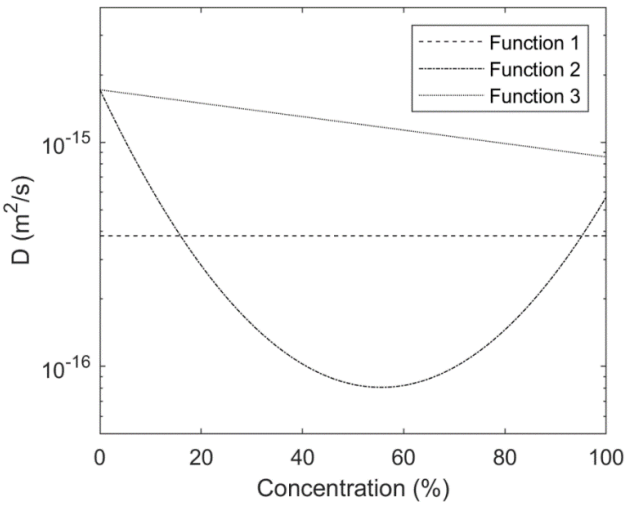

Figure 10.3 plots depicting the functions used to simulate the concentration profiles in this section numerically

Table 10.4: Simulation input parameters for the single-phase binary system

$C(x,0) = I(x)$	Initial condition
$C(\infty, t) = 0$	Right end boundary condition
$C(-\infty, t) = 100$	Left end boundary condition

Table 10.5: Simulation input parameters for the two-phase binary system

Phase A	**Phase B**
$C_A(x,0) = I_A(x)$	$C_B(x,0) = I_B(x)$
$C(-\infty, t) = 100$	$C_B(s,t) = 40$
$C_A(s,t) = 60$	$C_B(\infty, t) = 0$

used to simulate the pre-existing initial solute distribution. The diffusion time for this first pre-existing solute distribution is 0-20 hrs. Subsequently, using the pre-existing solute distribution as the initial condition (I(x)), the final concentration profiles are simulated for each D(C) presented in Equations 10.15-10.17. The duration of the final stage of diffusion is 0-50 hrs. The second set of simulations was also performed by using the pre-existing solute distribution as the initial condition (I(x)), but for a diffusion time of 0-30 hrs. Therefore, two sets of distributions are produced for the two binary systems with the pre-existing non-uniform solute distribution, they are 0-30 hrs and 0-50 hrs.

In the systems without a non-uniform pre-existing solute distribution, the initial diffusion condition is a concentration which is a step function in space. In this system, the diffusion simulations are performed directly for 0-50 hrs by using the three D(C) functions in Equations 10.15-10.17.

The simulated profiles were then analyzed and discussed in the subsequent section.

10.4 Results and Discussion

10.4.1 Concentration dependent interdiffusion coefficient between two non-isothermal concentration profile

This section investigates the reliability of the SF and the new methods in both the single-phase and two-phase systems, with or without a pre-existing non-uniform initial solute distribution. The D(C) extracted by using both methods will be compared to the actual D(C) used to numerically simulate the concentration profiles.

10.4.2 Systems without initial non-uniform solute distribution

The concentration profiles produced by using the three functions in single-phase systems with no pre-existing non-uniform solute distributions are presented in Figure 10.4. The new method and the SF method are used to calculate the D(C) from the concentration profiles in Figure 10.4. The D(C) from both the analytical methods and the actual functions used to simulate each profile are reported in Figure 10.5. As shown in Figure 10.5, the new and SF methods accurately extract the D(C) in systems without a non-uniform initial solute distribution prior to diffusion. The same comparison of the actual D(C) against the calculated functions obtained by the new and the SF methods, is repeated in the two-phase system. The profiles produced for each D(C) in the two-phase system are shown in Figure 10.6. The D(C) are calculated by using the new and SF methods. The calculated D(C) are compared to the actual D(C) used to simulate the concentration profiles. The compared D(C) are presented in Figure 10.7, and the figure shows that both methods are accurate in the absence of uniform initial solute distributions. These results in the single and two-phase systems confirm that the new method tends to the standard analytical methods when there is the absence of a non uniform initial solute distribution before the final diffusion process takes place.

10.4.1 Concentration-dependent interdiffusion coefficient operative between two isothermal profiles

This section will evaluate the D(C) when a non-uniform initial solute distribution exists prior to the final diffusion process. As discussed in the introduction, these diffusion processes are common. The D(C), which is extracted by using the new method, and the SF method that assumes a non-

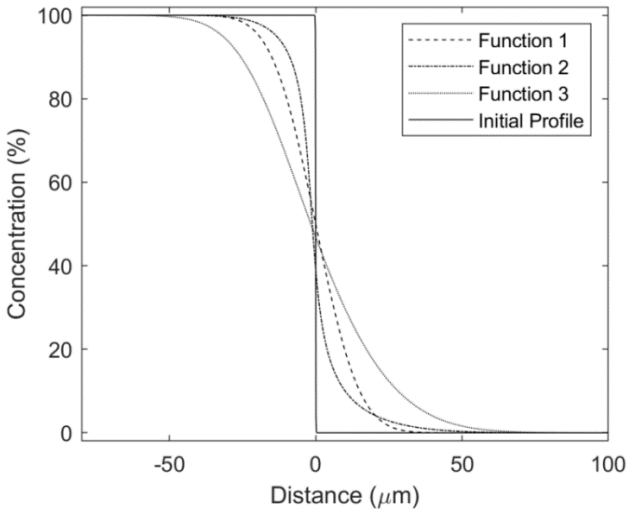

Figure 10.4 Concentration profiles in single-phase systems in the absence of an initial non-uniform solute profile

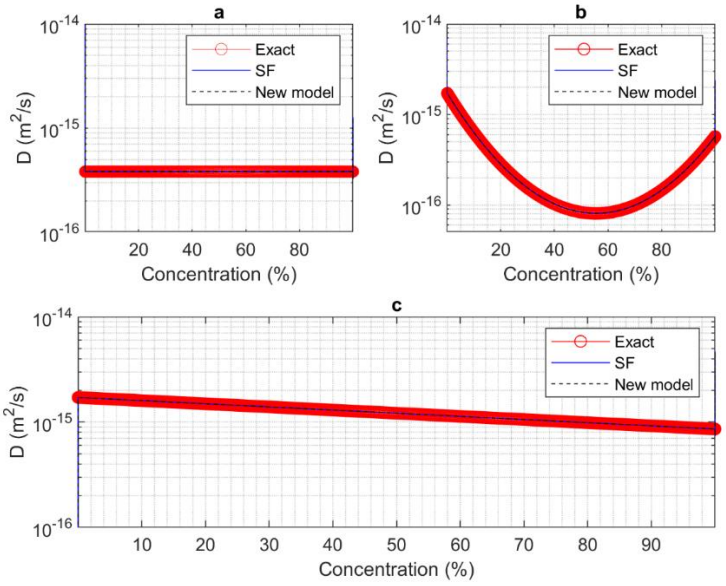

Figure 10.5 Single-phase concentration dependence of interdiffusion coefficient without pre-existing non-uniform solute profile for the three D(C) of (a) Function 1 (b) Function 2 (c) Function 3

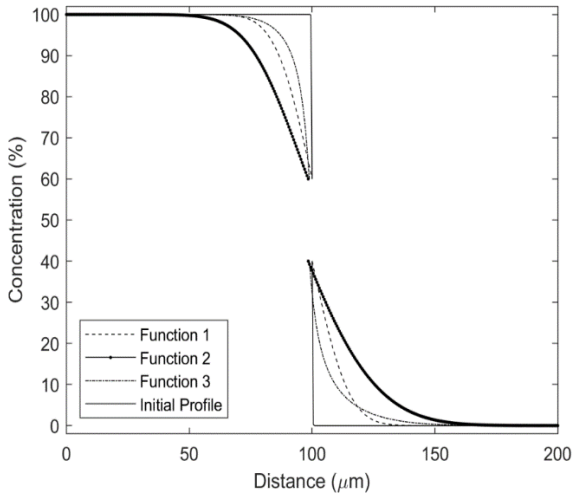

Figure 10.6 Concentration profiles in the binary two-phase systems without pre-existing non-uniform profile

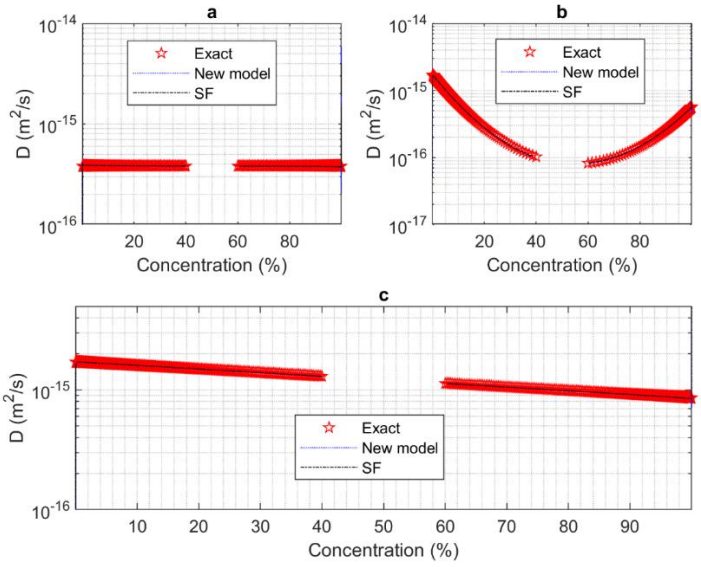

Figure 10.7 Two-phase concentration dependence of interdiffusion coefficient without non-uniform pre-existing solute profile for the three D(C) of (a) Function 1 (b) Function 2 (c) Function 3

uniform initial solute distribution does not exist, will be compared to the actual D(C) functions. The initial profiles prior to diffusion at 0 hrs and the profiles generated after 30 hrs are presented in Figure 10.8a, while the final concentration profiles at 50 hrs are shown in Figure 10.8b. The new method is used to calculate the D(C) operative between 30 and 50 hrs. The SF method, which assumes that a non-uniform solute distribution does not exist, is applied to the final profile to extract the operative D(C). The calculated and actual D(C) are plotted in Figure 10.9. The results in Figure 10.9 show that using the SF method can be erroneous. In contrast, the new method is accurate for all three functions. The analysis is also carried out in the two-phase system. The non-uniform initial concentration profiles at 0, 30 and 50 hrs are shown in Figure 10.10. The D(C) operative between 30-50 hrs and 50 hrs are calculated by using the new and standard methods, respectively. The calculated D(C) from the two methods and the exact D(C) used to simulate the final profiles are reported in Figure 10.11. As shown in Figure 10.11, the SF method also produces an inaccurate D(C). In contrast, the new method re-produces the exact D(C) which was used to final concentration profiles. The new method is applicable to diffusion systems because metal joining processes done prior to diffusion such as electrodeposition [52], [53], hot isostatic pressing[30], electrospark deposition [110], and forced contact [108], produce a non-uniform solute distribution prior to the final diffusion process. Another application of this method is for diffusion processes with multiple stages, where a diffusion stage precedes the final stage of diffusion. An example is the isothermal solidification stage in TLP bonding, which takes place after the base metal dissolution stage [43]. This approach enables the accurate representation of the true initial conditions prior to diffusion. Therefore, the standard analytical methods commonly used to extract the D(C) can result in an erroneous D(C) when a starting solute distribution exists,

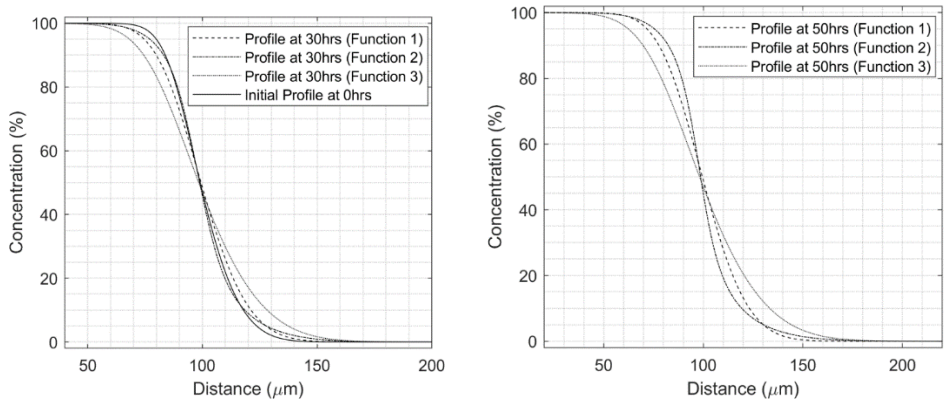

(a) (b)

Figure 10.8 Concentration profiles in binary single-phase systems with pre-existing non-uniform profile, for the three diffusivity functions at two diffusion times (a) Initial solute profile at 0 hrs, and at 30 hrs (b) solute profiles at 50 hrs

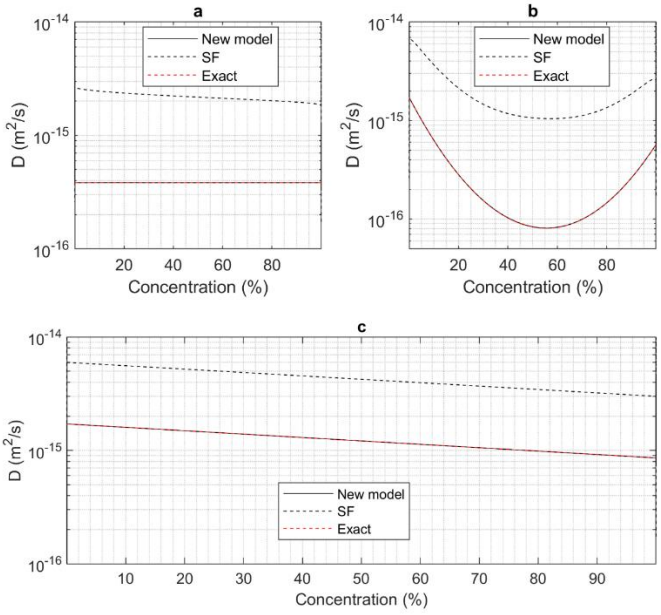

Figure 10.9 Single-phase concentration dependence of interdiffusion coefficient with non-uniform pre-existing solute profile for the three D(C) of (a) Function 1 (b) Function 2 (c) Function 3

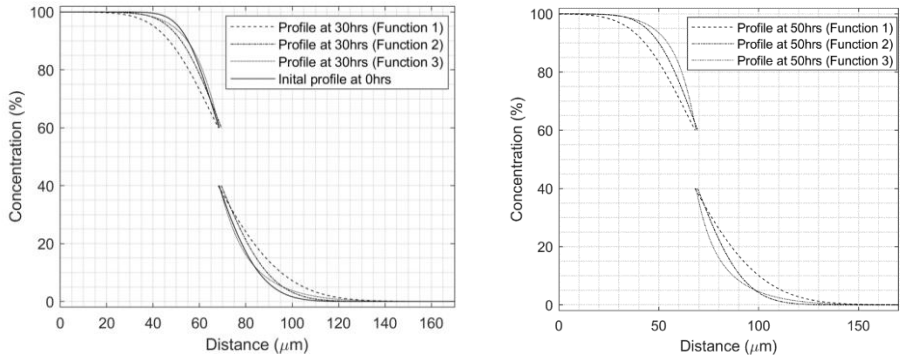

(a) (b)

Figure 10.10 Concentration profiles in binary two-phase systems with pre-existing non-uniform profile, for the three diffusivity functions at two diffusion times (a) Initial solute profile at 0 hrs, and at 30 hrs (b) solute profiles at 50 hrs

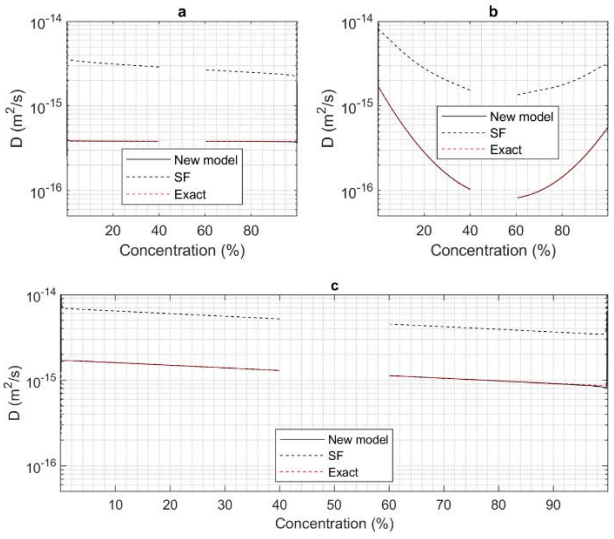

Figure 10.11 Two-phase concentration dependence of interdiffusion coefficient with non-uniform pre-existing solute profile for the three D(C) of (a) Function 1 (b) Function 2 (c) Function 3

as is commonly the case. In contrast, the new method can be used to calculate reliable D(C) regardless of the initial solute distribution.

10.5 Error Analysis

The BM and SF methods are generally utilized when the pre-diffusion solute distribution is small compared to the final distribution [108], [109]. Nevertheless, there is no defined limit or quantity of non-uniform solute distribution prior to diffusion that specifies when to use the SF and BM methods. Therefore, the error between the D(C) calculated by using the new model, SF method, and the actual D(C) will be compared for all cases of diffusion between the two limits of (a) a negligible pre-existing non-uniform solute distribution and (b) a significant pre-existing non-uniform solute distribution. The initial profile generated for the single-phase system with a pre-existing non-uniform solute distribution in section 10.3 is used as the initial diffusion condition for this task. The diffusion is simulated numerically for a diffusion time of 0 to 10,000 hrs using the D(C) in Equation 10.17. This simulation ensures a wide range of diffusion data, such that compared to the final solute distribution, the initial distribution is negligible and significant at long and short diffusion times, respectively. The solute distributions at 0, 100, and 10,000 are reported in Figure 10.12. The new and SF methods are used to calculate the D(C) operative between 0 hrs and other diffusion times. The concentration-averaged diffusivity (D_{ave}) for each method and actual function are calculated by using Equation 2.47. The calculated D_{ave} for the three functions at different durations of diffusion are plotted in Figure 10.13. The results show that the new method results in an accurate D_{ave} for all diffusion times, notwithstanding the initial solute distribution. Conversely, the SF method can provide erroneous results in situations where the initial solute distribution is significant when compared to the final solute distribution.

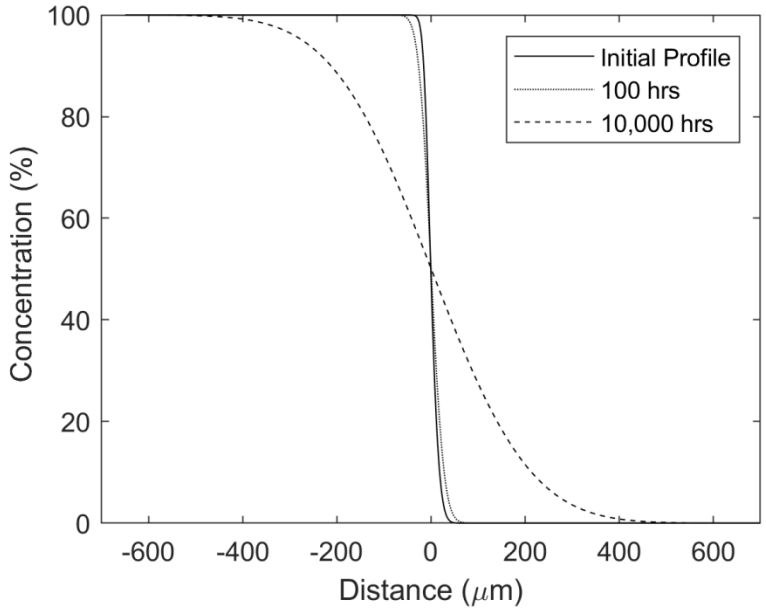

Figure 10.12 Sample numerically generated solute profiles at 0hrs, 100hrs**,** and 10,000 hrs

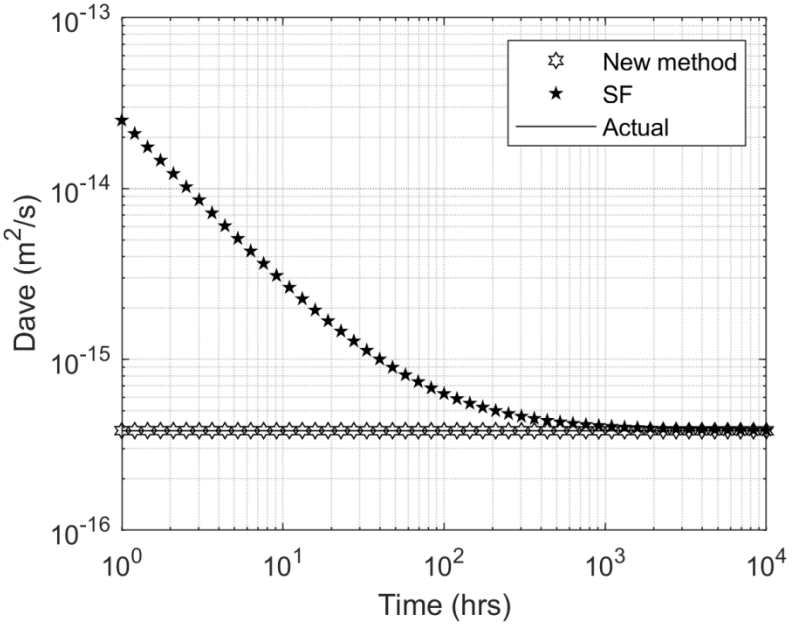

Figure 10.13 D_{ave} computed from the new method, the SF method, and actual function from the duration of significant to negligible non-uniform pre-existing solute distribution

The next task involves quantifying the error when using the new and SF methods. In the literature, an error of 10% is deemed acceptable when comparing different methods of calculating the D(C) from concentration profiles [67]. In this investigation, the percentage root-mean-squared (RMS) error (Equation 10.18) quantifies the error when using the new and the SF methods between 1 hr and 10,000 hrs of diffusion. Compositions of 1% to 99% are considered in determining the error. The errors calculated at selected diffusion times, using both the new method and SF method, are presented in Figure 10.14. The error that results from using the SF method is as high as 7000% for a short diffusion time of 1 hr, with a considerable initial solute distribution, and less than 1% when the initial solute distribution is insignificant at 10,000 hrs. In contrast, the new method has less than 1% error for all diffusion times, regardless of the comparability of the initial and final solute distributions. The error analysis thus validates the use of the new method in binary alloy systems, notwithstanding the initial solute distribution in the system.

$$\%Error = \frac{RMSE}{D_{actual,average}} \times 100\% \qquad 10.18$$

10.6 Experimental Verification of the New Analytical Method

Interface migration and solute distribution are two separate phenomena that are both controlled by diffusion. The simulation of interphase boundary migration is a major application of the D(C) extracted from concentration profiles. Numerical methods are used to predict the interface migration as there is no analytical model to do so when the D(C) depends on the concentration [130]. A reliable way to verify the validity of the calculated D(C) is to use the calculated D(C) to

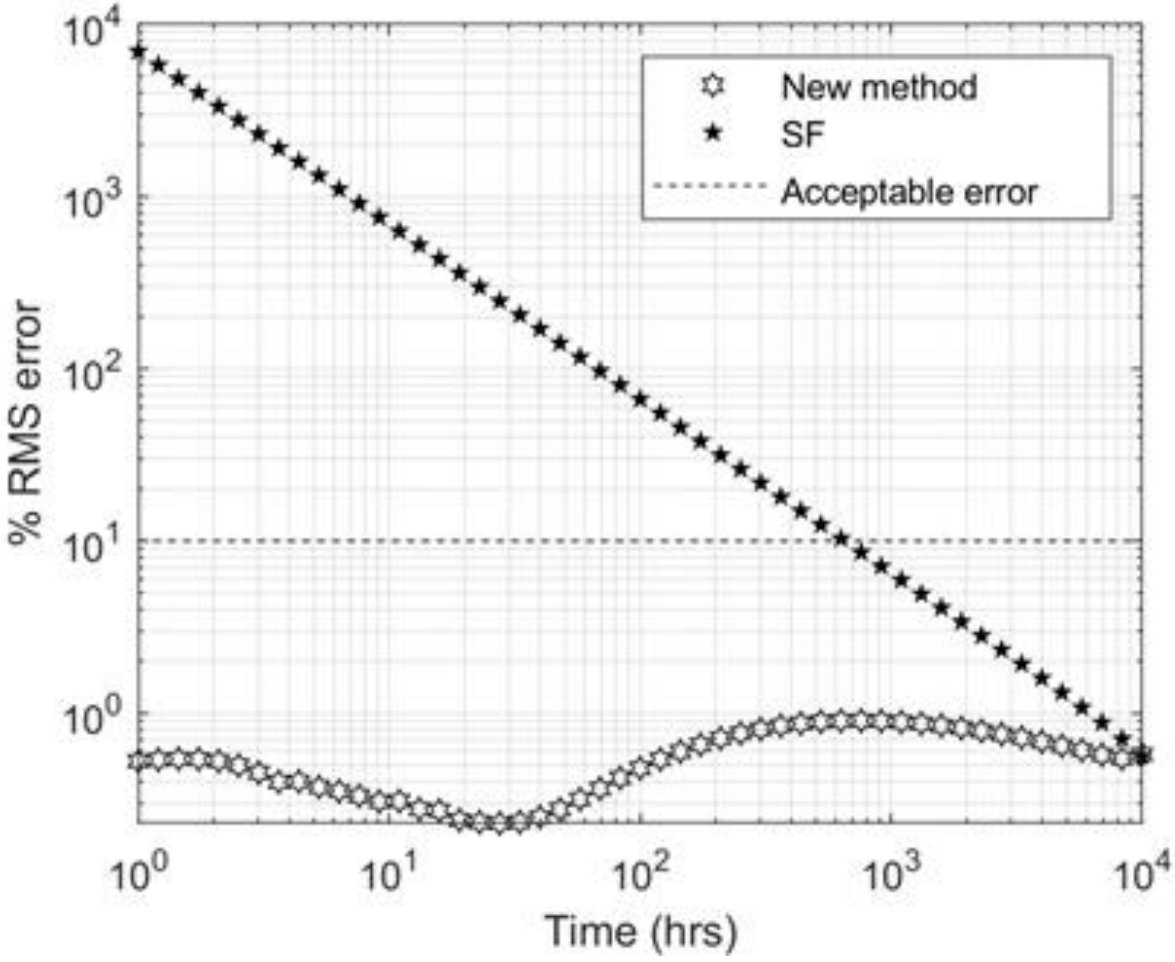

Figure 10.14 The root-mean-squared errors of D_{ave} for the new method, the SF method at periods ranging from significant to negligible initial non-uniform solute distribution

predict the interphase migration distance. A good agreement between the predicted and experimental results validates the D(C) extracted from the experimental concentration profiles. In Kirkendall et al. [35], the distance of the interface migration and concentration profiles were reported at different diffusion times and temperatures for alpha-beta brass couples. The concentration profiles at different times are presented in Figure 10.15 for a temperature of 600ºC. The D(C) operative between successive diffusion times of 2 hrs – 9 hrs, 9 hrs - 24 hrs, 24 hrs - 96 hrs, and 96 hrs - 339 hrs are calculated by using the new analytical method. The D(C) calculated are presented in Figure 10.16. The D(C) was used to calculate the interface migration distance between the two profiles. The predicted and experimentally measured interface migration distances are shown in Figure 10.17. A comparison between the predicted and experimentally measured interface migration distances at different time intervals, thus, experimentally validates the calculated D(C) and the new method proposed in this chapter.

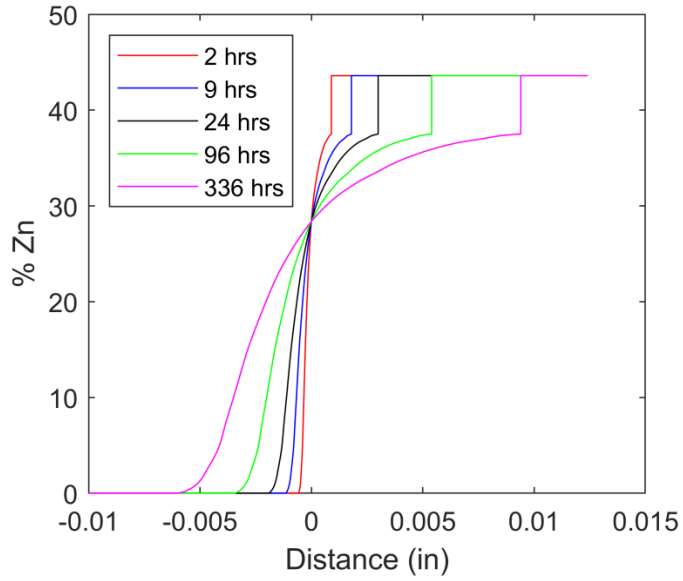

Figure 10.15 Alpha-Beta Cu-Zn concentration profiles at 600 ^{o}C [35]

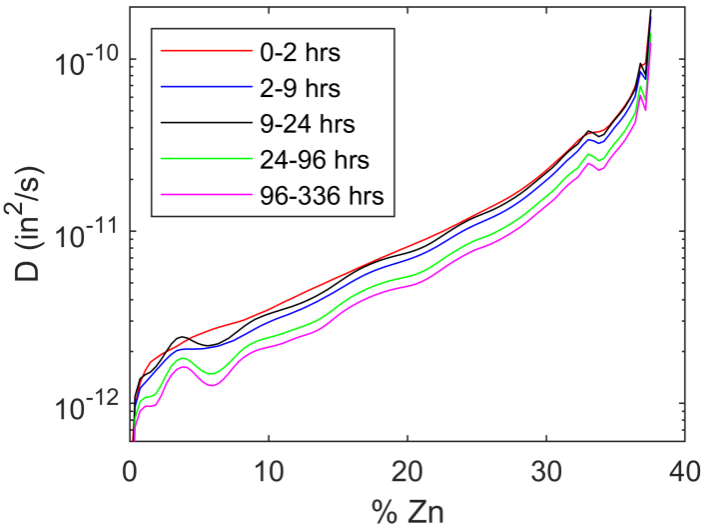

Figure 10.16 Sample concentration dependence of interdiffusion coefficient calculated between consecutive profiles at 600 ^{o}C

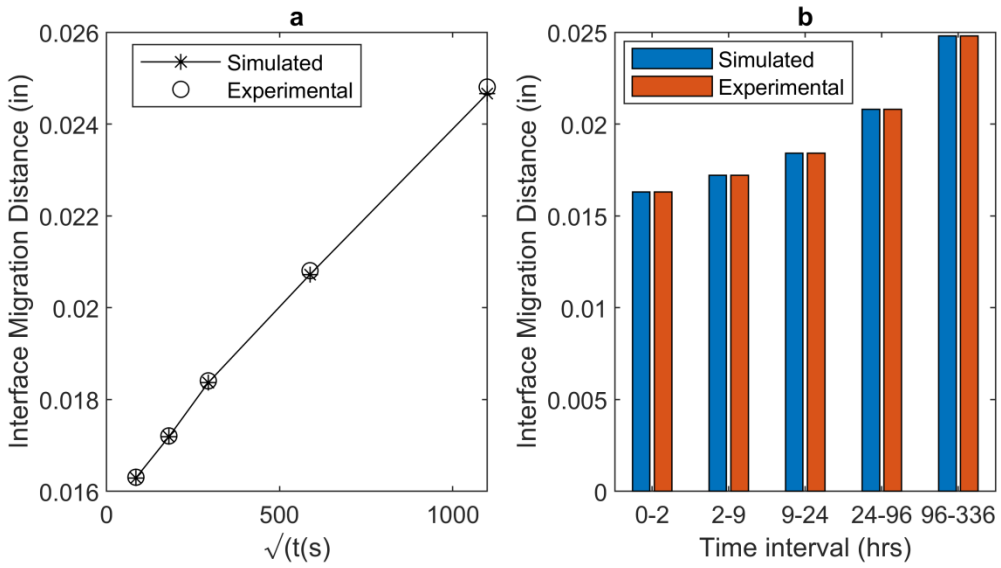

Figure 10.17 Predicted and experimental interphase migration at different time duration of diffusion at $600^{o}C$ for (a) interface migration against the square-root of time (b) interface migration for each time interval

CHAPTER ELEVEN

11 SUMMARY AND CONCLUSIONS

11.1 Summary

The outcomes of this research work can be summarized in the following findings.

11.1.1 Development of a theoretical model to calculate D(C) under DIS conditions

The key summary of this new model are:

1. A theoretical model for calculating D(C) under the influence of DIS is developed.
2. The developed D(C) model is verified by showing that it applies to all binary systems between and at the Darken and Nernst-Planck diffusion limits.
3. The developed pressure distribution equation considers DIS generation and relaxation.
4. The solute distribution equation under DIS is developed from first the principles using the intrinsic diffusivity that considers chemical and stress/pressure potentials.

11.1.2 Development of a new numerical model for extracting D(C) from experimental data

An explicit model based on the Leapfrog/DF scheme is utilized to enhance the stability and computational efficiency of diffusion systems of equations with multiple phases with moving boundaries. The models can simulate single-phase systems and extend to any number of multi-phase planar systems. The key findings are:

1. The new model can be applied to diffusion in planar, cylindrical, and spherical geometries, where the diffusion interface migrates in 1D, 2D and 3D.
2. In this new model, the solute is conserved, and there are no computational assumptions associated with implicit schemes.
3. The appropriate roots for each geometry and condition have been identified to eliminate computational assumptions and explicitly solve the mass conservation equation at the interface.
4. The improved stability reduces the number of grids required to calculate the nonlinear equations accurately, thus resulting in enhanced computational accuracy and efficiency.
5. This new model has been experimentally validated with an experimental data with variable diffusivity.
6. The new model has been extended to planar systems with any number of phases.

11.1.3 Time variation of concentration-dependent interdiffusion coefficient

The variability of the concentration dependence of diffusivity with time has been carefully investigated theoretically and validated experimentally in this work. The DIS equations with stress generation and relaxation were used for the theoretical study to simulate the theoretical distribution of stress and concentration profiles during diffusion. Experimental validation was performed by extracting D(C) from solid-liquid Ag-Cu and solid-solid Cu-Ni systems. The experimental analysis was done by coupling a newly developed numerical model that conserves solutes with the robust FSM to address the flaws in conventional methods like the BM, SF, and Hall procedures. The results obtained are as follows:

1. Theoretically, D(C) can isothermally change with diffusion time.

2. The effect of time increases with increasing differences in mobility, which results in a difference in DIS.
3. A system with a very low viscosity has no significant effect of time on D(C) during diffusion. Also, a very slow relaxation from high viscosity results in a different effective D(C), which does not significantly change with time. In contrast, a moderate viscosity leads to a significant effect of time on the effective D(C).
4. Isothermal systems with different stress-free impurity diffusivity and a comparable molar volume will have the greatest time effect.
5. Isothermal systems with different molar volumes and a comparable stress-free impurity diffusivity will have the greatest effect of time on the effective D(C).
6. The experimental results confirm the isothermal time variation of D(C).
7. The experimental time variation of the D(C) observed in this work is not attributable to grain growth because the grains showed no considerable growth. The time variation cannot be ascribed to residual stress because the samples were not subjected to mechanical loading prior to diffusion, and the diffusion took place at temperatures higher than the stress-relief temperatures of the substrates. However, the time variation is attributable to diffusion-induced stress/strain.
8. Experimental isothermal change in the D(C) with time is as high as 57% in the Ag-Cu system and 65% in the Cu-Ni system, which is significant compared to the 12% and 10% uncertainty in the Ag-Cu and Cu-Ni systems, respectively.
9. The study shows that the common practice of using a single experimental diffusion time to determine the isothermal D(C), using the BM, SF, and Hall methods, can become grossly unreliable when the dependence of diffusivity on concentration varies with time.

10. Unawareness or disregard of the fundamental concept elucidated in this study can lead to serious experimental consequences, including the identification of the underlying mechanism of microstructural changes through phase transformation reactions.

11.1.4 Effect of temperature on concentration-dependent interdiffusion coefficient

The D(C) evaluated theoretically and experimentally at different diffusion times and temperatures are used to calculate the Q(C) and D_0(C) in each system. The following conclusions are subsequently made:

1. Contrary to what has been generally assumed in the literature, theoretically, the Q(C) and D_0(C) are found to vary with time.
2. Experimentally, the time change in the Q(C) is found to be as high as 49% and 89% in the Cu-Ni and Ag-Cu diffusion couples, respectively.
3. Experimentally, the time variation of the natural log of the D_0(C) is found to change by a difference as high as 25% and 15% in the Cu-Ni and Ag-Cu systems, respectively.
4. For certain concentrations, the diffusion coefficient at a lower temperature can be larger than the diffusion coefficient at a higher temperature. This contrasts with expectations in the literature, where diffusivity is expected to increase with an increase in temperature.
5. A common expectation that diffusion-controlled kinetics increase with increased temperature may not always apply for all time durations.
6. The anomalous temperature dependence of the diffusion coefficient observed in this work can be explained by the concept of diffusion-induced stress/strain, and this has not been previously reported in the literature.

7. This study demonstrates that the common tendency to use constant Q(C) and D_0(C) to predict diffusion effects, such as solute distribution, penetration depth, and process kinetics, can lead to significant errors at various times during isothermal diffusion.

11.1.5 Analysis of concentration-dependent interdiffusion coefficient under the condition of pre-existing non-uniform solute distribution

Theoretically, equations for simulating diffusion DIS can be used to study the effect of pre-existing non-uniform solute distribution on D(C). The results were experimentally validated by using a numerical inverse method to calculate the D(C) when there is a pre-existing non-uniform solute distribution, which is impossible to do with standard methods, including the BM, SF, Hall, and Wagner methods. The key conclusions made are:

1. In contrast to what has been implicitly assumed in the literature, theoretically and experimentally, D(C) can be significantly influenced by a non-uniform solute distribution that already exists in a material prior to the diffusion process.
2. Increasing the non-uniform initial solute distribution in a two-stage diffusion process enhances the effect of the non-uniform initial solute distribution on D(C).
3. Increasing the final diffusion time decreases the effect of the non-uniform initial solute distribution on the D(C).
4. Inducing a significant amount of non-uniform initial solute relative to the final solute distribution will significantly affect the effective D(C) if the final diffusion process takes place for a short time and/or at a slow diffusion rate.

5. The use of D(C) obtained by the standard techniques in one stage diffusion to model, predict, or analyze diffusion effects during materials processes with multiple stages can be considerably unreliable.

11.1.6 Analysis of concentration dependence of interdiffusion coefficient under the condition of a time-varying surface concentration

This study investigates the long-held common assumption that the D(C) obtained by standard analytical techniques with a constant SC applies to cases where the SC changes with time. In this study, the common assumption is investigated both experimentally and theoretically. A numerical inverse method coupled with the FSM is used to extract accurate D(C) values from experimental concentration profiles obtained under both constant and time-varying SC conditions, which is not possible by using standard analytical methods. The key findings are:

1. Experimentally and theoretically, the D(C) obtained under constant and time-varying SC differ significantly.
2. The experimental difference in the concentration-averaged interdiffusion coefficients obtained under constant and time-varying SC is as high as 43%, which is considerably higher than the 15% uncertainty.
3. The use of D(C) obtained under a constant SC, which is the only type of SC possible by using standard analytical methods to model or analyze diffusion effects when the SC changes with time, such as during homogenization heat treatments, sintering, diffusion bonding, coating and surface alloying, can cause significant errors.

11.1.7 Effect of solute-source composition on composition-dependent interdiffusion coefficient

In summary, the influence of the values of solute-source composition on D(C) has been carefully investigated theoretically and experimentally. The D(C) are calculated theoretically using the numerical model developed in this study and experimentally from pure-metal/pure-metal and pure-metal/alloy diffusion couples in the Cu-Ni system. The key conclusions are as follows:

1. The theoretical and experimental studies show that the D(C) can significantly change with solute-source concentration.
2. Experimental changes in the isothermal concentration-averaged interdiffusion coefficient for the same compositional range when the solute-source composition changes from 1.0 to 0.1, is found to be as high as 76%. This is significant, considering that the uncertainty in the experimental data is at most 15%.
3. Accordingly, the common tendency to use D(C) obtained from pure-metal/pure-metal diffusion couples to predict or analyze diffusion data when the solute source is an alloy instead of a pure metal can lead to significant errors.

11.1.8 Effect of 1D and 2D Migration of Diffusion Interface on Concentration-Dependent Interdiffusion Coefficient

The common expectation that analytical 1D planar models can reliably extract D(C) profiles from non-planar diffusion systems, and that **D(C)** is an isothermal constant independent of geometry has been theoretically investigated. The results are validated experimentally. The results of the theoretical study, corroborated by experimental data, concur with the findings in [7] that the

effective **D(C)** can change with diffusion geometry, contrary to assumptions. The results are summarized as follows:

1. The common use of 1D planar methods to extract the D(C) when diffusion is non-planar can result in an erroneous D(C).
2. The calculated D(C) error increases with decreasing initial interface thickness, such as the radius of wires, holes, and balls, prior to the welding stage of the diffusion heat treatment.
3. Increasing the duration of diffusion reduces the reliability of the D(C) determined by using 1D planar methods.
4. Theoretically and experimentally, the D(C) operative in a non-planar system is different from that in a planar system.
5. The difference in the concentration-averaged interdiffusion coefficients obtained when the diffusion interface moves in 1D and 2D in planar and cylindrical systems, respectively, is as high as 45%, which is considerably larger than the 15% uncertainty.
6. A new equation has been developed to calculate the initial position of the interface from concentration profiles obtained from systems with 1D, 2D, and 3D migration of the interface.
7. Therefore, the indiscriminate use of **D(C)** reported in the literature, which is normally obtained from samples with a planar geometry, to predict or analyze diffusion data in other geometrical domains, such as cylindrical and spherical systems, can lead to significant errors in diffusion analyses.

11.1.9 A New Analytical Method for Computing Concentration-Dependent Interdiffusion Coefficient in Binary Systems with Pre-Existing Solute Concentration Gradient

A new analytical method for calculating D(C) when a non-uniform solute distribution already exists in a substrate prior to diffusion in a binary system, which can not be achieved by using existing analytical methods, such as the BM, SF and Wagner methods, has been developed. The key concept of the new method is validated by experimental data reported in the literature. This new method addresses the limitations of previous analytical techniques, which are restricted to a single solute concentration profile without a non-uniform initial solute state. The analyses of numerically simulated concentration profiles show that previous methods are erroneous when calculating the D(C) in binary systems with significant non-uniform initial solute distributions. In contrast, the new analytical method can reliably calculate the D(C) operative between two isothermal concentration profiles obtained at different diffusion times. Practically, this method can be used to extract D(C) from planar diffusion systems with non-uniform initial solute distribution prior to diffusion or caused by diffusion processes that have multiple stages.

11.2 Conclusions

The following major conclusions are drawn from this research work:

1. It has been established theoretically and verified experimentally that contrary to the common expectation that **D(C)** is isothermally constant, the **D(C)** can indeed vary isothermally by factors that influence concentration gradient at a given concentration due to DIS.

2. The indiscriminate use of **D(C)** reported in the literature as an isothermally constant material parameter can lead to significant errors in diffusion analyses.
3. Therefore, proper consideration of the factors that can cause the **D(C)** to isothermally change, as identified in the present work, is imperative to enhancing the reliability of theoretical predictions and analyses of diffusion effects in materials.

12 LIMITATIONS AND RECOMMENDATIONS FOR FUTURE WORK

12.1 Limitations of the Present Work

1. This work is focused on isothermal variation in the concentration-dependent interdiffusion coefficient. Nevertheless, the theoretical and experimental analyses performed in the present work suggest that aside from the interdiffusion coefficient, the impurity diffusion coefficient can equally be isothermally affected by the factors studied in the present work. Concentration-dependent interdiffusion coefficient studied in the present work is sufficient to describe diffusion in binary alloy systems; however, in ternary and multicomponent systems, the use of mobility parameters may be required. To assess mobility parameters, an impurity diffusion coefficient would become necessary in addition to the interdiffusion coefficient.

2. This work is focused on diffusion in binary alloy systems. Nonetheless, the key findings are crucially relevant in ternary and other multicomponent systems, which use mobility for diffusion analysis, as a key factor that fundamentally influences mobility is the concentration-dependent interdiffusion coefficient obtained in the binary systems.

3. Aside from the numerical model developed in the present work for extracting D(C) from experimental data when diffusion interface migrates in 1D, 2D, and 3D, a new analytical method that addresses a key limitation in conventional analytical methods like BM, SF, and Wagner methods for calculating D(C) from experimental data is also developed. The analytical method is developed for users who may not be sufficiently skilled in using the numerical model. However, the new analytical method is limited to cases where the

diffusion interface migrates in 1D. In cases where the diffusion interface migrates in 2D and 3D, the numerical model developed in the present work is needed for calculation D(C).

4. The forward simulation technique is limited when the surface concentration significantly changes with time. This is due to the lost concentrations at the final time that cannot be adjusted during iterations in the future time. In the present work, care was taken to work between times with no significant change in composition and a system with an uncomplicated D(C).

12.2 Recommendations For Future Work

In view of the limitations listed above, the following are recommended for future work:

1. It is suggested that studies be carried out to carefully study how impurity diffusion coefficient and concentration-dependent interdiffusion coefficient in ternary and other multi-components systems are affected by the key DIS factors studied in the present work.
2. It is recommended that a rigorous study should be performed to extend the new analytical method developed in the present work for cases where the diffusion interface migrates in 2D and 3D, and when the surface composition changes with time. This will make it possible for users who are not well skilled in using the numerical model to use the method for extracting D(C) from experimental data.
3. It is suggested that the explicit solutions to the DIS pressure and solute distribution equation should be made more efficient. The solutions should be stabilized and checked for consistency. The consistency analysis can be carried out using the Truncation error analysis, while the stability analysis can be done using the Von Neumann stability analysis.

Von-Neumann's analysis shows that applying the Duforth-Frankel scheme stabilizes both pressure and solute distribution equations. That is substituting $C_i^k = \frac{C_i^{k+1} + C_i^{k-1}}{2}$ and $P_i^k = \frac{P_i^{k+1} + P_i^{k-1}}{2}$ into the pressure and solute distribution equations stabilizes the solution and reduces the present limitation of using a small time step.

4. It is proposed that variable molar volumes or mole fraction dependent molar volumes should be introduced into the new model developed in section 3.3. To carry out this task, the following steps should be taken:

    a) Concentration should be replaced with $c = C/V$ (from Equation 2.41).

    b) A function of the dependence of V on C can be assumed (V=**F(C)**). A common function is a linear relationship called Vegard's law, which relates molar volume to the mole fractions and molar volumes of each element in the binary system. Vegard's law for molar volume is $V = V_1C + V_2(1-C)$. Other functions can be determined as found in the literature.

    A proposed approach to verify the model is outlined below:

        i. Use the model along with an assumed D(C) function to simulate concentration profiles under the condition of no solute build-up.

        ii. Use an established process (or method) to extract the D(C) from the simulated profiles. There are two established processes (or methods) - Wagner for systems without initial solute and our new analytical method for systems with or without initial solute. To reduce the uncertainties at

the boundaries, the exact simulated profiles should be used to extract D(C), and the solute must not get to the end.

iii. The D(C) used to simulate the profiles and the actual D(C) extracted using Equation 10.14c can be compared to determine the validity of the new model.

iv. The second stage involves comparing FSM coupled with the model and the new analytical method on experimental profiles, which usually have uncertainties around the boundaries (sometimes due to smoothing). The result of this stage will show that the FSM is reliable in all regions when coupled with the new model.

5. It is proposed that the new model should be extended to non-planar multi-phase cylindrical and spherical systems with 2D and 3D interface migration, respectively.
6. A backward diffusion method is proposed for cases with changing surface concentration. This method works by:
   a) Solving the diffusion equation backward in time (backward diffusion).
   b) Comparing the backward simulated and initial concentration gradient
   c) Adjusting the full concentration range of diffusion coefficient.
   d) Repeating steps a-c until there is convergence at step b.

The major drawback of this recommendation is the difficulty in solving the backward diffusion equation. The solution easily becomes unstable due to a quick amplification of errors.

13 RESEARCH CONTRIBUTIONS FROM THIS WORK

13.1 Peer-reviewed Journal Publications:

[1] **O. Olaye** and O. A. Ojo, "Leapfrog / Dufort-Frankel explicit scheme for diffusion-controlled moving interphase boundary problems with variable diffusion coefficient and solute conservation," *Model. Simul. Mater. Sci. Eng.*, vol. 28, no. 1, pp. 1–24, 2019.

[2] **O. Olaye** and O. A. Ojo, "Change in Concentration-Dependent Diffusion Activation Energy and Frequency Factor with Time: Identified by Numerical Analyses of Experimental Data," *Metall. Mater. Trans. A*, vol. 51, no. 12, pp. 6482–6497, 2020.

[3] **O. Olaye** and O. A. Ojo, "Time variation of concentration-dependent interdiffusion coefficient obtained by numerical simulation analysis," *Materialia*, vol. 16, no. February, p. 101056, 2021.

[4] **O. Olaye** and O. A. Ojo, "A new analytical method for computing concentration-dependent interdiffusion coefficient in systems with pre-existing solute concentration gradient," *Journal of Phase Equilibria and Diffusion, 2021.*

[5] **O. Olaye** and O. A. Ojo, "Analysis of Concentration Dependent Interdiffusion Coefficient under the Condition of Pre-Existing Non-uniform Solute Distribution," *Metall. Mater. Trans. A, 2021.*

[6] **O. Olaye** and O. A. Ojo, "The disparity in the Concentration Dependence of Interdiffusion Coefficient under 1D and 2D Diffusion Interface Migration," *Results in Physics,* Accepted.

[7] **O. Olaye** and O. A. Ojo, “Analysis of Concentration Dependence of Interdiffusion Coefficient under the Condition of a Time-Varying Surface Concentration,” *Materials Transactions,* Accepted.

[8] **O. Olaye** and O. A. Ojo, “Influence of Solute-Source Composition on Composition-Dependent Interdiffusion Coefficient,” *Results in Physics,* Under review.

13.2 Conference Presentations

[1] **O. Olaye** and O. A. Ojo, “A new numerical model for simulating diffusion-controlled moving interphase boundary problems” Canadian Materials Science Conference, Queen’s University, Ontario, June 1 - 4, 2021.

[2] **O. Olaye** and O. A. Ojo, “Time Variation of Concentration-dependent Interdiffusion Coefficient” TMS Conference 2022, Anaheim, California, USA, February 27 – March 3, 2022.

REFERENCE

[1] A. Fick, "Ueber Diffusion," *Ann. Phys.*, vol. 170, no. 1, pp. 59–86, 1855, doi: 10.1002/andp.18551700105.

[2] R. Gaur, L. Mishra, and S. K. Sen Gupta, "Diffusion and Transport of Molecules In Living Cells," in *Modelling and Simulation of Diffusive Processes. Simulation Foundations, Methods and Applications*, no. April, 2014, pp. 27–49.

[3] T. C. Illingworth, I. O. Golosnoy, V. Gergely, and T. W. Clyne, "Numerical modelling of transient liquid phase bonding and other diffusion controlled phase changes," *J. Mater. Sci.*, vol. 40, pp. 2505–2511, 2005, [Online]. Available: https://link-springer-com.uml.idm.oclc.org/content/pdf/10.1007%2Fs10853-005-1983-y.pdf.

[4] Z. Wang, L. Fang, I. Cotton, and R. Freer, "Ni-Cu interdiffusion and its implication for ageing in Ni-coated Cu conductors," *Mater. Sci. Eng. B Solid-State Mater. Adv. Technol.*, vol. 198, pp. 86–94, 2015, doi: 10.1016/j.mseb.2015.04.006.

[5] R. E. Robissoz, "Interdiffusion in a Bulk Couple of Lead and Lead-50wt% Indium Alloy," *Acta Mater.*, vol. 24, pp. 609–614, 1976.

[6] G. B. Stephenson, "Deformation During Interdiffusion," *Acta Metall.*, vol. 36, no. 10, pp. 2663–2683, 1988, doi: https://doi.org/10.1016/0001-6160(88)90114-9.

[7] F. C. Larche and J. W. Cahn, "The Effect of Self-Stress In Solids," *Acta Metall.*, vol. 30, pp. 1835–1845, 1982, doi: 10.1016/0001-6160(82)90023-2.

[8] R. K. Jain and R. J. van Overstraeten, "Calculation of the diffusion induced stresses in silicon," *Phys. Status Solidi*, vol. 25, no. 1, pp. 125–130, 1974, doi:

10.1002/pssa.2210250109.

[9] I. Daruka, I. A. Szabó, D. L. Beke, C. Cserháti, A. Kodentsov, and F. J. J. Van Loo, "Diffusion-induced bending of thin sheet couples: Theory and experiments in Ti-Zr system," *Acta Mater.*, vol. 44, no. 12, pp. 4981–4993, 1996, doi: 10.1016/S1359-6454(96)00099-7.

[10] T. Yamane, N. Mori, M. Yoritoshi, M. Yoshinari, K. Mitsue, and T. Takahashi, "Effect of High Pressure on Interdiffusion in Cu-Zn Alloys at Temperatures near the Melting Point," *Metall. Trans. A*, vol. 19A, pp. 467–471, 1988, doi: 10.1007/BF02649260.

[11] L. A. Girifalco and G. H. Hubert, "The Theory of Diffusion In Strained Systems," Ohio, 1958. [Online]. Available: https://ntrs.nasa.gov/search.jsp?R=19930085264.

[12] S. W. Donald and P. W. Gordon, "Diffusion-Induced Stresses and Plastic Deformation," *Metall. Trans. A*, vol. 8, no. October, pp. 1977–1531, 1977, doi: 10.1007/BF02644856.

[13] N. E. B. Cowern, "Diffusion in Strained Si(Ge)," *Phys. Rev. Lett.*, vol. 72, no. 16, pp. 2585–2588, 1994, doi: 10.1103/PhysRevLett.72.2585.

[14] D. L. Beke, I. A. Szabó, Z. Erdélyi, and G. Opposits, "Diffusion-induced stresses and their relaxation," *Mater. Sci. Eng. A*, vol. 387–389, no. 1-2 SPEC. ISS., pp. 4–10, 2004, doi: 10.1016/j.msea.2004.01.065.

[15] L. A. Girifalco and H. H. Grimes, "Effect of static strains on diffusion," *Phys. Rev.*, vol. 121, no. 4, pp. 982–991, 1961, doi: 10.1103/PhysRev.121.982.

[16] D. L. Beke, Z. Erdélyi, and B. Parditka, "Effect of diffusion induced driving forces on interdiffusion - Stress development/relaxation and kinetics of diffusion processes," *Defect*

Diffus. Forum, vol. 309–310, pp. 113–120, 2011, doi: 10.4028/www.scientific.net/DDF.309-310.113.

[17] G. Opposits, S. Szabó, D. L. Beke, Z. Guba, and I. A. Szabó, "Diffusion-induced bending of Cu-Ni thin sheet diffusion couples," *Scr. Mater.*, vol. 39, no. 7, pp. 977–983, 1998, doi: 10.1016/S1359-6462(98)00228-0.

[18] J. L. Chu and S. Lee, "The effect of chemical stresses on diffusion," *J. Appl. Phys.*, vol. 75, no. 6, pp. 2823–2829, 1994, doi: 10.1063/1.356174.

[19] Y. Iijima, K. Hirano, T. Ohezeki, and K. Suzuki, "Interdiffusion in Gold-Iron Alloys," in *Diffusion and Defect Monograph Series*, 1983, pp. 401–404.

[20] "Solid Solution of Metals: With Diagram | Metallurgy." https://www.engineeringnotes4u.com/2019/11/solid-solution-of-metals-with-diagram.html (accessed Mar. 16, 2021).

[21] L. Zhu, Z. Chen, W. E. I. Zhong, C. Wei, and G. Cai, "Measurement of Diffusion Coefficients in the bcc Phase of the Ti-Sn and Zr-Sn Binary Systems," *Metall. Mater. Trans. A*, vol. 50, no. 3, pp. 1409–1420, 2019, doi: 10.1007/s11661-018-05107-7.

[22] W. Zhong and J. Zhao, "First experimental measurement of calcium diffusion in magnesium using novel liquid-solid diffusion couples and forward-simulation analysis," *Scr. Mater.*, vol. 127, pp. 92–96, 2017, doi: 10.1016/j.scriptamat.2016.09.008.

[23] W. Zhong and J. Zhao, "First Reliable Diffusion Coefficients for Mg-Y and Additional Reliable Diffusion Coefficients for Mg-Sn and Mg-Zn," *Metall. Mater. Trans. A*, vol. 48, no. 12, pp. 5778–5782, 2017, doi: 10.1007/s11661-017-4378-1.

[24] Q. Zhang and J. Zhao, “Extracting interdiffusion coefficients from binary diffusion couples using traditional methods and a forward-simulation method,” *Intermetallics*, vol. 34, pp. 132–141, 2013, doi: 10.1016/j.intermet.2012.11.012.

[25] Q. Zhang, Z. Chen, W. Zhong, and J. C. Zhao, “Accurate and efficient measurement of impurity (dilute) diffusion coefficients without isotope tracer experiments,” *Scr. Mater.*, vol. 128, pp. 32–35, 2017, doi: 10.1016/j.scriptamat.2016.09.040.

[26] L. Greta *et al.*, “Diffusion in the Ti-Al-V System,” *J. Phase Equilibria Diffus.*, vol. 39, no. 5, pp. 731–746, 2018, doi: 10.1007/s11669-018-0673-9.

[27] C. M. E. Jr and J. Zhao, “Phase Equilibria and Diffusion in the Ni-Cr-Pt System at 1200 ° C,” *J. Phase Equilibria Diffus.*, vol. 40, no. 4, pp. 542–552, 2019, doi: 10.1007/s11669-019-00753-9.

[28] Z. Chen, Q. Zhang, and J. Zhao, “pydiffusion : A Python Library for Diffusion Simulation and Data Analysis,” *J. Open Res. Softw.*, vol. 7, no. 13, pp. 1–7, 2019, doi: https://doi.org/10.5334/jors.255.

[29] Z. Chen, Z. Liu, and J. Zhao, “Experimental Determination of Impurity and Interdiffusion Coefficients in Seven Ti and Zr Binary Systems Using Diffusion Multiples,” *Metall. Mater. Trans. A*, vol. 49, no. 7, pp. 3108–3116, 2018, doi: 10.1007/s11661-018-4645-9.

[30] L. Zhu, Q. Zhang, Z. Chen, C. Wei, and G. Cai, “Measurement of interdiffusion and impurity diffusion coefficients in the bcc phase of the Ti – X (X 5 Cr , Hf , Mo , Nb , V , Zr) binary systems using diffusion multiples,” *J Mater Sci*, vol. 52, pp. 3255–3268, 2017, doi: 10.1007/s10853-016-0614-0.

[31] Z. L. Bryan, P. Alieninov, I. S. Berglund, and M. V. Manuel, “A diffusion mobility database for magnesium alloy development,” *Calphad Comput. Coupling Phase Diagrams Thermochem.*, vol. 48, pp. 123–130, 2015, doi: 10.1016/j.calphad.2014.12.001.

[32] M. T. Modes, “Kinetics of Concentration Polarization,” in *Electrochemistry and Corrosion Science*, 2006, p. 124.

[33] O. Karabelchtchikova and R. D. Sisson, “Carbon diffusion in steels: A numerical analysis based on direct integration of the flux,” *J. Phase Equilibria Diffus.*, vol. 27, no. 6, pp. 598–604, 2006, doi: 10.1361/154770306X153611.

[34] O. Karabelchtchikova and R. D. Sisson, “Calculation of gas carburizing kinetics from carbon concentration profiles based on direct flux integration,” *Defect Diffus. Forum*, vol. 266, pp. 171–180, 2007, doi: 10.4028/3-908451-45-0.171.

[35] E. Kirkendall, L. Thomassen, and C. Uethegrove, “Rates of Diffusion of Copper and Zinc in Alpha Brass,” *Trans. Am. Inst. Min. Metall. Eng.*, vol. 133, no. 967, pp. 186–203, 1939, [Online]. Available: http://www.aimehq.org/doclibrary-assets/books/AIME Technical Publications – 1938 - A-E/AIME Technical Publications – 1938 - A-E - 076.pdf.

[36] R. W. Balluffi, S. M. Allen, and W. C. Carter, “Driving Forces and Fluxes for Diffusion,” in *Kinetics of Materials*, Hoboken, New Jersey: John Wiley & Sons, Inc., 2005.

[37] S. Banerjee and P. Mukhopadhyay, “Diffusional Transformations,” in *Phase Transformations: Examples from Titanium and Zirconium Alloys*, Pergamon M., vol. 12, Elsevier, Academic Press, 2007, pp. 555–716.

[38] C. E. Birchenall, “The mechanism of diffusion in the solid state,” *Metall. Rev.*, vol. 3, no.

1, pp. 235–277, 1958, doi: 10.1179/mtlr.1958.3.1.235.

[39] P. Shewmon, *Diffusion In Solids*, Second. Switzerland: The Minerals, Metals & Materials Society, 2016.

[40] G. Borchardt, K. Gömann, M. Kilo, and H. Schmidt, *Diffusion in Ceramics*, vol. 1–4. 2013.

[41] Y. Mishin, C. Herzig, J. Bernardini, and W. Gust, "Grain boundary diffusion : fundamentals to recent developments," vol. 42, no. 4, 1997.

[42] Y. Chen and C. A. Schuh, "Geometric considerations for diffusion in polycrystalline solids," *J. Appl. Phys.*, vol. 101, no. 6, 2007, doi: 10.1063/1.2711820.

[43] Y. Zhou, W. F. Gale, and T. H. North, "Modelling of transient liquid phase bonding," *Int. Mater. Rev.*, vol. 40, no. 5, pp. 181–196, 1995, doi: 10.1179/imr.1995.40.5.181.

[44] J. Bruchon, D. Pino-Muñoz, F. Valdivieso, and S. Drapier, "Finite element simulation of mass transport during sintering of a granular packing. Part I. Surface and lattice diffusions," *J. Am. Ceram. Soc.*, vol. 95, no. 8, pp. 2398–2405, 2012, doi: 10.1111/j.1551-2916.2012.05073.x.

[45] A. Einstein, "Über die von der molekularkinetischen Theorie der Wärme geforderte Bewegung von in ruhenden Flüssigkeiten suspendierten Teilchen," *Ann. Phys.*, vol. 17, pp. 549–560, 1905, doi: 10.1063/1.3071085.

[46] A. N. Gorban, H. P. Sargsyan, and H. A. Wahab, "Quasichemical models of multicomponent nonlinear diffusion," *Math. Model. Nat. Phenom.*, vol. 6, no. 5, pp. 184–262, 2011, doi: 10.1051/mmnp/20116509.

[47] G. Peskir, "On the diffusion coefficient: The Einstein relation and beyond," *Stoch. Model.*,

vol. 19, no. 3, pp. 383–405, 2003, doi: 10.1081/STM-120023566.

[48] T. Teorell, “Studies on the ‘Diffusion Effect’ upon Ionic Distribution. Some Theoretical Considerations,” *Proc. Natl. Acad. Sci.*, vol. 21, no. 3, pp. 152–161, 1935, doi: 10.1073/pnas.21.3.152.

[49] V. Y. Paul’s, V. N. Kuskov, and N. I. Smolin, “Simulation of alloying-element diffusion during electrodiffusion heat treatment of steels,” *Russ. Metall.*, vol. 2007, no. 1, pp. 29–32, 2007, doi: 10.1134/S0036029507010065.

[50] H.-J. Stepper and H. Wever, “Electrodiffusion in dilute copper alloys,” *J. Phys. Chem. Solids*, vol. 28, no. 7, pp. 1103–1108, 1967, doi: 10.1016/0022-3697(67)90054-6.

[51] F. Lantelme and S. Belaidouni, “Electrochemical study of the diffusion at solid state. Gold—copper system,” *Electrochim. Acta*, vol. 26, no. 9, pp. 1225–1236, 1981, doi: 10.1016/0013-4686(81)85103-1.

[52] J. Lienig and M. Thiele, “Fundamentals of Electromigration Having,” in *Fundamentals of Electromigration- Aware Integrated Circuit Design*, Cham, Switzerland, 2018, pp. 13–26.

[53] B. Chao, S. H. Chae, X. Zhang, K. H. Lu, J. Im, and P. S. Ho, “Investigation of diffusion and electromigration parameters for Cu-Sn intermetallic compounds in Pb-free solders using simulated annealing,” *Acta Mater.*, vol. 55, no. 8, pp. 2805–2814, 2007, doi: 10.1016/j.actamat.2006.12.019.

[54] L. S. Darken and R. A. Oriani, “Thermal diffusion in solid alloys,” *Acta Metall.*, vol. 2, no. 6, pp. 841–847, 1954, doi: 10.1016/0001-6160(54)90038-3.

[55] Z. Erdélyi and L. Beke, “Stress effects on diffusional interface sharpening in ideal binary

alloys," *Phys. Rev. B - Condens. Matter Mater. Phys.*, vol. 68, no. 9, pp. 2–5, 2003, doi: 10.1103/PhysRevB.68.092102.

[56] Z. Erdélyi, B. Parditka, and D. L. Beke, "Stress effects on the kinetics of nanoscale diffusion processes," *Scr. Mater.*, vol. 64, no. 10, pp. 938–941, 2011, doi: 10.1016/j.scriptamat.2011.01.040.

[57] W. V. Youdelis, D. R. Colton, and J. Cahoon, "On the Theory of Diffusion in a Magnetic Field," *Can. J. Phys.*, vol. 42, no. 11, pp. 2217–2237, 1964, doi: 10.1139/p64-204.

[58] Y. Wu, G. Duan, and X. Zhao, "Effects of magnetic field intensity on carbon diffusion coefficient in pure iron in γ-Fe temperature region," *Int. J. Mod. Phys. B*, vol. 29, no. 10–11, pp. 1–8, 2015, doi: 10.1142/S0217979215400019.

[59] Y. Wu, H. H. Li, G. S. Duan, and X. Zhao, "Effects of Magnetic Field Intensity on Carbon Diffusion Behavior in Pure Iron in α-Fe temperature region," 2015, doi: 10.1142/S0217979215400019.

[60] F. J. J. Van Loo, "On the determination of diffusion coefficients in a binary metal system," *Acta Metall.*, vol. 18, no. 10, pp. 1107–1111, 1970, doi: 10.1016/0001-6160(70)90009-X.

[61] S. Shankar and L. L. Seigle, "Interdiffusion and intrinsic diffusion in the Ni AI (δ) phase of the Al-Ni system," *Metall. Trans. A*, vol. 9, no. 10, pp. 1467–1476, 1978, doi: 10.1007/BF02661819.

[62] L. S. Darken, "Diffusion, Mobility and Their Interrelation through Free Energy in Binary Metallic Systems," *Trans. AIME*, vol. 175, pp. 184–201, 1948.

[63] M. A. Dayananda, "Average effective interdiffusion coefficients and the matano plane

composition," *Metall. Mater. Trans. A Phys. Metall. Mater. Sci.*, vol. 27, no. 9, pp. 2504–2509, 1996, doi: 10.1007/bf02652344.

[64] M. A. Dayananda, "Average Effective Interdiffusion Coefficients in Binary and Multicomponent Alloys," *Defect Diffus. Forum*, vol. 95–98, pp. 521–536, 1993, doi: 10.4028/www.scientific.net/ddf.95-98.521.

[65] H. Mehrer, "Interdiffusion and Kirkendall Effect," in *Diffusion in Solids*, Springer, Berlin, Heidelberg, 2007, p. 165.

[66] T. Ahmed, I. V Belova, and G. E. Murch, "Finite Difference Solution of the Diffusion Equation and Calculation of the Interdiffusion Coefficient using the Sauer-Freise and Hall Methods in Binary Systems," *Procedia Eng.*, vol. 105, no. Icte 2014, pp. 570–575, 2015, doi: 10.1016/j.proeng.2015.05.034.

[67] S. Santra and A. Paul, "Role of the Molar Volume on Estimated Diffusion Coefficients," *Metall. Mater. Trans. A*, vol. 46, no. 9, pp. 3887–3899, 2015, doi: 10.1007/s11661-015-2988-z.

[68] L. D. Hall, "An Analytical Method of Calculating Variable Diffusion Coefficients," *J. Chem. Phys.*, vol. 21, no. 1, pp. 87–89, 1953, doi: 10.1063/1.1698631.

[69] R. F. Sekerka and S.-L. Wang, "Moving phase boundary problems," in *Lectures on the Theory of Phase Transformations*, Second., H. I. Aaronson, Ed. Wiley-TMS, 2000, pp. 231–284.

[70] J. CRANK, *The Mathematics of Diffusion*, SECOND EDI. Oxford: CLARENDON PRESS, 1975.

[71] R. Asthana, “An Analysis for Moving Boundary Diffusion Controlled Growth in a Finite Domain with a Concentration-Dependent Diffusion Coefficient,” *Jurnal of Colloid and Interface Science*, vol. 158. pp. 146–151, 1993, doi: 0021-9797/93.

[72] H. Nakagawa, C. H. Lee, and T. H. North, “Modeling of base metal dissolution behavior during transient liquid-phase brazing,” *Metall. Trans. A*, vol. 22, no. 2, pp. 543–555, 1991, doi: 10.1007/BF02656822.

[73] T. Shinmura, K. Ohsasa, and T. Narita, “Isothermal Solidification Behavior During the Transient Liquid Phase Bonding Process of Nickel Using Binary Filler Metals,” *Mater. Trans.*, vol. 42, no. 2, pp. 292–297, 2001, doi: https://doi.org/10.2320/matertrans.42.292.

[74] J. F. Li, P. A. Agyakwa, and C. M. Johnson, “A fixed-grid numerical modelling of transient liquid phase bonding and other diffusion-controlled phase changes,” *J. Mater. Sci.*, vol. 45, no. 9, pp. 2340–2350, 2010, doi: 10.1007/s10853-009-4199-8.

[75] S. K. Pabi, “Computer simulation of the two-phase diffusion-controlled dissolution in the planar finite multilayer couples,” *Phys. Status Solidi*, vol. 51, no. 1, pp. 281–289, 1979, doi: 10.1002/pssa.2210510133.

[76] W. D. Murray and F. Landis, “Numerical and Machine Solutions of Transient Heat-Conduction Problems Involving Melting or Freezing: Part I—Method of Analysis and Sample Solutions,” *J. Heat Transfer*, vol. 81, no. 2, pp. 106–112, 1959, doi: 10.1115/1.4008149.

[77] R. W. Heckel, A. J. Hickl, R. J. Zaehring, and R. A. Tanzilli, “Transient Growth of Second Phases During Solution Treatment.,” *Met. Trans*, vol. 3, no. 10, pp. 2565–2569, 1972, doi: 10.1007/BF02644230.

[78] T. C. Illingworth and I. O. Golosnoy, “Numerical solutions of diffusion-controlled moving boundary problems which conserve solute,” *J. Comput. Phys.*, vol. 209, no. 1, pp. 207–225, 2005, doi: 10.1016/j.jcp.2005.02.031.

[79] G. B. Stephenson, “Diffusion-Induced Flow and Stress during Interdiffusion in Amorphous Systems,” *Defect Diffus. Forum*, vol. 95–98, pp. 507–520, 1993, doi: 10.4028/www.scientific.net/ddf.95-98.507.

[80] W. Zhong and J. Zhao, “First experimental measurement of calcium diffusion in magnesium using novel liquid-solid diffusion couples and forward-simulation analysis,” *Scr. Mater.*, vol. 127, pp. 92–96, 2017, doi: 10.1016/j.scriptamat.2016.09.008.

[81] S. Gasparin, J. Berger, D. Dutykh, and N. Mendes, “Stable explicit schemes for simulation of nonlinear moisture transfer in porous materials,” *J. Build. Perform. Simul.*, vol. 11, no. 2, pp. 129–144, 2018, doi: 10.1080/19401493.2017.1298669.

[82] D. F. Fletcher, *Computational techniques for fluid dynamics*, vol. 70, no. 1. 1992.

[83] L. Wu, “Dufort–Frankel-Type Methods for Linear and Nonlinear Schrödinger Equations,” *SIAM J. Numer. Anal. 33(4), 1526–1533*, vol. 33, no. 4, pp. 1526–1533, 1996, doi: 10.1137/s0036142994270636.

[84] J. C. Strikwerda, *Finite Difference Schemes and Partial Differential Equations*, Second Edi. Society for Industrial and Applied Mathematics Philadelphia, 2004.

[85] T. F. Chant, “Stability Analysis of Finite Difference Schemes for the Advection-Diffusion Equation,” *SIAM J. Numer. Anal.*, vol. 21, no. 2, pp. 272–284, 1984, doi: https://doi.org/10.1137/0721020.

[86] J. C. Tannehill, D. A. Anderson, and R. H. Pletcher, “Computational fluid mechanics and heat transfer.” p. 225, 1984, doi: 10.2307/2008017.

[87] B. Cushman-Roisin, “Analytical, linear stability criteria for the leap-frog, Dufort-Frankel method,” *J. Comput. Phys.*, vol. 53, no. 2, pp. 227–239, 1984, doi: 10.1016/0021-9991(84)90039-1.

[88] Q. Zhang and J. Zhao, “Extracting interdiffusion coefficients from binary diffusion couples using traditional methods and a forward-simulation method,” *Intermetallics*, vol. 34, pp. 132–141, 2013, doi: 10.1016/j.intermet.2012.11.012.

[89] S. Prussin, “Generation and distribution of dislocations by solute diffusion,” *J. Appl. Phys.*, vol. 32, no. 10, pp. 1876–1881, 1961, doi: 10.1063/1.1728256.

[90] I. Gregor and D. Patra, “Statistical Analysis of Diffusion Coefficient Determination,” *J. ofFluorescence*, vol. 15, no. 3, pp. 415–422, 2005, doi: 10.1007/s10895-005-2633-0.

[91] C. D. Le, “Measurement of Diffusion Coefficients of Binary Liquid Systems By The Mjire Pattern Method,” McMaster University, Canada (Thesis), 1968.

[92] S. T. Oyama, “Membrane Science and Technology,” in *Inorganic Polymeric and Composite Membranes*, vol. 14, S. T. Oyama and S. M. Stagg-Williams, Eds. Blacksburg, USA: Elsevier, 2011, p. 158.

[93] S. Bader, W. Gust, and H. Hieber, “Rapid formation of intermetallic compounds interdiffusion in the CuSn and NiSn systems,” *Acta Metall. Mater.*, vol. 43, no. 1, pp. 329–337, 1995, doi: 10.1016/0956-7151(95)90289-9.

[94] J. Shen, Y. C. Chan, and S. Y. Liu, “Growth mechanism of Ni3Sn4 in a Sn/Ni liquid/solid

interfacial reaction," *Acta Mater.*, vol. 57, no. 17, pp. 5196–5206, 2009, doi: 10.1016/j.actamat.2009.07.021.

[95] J. F. Li, P. A. Agyakwa, and C. M. Johnson, "Kinetics of Ag3Sn growth in Ag-Sn-Ag system during transient liquid phase soldering process," *Acta Mater.*, vol. 58, no. 9, pp. 3429–3443, 2010, doi: 10.1016/j.actamat.2010.02.018.

[96] U. Gösele and K. N. Tu, "Growth kinetics of planar binary diffusion couples : '' Thinfilm case '' versus '' bulk cases'','' *J. Appl. Phys.*, vol. 53, no. 4, pp. 3252–3260, 1982, doi: 10.1063/1.331028.

[97] S. M. Schwarz, B. W. Kempshall, and L. A. Giannuzzi, "Effects of diffusion induced recrystallization on volume diffusion in the copper-nickel system," *Acta Mater.*, vol. 51, no. 10, pp. 2765–2776, 2003, doi: 10.1016/S1359-6454(03)00082-X.

[98] G. B. Gibbs, "On the temperature dependence of the activation energy for diffusion," *Acta Metall.*, vol. 13, no. 8, pp. 926–927, 1965, doi: 10.1016/0001-6160(65)90085-4.

[99] H. M. Morrison, "The analysis of curved Arrhenius plots in diffusion experiments," *Philos. Mag.*, vol. 31, no. 2, pp. 243–254, 1975, doi: 10.1080/14786437508228929.

[100] G. De Vries, "The temperature dependence of the activation energy for diffusion," *Phys. Status Solidi*, vol. 28, no. 1, pp. K61–K63, 1975, doi: 10.1002/pssa.2210280161.

[101] G. Brunel, G. Cizeron, and P. Lacombe, "Determination of diffusion coefficients in volume at infinite dilution of nickel in pure copper and in the alloy Cu+0.8% chromium and the effects of the chromium addition during the diffusion process," *Comptes Rendus Hebd. des Seances l'Academie Sci. Ser. C*, vol. 270, p. 895, 1970.

[102] R. Resnick and R. W. Balluffi, “Diffusion of Zinc and Copper in Alpha and Beta Brasses,” *Jom*, vol. 7, no. 9, pp. 1004–1010, 1955, doi: 10.1007/bf03377601.

[103] W. Sprengel, M. Denkinger, and H. Mehrer, “Multiphase diffusion in the CoNb and NiNb systems: Part II. Interdiffusion,” *Intermetallics*, vol. 2, no. 2, p. 141,144, 1994, doi: 10.1016/0966-9795(94)90008-6.

[104] C. Zhong *et al.*, “Protective diffusion coatings on magnesium alloys: A review of recent developments,” *J. Alloys Compd.*, vol. 520, pp. 11–21, 2012, doi: 10.1016/j.jallcom.2011.12.124.

[105] N. Method and F. O. R. Simulating, “Scientific Research and Development Numerical Method for Simulating Sintering,” *Refract. Ind. Ceram.*, vol. 50, no. 3, pp. 191–197, 2009.

[106] M. Liu *et al.*, “Precipitation kinetics and hardening mechanism in Al-Si solid solutions processed by high pressure solution treatment,” *Mater. Sci. Eng. A*, vol. 712, no. December 2017, pp. 757–764, 2018, doi: 10.1016/j.msea.2017.12.033.

[107] Y. I. Komizo and K. Ogawa, “Interface migration and diffusion behavior on bonding interface of dissimilar materials,” *Yosetsu Gakkai Ronbunshu/Quarterly J. Japan Weld. Soc.*, vol. 15, no. 3, pp. 425–431, 1997, doi: 10.2207/qjjws.15.425.

[108] D. Ansel, I. Thibon, M. Boliveau, and J. Debuigne, “Interdiffusion in the body cubic centered β-phase of TA-TI alloys,” *Acta Mater.*, vol. 46, no. 2, pp. 423–430, 1998, doi: 10.1016/S1359-6454(97)00272-3.

[109] G. L. E. Gall and J. Debuigne, “Interdiffusion In The Body Cubic Centered P-Phase Of Titanium-Hafnium Alloys,” *Acta Mater.*, vol. 35, no. 9, pp. 2297–2305, 2000.

[110] S. K. Tang, “The Process Fundamentals and Parameters of Electro-Spark Deposition,” University of Waterloo, 2009.

[111] E. M. Dietze and P. N. Plessow, “Kinetic Monte Carlo Model for Gas Phase Diffusion in Nanoscopic Systems,” *J. Phys. Chem. C*, vol. 122, no. 21, pp. 11524–11531, 2018, doi: 10.1021/acs.jpcc.8b01816.

[112] X. Wu, J. Zhong, and L. Zhang, “A general approach to quantify the uncertainty of interdiffusion coef fi cients in binary , ternary and multicomponent systems evaluated using Matano-based methods,” *Acta Mater.*, vol. 188, pp. 665–676, 2020, doi: 10.1016/j.actamat.2020.02.042.

[113] W. A. Johnson, “Diffusion experiments on gold-silver alloy by chemical and radioactive tracer methods,” *Am. Inst. Min. Metall. Eng. -- Trans.*, vol. 147, pp. 331–346, 1942.

[114] V. A. Baheti and A. Paul, “Development of different methods and their efficiencies for the estimation of diffusion coefficients following the diffusion couple technique,” *Acta Mater.*, vol. 156, pp. 420–431, 2018, doi: 10.1016/j.actamat.2018.04.051.

[115] S. Rudinsky and M. Brochu, “Interdiffusion between copper and nickel powders and sintering map development during spark plasma sintering,” *Scr. Mater.*, vol. 100, pp. 74–77, 2015, doi: 10.1016/j.scriptamat.2014.12.017.

[116] W. Gong, L. Zhang, D. Yao, and C. Zhou, “Diffusivities and atomic mobilities in fcc Ni-Pt alloys,” *Scr. Mater.*, vol. 61, no. 1, pp. 100–103, 2009, doi: 10.1016/j.scriptamat.2009.03.010.

[117] V. D. Divya, S. S. K. Balam, U. Ramamurty, and A. Paul, “Interdiffusion in the Ni-Mo

system," *Scr. Mater.*, vol. 62, no. 8, pp. 621–624, 2010, doi: 10.1016/j.scriptamat.2010.01.008.

[118] M. Paliwal, S. K. Das, J. Kim, and I. H. Jung, "Diffusion of Nd in hcp Mg and interdiffusion coefficients in Mg-Nd system," *Scr. Mater.*, vol. 108, pp. 11–14, 2015, doi: 10.1016/j.scriptamat.2015.06.010.

[119] W. Chen, Q. Li, and L. Zhang, "A novel approach to eliminate the effect of external stress on interdiffusivity measurement," *Materials (Basel).*, vol. 10, no. 8, pp. 1–11, 2017, doi: 10.3390/ma10080961.

[120] Q. Zhang, Z. Chen, W. Zhong, and J. Zhao, "Accurate and efficient measurement of impurity (dilute) diffusion coefficients without isotope tracer experiments," *Scr. Mater.*, vol. 128, pp. 32–35, 2017, doi: 10.1016/j.scriptamat.2016.09.040.

[121] J. E. Morral, "Rate constants for interdiffusion," *Scr. Metall.*, vol. 18, no. 11, pp. 1251–1256, 1984, doi: 10.1016/0036-9748(84)90116-9.

[122] A. M. Gusak and M. V Yarmolenko, "A simple way of describing the diffusion phase growth in cylindrical and spherical samples," *J. Appl. Phys.*, vol. 73, no. 10, pp. 4881–4884, 1993.

[123] M. C. Tringides and R. Gomer, "Adsorbate-adsorbate interaction effects in surface diffusion," *Surf. Sci.*, vol. 265, no. 1–3, pp. 283–292, 1992, doi: 10.1016/0039-6028(92)90508-4.

[124] B. Ostrowska and Å. Narębska, "Diffusion of dyes in polyester fibers. II. Diffusion coefficients from the radial distribution curves," *J. Appl. Polym. Sci.*, vol. 25, no. 12, pp.

2845–2855, 1980, doi: 10.1002/app.1980.070251216.

[125] F. Sauer and V. Freise, “Diffusion in binaren Gemischen mit Volumenanderung,” *Zeitschrift für Elektrochemie*, vol. 66, no. 4, pp. 353–362, 1962.

[126] C. Wagner, “The evaluation of data obtained with diffusion couples of binary single-phase and multiphase systems,” *Acta Metall.*, vol. 17, no. 2, pp. 99–107, 1969, doi: 10.1016/0001-6160(69)90131-X.

[127] T. Ahmed, I. V. Belova, A. V. Evteev, E. V. Levchenko, and G. E. Murch, “Comparison of the Sauer-Freise and Hall Methods for Obtaining Interdiffusion Coefficients in Binary Alloys,” *J. Phase Equilibria Diffus.*, vol. 36, no. 4, pp. 366–374, 2015, doi: 10.1007/s11669-015-0392-4.

[128] E. O. Kirkendall, “Diffusion of zinc in alpha brass,” *Trans. Am. Inst. Min. Metall. Eng.*, vol. 147, pp. 104–109, 1942.

[129] A. D. Smigelskas and E. O. Kirkendall, “Zinc Diffusion in Alpha Brass,” *Trans. AIME*, vol. 171, no. 1942, pp. 130–142, 1947.

[130] O. Olaye and O. A. Ojo, “Leapfrog / Dufort-Frankel explicit scheme for diffusion-controlled moving interphase boundary problems with variable diffusion coefficient and solute conservation,” *Model. Simul. Mater. Sci. Eng.*, vol. 28, no. 1, pp. 1–24, 2019, [Online]. Available: https://doi.org/10.1088/1361-%0A651X/ab58f3.

APPENDIX

A. DETAILED DERIVATION OF MODELS

A.1 Diffusion Induced Stress Equations

The intrinsic flux of each component is given as:

$$J_i = -\left(D_i^* \theta \nabla \rho_i + \frac{D_i^* \rho_i}{KT} \nabla (V_i P) \right) \quad \text{A.1}$$

where D^*_i is the stress-free impurity tracer diffusivity of component i, C is the concentration of component i, ρ is the density (mole density or mass density), R is the gas constant, T is the temperature, and θ is a thermodynamic factor.

$$\sum_{i=1}^{2} \rho_i V_i = 1 \quad \text{A.2}$$

The relationship between the molar density and mole fraction (C) is

$$C = \frac{\rho_1}{\rho} \quad \text{A.3}$$

The equation of the thermodynamic factor (θ) which gives unity at the pure boundaries obtained from Stephenson [79] is:

$$\theta = 1 - \frac{2\alpha}{RT} C(1-C) \quad \text{A.4}$$

Taking Equation A.3 into consideration, Equation A.1 can be re-written as:

$$J_i = -\rho \left(D_i^* \theta \nabla C_i + \frac{D_i^* C_i V_i}{KT} \nabla P \right) \quad \text{A.5}$$

A.1.1 Derivation of equations for pressure distribution under DIS

The total strain in a diffusing system is taken to be the sum of the elastic, plastic and stress-free strains.

$$\varepsilon^T = \varepsilon^{SF} + \varepsilon^P + \varepsilon^E \qquad \text{A.6}$$

The stress-free strain is due to volume transport with an isotropic deformation. The rate of the stress-free deformation in 1D planar systems can be given as [6]:

$$\frac{D\varepsilon^{SF}}{Dt} = \frac{1}{3}\left(V_1 \frac{\partial}{\partial r}(J_1) + V_2 \frac{\partial}{\partial r}(J_2)\right) \qquad \text{A.7}$$

The plastic strain rate is that of an incompressible Newtonian flow with shear viscosity η, and hence, for an isotropic system:

$$\frac{D\varepsilon^P}{Dt} = \frac{1}{3}\frac{\sigma}{2\eta} \qquad \text{A.8}$$

where σ is the diffusion induced stress, and η is the viscosity.

The elastic strain rate is negligible[6], and hence will not be discussed. Therefore, the total strain rate from Equation A.6 is given as:

$$\frac{D\varepsilon^T}{Dt} = \frac{D\varepsilon^{SF}}{Dt} + \frac{D\varepsilon^P}{Dt} \qquad \text{A.9}$$

Substituting Equations A.7 and A.8 into Equation A.9 gives:

$$\frac{D\varepsilon^{T}}{Dt} = \frac{1}{3}\left(V_1 \frac{\partial}{\partial r}(J_1) + V_2 \frac{\partial}{\partial r}(J_2)\right) + \frac{\sigma}{6\eta} \quad \text{A.10}$$

Poisson's ratio is υ, and η is the shear viscosity

The relationship between viscosity and mobility of the slower moving component is given by the Stokes-Einstein relation presented in Equation A.11.

$$\eta = \frac{\rho d_{SE}^{2}}{C_{SE} \min(M_1, M_2)} \quad \text{A.11}$$

where C_{SE} and d_{SE} are the geometrical constant and atomic size respectively.

The stress-strain relation for isotropic films is:

$$\sigma = \varepsilon \frac{E}{(1-\upsilon)} \quad \text{A.12}$$

where E is the Young's modulus.

Substituting Equation A.12 into Equation A.10 provides:

$$\frac{(1-\upsilon)}{E}\frac{D\sigma}{Dt} = \frac{1}{3}\left(V_1 \frac{\partial}{\partial r}(J_1) + V_2 \frac{\partial}{\partial r}(J_2)\right) + \frac{\sigma}{6\eta} \quad \text{A.13}$$

The relationship between the local pressure and stress in an isotropic material is given as [6], [55]:

$$\sigma = -\frac{3}{2}P \quad \text{A.14}$$

where P is the pressure induced by diffusion.

Substituting Equation A.14 into Equation A.13 results in:

$$-\frac{(1-\upsilon)}{E}\frac{3}{2}\frac{DP}{Dt}=\frac{1}{3}\left(V_1\frac{\partial}{\partial r}(J_1)+V_2\frac{\partial}{\partial r}(J_2)\right)+\frac{3}{2}\frac{P}{6\eta} \quad \text{A.15}$$

Further simplification of Equation A.15 gives the time rate of the pressure change equation defined in Equation A.16 which is the pressure changes in a system with isotropic stress along with pressure development and relaxation[6]: .

$$\frac{DP}{Dt}=-\frac{2}{9}\frac{E}{(1-\upsilon)}\left(\left(V_1\frac{\partial}{\partial r}(J_1)+V_2\frac{\partial}{\partial r}(J_2)\right)+\frac{3P}{4\eta}\right) \quad \text{A.16}$$

The material derivative is approximately equal to the Euler derivative.

$$\frac{\partial P}{\partial t}=\frac{DP}{Dt}-v\frac{\partial P}{\partial r}=\frac{-2E}{9(1-\upsilon)}\left[\sum_{i=1}^{2}V_i\nabla J_i+\frac{3}{4\eta}P\right]-v\frac{\partial P}{\partial r} \quad \text{A.17}$$

$$\frac{DP}{Dt}\cong\frac{\partial P}{\partial t}=\frac{-2E}{9(1-\upsilon)}\left[\sum_{i=1}^{2}V_i\nabla J_i+\frac{3}{4\eta}P\right] \quad \text{A.18}$$

Substituting the fluxes, Equation A.18 is transformed into Equation A.19:

$$\frac{\partial P}{\partial t}=\frac{-2E}{9(1-\upsilon)}\left[-\frac{\partial}{\partial r}\left(\left(D_1^*V_1-D_2^*V_2\right)\theta\nabla C+\left(\frac{D_1^*CV_1V_1}{KT}+\frac{D_2^*(1-C)V_2V_2}{KT}\right)\frac{\partial P}{\partial r}\right)+\frac{3}{4\eta}P\right] \quad \text{A.19}$$

$P=P(t=0)\exp\left(\frac{-Et}{6(1-\upsilon)\eta}\right)$ is the solution of Equation A.19 if the divergences of the atomic fluxes are negligible. This solution shows relaxation of pressure.

When the solute changes, the relative magnitude of the relaxation term and divergences of the atomic fluxes determine if the stress is relaxed or generated. For stress relaxation $\sum_{i=1}^{2} V_i \nabla J_i > \frac{3}{4\eta} P$ whereas, for stress relaxation $\sum_{i=1}^{2} V_i \nabla J_i < \frac{3}{4\eta} P$.

A.1.2 Derivation of the equation for solute distribution under DIS

The relationship among the interdiffusion flux, intrinsic flux, density and Kirkendall velocity (v) is:

$$\bar{J}_i = J_i + v\rho_i \qquad \text{A.20}$$

According to solute conservation, the total interdiffusion flux is zero. Hence:

$$\bar{J}_1 + \bar{J}_2 = J_1 + v\rho_1 + J_2 + v\rho_2 = 0 \qquad \text{A.21}$$

The Kirkendall velocity derived from Equation A.21 becomes:

$$v = -\frac{(J_1 + J_2)}{\rho_1 + \rho_2} = -\frac{(J_1 + J_2)}{\rho} \qquad \text{A.22}$$

Equation A.22 can be substituted into Equation A.20, thus, resulting in the interdiffusion flux of Equation A.23:

$$\bar{J}_1 = J_1 - \frac{\rho_1}{\rho}(J_1 + J_2) = J_1 - C(J_1 + J_2) = J_1(1-C) - CJ_2 \qquad \text{A.23}$$

Equations A.5 can be substituted into Equation A.23, for each component, thus resulting in:

$$\bar{J}_1 = -\rho\left(D_1^* \theta \nabla C + \frac{D_1^* C V_1}{KT} \nabla P \right)(1-C) - \left[-\rho\left(-D_2^* \theta \nabla C + \frac{D_2^* (1-C) V_2}{KT} \nabla P \right) C \right] \quad \text{A.24}$$

Equation A.24 can be expanded to:

$$\bar{J}_1 = -\rho\left(D_1^* \theta (1-C) \nabla C + D_2^* \theta C \nabla C + \frac{D_1^* C (1-C) V_1}{KT} \nabla P - \frac{D_2^* C (1-C) V_2}{KT} \nabla P \right) \quad \text{A.25}$$

Equation A.26 can be further simplified to:

$$\bar{J}_1 = -\rho\left(\left(D_1^* (1-C) + D_2^* C \right) \theta \nabla C + \frac{C(1-C)}{KT} \left(D_1^* V_1 - D_2^* V_2 \right) \nabla P \right) \quad \text{A.26}$$

Using the continuity equation of Fick's second law, the Fick's second law for a stressed system is written as:

$$\frac{\rho \partial C}{\partial t} = \frac{\partial}{\partial r}\left(\left((1-C) D_1^* \theta + C D_2^* \theta \right) \frac{\partial C}{\partial r} + \frac{C(1-C)\left(D_1^* V_1 - D_2^* V_2 \right)}{KT} \frac{\rho \partial P}{\partial r} \right) \quad \text{A.27}$$

Equation A.28 can also be re-written as:

$$\frac{\rho \partial C}{\partial t} = \frac{\partial}{\partial r}\left(\left[\left((1-C) D_1^* \theta + C D_2^* \theta \right) + \frac{C(1-C)\left(D_1^* V_1 - D_2^* V_2 \right)}{KT} \frac{\partial P}{\partial C} \right] \frac{\rho \partial C}{\partial r} \right) \quad \text{A.28}$$

The form of Equation A.27 avoids the indeterminate problem when $P \to 0$ and $C \to 0$.

A.1.3 Effective interdiffusion coefficient

From Fick's first law

$$\bar{J}_1 = -\bar{D}\nabla C_1 \qquad \text{A.29}$$

Comparing Equations A.26 and A.29, the effective interdiffusion coefficient ($\bar{D}(C)$) which satisfies the Fick's first law is given as:

$$\bar{D}(C) = \left(C_2 D_1^* \theta + C_1 D_2^* \theta\right) + \frac{C_2 C_1}{KT}\left(D_1^* V_1 - D_2^* V_2\right)\frac{\nabla P}{\nabla C_1} \qquad \text{A.30}$$

Similarly, from the Fick's second law, we have:

$$\frac{\rho \partial C}{\partial t} = \frac{\partial}{\partial r}\left(\bar{D}(C)\frac{\rho \partial C}{\partial r}\right) \qquad \text{A.31}$$

Comparing Equations A.31 and A.28, the effective interdiffusion coefficient (Deff), which satisfies Fick's second law of diffusion, is given as Equation A.32. Equations A.32 and A.20 are the same.

$$\bar{D}(C) = \left((1-C)D_1^* \theta + C D_2^* \theta\right) + \frac{C(1-C)\left(D_1^* V_1 - D_2^* V_2\right)}{KT}\frac{\partial P}{\partial C} \qquad \text{A.32}$$

The effective interdiffusion coefficient can also be re-written in terms of mobility $\left(M_i = \frac{D_i^*}{KT}\right)$ as:

$$\bar{D}(C) = \left((1-C)D_1^* \theta + C D_2^* \theta\right) + C(1-C)\left(M_1 V_1 - M_2 V_2\right)\frac{\partial P}{\partial C} \qquad \text{A.33}$$

A.1.4 Diffusion induced stress equations in the generalized coordinate system

The pressure equation in Stephenson [6] for coupled differential equations for diffusion in an isotropic binary system, which considers the generation and relaxation of DIS , will be extended from planar systems to cylindrical and spherical geometries to address the second objective. The general pressure equation in Stephenson [8] is:

$$\frac{\partial P}{\partial t} = -\frac{2}{9}\frac{E}{(1-\upsilon)}\left(\sum_{i=1}^{2}\left(V_i \frac{\partial}{\partial t} C_i\right) + \frac{3P}{4\eta}\right), \qquad \text{A.34}$$

where P is the pressure due to diffusion-induced stress, t is the time, r is the distance, V the molar volume, E the Young's modulus, η is the viscosity, and ν the Poisson's ratio.

Equation A.34 is further developed into Equation A.35 [56] for planar systems.

$$\frac{\partial P}{\partial t} = -\frac{2}{9}\frac{E}{(1-\upsilon)}\left(\sum_{i=1}^{2}\left(V_i \frac{\partial}{\partial r} J_i\right) + \frac{3P}{4\eta}\right) \qquad \text{A.35}$$

However, modifying Equation A.35 for the generalized coordinate system, the sum of the product of the divergence of fluxes and volume fraction in the generalized coordinate systems will be incorporated into Equation A.35 to give:

$$\frac{\partial P}{\partial t} = -\frac{2}{9}\frac{E}{(1-\upsilon)}\left(\frac{V_1}{r^n}\frac{\partial}{\partial r}\left(r^n J_1\right) + \frac{V_2}{r^n}\frac{\partial}{\partial r}\left(r^n J_2\right) + \frac{3P}{4\eta}\right) \qquad \text{A.36}$$

where n = 0, 1, and 2 in the planar, cylindrical, and spherical geometries, respectively.

Fick's second law with variable molar densities or volumes is given as:

$$\frac{\rho\partial C}{\partial t} = \frac{\partial}{r^n \partial r}\left(r^n \overline{D}(C)\frac{\rho\partial C}{\partial r}\right) \qquad \textit{A.37}$$

The continuity equation in non-planar systems is given as:

$$\frac{\rho\partial N}{\partial t} = \frac{1}{r^n}\nabla r^n \left(CJ_2 - (1-C)J_1\right) \qquad \text{A.38}$$

Substituting the flux equations to give the equation for solute distribution under the influence of DIS, the solute distribution equation is:

$$\frac{\rho\partial C}{\partial t} = \frac{\partial}{r^n \partial r}\left(\left[\left(D_2^*\theta C + D_1^*\theta(1-C)\right)\frac{\rho\partial C}{\partial r} + \left(\frac{-D_2^* C(1-C)V_2 + D_1^*(1-C)CV_1}{RT}\right)\rho\frac{\partial P}{\partial r}\right] r^n\right) \qquad \text{A.39}$$

Equation 3.30 can be re-written as Equation 3.31.

$$\frac{\rho\partial C}{\partial t} = \frac{\partial}{r^n \partial r}\left(\left[D_2^*\theta C + D_1^*\theta(1-C) + \left(\frac{-D_2^* C(1-C)V_2 + D_1^*(1-C)CV_1}{RT}\right)\frac{\partial P}{\partial C}\right] r^n \frac{\rho\partial C}{\partial r}\right) \qquad \text{A.40}$$

Comparing Equations A.37 and A.40, the effective concentration-dependent interdiffusion coefficient (D_{eff}) can be determined. D_{eff} in the generalized coordinate system is given as:

$$D_{eff} = \left(D_2^* C + D_1^*(1-C)\right)\theta + \left(\frac{-D_2^* C(1-C)V_2 + D_1^*(1-C)CV_1}{KT}\right)\frac{\partial P}{\partial C} \qquad \text{A.41}$$

Similarly, for the pressure distribution, the equation is:

$$\frac{\partial P}{\partial t} = \frac{-2E}{9(1-\upsilon)}\left[-\frac{\partial}{r^n \partial r}\left(r^n\left(D_1^* V_1 - D_2^* V_2\right)\theta\nabla C + r^n\left(\frac{D_1^* C V_1 V_1}{KT} + \frac{D_2^*(1-C)V_2 V_2}{KT}\right)\frac{\partial P}{\partial r}\right) + \frac{3}{4\eta}P\right]$$

A.42

For the numerical simulation of the diffusion in a sample of length L, Equations A.43 and A.46 for the pressure and solute distributions respectively are transformed to forms that contain only dimensionless variables, which are:

$$r' = r/L \qquad t' = t\max(D_i)/L^2 \qquad P' = P/E \qquad D_i^{'} = D_i/\max(D_i) \qquad D_{eff}^{'} = D_{eff}/\max(D_i)$$

$$\eta' = \eta\max(D_i)/EL^2 \qquad V_i^{'} = V_i/V_{\max} \qquad T^{'} = \frac{KT}{EV_{\max}} \qquad \alpha' = \frac{2\alpha}{KT}$$

The dimensionless equations for pressure, solute distributions and effective diffusion coefficient are respectively:

$$\frac{dP'}{dt'} = \frac{-2}{9(1-\upsilon)}\left[\frac{\partial}{r'^n\partial r'}\left(r'^n\left(D_2^{*'}V_2^{'} - D_1^{*'}V_1^{'}\right)\theta\nabla C - \frac{r'^n}{T'}\left(D_1^{*'}CV_1^{'}V_1^{'} + D_2^{*'}(1-C)V_2^{'}V_2^{'}\right)\frac{\partial P^{'}}{\partial r'}\right) + \frac{3}{4\eta'}P^{'}\right]$$

A.43

$$\frac{\rho'\partial C}{\partial t'} = \frac{\partial}{r'^n\partial r'}\left(\left[\left(D_2^{*'}\theta C + D_1'^{*}\theta(1-C)\right)\frac{\rho'\partial C}{\partial r'} + \left(\frac{-D_2^{*'}C(1-C)V_2' + D_1^{*'}(1-C)CV_1'}{T'}\right)\rho'\frac{\partial P'}{\partial r'}\right]r'^n\right)$$

A.44

$$\frac{\rho'\partial C}{\partial t'} = \frac{\partial}{r'^n\partial r'}\left(\left[D_2^{*'}\theta C + D_1'^{*}\theta(1-C) + \left(\frac{-D_2^{*'}C(1-C)V_2' + D_1^{*'}(1-C)CV_1'}{T'}\right)\frac{\partial P'}{\partial C}\right]r'^n\frac{\rho'\partial C}{\partial r'}\right)$$

A.45

$$D_{eff}' = D_2'^{*'}\theta C + D_1'\theta(1-C) + \left(\frac{-D_2^{*'}C(1-C)V_2' + D_1^{*'}(1-C)CV_1'}{T'}\right)\frac{\partial P'}{\partial C} \qquad \text{A.46}$$

A.2 Development of a New Numerical Model for Extracting Interdiffusion Coefficient from Experimental Data

Following Illingworth and Golosnoy [78], the set of equations that govern a diffusion-controlled two-phase system can be written as:

$$r^{\lambda\lambda-1}\frac{\partial C(r,t)}{\partial t}=\frac{\partial}{\partial t}\left(r^{\lambda\lambda-1}D_A[r,t]\frac{\partial C(r,t)}{\partial r}\right) \qquad 0\le r\le s(t) \quad \text{A.47}$$

$$r^{\lambda\lambda-1}\frac{\partial C(r,t)}{\partial t}=\frac{\partial}{\partial r}\left(r^{\lambda\lambda-1}D_B\left[C(r,t)\right]\frac{\partial C(r,t)}{\partial r}\right) \qquad s(t)\le r\le R \quad \text{A.48}$$

$$D_A\left[C(r,t)\right]\frac{\partial C(r,t)}{\partial r}\bigg|_{r=s(t)^-}-D_B\left[C(r,t)\right]\frac{\partial C(r,t)}{\partial r}\bigg|_{r=s(t)^+}=\left[C_B-C_A\right]\frac{ds}{dt},\quad r=s(t) \quad \text{A.49}$$

The solute distribution and diffusion in the first and second phases, A and B, respectively, are described by using Equations A.47 and A.48. Equation A.49 mathematically describes the equation for the interface migration. The value of λλ defines the geometry of the system, such that λλ=1 applies to the 1D planar geometry, λλ=2 to the cylindrical geometry, and λλ=3 to the spherical geometry. Zero flux conditions are imposed at the boundaries ($r = 0$ and $r = R$).

The new transformation coordinates,

$$r=su \text{ and } r=(R-s)v+s \qquad \text{A.50}$$

The Landau transformations of Equations A.47 – A.49 are given as:

$$[us]^{\lambda\lambda-1}\left(\frac{\partial p}{\partial t}-\frac{ds}{dt}\frac{u}{s}\frac{\partial p}{\partial u}\right)=\frac{\partial}{\partial u}\left(\frac{[us]^{\lambda\lambda-1}D_A(p)}{s^2}\frac{\partial p}{\partial u}\right),\quad 0\le u\le 1 \qquad \text{A.51}$$

$$\left[v\left(R-s\right)+s\right]^{\lambda\lambda-1}\left(\frac{\partial q}{\partial t}-\frac{ds}{dt}\frac{u}{s}\frac{\partial q}{\partial u}\right)=\frac{\partial}{\partial v}\left(\frac{\left[v\left(L-s\right)+s\right]^{\lambda\lambda-1}D_B\left(q\right)}{\left(R-s\right)^2}\frac{\partial q}{\partial v}\right),\quad 0\le v\le 1 \qquad \text{A.52}$$

$$\frac{D_A\left(p\right)}{s}\frac{\partial p}{\partial u}\bigg|_{u=1}-\frac{D_B\left(q\right)}{\left(R-s\right)}\frac{\partial q}{\partial v}\bigg|_{v=0}=\left[C_B-C_A\right]\frac{ds}{dt},\qquad u=1,\ v=0 \qquad \text{A.53}$$

To obtain the interface equation that conserves solute, Equations A.51 and A.52 are transformed into the form below:

$$\frac{\partial}{\partial t}\left(ps\left[us\right]^{\lambda\lambda-1}\right)=\frac{\partial}{\partial u}\left(\left[us\right]^{\lambda\lambda-1}\left\{\frac{ds}{dt}pu+\frac{D_A\left(p\right)}{s}\frac{\partial p}{\partial u}\right\}\right),\quad 0\le u\le 1 \qquad \text{A.54}$$

$$\frac{\partial}{\partial t}\left(q\left(R-s\right)\left[v\left(R-s\right)+s\right]^{\lambda\lambda-1}\right)=\frac{\partial}{\partial v}\left(\left[v\left(R-s\right)+s\right]^{\lambda\lambda-1}\left\{\frac{ds}{dt}q\left(1-v\right)+\frac{D_B\left(q\right)}{\left(R-s\right)}\frac{\partial q}{\partial v}\right\}\right),\quad 0\le v\le 1$$

A.55

To ensure solute conservation, the total amount of solute throughout the diffusion system must be the same for all diffusion times.

$$\frac{\partial}{\partial t}\left(s\int_0^1 p\left[us\right]^{\lambda\lambda-1}du+\left(R-s\right)\int_0^1 q\left[v\left(R-s\right)+s\right]^{\lambda\lambda-1}dv\right)=0 \qquad \text{A.56}$$

The interface migration equation is obtained by integrating Equations A.56 over space and a time step. To ensure an explicit solution, Equations A.54 and A.55 are analyzed by using explicit schemes.

A.2.1 LeapFrog/Dufort-Frankel scheme

Numerically integrating Equations A.54 and A.55 by using a leapfrog/Dufort-Frankel algorithm gives:

$$\int_{u_{i-1/2}}^{u_{i+1/2}}\int_{t^{k-1}}^{t^{k+1}} \frac{\partial}{\partial t}\left(ps\left[us\right]^{\lambda\lambda-1}\right)dtdu = \int_{t^{k-1}}^{t^{k+1}}\int_{u_{i-1/2}}^{u_{i+1/2}} \frac{\partial}{\partial u}\left(\left[us\right]^{\lambda\lambda-1}\left\{\frac{ds}{dt}\,pu + \frac{D_A(p)}{s}\frac{\partial p}{\partial u}\right\}\right)dudt \qquad \text{A.57}$$

The integration gives:

$$\int_{u_{i-1/2}}^{u_{i+1/2}}\left(p^{k+1}s^{k+1}\left[us^{k+1}\right]^{\lambda\lambda-1} - p^{k-1}s^{k-1}\left[us^{k-1}\right]^{\lambda\lambda-1}\right)du =$$
$$\int_{t^{k-1}}^{t^{k+1}}\left\{\left(su_{i+1/2}\right)^{\lambda\lambda-1}\left(\dot{s}p_{i+1/2}u_{i+1/2} + \frac{\left[D_A(p)\right]\Big|_{i+1/2}}{s}\frac{\partial p}{\partial u}\Big|_{i+1/2}\right) - \left(su_{i-1/2}\right)^{\lambda\lambda-1}\left(\dot{s}p_{i-1/2}u_{i-1/2} + \frac{\left[D_A(p)\right]\Big|_{i-1/2}}{s}\frac{\partial p}{\partial u}\Big|_{i-1/2}\right)\right\}dt$$

A.58

The left side of Equation A.58 is independent of time; hence u in the square brackets is the only function of u and can be integrated.

$$\int_{u_{i-1/2}}^{u_{i+1/2}}\left(p^{k+1}s^{k+1}\left[us^{k+1}\right]^{\lambda\lambda-1} - p^{k-1}s^{k-1}\left[us^{k-1}\right]^{\lambda\lambda-1}\right)du =$$
$$\frac{p^{k+1}}{\lambda}\left\{\left(r_{i+1/2}^{k+1}\right)^{\lambda\lambda} - \left(r_{i-1/2}^{k+1}\right)^{\lambda\lambda}\right\} - \frac{p^{k-1}}{\lambda\lambda}\left\{\left(r_{i+1/2}^{k-1}\right)^{\lambda\lambda} - \left(r_{i-1/2}^{k-1}\right)^{\lambda\lambda}\right\} \qquad \text{A.59}$$

Hence, from Equations A.58 and A.59,

$$\frac{1}{\left(t^{k+1}-t^{k-1}\right)}\left[\frac{p_i^{k+1}}{\lambda}\left\{\left(r_{i+1/2}^{k+1}\right)^{\lambda\lambda} - \left(r_{i-1/2}^{k+1}\right)^{\lambda\lambda}\right\} - \frac{p_i^{k-1}}{\lambda\lambda}\left\{\left(r_{i+1/2}^{k-1}\right)^{\lambda\lambda} - \left(r_{i-1/2}^{k-1}\right)^{\lambda\lambda}\right\}\right]$$
$$= \left[\left(r_{i+1/2}^{k-1}\right)^{\lambda\lambda-1}\left(\dot{s}p_{i+1/2}^{k}u_{i+1/2} + \frac{\left[D_A(p)\right]\Big|_{i+1/2}}{s}\frac{\partial p}{\partial u}\Big|_{i+1/2}\right) - \left(r_{i-1/2}^{k-1}\right)^{\lambda\lambda-1}\left(\dot{s}p_{i+1/2}^{k}u_{i-1/2} + \frac{\left[D_A(p)\right]\Big|_{i-1/2}}{s}\frac{\partial p}{\partial u}\Big|_{i-1/2}\right)\right]$$

A.60

Applying $p_i^k = \frac{p_i^{k+1} + p_i^{k-1}}{2}$ and $\dot{s} = \left(\frac{s^{k+1} - s^{k-1}}{t^{k+1} - t^{k-1}} \right)$, $p_{i+1/2}^k = \beta p_{i+1}^k + \alpha p_i^k$ and $p_{i-1/2}^k = \beta p_i^k + \alpha p_{i-1}^k$ to

Equation A.60 gets:

$$\frac{1}{\left(t^{k+1} - t^{k-1}\right)} \left[\frac{p_i^{k+1}}{\lambda\lambda} \left\{ \left(r_{i+1/2}^{k+1}\right)^{\lambda\lambda} - \left(r_{i-1/2}^{k+1}\right)^{\lambda\lambda} \right\} - \frac{p_i^{k-1}}{\lambda\lambda} \left\{ \left(r_{i+1/2}^{k-1}\right)^{\lambda\lambda} - \left(r_{i-1/2}^{k-1}\right)^{\lambda\lambda} \right\} \right]$$
$$= \left[\left(r_{i+1/2}^{k-1}\right)^{\lambda\lambda-1} \left(\dot{s}\alpha u_{i+1/2} - \frac{\left(D_A\right)_{i+1/2}^k}{s^k} \left(\frac{1}{u_{i+1} - u_i} \right) \right) - \left(r_{i-1/2}^{k-1}\right)^{\lambda\lambda-1} \left(\dot{s}\beta u_{i-1/2} + \frac{\left(D_A\right)_{i-1/2}^k}{s^k} \left(\frac{1}{u_i - u_{i-1}} \right) \right) \right] \left(\frac{p_i^{k+1} + p_i^{k-1}}{2} \right)$$
$$+ \left[\left(r_{i+1/2}^{k-1}\right)^{\lambda\lambda-1} \left(\dot{s}\beta p_{i+1}^k u_{i+1/2} + \frac{\left(D_A\right)_{i+1/2}^k}{s^k} \left(\frac{p_{i+1}^k}{u_{i+1} - u_i} \right) \right) - \left(r_{i-1/2}^{k-1}\right)^{\lambda\lambda-1} \left(\dot{s}\alpha p_{i-1}^k u_{i-1/2} - \frac{\left(D_A\right)_{i-1/2}^k}{s^k} \left(\frac{p_{i-1}^k}{u_i - u_{i-1}} \right) \right) \right]$$

A.61

Collecting the terms, the finite difference scheme for Phase A is

$$\delta_{p1} p_i^{k+1} = \delta_{p2} p_i^{k-1} + \delta_{p3} p_{i+1}^k + \delta_{p4} p_{i-1}^k$$

A.62

where

$$\delta_{p1} = \frac{\left(r_{i+1/2}^{k+1}\right)^{\lambda\lambda} - \left(r_{i-1/2}^{k+1}\right)^{\lambda\lambda}}{\lambda\lambda\left(t^{k+1} - t^{k-1}\right)} - \frac{1}{2}\left(r_{i+1/2}^{k-1}\right)^{\lambda\lambda-1} \left(\dot{s}\alpha u_{i+1/2} - \frac{\left(D_A\right)_{i+1/2}^k}{s^k\left(u_{i+1} - u_i\right)} \right) + \frac{1}{2}\left(r_{i-1/2}^{k-1}\right)^{\lambda\lambda-1} \left(\dot{s}\beta u_{i-1/2} + \frac{\left(D_A\right)_{i-1/2}^k}{s^k\left(u_i - u_{i-1}\right)} \right)$$

A.63

$$\delta_{p2} = \frac{\left(r_{i+1/2}^{k-1}\right)^{\lambda\lambda} - \left(r_{i-1/2}^{k-1}\right)^{\lambda\lambda}}{\lambda\lambda\left(t^{k+1} - t^{k-1}\right)} + \frac{1}{2}\left(r_{i+1/2}^{k-1}\right)^{\lambda\lambda-1} \left(\dot{s}\alpha u_{i+1/2} - \frac{\left(D_A\right)_{i+1/2}^k}{s^k\left(u_{i+1} - u_i\right)} \right) - \frac{1}{2}\left(r_{i-1/2}^{k-1}\right)^{\lambda\lambda-1} \left(\dot{s}\beta u_{i-1/2} + \frac{\left(D_A\right)_{i-1/2}^k}{s^k\left(u_i - u_{i-1}\right)} \right)$$

A.64

$$\delta_{p3} = \left(r_{i+1/2}^{k-1}\right)^{\lambda\lambda-1} \left(\dot{s}\beta u_{i+1/2} + \frac{\left(D_A\right)_{i+1/2}^k}{s^k\left(u_{i+1} - u_i\right)} \right)$$

A.65

$$\delta_{p4} = -\left(r_{i-1/2}^{k-1}\right)^{\lambda\lambda-1}\left(\dot{s}\,\alpha u_{i-1/2} - \frac{\left(D_A\right)_{i-1/2}^{k}}{s^k\left(u_i - u_{i-1}\right)}\right) \quad \text{A.66}$$

For the left boundary (i=1 node) with zero flux, the discretized boundary conditions for Phase A are:

$$\delta_{p5} p_1^{k+1} = \delta_{p6} p_1^{k-1} + \delta_{p7} p_2^{k}$$

$$\delta_{p5} = \frac{\left(r_{1+1/2}^{k+1}\right)^{\lambda\lambda}}{\lambda\lambda\left(t^{k+1} - t^{k-1}\right)} - \frac{1}{2}\left(r_{1+1/2}^{k-1}\right)^{\lambda\lambda-1}\left(\dot{s}\,\alpha u_{1+1/2} - \frac{\left(D_A\right)_{1+1/2}^{k}}{s^k\left(u_{1+1} - u_1\right)}\right) \quad \text{A.67}$$

$$\delta_{p6} = \frac{\left(r_{1+1/2}^{k+1}\right)^{\lambda\lambda}}{\lambda\lambda\left(t^{k+1} - t^{k-1}\right)} + \frac{1}{2}\left(r_{1+1/2}^{k-1}\right)^{\lambda\lambda-1}\left(\dot{s}\,\alpha u_{1+1/2} - \frac{\left(D_A\right)_{1+1/2}^{k}}{s^k\left(u_{1+1} - u_1\right)}\right) \quad \text{A.68}$$

$$\delta_{p7} = \left(r_{1+1/2}^{k-1}\right)^{\lambda\lambda-1}\left(\dot{s}\,\alpha u_{1+1/2} - \frac{\left(D_A\right)_{1+1/2}^{k}}{s^k\left(u_{1+1} - u_1\right)}\right) \quad \text{A.69}$$

The discretized boundary equation for the interface (i=m+1) in Phase A with a constant concentration is:

$$p_{m+1}^{k+1} = p_{m+1}^{k} + p_{m+1}^{k-1} = C_{AB} \quad \text{A.70}$$

R is the sample length, while u and v are dimensionless numbers from 0 to 1.

The above procedure is repeated in Phase B, and the discretized expression for Phase B is:

$$\delta_{q1} q_i^{k+1} = \delta_{q2} q_i^{k-1} + \delta_{q3} q_{i+1}^{k} + \delta_{q4} q_{i-1}^{k} \quad \text{A.71}$$

where

$$\delta_{q1}=\frac{\left(l_{i+1/2}^{k+1}\right)^{\lambda\lambda}-\left(l_{i-1/2}^{k+1}\right)^{\lambda\lambda}}{\lambda\lambda\left(t^{k+1}-t^{k-1}\right)}-\frac{1}{2}\left(l_{i+1/2}^{k-1}\right)^{\lambda\lambda-1}\left(\dot{s}\alpha\left(1-v_{i+1/2}\right)-\frac{\left(D_B\right)_{i+1/2}^{k}}{\left(R-s^k\right)\left(v_{i+1}-v_i\right)}\right)$$
$$+\frac{1}{2}\left(l_{i-1/2}^{k-1}\right)^{\lambda\lambda-1}\left(\dot{s}\beta\left(1-v_{i-1/2}\right)+\frac{\left(D_B\right)_{i-1/2}^{k}}{\left(R-s^k\right)\left(v_i-v_{i-1}\right)}\right) \quad \text{A.72}$$

$$\delta_{q2}=\frac{\left(l_{i+1/2}^{k+1}\right)^{\lambda\lambda}-\left(l_{i-1/2}^{k+1}\right)^{\lambda\lambda}}{\lambda\lambda\left(t^{k+1}-t^{k-1}\right)}+\frac{1}{2}\left(l_{i+1/2}^{k-1}\right)^{\lambda\lambda-1}\left(\dot{s}\alpha\left(1-v_{i+1/2}\right)-\frac{\left(D_B\right)_{i+1/2}^{k}}{\left(R-s^k\right)\left(v_{i+1}-v_i\right)}\right)$$
$$-\frac{1}{2}\left(l_{i-1/2}^{k-1}\right)^{\lambda\lambda-1}\left(\dot{s}\beta\left(1-v_{i-1/2}\right)+\frac{\left(D_B\right)_{i-1/2}^{k}}{\left(R-s^k\right)\left(v_i-v_{i-1}\right)}\right) \quad \text{A.73}$$

$$\delta_{q3}=\left(l_{i+1/2}^{k-1}\right)^{\lambda\lambda-1}\left(\dot{s}\beta\left(1-v_{i+1/2}\right)+\frac{\left(D_B\right)_{i+1/2}^{k}}{\left(R-s^k\right)\left(v_{i+1}-v_i\right)}\right) \quad \text{A.74}$$

$$\delta_{q4}=-\left(l_{i-1/2}^{k-1}\right)^{\lambda\lambda-1}\left(\dot{s}\alpha\left(1-v_{i-1/2}\right)-\frac{\left(D_B\right)_{i-1/2}^{k}}{\left(R-s^k\right)\left(v_i-v_{i-1}\right)}\right) \quad \text{A.75}$$

The discretized boundary equation for the interface (i=1) at Phase B with a constant concentration is:

$$q_1^{k+1}=q_1^k=q_1^{k-1}=C_{BA} \quad \text{A.76}$$

In Phase B, there is a zero flux at the right boundary (i=M+1 node) with a discretized boundary condition given as:

$$\delta_{q5}q_{m+1}^{k+1}=\delta_{q6}q_{m+1}^{k-1}+\delta_{q7}q_m^k \quad \text{A.77}$$

$$\delta_{q5}=\frac{(R)^{\lambda\lambda}-\left(l_{M+1/2}^{k+1}\right)^{\lambda\lambda}}{\lambda\lambda\left(t^{k+1}-t^{k-1}\right)}+\frac{1}{2}\left(l_{M+1/2}^{k-1}\right)^{\lambda\lambda-1}\left(\dot{s}\,\beta\left(1-v_{M+1/2}\right)+\frac{\left(D_B\right)_{M+1/2}^{k}}{\left(R-s^{k}\right)\left(v_{M+1}-v_M\right)}\right) \qquad \text{A.78}$$

$$\delta_{q6}=\frac{(R)^{\lambda\lambda}-\left(l_{M+1/2}^{k+1}\right)^{\lambda\lambda}}{\lambda\lambda\left(t^{k+1}-t^{k-1}\right)}-\frac{1}{2}\left(l_{M+1/2}^{k-1}\right)^{\lambda\lambda-1}\left(\dot{s}\,\beta\left(1-v_{M+1/2}\right)+\frac{\left(D_B\right)_{M+1/2}^{k}}{\left(R-s^{k}\right)\left(v_{M+1}-v_M\right)}\right) \qquad \text{A.79}$$

$$\delta_{q7}=-\left(l_{M+1/2}^{k-1}\right)^{\lambda\lambda-1}\left(\dot{s}\,\alpha\left(1-v_{M+1/2}\right)-\frac{\left(D_B\right)_{M+1/2}^{k}}{\left(R-s^{k}\right)\left(v_{M+1}-v_M\right)}\right) \qquad \text{A.80}$$

At each consecutive time step, the total amount of solute must be conserved, hence:

$$\left[\begin{array}{l}\sum\ \dfrac{\mathrm{p_i^{k+1}}}{\lambda\lambda}\left\{\left(\mathrm{r_{i+1/2}^{k+1}}\right)^{\lambda\lambda}-\left(\mathrm{r_{i-1/2}^{k+1}}\right)^{\lambda\lambda}\right\}-\dfrac{\mathrm{p_i^{k}}}{\lambda\lambda}\left\{\left(\mathrm{r_{i+1/2}^{k}}\right)^{\lambda\lambda}-\left(\mathrm{r_{i-1/2}^{k}}\right)^{\lambda\lambda}\right\}\\ +\dfrac{\mathrm{q_i^{k+1}}}{\lambda\lambda}\left\{\left(\mathrm{l_{i+1/2}^{k+1}}\right)^{\lambda\lambda}-\left(\mathrm{l_{i-1/2}^{k+1}}\right)^{\lambda\lambda}\right\}-\dfrac{\mathrm{q_i^{k}}}{\lambda\lambda}\left\{\left(\mathrm{l_{i+1/2}^{k}}\right)^{\lambda\lambda}-\left(\mathrm{l_{i-1/2}^{k}}\right)^{\lambda\lambda}\right\}\end{array}\right]=0 \qquad \text{A.81}$$

Applying $\mathrm{p_i^{k-1}}=2\mathrm{p_i^{k}}-\mathrm{p_i^{k+1}}$ and $\mathrm{q_i^{k-1}}=2\mathrm{q_i^{k}}-\mathrm{q_i^{k+1}}$

Hence, the interface equation which conserves solute is given as:

$$\begin{array}{l}\lambda\lambda\left(t^{k+1}-t^{k}\right)\left(r_{m+1/2}^{k}\right)^{\lambda\lambda-1}\left[\dfrac{\left(s^{k+1}-s^{k}\right)}{\left(t^{k+1}-t^{k}\right)}p_{m+1/2}^{k}u_{N+1/2}^{k}+\dfrac{\left(D_A\right)_{m+1/2}^{k}}{s^{k}}\left.\dfrac{\partial p}{\partial u}\right|_{m+1/2}^{k}\right]\\ +C_A\left[\left(s^{k+1}\right)^{\lambda\lambda}-\left(s^{k}\right)^{\lambda\lambda}-\left(r_{m+1/2}^{k+1}\right)^{\lambda\lambda-1}+\left(r_{m+1/2}^{k}\right)^{\lambda\lambda-1}\right]=\\ -C_B\left[-\left(s^{k+1}\right)^{\lambda\lambda}+\left(s^{k}\right)^{\lambda\lambda}+\left(r_{m+1/2}^{k+1}\right)^{\lambda\lambda-1}-\left(r_{m+1/2}^{k}\right)^{\lambda\lambda-1}\right]\\ +\lambda\lambda\left(t^{k+1}-t^{k}\right)\left(r_{m+1+1/2}^{k}\right)^{\lambda\lambda-1}\left[\dfrac{\left(s^{k+1}-s^{k}\right)}{\left(t^{k+1}-t^{k}\right)}q_{1+1/2}^{k}\left(1-v_{1+1/2}^{k}\right)+\dfrac{\left(D_B\right)_{1+1/2}^{k}}{R-s^{k}}\left.\dfrac{\partial q}{\partial v}\right|_{1+1/2}^{k}\right]\end{array} \qquad \text{A.82}$$

A.2.2 Extending the new model to a multi-phase Systems

Single and 2D planar phase systems have been discussed; however, for systems with more than two phases, there are interphases. Unlike the two end phases, both interfaces of the inner phases have moving boundaries.

$$\frac{\partial c_1(r,t)}{\partial t} = \frac{\partial}{\partial t}\left(D_1[c_1(r,t)]\frac{\partial c_1(r,t)}{\partial t}\right) \qquad 0 \le r \le s_1(t) \qquad \text{A.83}$$

$$\frac{\partial c_{nn}(r,t)}{\partial t} = \frac{\partial}{\partial t}\left(D_{nn}\left[c_{nn}(r,t)\right]\frac{\partial c_{nn}(r,t)}{\partial t}\right) \qquad s_{nn}(t) \le r \le s_{nf-1}(t) \qquad \text{A.84}$$

$$\frac{\partial c_{nf}(r,t)}{\partial t} = \frac{\partial}{\partial t}\left(D_{nf}\left[c_{nf}(r,t)\right]\frac{\partial c_{nf}(r,t)}{\partial t}\right) \qquad s_{nf-1}(t) \le r \le s_{nf}(t) = R \qquad \text{A.85}$$

n = 2… nf-1

n is the intermediate phase and nf-1 is the right boundary phase and the interface nf is the extreme right boundary.

The solution to Equations A.84 is presented below.

$$w_n = \frac{r - s_{n-1}(t)}{s_n(t) - s_{n-1}(t)} \qquad \text{A.86}$$

$$z(w,t) = c_n(r,t) \qquad \text{A.87}$$

The Landau transformation yields:

$$\frac{\partial z}{\partial t} - \frac{\left[\frac{ds_1}{dt} + w\left(\frac{ds_2}{dt} - \frac{ds_1}{dt}\right)\right]}{(s_2 - s_1)}\frac{\partial z}{\partial w} = \frac{1}{(s_2 - s_1)^2}\frac{\partial}{\partial w}\left(D_E \frac{\partial z}{\partial w}\right) \qquad \text{A.88}$$

This can be simplified to:

$$(s_2 - s_1)\frac{\partial z}{\partial t} - \left[\frac{ds_1}{dt} + w\left(\frac{ds_2}{dt} - \frac{ds_1}{dt}\right)\right]\frac{\partial z}{\partial w} = \frac{1}{(s_2 - s_1)}\frac{\partial}{\partial w}\left(D_E \frac{\partial z}{\partial w}\right) \quad \text{A.89}$$

Applying further transformations, such that:

$$\frac{\partial z(s_2 - s_1)}{\partial t} = (s_2 - s_1)\frac{\partial z}{\partial t} + z\left(\frac{ds_2}{dt} - \frac{ds_1}{dt}\right) \quad \text{A.90}$$

$$\frac{\partial}{\partial w}\left[z\left(\frac{ds_1}{dt} + w\left(\frac{ds_2}{dt} - \frac{ds_1}{dt}\right)\right)\right] = \left[\frac{ds_1}{dt} + w\left(\frac{ds_2}{dt} - \frac{ds_1}{dt}\right)\right]\frac{\partial z}{\partial w} + z\left(\frac{ds_2}{dt} - \frac{ds_1}{dt}\right) \quad \text{A.91}$$

The difference between Equations A.90 and A.91 yields the left side of Equation A.89:

$$\frac{\partial[z(s_2 - s_1)]}{\partial t} - \frac{\partial}{\partial w}\left[z\left(\frac{ds_1}{dt} + w\left(\frac{ds_2}{dt} - \frac{ds_1}{dt}\right)\right)\right] = \frac{1}{(s_2 - s_1)}\frac{\partial}{\partial w}\left(D_E \frac{\partial z}{\partial w}\right)$$

A.92

Re-arranging Equation A.82 yields Equation A.93 which can be further simplified to Equation A.94, which is the equation for the inner phase with moving interfaces at both boundaries.

$$\frac{\partial[z(s_2 - s_1)]}{\partial t} = \frac{\partial}{\partial w}\left[z\left(\frac{ds_1}{dt} + w\left(\frac{ds_2}{dt} - \frac{ds_1}{dt}\right)\right)\right] + \frac{1}{(s_2 - s_1)}\frac{\partial}{\partial w}\left(D_E \frac{\partial z}{\partial w}\right)$$

A.93

$$\frac{\partial[z(s_2 - s_1)]}{\partial t} = \frac{\partial}{\partial w}\left[z\left(\frac{ds_1}{dt} + w\left(\frac{ds_2}{dt} - \frac{ds_1}{dt}\right)\right) + \frac{D_E}{(s_2 - s_1)}\frac{\partial z}{\partial w}\right] \quad \text{A.94}$$

It is important to note that Equation A.94 can be converted to the Phase A and B equations by applying the necessary interface condition. For example, for 1D planar conditions with a fixed left boundary, Equation A.94 is the same as Equation A.54. Similarly, when the right boundary is fixed, Equation A.94 is the same as Equation A.55 for 1D planar systems.

Numerically integrating Equation A.94 using a leapfrog/DF algorithm gives:

$$\int_{u_{i-1/2}}^{u_{i-1/2}}\int_{t^{k-1}}^{t^{k+1}}\frac{\partial}{\partial t}\left[z\left(s_2-s_1\right)\right]dtdw=\int_{u_{i-1/2}}^{u_{i-1/2}}\int_{t^{k-1}}^{t^{k+1}}\frac{\partial}{\partial w}\left[z\left(\frac{ds_1}{dt}+w\left(\frac{ds_2}{dt}-\frac{ds_1}{dt}\right)\right)+\frac{D_E}{\left(s_2-s_1\right)}\frac{\partial z}{\partial w}\right]dwdt \qquad \text{A.95}$$

The integration gives:

$$\int_{u_{i-1/2}}^{u_{i-1/2}}\left[z_i^{k+1}\left(s_2^{k+1}-s_1^{k+1}\right)-z_i^{k-1}\left(s_2^{k-1}-s_1^{k-1}\right)\right]dw=\int_{t^{k-1}}^{t^{k+1}}\left[\begin{array}{l} z_{i+1/2}^{k}\left(\frac{ds_1}{dt}\left(1-w_{i+1/2}\right)+\frac{ds_2}{dt}w_{i+1/2}\right)+\frac{D_{E\,i+1/2}^{\;k}}{\left(s_2-s_1\right)}\frac{\partial z}{\partial w}\Big|_{i+1/2} \\ -z_{i-1/2}^{k}\left(\frac{ds_1}{dt}\left(1-w_{i-1/2}\right)+\frac{ds_2}{dt}w_{i-1/2}\right)+\frac{D_{E\,i-1/2}^{\;k}}{\left(s_2-s_1\right)}\frac{\partial z}{\partial w}\Big|_{i-1/2}\end{array}\right]dt$$

A.96

For the left side of Equation A.96, z is at a constant time; hence u in the square brackets is the only function of w and can be integrated with $s^{k+1}=\Delta s+s^{k-1}$ and $\delta t=t^{k+1}-t^{k-1}$.

$$\left[z_i^{k+1}\left(s_2^{k+1}-s_1^{k+1}\right)-z_i^{k-1}\left(s_2^{k-1}-s_1^{k-1}\right)\right]\left(w_{i+1/2}-w_{i-1/2}\right)=z_{i+1/2}^{k}\left(\Delta s_1\left(1-w_{i+1/2}\right)+\Delta s_2 w_{i+1/2}\right)+\frac{D_{E\,i+1/2}^{\;k}\delta t}{\left(s_2-s_1\right)}\frac{\partial z}{\partial w}\Big|_{i+1/2}$$
$$-z_{i-1/2}^{k}\left(\Delta s_1\left(1-w_{i-1/2}\right)+\Delta s_2 w_{i-1/2}\right)-\frac{D_{E\,i-1/2}^{\;k}\delta t}{\left(s_2-s_1\right)}\frac{\partial z}{\partial w}\Big|_{i-1/2}$$

A.97

$$\left[z_i^{k+1}\left(s_2^{k+1}-s_1^{k+1}\right)-z_i^{k-1}\left(s_2^{k-1}-s_1^{k-1}\right)\right]\left(w_{i+1/2}-w_{i-1/2}\right)=z_{i+1/2}^{k}\left(\Delta s_1\left(1-w_{i+1/2}\right)+\Delta s_2 w_{i+1/2}\right)+\frac{D_{E\,i+1/2}^{\;k}\delta t}{\left(s_2-s_1\right)}\frac{\left(z_{i+1}^{k}-z_i^{k}\right)}{\left(w_{i+1}-w_i\right)}$$
$$-z_{i-1/2}^{k}\left(\Delta s_1\left(1-w_{i-1/2}\right)+\Delta s_2 w_{i-1/2}\right)-\frac{D_{E\,i-1/2}^{\;k}\delta t}{\left(s_2-s_1\right)}\frac{\left(z_i^{k}-z_{i-1}^{k}\right)}{\left(w_i-w_{i-1}\right)}$$

A.98

Setting $z_{i+1/2}^{k} = \beta z_{i+1}^{k} + \alpha z_{i}^{k}$ and $z_{i-1/2}^{k} = \beta z_{i}^{k} + \alpha z_{i-1}^{k}$ and collecting the z_{i}^{k} terms

$$\left[z_i^{k+1}\left(s_2^{k+1}-s_1^{k+1}\right)-z_i^{k-1}\left(s_2^{k-1}-s_1^{k-1}\right)\right]\left(w_{i+1/2}-w_{i-1/2}\right)=\left(\beta z_{i+1}^{k}+\alpha z_i^{k}\right)\left(\Delta s_1\left(1-w_{i+1/2}\right)+\Delta s_2 w_{i+1/2}\right)+\frac{D_{Ei+1/2}^{k}\delta t}{\left(s_2-s_1\right)}\frac{\left(z_{i+1}^{k}-z_i^{k}\right)}{\left(w_{i+1}-w_i\right)}$$
$$-\left(\beta z_i^{k}+\alpha z_{i-1}^{k}\right)\left(\Delta s_1\left(1-w_{i-1/2}\right)+\Delta s_2 w_{i-1/2}\right)-\frac{D_{Ei-1/2}^{k}\delta t}{\left(s_2-s_1\right)}\frac{\left(z_i^{k}-z_{i-1}^{k}\right)}{\left(w_i-w_{i-1}\right)}$$

A.99

$$\left[z_i^{k+1}\left(s_2^{k+1}-s_1^{k+1}\right)-z_i^{k-1}\left(s_2^{k-1}-s_1^{k-1}\right)\right]\left(w_{i+1/2}-w_{i-1/2}\right)=\frac{D_{Ei+1/2}^{k}\delta t}{\left(s_2-s_1\right)}\frac{\left(z_{i+1}^{k}\right)}{\left(w_{i+1}-w_i\right)}+\frac{D_{Ei-1/2}^{k}\delta t}{\left(s_2-s_1\right)}\frac{\left(z_{i-1}^{k}\right)}{\left(w_i-w_{i-1}\right)}$$
$$\left(\beta z_{i+1}^{k}\right)\left(\Delta s_1\left(1-w_{i+1/2}\right)+\Delta s_2 w_{i+1/2}\right)-\left(\alpha z_{i-1}^{k}\right)\left(\Delta s_1\left(1-w_{i-1/2}\right)+\Delta s_2 w_{i-1/2}\right)$$
$$+z_i^{k}\left[\begin{array}{l}-\dfrac{D_{Ei+1/2}^{k}\delta t}{\left(s_2-s_1\right)\left(w_{i+1}-w_i\right)}-\dfrac{D_{Ei-1/2}^{k}\delta t}{\left(s_2-s_1\right)\left(w_i-w_{i-1}\right)}\\ +\alpha\left(\Delta s_1\left(1-w_{i+1/2}\right)+\Delta s_2 w_{i+1/2}\right)-\beta\left(\Delta s_1\left(1-w_{i-1/2}\right)+\Delta s_2 w_{i-1/2}\right)\end{array}\right]$$

A.100

To stabilize the model, Equation A.100, set $z_i^{k}=\dfrac{z_i^{k+1}+z_i^{k-1}}{2}$

$$\left[z_i^{k+1}\left(s_2^{k+1}-s_1^{k+1}\right)-z_i^{k-1}\left(s_2^{k-1}-s_1^{k-1}\right)\right]\left(w_{i+1/2}-w_{i-1/2}\right)=\frac{D_{Ei+1/2}^{k}\delta t}{\left(s_2-s_1\right)}\frac{\left(z_{i+1}^{k}\right)}{\left(w_{i+1}-w_i\right)}+\frac{D_{Ei-1/2}^{k}\delta t}{\left(s_2-s_1\right)}\frac{\left(z_{i-1}^{k}\right)}{\left(w_i-w_{i-1}\right)}$$
$$\left(\beta z_{i+1}^{k}\right)\left(\Delta s_1\left(1-w_{i+1/2}\right)+\Delta s_2 w_{i+1/2}\right)-\left(\alpha z_{i-1}^{k}\right)\left(\Delta s_1\left(1-w_{i-1/2}\right)+\Delta s_2 w_{i-1/2}\right)$$
$$+\frac{z_i^{k+1}+z_i^{k-1}}{2}\left[\begin{array}{l}-\dfrac{D_{Ei+1/2}^{k}\delta t}{\left(s_2-s_1\right)\left(w_{i+1}-w_i\right)}-\dfrac{D_{Ei-1/2}^{k}\delta t}{\left(s_2-s_1\right)\left(w_i-w_{i-1}\right)}\\ +\alpha\left(\Delta s_1\left(1-w_{i+1/2}\right)+\Delta s_2 w_{i+1/2}\right)-\beta\left(\Delta s_1\left(1-w_{i-1/2}\right)+\Delta s_2 w_{i-1/2}\right)\end{array}\right]$$

A.101

$$z_i^{k+1}\left[\left(s_2^{k+1}-s_1^{k+1}\right)\left(w_{i+1/2}-w_{i-1/2}\right)-\frac{1}{2}\left[\begin{array}{l}-\dfrac{D_{E\,i+1/2}^{\;k}\delta t}{\left(s_2-s_1\right)\left(w_{i+1}-w_i\right)}-\dfrac{D_{E\,i-1/2}^{\;k}\delta t}{\left(s_2-s_1\right)\left(w_i-w_{i-1}\right)}\\ +\alpha\left(\Delta s_1\left(1-w_{i+1/2}\right)+\Delta s_1 w_{i+1/2}\right)-\beta\left(\dfrac{ds_1}{dt}\left(1-w_{i-1/2}\right)+\Delta s_2 w_{i-1/2}\right)\end{array}\right]\right]$$

$$-z_i^{k-1}\left[\left(s_2^{k-1}-s_1^{k-1}\right)\left(w_{i+1/2}-w_{i-1/2}\right)+\frac{1}{2}\left[\begin{array}{l}-\dfrac{D_{E\,i+1/2}^{\;k}\delta t}{\left(s_2-s_1\right)\left(w_{i+1}-w_i\right)}-\dfrac{D_{E\,i-1/2}^{\;k}\delta t}{\left(s_2-s_1\right)\left(w_i-w_{i-1}\right)}\\ +\alpha\left(\Delta s_1\left(1-w_{i+1/2}\right)+\Delta s_2 w_{i+1/2}\right)-\beta\left(\Delta s_1\left(1-w_{i-1/2}\right)+\Delta s_2 w_{i-1/2}\right)\end{array}\right]\right]$$

$$=\frac{D_{E\,i+1/2}^{\;k}\delta t}{\left(s_2-s_1\right)}\frac{\left(z_{i+1}^{k}\right)}{\left(w_{i+1}-w_i\right)}+\frac{D_{E\,i-1/2}^{\;k}\delta t}{\left(s_2-s_1\right)}\frac{\left(z_{i-1}^{k}\right)}{\left(w_i-w_{i-1}\right)}+\left(\beta z_{i+1}^{k}\right)\left(\Delta s_1\left(1-w_{i+1/2}\right)+\Delta s_2 w_{i+1/2}\right)-\left(\alpha z_{i-1}^{k}\right)\left(\Delta s_1\left(1-w_{i-1/2}\right)+\Delta s_2 w_{i-1/2}\right)$$

A.102

$$z_i^{k+1}\left[\left(s_2^{k+1}-s_1^{k+1}\right)\left(w_{i+1/2}-w_{i-1/2}\right)-\frac{1}{2}\left[\begin{array}{l}-\dfrac{D_{E\,i+1/2}^{\;k}\delta t}{\left(s_2-s_1\right)\left(w_{i+1}-w_i\right)}-\dfrac{D_{E\,i-1/2}^{\;k}\delta t}{\left(s_2-s_1\right)\left(w_i-w_{i-1}\right)}\\ +\alpha\left(\Delta s_1\left(1-w_{i+1/2}\right)+\Delta s_2 w_{i+1/2}\right)-\beta\left(\Delta s_1\left(1-w_{i-1/2}\right)+\Delta s_2 w_{i-1/2}\right)\end{array}\right]\right]$$

$$=z_i^{k-1}\left[\left(s_2^{k-1}-s_1^{k-1}\right)\left(w_{i+1/2}-w_{i-1/2}\right)+\frac{1}{2}\left[\begin{array}{l}-\dfrac{D_{E\,i+1/2}^{\;k}\delta t}{\left(s_2-s_1\right)\left(w_{i+1}-w_i\right)}-\dfrac{D_{E\,i-1/2}^{\;k}\delta t}{\left(s_2-s_1\right)\left(w_i-w_{i-1}\right)}\\ +\alpha\left(\Delta s_1\left(1-w_{i+1/2}\right)+\Delta s_2 w_{i+1/2}\right)-\beta\left(\Delta s_1\left(1-w_{i-1/2}\right)+\Delta s_2 w_{i-1/2}\right)\end{array}\right]\right]$$

$$+\frac{D_{E\,i+1/2}^{\;k}\delta t}{\left(s_2-s_1\right)}\frac{\left(z_{i+1}^{k}\right)}{\left(w_{i+1}-w_i\right)}+\frac{D_{E\,i-1/2}^{\;k}\delta t}{\left(s_2-s_1\right)}\frac{\left(z_{i-1}^{k}\right)}{\left(w_i-w_{i-1}\right)}+\left(\beta z_{i+1}^{k}\right)\left(\Delta s_1\left(1-w_{i+1/2}\right)+\Delta s_2 w_{i+1/2}\right)-\left(\alpha z_{i-1}^{k}\right)\left(\Delta s_1\left(1-w_{i-1/2}\right)+\Delta s_2 w_{i-1/2}\right)$$

A.103

$$z_i^{k+1}\left[\left(s_2^{k+1}-s_1^{k+1}\right)\left(w_{i+1/2}-w_{i-1/2}\right)-\frac{1}{2}\left[\begin{array}{l}-\dfrac{D_{Ei+1/2}^{k}\delta t}{\left(s_2-s_1\right)\left(w_{i+1}-w_i\right)}-\dfrac{D_{Ei-1/2}^{k}\delta t}{\left(s_2-s_1\right)\left(w_i-w_{i-1}\right)}\\ +\alpha\left(\Delta s_1\left(1-w_{i+1/2}\right)+\Delta s_2 w_{i+1/2}\right)-\beta\left(\Delta s_1\left(1-w_{i-1/2}\right)+\Delta s_2 w_{i-1/2}\right)\end{array}\right]\right]$$
$$=z_i^{k-1}\left[\left(s_2^{k-1}-s_1^{k-1}\right)\left(w_{i+1/2}-w_{i-1/2}\right)+\frac{1}{2}\left[\begin{array}{l}-\dfrac{D_{Ei+1/2}^{k}\delta t}{\left(s_2-s_1\right)\left(w_{i+1}-w_i\right)}-\dfrac{D_{Ei-1/2}^{k}\delta t}{\left(s_2-s_1\right)\left(w_i-w_{i-1}\right)}\\ +\alpha\left(\Delta s_1\left(1-w_{i+1/2}\right)+\Delta s_2 w_{i+1/2}\right)-\beta\left(\Delta s_1\left(1-w_{i-1/2}\right)+\Delta s_2 w_{i-1/2}\right)\end{array}\right]\right]$$
$$+z_{i+1}^{k}\left[\frac{D_{Ei+1/2}^{k}\delta t}{\left(s_2-s_1\right)\left(w_{i+1}-w_i\right)}+\beta\left(\Delta s_1\left(1-w_{i+1/2}\right)+\Delta s_2 w_{i+1/2}\right)\right]$$
$$+z_{i-1}^{k}\left[\frac{D_{Ei-1/2}^{k}\delta t}{\left(s_2-s_1\right)\left(w_i-w_{i-1}\right)}-\alpha\left(\Delta s_1\left(1-w_{i-1/2}\right)+\Delta s_2 w_{i-1/2}\right)\right]$$

A.104

Collecting the terms, the finite difference scheme for the inner phase is

$$\delta_{z1}z_i^{k+1}=\delta_{z2}z_i^{k-1}+\delta_{z3}z_{i+1}^{k}+\delta_{z4}z_{i-1}^{k}$$

A.105

$$\delta_{z1}=\left(s_2^{k+1}-s_1^{k+1}\right)\left(w_{i+1/2}-w_{i-1/2}\right)-\frac{1}{2}\left[\begin{array}{l}-\dfrac{D_{Ei+1/2}^{k}\delta t}{\left(s_2-s_1\right)\left(w_{i+1}-w_i\right)}-\dfrac{D_{Ei-1/2}^{k}\delta t}{\left(s_2-s_1\right)\left(w_i-w_{i-1}\right)}\\ +\alpha\left(\Delta s_1\left(1-w_{i+1/2}\right)+\Delta s_2 w_{i+1/2}\right)-\beta\left(\Delta s_1\left(1-w_{i-1/2}\right)+\Delta s_2 w_{i-1/2}\right)\end{array}\right]$$

A.106

$$\delta_{z2}=\left[\left(s_2^{k-1}-s_1^{k-1}\right)\left(w_{i+1/2}-w_{i-1/2}\right)+\frac{1}{2}\left[\begin{array}{l}-\dfrac{D_{Ei+1/2}^{k}\delta t}{\left(s_2-s_1\right)\left(w_{i+1}-w_i\right)}-\dfrac{D_{Ei-1/2}^{k}\delta t}{\left(s_2-s_1\right)\left(w_i-w_{i-1}\right)}\\ +\alpha\left(\Delta s_1\left(1-w_{i+1/2}\right)+\Delta s_2 w_{i+1/2}\right)-\beta\left(\Delta s_1\left(1-w_{i-1/2}\right)+\Delta s_2 w_{i-1/2}\right)\end{array}\right]\right]$$

A.107

$$\delta_{z3}=\frac{D_{Ei+1/2}^{k}\delta t}{\left(s_2-s_1\right)\left(w_{i+1}-w_i\right)}+\beta\left(\Delta s_1\left(1-w_{i+1/2}\right)+\Delta s_2 w_{i+1/2}\right)$$

A.108

$$\delta_{z4} = \frac{D_{E\,i-1/2}^{\,k}\delta t}{(s_2 - s_1)(w_i - w_{i-1})} - \alpha\left(\Delta s_1(1 - w_{i-1/2}) + \Delta s_2 w_{i-1/2}\right) \qquad \text{A.109}$$

The boundary conditions are constant interface concentrations.

$$z_1^{k-1} = z_1^k = z_1^{k+1} \qquad \text{A.110}$$

$$z_{m+1}^{k-1} = z_{m+1}^k = z_{m+1}^{k+1} \qquad \text{A.111}$$

A.2.3 Solute balance in multi-phase one-dimensional planar systems

To ensure solute conservation, the total amount of solute throughout the diffusion system must be the same for all diffusion times, and by implication, the time rate of change in the total solute is zero. Therefore, consider a system with interface positions $s_0, s_1, s_2, \ldots, s_{nf-1}, s_{nf}$. The first phase has a left boundary with zero flux, while the right boundary of the last phase has zero flux.

$$\frac{\partial}{\partial t}\left((s_1 - s_0)\int_0^1 z_1 dw_1 + (s_2 - s_1)\int_0^1 z_2 dw_2 + (s_3 - s_2)\int_0^1 z_3 dw_3 + \ldots + (s_{n-1} - s_{n-2})\int_0^1 z_{n-1} dw_{n-1} + (s_{nf} - s_{n-1})\int_0^1 z_n dw_n\right) = 0$$

A.112

The summation is done for each phase.

In the first phase with zero flux at the left boundary:

$$\frac{\partial}{\partial t}\left((s_1 - s_0)\int_0^1 z_1 dw_1\right) \qquad \text{A.113}$$

This becomes

$$\left(\left(s_1^{k+1}-s_0^{k+1}\right)\left[z_{1,1}^{k+1}\frac{w_{1,2}-w_{1,1}}{2}+\sum_{i=2}^{N}z_{1,i}^{k+1}\frac{w_{1,i+1}-w_{1,i}}{2}\right]+z_{1,N+1,1}^{k+1}\frac{w_{1,N+1}-w_{1,N}}{2}\right)$$
$$-\left(\left(s_1^{k-1}-s_0^{k-1}\right)\left[z_{1,1}^{k-1}\frac{w_{1,2}-w_{1,1}}{2}+\sum_{i=2}^{N}z_{1,i}^{k-1}\frac{w_{1,i+1}-w_{1,i}}{2}\right]+z_{1,N+1,1}^{k-1}\frac{w_{1,N+1}-w_{1,N}}{2}\right) \quad \text{A.114}$$

Rearranging Equation A.114 gets:

$$\left[\left(s_1^{k+1}-s_0^{k+1}\right)z_{1,1}^{k+1}-\left(s_1^{k-1}-s_0^{k-1}\right)z_{1,1}^{k-1}\right]\left(\frac{w_{1,2}-w_{1,1}}{2}\right)$$
$$+\sum_{i=2}^{N}\left[\left(s_1^{k+1}-s_0^{k+1}\right)z_{1,i}^{k+1}-\left(s_1^{k-1}-s_0^{k-1}\right)z_{1,i}^{k-1}\right]\left(\frac{w_{1,i+1}-w_{1,i}}{2}\right) \quad \text{A.115}$$
$$\left[\left(s_1^{k+1}-s_0^{k+1}\right)z_{1,m+1}^{k+1}-\left(s_1^{k-1}-s_0^{k-1}\right)z_{1,m+1}^{k-1}\right]\left(\frac{w_{1,m+1}-w_{1,m}}{2}\right)$$

Applying the Equation A.115 gets:

$$\sum_{i=2}^{N}\left[\left(s_1^{k+1}-s_0^{k+1}\right)z_{0,i}^{k+1}-\left(s_1^{k-1}-s_0^{k-1}\right)z_{0,i}^{k-1}\right]\left(\frac{w_{i+1}-w_i}{2}\right)=-z_{2-1/2}^{k}\left(\Delta s_0\left(1-w_{2-1/2}\right)+\Delta s_1 w_{2-1/2}\right)-\frac{D_{1,2-1/2}^{\ k}\delta t}{\left(s_2-s_1\right)}\frac{\left(z_2^k-z_1^k\right)}{\left(w_2-w_1\right)}$$
$$+z_{m+1/2}^{k}\left(\Delta s_0\left(1-w_{m+1/2}\right)+\Delta s_1 w_{m+1/2}\right)+\frac{D_{1,N+1/2}^{\ k}\delta t}{\left(s_2-s_1\right)}\frac{\left(z_{m+1}^k-z_m^k\right)}{\left(w_{m+1}-w_m\right)} \quad \text{A.116}$$

Substituting Equation A.116 into Equation A.117 results in:

$$\left[\left(s_1^{k+1}-s_0^{k+1}\right)z_{1,1}^{k+1}-\left(s_1^{k-1}-s_0^{k-1}\right)z_{1,1}^{k-1}\right]\left(\frac{w_{1,2}-w_{1,1}}{2}\right)-z_{1,1+1/2}^{k}\left(\Delta s_0\left(1-w_{1,1+1/2}\right)+\Delta s_1 w_{1,1+1/2}\right)-\frac{D_{1,1+1/2}^{\ k}\delta t}{\left(s_0-s_1\right)}\frac{\left(z_{1,2}^k-z_{1,1}^k\right)}{\left(w_{1,2}-w_{1,1}\right)}$$
$$+z_{1,m+1/2}^{k}\left(\Delta s_0\left(1-w_{1,m+1/2}\right)+\Delta s_1 w_{1,m+1/2}\right)+\frac{D_{1,m+1/2}^{\ k}\delta t}{\left(s_0-s_1\right)}\frac{\left(z_{1,m+1}^k-z_{1,m}^k\right)}{\left(w_{1,m+1}-w_{1,m}\right)}+\left[\left(s_1^{k+1}-s_0^{k+1}\right)z_{1,m+1,1}^{k+1}-\left(s_1^{k-1}-s_0^{k-1}\right)z_{1,m+1}^{k-1}\right]\left(\frac{w_{1,m+1}-w_{1,m}}{2}\right) \quad \text{A.117}$$

The interface concentration does not change $z_{1,1}^{k-1}=z_{1,1}^{k+1}=z_{1,1}$ and $z_{1,m+1}^{k-1}=z_{1,m+1}^{k+1}=z_{1,m+1}$

$$(\Delta s_1 - \Delta s_0) z_{1,1}\left(\frac{w_{1,2} - w_{1,1}}{2}\right) - z^k_{1,1+1/2}\left(\Delta s_0\left(1 - w_{1,1+1/2}\right) + \Delta s_1 w_{1,1+1/2}\right) - \frac{D^k_{1,1+1/2}\delta t}{(s_0 - s_1)}\frac{\left(z^k_{1,2} - z^k_{1,1}\right)}{\left(w_{1,2} - w_{1,1}\right)}$$
$$+ z^k_{1,m+1/2}\left(\Delta s_0\left(1 - w_{1,m+1/2}\right) + \Delta s_1 w_{1,m+1/2}\right) + \frac{D^k_{1,m+1/2}\delta t}{(s_0 - s_1)}\frac{\left(z^k_{1,m+1} - z^k_{1,m}\right)}{\left(w_{1,m+1} - w_{1,m}\right)} + (\Delta s_1 - \Delta s_0) z_{1,m+1}\left(\frac{w_{1,m+1} - w_{1,m}}{2}\right)$$

A.118

Collecting the terms results in:

$$\Delta s_0\left(-z^k_{1,1+1/2}\left(1 - w_{1,1+1/2}\right) - z_{1,1}\left(\frac{w_{1,2} - w_{1,1}}{2}\right)\right) + \Delta s_1\left(-z^k_{1,1+1/2} w_{1,1+1/2} + z_{1,1}\left(\frac{w_{1,2} - w_{1,1}}{2}\right)\right) - \frac{D^k_{1,1+1/2}\delta t}{(s_1 - s_0)}\frac{\left(z^k_{1,2} - z^k_{1,1}\right)}{\left(w_{1,2} - w_{1,1}\right)}$$
$$+ \Delta s_0\left(z^k_{1,m+1/2}\left(1 - w_{1,m+1/2}\right) - z_{1,m+1}\left(\frac{w_{1,m+1} - w_{1,m}}{2}\right)\right) + \Delta s_1\left(z^k_{1,m+1/2} w_{1,m+1/2} + z_{1,m+1}\left(\frac{w_{1,m+1} - w_{1,m}}{2}\right)\right) + \frac{D^k_{1,m+1/2}\delta t}{(s_1 - s_0)}\frac{\left(z^k_{1,m+1} - z^k_{1,m}\right)}{\left(w_{1,m+1} - w_{1,m}\right)}$$

A.119

Equation A.119 is a general equation that can be applied to any phase.

Considering the first phase with zero flux at the left boundary, the zero-flux condition will be applied to Equation A.119 to obtain:

$$\left[\left(s_1^{k+1} - s_0^{k+1}\right) z_{1,1}^{k+1} - \left(s_1^{k-1} - s_0^{k-1}\right) z_{1,1}^{k-1}\right]\left(\frac{w_{1,2} - w_{1,1}}{2}\right) - z^k_{1,1+1/2}\left(\Delta s_0\left(1 - w_{1,1+1/2}\right) + \Delta s_1 w_{1,1+1/2}\right) - \frac{D^k_{1,1+1/2}\delta t}{(s_1 - s_0)}\frac{\left(z^k_{1,2} - z^k_{1,1}\right)}{\left(w_{1,2} - w_{1,1}\right)}$$
$$= \Delta s_0\left(-z^k_{1,1+1/2}\left(1 - w_{1,1+1/2}\right) - z_{1,1}\left(\frac{w_{1,2} - w_{1,1}}{2}\right)\right) + \Delta s_1\left(-z^k_{1,1+1/2} w_{1,1+1/2} + z_{1,1}\left(\frac{w_{1,2} - w_{1,1}}{2}\right)\right) - \frac{D^k_{1,1+1/2}\delta t}{(s_1 - s_0)}\frac{\left(z^k_{1,2} - z^k_{1,1}\right)}{\left(w_{1,2} - w_{1,1}\right)}$$
$$= 0$$

A.120

Hence, for the first phase with zero flux at the left boundary, the equation becomes:

$$\Delta s_0\left(z^k_{1,m+1/2}\left(1-w_{1,m+1/2}\right)-z_{1,m+1}\left(\frac{w_{1,m+1}-w_{1,m}}{2}\right)\right)+\Delta s_1\left(z^k_{1,m+1/2}w_{1,m+1/2}+z_{1,m+1}\left(\frac{w_{1,m+1}-w_{1,m}}{2}\right)\right)+\frac{D^{\,k}_{1,m+1/2}\delta t}{\left(s_1-s_0\right)}\frac{\left(z^k_{1,m+1}-z^k_{1,m}\right)}{\left(w_{1,m+1}-w_{1,m}\right)}$$

A.121

The second phase which uses Equation A.119, results in:

$$\Delta s_1\left(-z^k_{2,1+1/2}\left(1-w_{2,1+1/2}\right)-z_{2,1}\left(\frac{w_{2,2}-w_{2,1}}{2}\right)\right)+\Delta s_2\left(-z^k_{2,1+1/2}w_{2,1+1/2}+z_{2,1}\left(\frac{w_{2,2}-w_{2,1}}{2}\right)\right)-\frac{D^{\,k}_{2,1+1/2}\delta t}{\left(s_2-s_1\right)}\frac{\left(z^k_{2,2}-z^k_{2,1}\right)}{\left(w_{2,2}-w_{2,1}\right)}$$
$$+\Delta s_1\left(z^k_{2,m+1/2}\left(1-w_{2,m+1/2}\right)-z_{2,m+1}\left(\frac{w_{2,m+1}-w_{2,m}}{2}\right)\right)+\Delta s_2\left(z^k_{2,m+1/2}w_{2,m+1/2}+z_{2,m+1}\left(\frac{w_{2,m+1}-w_{2,m}}{2}\right)\right)+\frac{D^{\,k}_{2,m+1/2}\delta t}{\left(s_2-s_1\right)}\frac{\left(z^k_{2,m+1}-z^k_{2,m}\right)}{\left(w_{2,m+1}-w_{2,m}\right)}$$

A.122

Similarly, for the third phase, Equation A.119 results in:

$$\Delta s_2\left(-z^k_{3,1+1/2}\left(1-w_{3,1+1/2}\right)-z_{3,1}\left(\frac{w_{3,2}-w_{3,1}}{2}\right)\right)+\Delta s_3\left(-z^k_{3,1+1/2}w_{3,1+1/2}+z_{3,1}\left(\frac{w_{3,2}-w_{3,1}}{2}\right)\right)-\frac{D^{\,k}_{3,1+1/2}\delta t}{\left(s_3-s_2\right)}\frac{\left(z^k_{3,2}-z^k_{3,1}\right)}{\left(w_{3,2}-w_{3,1}\right)}$$
$$+\Delta s_2\left(z^k_{3,m+1/2}\left(1-w_{3,m+1/2}\right)-z_{3,m+1}\left(\frac{w_{3,m+1}-w_{3,m}}{2}\right)\right)+\Delta s_3\left(z^k_{3,m+1/2}w_{3,m+1/2}+z_{3,m+1}\left(\frac{w_{3,m+1}-w_{3,m}}{2}\right)\right)+\frac{D^{\,k}_{3,m+1/2}\delta t}{\left(s_3-s_2\right)}\frac{\left(z^k_{3,m+1}-z^k_{3,m}\right)}{\left(w_{3,m+1}-w_{3,m}\right)}$$

A.123

In the nn-th phase:

$$\Delta s_{nn-1}\left(-z^k_{nn,1+1/2}\left(1-w_{nn,1+1/2}\right)-z_{nn,1}\left(\frac{w_{nn,2}-w_{nn,1}}{2}\right)\right)+\Delta s_{nn}\left(-z^k_{nn,1+1/2}w_{nn,1+1/2}+z_{nn,1}\left(\frac{w_{nn,2}-w_{nn,1}}{2}\right)\right)-\frac{D^{\,k}_{nn,1+1/2}\delta t}{\left(s_{nn}-s_{nn-1}\right)}\frac{\left(z^k_{nn,2}-z^k_{nn,1}\right)}{\left(w_{nn,2}-w_{nn,1}\right)}$$
$$+\Delta s_{nn-1}\left(z^k_{nn,m+1/2}\left(1-w_{nn,m+1/2}\right)-z_{nn,m+1}\left(\frac{w_{nn,m+1}-w_{nn,m}}{2}\right)\right)+\Delta s_{nn}\left(z^k_{nn,m+1/2}w_{nn,m+1/2}+z_{nn,m+1}\left(\frac{w_{nn,m+1}-w_{nn,m}}{2}\right)\right)+\frac{D^{\,k}_{nn,m+1/2}\delta t}{\left(s_{nn}-s_{nn-1}\right)}\frac{\left(z^k_{nn,m+1}-z^k_{nn,m}\right)}{\left(w_{nn,m+1}-w_{nn,m}\right)}$$

A.124

The second to the last phase (nf-1):

$$\Delta s_{nf-2}\left(-z^{k}_{nf-1,1+1/2}\left(1-w_{nf-1,1+1/2}\right)-z_{nf-1,1}\left(\frac{w_{nf-1,2}-w_{nf-1,1}}{2}\right)\right)$$
$$+\Delta s_{nf-1}\left(-z^{k}_{nf-1,1+1/2}w_{nf-1,1+1/2}+z_{nf-1,1}\left(\frac{w_{nf-1,2}-w_{nf-1,1}}{2}\right)\right)-\frac{D^{k}_{nf-1,1+1/2}\delta t}{\left(s_{nf-1}-s_{nf-2}\right)}\frac{\left(z^{k}_{nf-1,2}-z^{k}_{nf-1,1}\right)}{\left(w_{nf,2}-w_{nf,1}\right)}$$
$$+\Delta s_{nf-2}\left(z^{k}_{nf-1,m+1/2}\left(1-w_{nf-1,m+1/2}\right)-z_{nf-1,m+1}\left(\frac{w_{nf-1,m+1}-w_{nf-1,m}}{2}\right)\right)$$
$$+\Delta s_{nf-1}\left(z^{k}_{nf-1,m+1/2}w_{nf-1,m+1/2}+z_{nf-1,m+1}\left(\frac{w_{nf-1,m+1}-w_{nf-1,m}}{2}\right)\right)+\frac{D^{k}_{nf-1,m+1/2}\delta t}{\left(s_{nf-1}-s_{nf-2}\right)}\frac{\left(z^{k}_{nf-1,m+1}-z^{k}_{nf-1,m}\right)}{\left(w_{nf-1,m+1}-w_{nf-1,m}\right)}$$

A.125

Similarly, for the last phase:

$$\Delta s_{nf-1}\left(-z^{k}_{nf,1+1/2}\left(1-w_{nf,1+1/2}\right)-z_{nf,1}\left(\frac{w_{nf,2}-w_{nf,1}}{2}\right)\right)+\Delta s_{nf}\left(-z^{k}_{nf,1+1/2}w_{nf,1+1/2}+z_{nf,1}\left(\frac{w_{nf,2}-w_{nf,1}}{2}\right)\right)-\frac{D^{k}_{nf,1+1/2}\delta t}{\left(s_{nf}-s_{nf-1}\right)}\frac{\left(z^{k}_{nf,2}-z^{k}_{nf,1}\right)}{\left(w_{nf,2}-w_{nf,1}\right)}$$
$$+\Delta s_{nf-1}\left(z^{k}_{nf,m+1/2}\left(1-w_{nf,m+1/2}\right)-z_{nf,m+1}\left(\frac{w_{nf,m+1}-w_{nf,m}}{2}\right)\right)+\Delta s_{nf}\left(z^{k}_{nf,m+1/2}w_{nf,m+1/2}+z_{nf,m+1}\left(\frac{w_{nf,m+1}-w_{nf,m}}{2}\right)\right)+\frac{D^{k}_{nf,m+1/2}\delta t}{\left(s_{nf}-s_{nf-1}\right)}\frac{\left(z^{k}_{nf,m+1}-z^{k}_{nf,m}\right)}{\left(w_{nf,m+1}-w_{nf,m}\right)}$$

A.126

In the last phase, the right boundary which has zero flux results in

$$\left[\left(s^{k+1}_{nf}-s^{k+1}_{nf-1}\right)z^{k+1}_{nf,m+1,1}-\left(s^{k-1}_{nf}-s^{k-1}_{nf-1}\right)z^{k-1}_{nf,m+1}\right]\left(\frac{w_{nf,m+1}-w_{nf,m}}{2}\right)+z^{k}_{nf,m+1/2}\left(\Delta s_{nf-1}\left(1-w_{nf,m+1/2}\right)+\Delta s_{nf}\right)+\frac{D^{k}_{nf,m+1/2}\delta t}{\left(s_{nf}-s_{nf-1}\right)}\frac{\left(z^{k}_{nf,m+1}-z^{k}_{nf,m}\right)}{\left(w_{nf,m+1}-w_{nf,m}\right)}$$
$$=\Delta s_{nf-1}\left(z^{k}_{nf,m+1/2}\left(1-w_{nf,m+1/2}\right)-z_{nf,m+1}\left(\frac{w_{nf,m+1}-w_{nf,m}}{2}\right)\right)+\Delta s_{nf}\left(z^{k}_{nf,m+1/2}w_{nf,m+1/2}+z_{nf,m+1}\left(\frac{w_{nf,m+1}-w_{nf,m}}{2}\right)\right)+\frac{D^{k}_{nf,m+1/2}\delta t}{\left(s_{nf}-s_{nf-1}\right)}\frac{\left(z^{k}_{nf,m+1}-z^{k}_{nf,m}\right)}{\left(w_{nf,m+1}-w_{nf,m}\right)}$$
$$=0$$

A.127

Hence, for the last phase, the equation becomes:

$$\Delta s_{nn-1}\left(-z^{k}_{nn,1+1/2}\left(1-w_{nn,1+1/2}\right)-z_{nn,1}\left(\frac{w_{nn,2}-w_{nn,1}}{2}\right)\right)+\Delta s_{nn}\left(-z^{k}_{nn,1+1/2}w_{nn,1+1/2}+z_{nn,1}\left(\frac{w_{nn,2}-w_{nn,1}}{2}\right)\right)-\frac{D^{k}_{nn,1+1/2}\delta t}{\left(s_{nn}-s_{nn-1}\right)}\frac{\left(z^{k}_{nn,2}-z^{k}_{nn,1}\right)}{\left(w_{nn,2}-w_{nn,1}\right)}$$

A.128

Taking the sum of all phases:

$$\Delta s_0\left(z^k_{1,m+1/2}\left(1-w_{1,m+1/2}\right)-z_{1,m+1}\left(\frac{w_{1,m+1}-w_{1,m}}{2}\right)\right)+\Delta s_1\left(z^k_{1,m+1/2}w_{1,m+1/2}+z_{1,m+1}\left(\frac{w_{1,m+1}-w_{1,m}}{2}\right)\right)+\frac{D^k_{1,m+1/2}\delta t}{\left(s_1-s_0\right)}\frac{\left(z^k_{1,m+1}-z^k_{1,m}\right)}{\left(w_{1,m+1}-w_{1,m}\right)}$$

$$+$$

$$\Delta s_1\left(-z^k_{2,1+1/2}\left(1-w_{2,1+1/2}\right)-z_{2,1}\left(\frac{w_{2,2}-w_{2,1}}{2}\right)\right)+\Delta s_2\left(-z^k_{2,1+1/2}w_{2,1+1/2}+z_{2,1}\left(\frac{w_{2,2}-w_{2,1}}{2}\right)\right)-\frac{D^k_{2,1+1/2}\delta t}{\left(s_2-s_1\right)}\frac{\left(z^k_{2,2}-z^k_{2,1}\right)}{\left(w_{2,2}-w_{2,1}\right)}$$

$$+\Delta s_1\left(z^k_{2,m+1/2}\left(1-w_{2,m+1/2}\right)-z_{2,m+1}\left(\frac{w_{2,m+1}-w_{2,m}}{2}\right)\right)$$

$$+\Delta s_2\left(z^k_{2,m+1/2}w_{2,m+1/2}+z_{2,m+1}\left(\frac{w_{2,m+1}-w_{2,m}}{2}\right)\right)+\frac{D^k_{2,m+1/2}\delta t}{\left(s_2-s_1\right)}\frac{\left(z^k_{2,m+1}-z^k_{2,m}\right)}{\left(w_{2,m+1}-w_{2,m}\right)}$$

$$+$$

$$\Delta s_{nn-1}\left(-z^k_{nn,1+1/2}\left(1-w_{nn,1+1/2}\right)-z_{nn,1}\left(\frac{w_{nn,2}-w_{nn,1}}{2}\right)\right)$$

$$+\Delta s_{nn}\left(-z^k_{nn,1+1/2}w_{nn,1+1/2}+z_{nn,1}\left(\frac{w_{nn,2}-w_{nn,1}}{2}\right)\right)-\frac{D^k_{nn,1+1/2}\delta t}{\left(s_{nn}-s_{nn-1}\right)}\frac{\left(z^k_{nn,2}-z^k_{nn,1}\right)}{\left(w_{nn,2}-w_{nn,1}\right)}+\Delta s_{nn-1}\left(z^k_{nn,N+1/2}\left(1-w_{nn,N+1/2}\right)-z_{nn,N+1}\left(\frac{w_{nn,N+1}-w_{nn,N}}{2}\right)\right)$$

$$+\Delta s_{nn}\left(z^k_{nn,m+1/2}w_{nn,m+1/2}+z_{nn,m+1}\left(\frac{w_{nn,m+1}-w_{nn,m}}{2}\right)\right)+\frac{D^k_{nn,m+1/2}\delta t}{\left(s_{nn}-s_{nn-1}\right)}\frac{\left(z^k_{nn,m+1}-z^k_{nn,m}\right)}{\left(w_{nn,m+1}-w_{nn,m}\right)}$$

$$+$$

$$\Delta s_{nf-2}\left(-z^k_{nf-1,1+1/2}\left(1-w_{nf-1,1+1/2}\right)-z_{nf-1,1}\left(\frac{w_{nf-1,2}-w_{nf-1,1}}{2}\right)\right)$$

$$+\Delta s_{nf-1}\left(-z^k_{nf-1,1+1/2}w_{nf-1,1+1/2}+z_{nf-1,1}\left(\frac{w_{nf-1,2}-w_{nf-1,1}}{2}\right)\right)-\frac{D^k_{nf-1,1+1/2}\delta t}{\left(s_{nf-1}-s_{nf-2}\right)}\frac{\left(z^k_{nf-1,2}-z^k_{nf-1,1}\right)}{\left(w_{nf,2}-w_{nf,1}\right)}$$

$$+\Delta s_{nf-2}\left(z^k_{nf-1,m+1/2}\left(1-w_{nf-1,m+1/2}\right)-z_{nf-1,m+1}\left(\frac{w_{nf-1,m+1}-w_{nf-1,m}}{2}\right)\right)$$

$$+\Delta s_{nf-1}\left(z^k_{nf-1,m+1/2}w_{nf-1,m+1/2}+z_{nf-1,m+1}\left(\frac{w_{nf-1,m+1}-w_{nf-1,m}}{2}\right)\right)+\frac{D^k_{nf-1,m+1/2}\delta t}{\left(s_{nf-1}-s_{nf-2}\right)}\frac{\left(z^k_{nf-1,m+1}-z^k_{nf-1,m}\right)}{\left(w_{nf-1,m+1}-w_{nf-1,m}\right)}$$

$$+$$

$$\Delta s_{nf-1}\left(-z^k_{nf,1+1/2}\left(1-w_{nf,1+1/2}\right)-z_{nf,1}\left(\frac{w_{nf,2}-w_{nf,1}}{2}\right)\right)+\Delta s_{nf}\left(-z^k_{nf,1+1/2}w_{nf,1+1/2}+z_{nf,1}\left(\frac{w_{nf,2}-w_{nf,1}}{2}\right)\right)$$

$$-\frac{D^k_{nf,1+1/2}\delta t}{\left(s_{nf}-s_{nf-1}\right)}\frac{\left(z^k_{nf,2}-z^k_{nf,1}\right)}{\left(w_{nf,2}-w_{nf,1}\right)}=0$$

A.129

The equilibrium condition dictates that the sum of the terms at the boundaries is zero, and this results in Equations A.130 to A.132.

$$\Delta s_0\left(z^k_{1,m+1/2}\left(1-w_{1,m+1/2}\right)-z_{1,m+1}\left(\frac{w_{1,m+1}-w_{1,m}}{2}\right)\right)+\Delta s_1\left(z^k_{1,m+1/2}w_{1,m+1/2}+z_{1,m+1}\left(\frac{w_{1,m+1}-w_{1,m}}{2}\right)\right)+\frac{D^k_{1,m+1/2}\delta t}{\left(s_1-s_0\right)}\frac{\left(z^k_{1,m+1}-z^k_{1,m}\right)}{\left(w_{1,m+1}-w_{1,m}\right)}+$$
$$\Delta s_1\left(-z^k_{2,1+1/2}\left(1-w_{2,1+1/2}\right)-z_{2,1}\left(\frac{w_{2,2}-w_{2,1}}{2}\right)\right)+\Delta s_2\left(-z^k_{2,1+1/2}w_{2,1+1/2}+z_{2,1}\left(\frac{w_{2,2}-w_{2,1}}{2}\right)\right)-\frac{D^k_{2,1+1/2}\delta t}{\left(s_2-s_1\right)}\frac{\left(z^k_{2,2}-z^k_{2,1}\right)}{\left(w_{2,2}-w_{2,1}\right)}=0$$

A.130

$$+\Delta s_1\left(z^k_{2,m+1/2}\left(1-w_{2,m+1/2}\right)-z_{2,m+1}\left(\frac{w_{2,m+1}-w_{2,m}}{2}\right)\right)+\Delta s_2\left(z^k_{2,m+1/2}w_{2,m+1/2}+z_{2,m+1}\left(\frac{w_{2,m+1}-w_{2,m}}{2}\right)\right)+\frac{D^k_{2,m+1/2}\delta t}{\left(s_2-s_1\right)}\frac{\left(z^k_{2,m+1}-z^k_{2,m}\right)}{\left(w_{2,m+1}-w_{2,m}\right)}+$$
$$\Delta s_2\left(-z^k_{3,1+1/2}\left(1-w_{3,1+1/2}\right)-z_{3,1}\left(\frac{w_{3,2}-w_{3,1}}{2}\right)\right)+\Delta s_3\left(-z^k_{3,1+1/2}w_{3,1+1/2}+z_{3,1}\left(\frac{w_{3,2}-w_{3,1}}{2}\right)\right)-\frac{D^k_{3,1+1/2}\delta t}{\left(s_3-s_2\right)}\frac{\left(z^k_{3,2}-z^k_{3,1}\right)}{\left(w_{3,2}-w_{3,1}\right)}=0$$

A.131

$$+\Delta s_{nf-2}\left(z^k_{nf-1,m+1/2}\left(1-w_{nf-1,m+1/2}\right)-z_{nf-1,m+1}\left(\frac{w_{nf-1,m+1}-w_{nf-1,m}}{2}\right)\right)+\Delta s_{nf-1}\left(z^k_{nf-1,m+1/2}w_{nf-1,m+1/2}+z_{nf-1,m+1}\left(\frac{w_{nf-1,m+1}-w_{nf-1,m}}{2}\right)\right)$$
$$+\frac{D^k_{nf-1,m+1/2}\delta t}{\left(s_{nf-1}-s_{nf-2}\right)}\frac{\left(z^k_{nf-1,m+1}-z^k_{nf-1,m}\right)}{\left(w_{nf-1,m+1}-w_{nf-1,m}\right)}+$$
$$\Delta s_{nf-1}\left(-z^k_{nf,1+1/2}\left(1-w_{nf,1+1/2}\right)-z_{nf,1}\left(\frac{w_{nf,2}-w_{nf,1}}{2}\right)\right)+\Delta s_{nf}\left(-z^k_{nf,1+1/2}w_{nf,1+1/2}+z_{nf,1}\left(\frac{w_{nf,2}-w_{nf,1}}{2}\right)\right)-\frac{D^k_{nf,1+1/2}\delta t}{\left(s_{nf}-s_{nf-1}\right)}\frac{\left(z^k_{nf,2}-z^k_{nf,1}\right)}{\left(w_{nf,2}-w_{nf,1}\right)}$$
$$=0$$

A.132

The first and last interfaces are stationary, hence $\Delta s_0=\Delta s_{nf}=0$

$$\Delta s_1\left(z^k_{1,m+1/2}w_{1,m+1/2}+z_{1,m+1}\left(\frac{w_{1,m+1}-w_{1,m}}{2}\right)-z^k_{2,1+1/2}\left(1-w_{2,1+1/2}\right)-z_{2,1}\left(\frac{w_{2,2}-w_{2,1}}{2}\right)\right)$$

$$\Delta s_2\left(-z^k_{2,1+1/2}w_{2,1+1/2}+z_{2,1}\left(\frac{w_{2,2}-w_{2,1}}{2}\right)\right)=\frac{D^{\,k}_{2,1+1/2}\delta t}{\left(s_2-s_1\right)}\frac{\left(z^k_{2,2}-z^k_{2,1}\right)}{\left(w_{2,2}-w_{2,1}\right)}-\frac{D^{\,k}_{1,N+1/2}\delta t}{\left(s_1-s_0\right)}\frac{\left(z^k_{1,N+1}-z^k_{1,N}\right)}{\left(w_{1,N+1}-w_{1,N}\right)} \qquad \text{A.133}$$

$$+\Delta s_1\left(z^k_{2,m+1/2}\left(1-w_{2,m+1/2}\right)-z_{2,m+1}\left(\frac{w_{2,N+1}-w_{2,N}}{2}\right)\right)$$

$$+\Delta s_2\left(z^k_{2,m+1/2}w_{2,m+1/2}+z_{2,m+1}\left(\frac{w_{2,m+1}-w_{2,m}}{2}\right)-z^k_{3,1+1/2}\left(1-w_{3,1+1/2}\right)-z_{3,1}\left(\frac{w_{3,2}-w_{3,1}}{2}\right)\right)+\frac{D^{\,k}_{2,N+1/2}\delta t}{\left(s_2-s_1\right)}\frac{\left(z^k_{2,N+1}-z^k_{2,N}\right)}{\left(w_{2,N+1}-w_{2,N}\right)}$$

$$+\Delta s_3\left(-z^k_{3,1+1/2}w_{3,1+1/2}+z_{3,1}\left(\frac{w_{3,2}-w_{3,1}}{2}\right)\right)=\frac{D^{\,k}_{3,1+1/2}\delta t}{\left(s_3-s_2\right)}\frac{\left(z^k_{3,2}-z^k_{3,1}\right)}{\left(w_{3,2}-w_{3,1}\right)}-\frac{D^{\,k}_{2,m+1/2}\delta t}{\left(s_2-s_1\right)}\frac{\left(z^k_{2,m+1}-z^k_{2,m}\right)}{\left(w_{2,m+1}-w_{2,m}\right)}$$

A.134

Equation A.134 can be generalized into Equation A.135 for the nth interface between two phases.

$$+\Delta s_{nn-1}\left(z^k_{nn,N+1/2}\left(1-w_{nn,N+1/2}\right)-z_{nn,N+1}\left(\frac{w_{nn,N+1}-w_{nn,N}}{2}\right)\right)$$

$$+\Delta s_{nn}\left(z^k_{nn,N+1/2}w_{nn,N+1/2}+z_{nn,N+1}\left(\frac{w_{nn,N+1}-w_{nn,N}}{2}\right)-z^k_{nn+1,1+1/2}\left(1-w_{nn+1,1+1/2}\right)-z_{nn+1,1}\left(\frac{w_{nn+1,2}-w_{nn+1,1}}{2}\right)\right)$$

$$+\Delta s_{n+1}\left(-z^k_{nn+1,1+1/2}w_{nn+1,1+1/2}+z_{nn+1,1}\left(\frac{w_{nn+1,2}-w_{nn+1,1}}{2}\right)\right)=\frac{D^{\,k}_{nn+1,1+1/2}\delta t}{\left(s_{nn+1}-s_{nn}\right)}\frac{\left(z^k_{nn+1,2}-z^k_{nn+1,1}\right)}{\left(w_{nn+1,2}-w_{nn+1,1}\right)}-\frac{D^k_{nn,N+1/2}\delta t}{\left(s_{nn}-s_{nn-1}\right)}\frac{\left(z^k_{nn,N+1}-z^k_{nn,N}\right)}{\left(w_{nn,N+1}-w_{nn,N}\right)}$$

A.135

The interface equation for the last interface is:

$$+\Delta s_{nf-2}\left(z^{k}_{nf-1,m+1/2}\left(1-w_{nf-1,m+1/2}\right)-z_{nf-1,m+1}\left(\frac{w_{nf-1,m+1}-w_{nf-1,m}}{2}\right)\right)$$

$$+\Delta s_{nf-1}\left(z^{k}_{nf-1,m+1/2}w_{nf-1,m+1/2}+z_{nf-1,m+1}\left(\frac{w_{nf-1,m+1}-w_{nf-1,m}}{2}\right)-z^{k}_{nf,1+1/2}\left(1-w_{nf,1+1/2}\right)-z_{nf,1}\left(\frac{w_{nf,2}-w_{nf,1}}{2}\right)\right)$$

$$=\frac{D^{k}_{nf,1+1/2}\delta t}{\left(s_{nf}-s_{nf-1}\right)}\frac{\left(z^{k}_{nf,2}-z^{k}_{nf,1}\right)}{\left(w_{nf,2}-w_{nf,1}\right)}-\frac{D_{nf,-1}{}^{k}_{m+1/2}\delta t}{\left(s_{nf-1}-s_{nf-2}\right)}\frac{\left(z^{k}_{nf-1,m+1}-z^{k}_{nf-1,m}\right)}{\left(w_{nf-1,m+1}-w_{nf-1,m}\right)}$$

A.136

The above equations can be solved by using a matrix:

The summation is done for each phase, and the equations can be solved by using a matrix:

The summation is done for each phase, and the equations can be solved by using a matrix:

$$\begin{bmatrix} a_1 & a_2 & & & & \\ \mathrm{K}_{n-1} & \mathrm{K}_{nn} & \mathrm{K}_{nn+1} & & & \\ & \cdot & \cdot & \cdot & & \\ & & \cdot & \cdot & \cdot & \\ & & & \cdot & \cdot & \cdot \\ & & & & \mathrm{K}_{nf-2} & \mathrm{K}_{nf-1} \end{bmatrix}\begin{bmatrix} \Delta s_1 \\ \Delta s_{nn} \\ \cdot \\ \cdot \\ \cdot \\ \Delta s_{nf-1} \end{bmatrix}=\begin{bmatrix} b_1 \\ b_{nn} \\ \cdot \\ \cdot \\ \cdot \\ b_{nf-1} \end{bmatrix}$$

A.137

The entries in the matrix are:

$$\mathrm{K}_1=\left(z^{k}_{1,m+1/2}w_{1,m+1/2}+z_{1,m+1}\left(\frac{w_{1,m+1}-w_{1,m}}{2}\right)-z^{k}_{2,1+1/2}\left(1-w_{2,1+1/2}\right)-z_{2,1}\left(\frac{w_{2,2}-w_{2,1}}{2}\right)\right)$$

$$\mathrm{K}_2=\left(-z^{k}_{2,1+1/2}w_{2,1+1/2}+z_{2,1}\left(\frac{w_{2,2}-w_{2,1}}{2}\right)\right)$$

$$b_1=\frac{D_{2,}{}^{k}_{1+1/2}\delta t}{\left(s_2-s_1\right)}\frac{\left(z^{k}_{2,2}-z^{k}_{2,1}\right)}{\left(w_{2,2}-w_{2,1}\right)}-\frac{D_{1,}{}^{k}_{m+1/2}\delta t}{\left(s_1-s_0\right)}\frac{\left(z^{k}_{1,m+1}-z^{k}_{1,m}\right)}{\left(w_{1,m+1}-w_{1,m}\right)}$$

$$\mathrm{K}_{nn-1} = \left(z^{k}_{nn,m+1/2}\left(1 - w_{nn,m+1/2}\right) - z_{nn,m+1}\left(\frac{w_{nn,m+1} - w_{nn,m}}{2} \right) \right)$$

$$\mathrm{K}_{nn} = \left(z^{k}_{nn,m+1/2} w_{nn,m+1/2} + z_{nn,m+1}\left(\frac{w_{nn,m+1} - w_{nn,m}}{2} \right) - z^{k}_{nn+1,1+1/2}\left(1 - w_{nn+1,1+1/2}\right) - z_{nn+1,1}\left(\frac{w_{nn+1,2} - w_{nn+1,1}}{2} \right) \right)$$

$$\mathrm{K}_{nn+1} = \left(-z^{k}_{nn+1,1+1/2} w_{nn+1,1+1/2} + z_{nn+1,1}\left(\frac{w_{nn+1,2} - w_{nn+1,1}}{2} \right) \right)$$

$$b_{nn} = \frac{D^{k}_{nn+1,1+1/2}\delta t}{\left(s_{nn+1} - s_{nn}\right)} \frac{\left(z^{k}_{nn+1,2} - z^{k}_{nn+1,1}\right)}{\left(w_{nn+1,2} - w_{nn+1,1}\right)} - \frac{D^{k}_{nn,m+1/2}\delta t}{\left(s_{nn} - s_{nn-1}\right)} \frac{\left(z^{k}_{nn,m+1} - z^{k}_{nn,m}\right)}{\left(w_{nn,m+1} - w_{nn,m}\right)}$$

$$\mathrm{K}_{nf-2} = \left(z^{k}_{nf-1,m+1/2}\left(1 - w_{nf-1,m+1/2}\right) - z_{nf-1,m+1}\left(\frac{w_{nf-1,m+1} - w_{nf-1,m}}{2} \right) \right)$$

$$\mathrm{K}_{nf-1} = \left(z^{k}_{nf-1,m+1/2} w_{nf-1,m+1/2} + z_{nf-1,m+1}\left(\frac{w_{nf-1,m+1} - w_{nf-1,m}}{2} \right) - z^{k}_{nf,1+1/2}\left(1 - w_{nf,1+1/2}\right) - z_{nf,1}\left(\frac{w_{nf,2} - w_{nf,1}}{2} \right) \right)$$

$$b_{nf-1} = \frac{D^{k}_{nf,1+1/2}\delta t}{\left(s_{nf} - s_{nf-1}\right)} \frac{\left(z^{k}_{nf,2} - z^{k}_{nf,1}\right)}{\left(w_{nf,2} - w_{nf,1}\right)} - \frac{D_{nf,-1}{}^{k}_{m+1/2}\delta t}{\left(s_{nf-1} - s_{nf-2}\right)} \frac{\left(z^{k}_{nf-1,m+1} - z^{k}_{nf-1,m}\right)}{\left(w_{nf-1,m+1} - w_{nf-1,m}\right)}$$

$$s^{k+1} = \Delta s + s^{k-1}$$